“INFLUENCE OF SUPPLEMENTARY CEMENTITIOUS MATERIALS AND COARSE AGGREGATES ON PROPERTIES OF THE NO-FINES CONCRETE”

A Thesis

Submitted in Fulfillment of the Requirements

For the award of the degree of

DOCTORATE OF PHILOSOPHY

IN

CIVIL ENGINEERING

TARUNBIR SINGH

(Registration No. 901602013)

UNDER THE SUPERVISION OF

Dr. RAFAT SIDDIQUE

Senior Professor

Dean, Research and Sponsored Projects

Dr. SHRUTI SHARMA

Professor

DEPARTMENT OF CIVIL ENGINEERING

THAPAR INSTITUTE OF ENGINEERING AND TECHNOLOGY,

DEEMED TO BE UNIVERSITY

PATIALA-147004

MARCH 2022

CERTIFICATE

Certify that the work which is being presented in the thesis entitled **"INFLUENCE OF SUPPLEMENTARY CEMENTITIOUS MATERIALS AND COARSE AGGREGATES ON PROPERTIES OF THE NO-FINES CONCRETE,"** which is submitted by Tarunbir Singh, in fulfillment of the requirements for the award of the Degree of Doctor of Philosophy and submitted in the Department of Civil Engineering of the Thapar Institute of Engineering and Technology, Patiala, is an authentic record of candidate`s own original and independent research work out by him under our supervision and guidance. The matter embodied in this thesis has not been submitted in part or full to any other University or Institute for the award of any degree.

Siddique

(Dr. Rafat Siddique)
Senior Professor
Department of Civil Engineering
Dean of Research and Sponsored Projects
TIET, Patiala
Punjab, India.

Shruti Sharma

(Dr. Shruti Sharma)
Professor
Department of Civil Engineering
TIET, Patiala
Punjab, India.

DECLARATION

I hereby declare that the research work presented in this thesis entitled **"INFLUENCE OF SUPPLEMENTARY CEMENTITIOUS MATERIALS AND COARSE AGGREGATES ON PROPERTIES OF THE NO-FINES CONCRETE"** submitted for the award of the Degree of Doctor of Philosophy and submitted in the Department of Civil Engineering of the Thapar Institute of Engineering and Technology, Patiala, is an authenticated record of my own work carried out under the supervision of **Dr. Rafat Siddique,** Senior Professor and DRSP and **Dr. Shruti Sharma,** Professor, Department of Civil Engineering and refers other researcher`s work is duly listed in the reference section.

The matter presented in the thesis has not been submitted by me for the award of any degree of this or any other University or Institute.

Tarunbir Singh

(Tarunbir Singh)

ACKNOWLEDGEMENT

|| ਅਵਲਿ ਅਲਹ ਨੂਰੁ ਉਪਾਇਆ ਕੁਦਰਤਿ ਕੇ ਸਭ ਬੰਦੇ

ਏਕ ਨੂਰ ਤੇ ਸਭੁ ਜਗੁ ਉਪਜਿਆ ਕਉਨ ਭਲੇ ਕੋ ਮੰਦੇ ||

- *At the outset, I would like to acknowledge my sincere gratitude and appreciation of my supervisors Dr. Rafat Siddique, Senior Professor and DRSP, and Dr. Shruti Sharma, Professor, Department of Civil Engineering, Thapar Institute of Engineering and Technology, Patiala, for their invaluable guidance and time throughout my research work. They were always available and eager to help and advice, whether my problem be professional or personal. Their cooperation, support, and motivation are the primary reason for completing this dissertation. This research would not have been possible without their inspiration.*
- *I would like to take this opportunity to express my sincere gratitude to all faculty members of the Department of Civil Engineering, especially advisory committee members, namely Dr. Prem Pal Bansal, Dr. Shweta Goyal, Dr. Puneet Sharma and Dr. Heaven Singh, for their valuable suggestions and feedbacks. The inputs provided by Dr. Prem Pal Bansal, Head Department of Civil Engineering, his interest, and his critical appraisal during the early stages of this research were invaluable.*
- *I would like to sincerely thank all the Department of Civil Engineering laboratory technical staff, TIET Patiala. The help and support provided by Er. Varinder Kumar Sharma and Shri Ram Sumiran during the entire research period are greatly appreciated. Special thanks go to Mr. Manreet Singh and Mr. Hitesh Bhardwaj for their untiring efforts in helping and facilitating the research work of Ph.D. students like me.*
- *I would express my dearest gratitude to my fellow research scholars, some of whom I have come to share a special bond throughout my thesis. Ankit Kumar and Amandeep Singh Sidhu are the one who helped me a lot, and the times we spent and the memories we shared will always be etched in my memory. They were always there as a friend whenever I needed him. Thank you for your unending support.*

- *I would also like to thank my fellow research scholars Devender Sharma, Ruby Priya, Pavitar Singh and Vivek Dhingra for their help, support, and good times we spent at Thapar Institute.*
- *No words of mine can be sufficient to express my thanks and respect to my Parents. Special thanks to my wife Gaganpreet Kaur and daughter Savreen Kaur. They have been a constant and untiring source of support and motivation to me all through this time. I am also grateful to my sisters and brothers-in-law, who were always there for me, as friends, guides, and elders, to share their experiences through this journey.*
- *In the end, I thank the Almighty for giving me his blessing throughout my research work and providing me with strength enough to accomplish this research work.*

LIST OF PUBLICATIONS

1. Singh T., Siddique R., and Sharma S., “Strength and Permeability of No-Fines Concrete made with Supplementary Cementitious Materials” ***Journal of Materials in Civil Engineering***, ***ASCE*** (2021) DOI: 10.1061/ (ASCE) MT.1943-5533.0004037.
2. Singh T., Siddique R., and Sharma S., “Effectiveness of using Metakaolin and Fly ash as Supplementary Cementitious Materials in Pervious Concrete” ***European Journal of Environmental and Civil Engineering, Taylor & Francis*** (2021), DOI: 10.1080/19648189.2021.1988715.

ABSTRACT

The rapid increase in infrastructural development escalates the problem of storm water runoff and flash flooding in rainy seasons in urban areas due to insufficient drainage. To overcome this problem, the permeability of conventional pavements is improved by replacing normal concrete with Pervious Concrete or No-Fines Concrete (NFC). Since NFC consist of extensive large volume of voids which contributes towards its highly porous nature, which can remedy the problem of the rainwater runoff, recharges the groundwater table near road pavements, city streets, and parking lots, and reduces noise from the vehicle tire movement. The exclusion of sand from NFC leads to a reduction in workability and strength, limiting its practical applications. Thereby, it is currently not feasible to use NFC mixtures in highway pavements due to their lower strength than conventional pavement quality concrete.

This research aimed to investigate the influence of supplementary cementitious materials such as fly ash, metakaolin, silica fume, and rice husk ash and different gradations of coarse aggregates on the properties of NFC. In NFC mixes, cement was replaced by supplementary cementitious materials up to 20% replacement levels. The effect of different gradations of coarse aggregates on the properties of NFC was also inspected. The following properties were evaluated: compressive strength, split tensile strength, flexural strength, abrasion resistance, water permeability, porosity, density, water absorption, and drying shrinkage up to 365-day.

The experimental results indicate that with the inclusion of Fly Ash (FA), the compressive strength decreased at an early curing age up to 28-day compared to the control NFC mix. The compressive strength increased concerning the control NFC mix at 90 and 365-day of curing. With the incorporation of metakaolin in the NFC mix, the compressive strength increased with the increasing percentage replacement of Metakaolin (MK) at all curing ages compared to the control NFC mix.

The optimum replacement level for SF was found to be 10% in terms of compressive strength at all curing ages compared to the control mix. The Rice Husk Ash (RHA) replacement reduced the compressive strength at 7 and 28-day. However, at later ages, the compressive strength was maximum at optimum 5% replacement. The overall compressive strength values were higher than

the control mix at all percentage replacement levels. The maximum compressive strength of 10.77 MPa was achieved at 365-day in NFC prepared with an aggregate size of 4.75 mm.

On replacing cement with FA, split tensile strength results seemed to follow the compressive strength trend with decreases at 7 and 28-day compared to control NFC but improved at 90-day. Hence, it can be concluded that no significant contribution by FA replacement in compressive and tensile strength is observed at early ages as it requires a longer curing period to reach strength comparable to cement. For MK replacement of cement, the split tensile strength increased at different curing ages. For SF in NFC mixes, an increase in split tensile strength at 7, 28, 90, and 365-day with an optimum replacement level of 10% compared with that of the control mix. When replacing cement with RHA, the split tensile strength decreased continuously as the percentage replacement level increased from 0% to 20% compared to the control mix. The NFC mix prepared with smaller-sized aggregates shows better split tensile strength than the NFC mixes made with larger ones.

Similar results were found in the flexural strength of NFC containing FA. The trends of flexural strength were similar to compressive and split tensile strength results of NFC mixes with different aggregates sizes such that the smaller size aggregates performed better than larger sized aggregates in NFC mixes.

The abrasion resistance increases as the amount of FA and MK replacement increases. The optimum level concerning abrasion was at 10% replacement with SF. In NFC mixes containing RHA, percentage mass loss consistently increased with increasing replacement increased with RHA, causing a drop in abrasion resistance. On the other hand, it was observed that the weight loss was more in NFC-9.5 mm size of aggregate concrete than the NFC-4.75 mm size aggregate concrete.

Permeation properties i.e., water permeability and porosity of NFC mixes containing MK slightly reduced but are well within acceptable limits as per ACI guidelines. On the other hand, increased FA levels in NFC mixes decreased water permeability and porosity due to pore size refinement and continuous voids. The permeability properties of permeability and porosity decrease marginally with increasing SF and RHA replacement at optimum levels without considerably affecting the drainage properties for use in road pavements. The permeation properties of NFC mixes improved slightly by using larger size aggregates. The water permeability of NFC mix prepared with 4.75 mm aggregates was 50% lower at 28-day as compared to NFC mix prepared with 9.5 mm sized aggregate.

The density of all NFC mixes prepared with FA, MK, SF, and RHA was reported in the acceptable range of 1600 to 2200 kg/m^3. The density of the NFC mixes decreases as the size of aggregates used increases. The maximum density was obtained with NFC-4.75 at all the curing ages.

The decrease in water absorption values was observed with increasing FA, MK, SF, and RHA replacement of cement in NFC but lies well within the acceptable limits for NFC. Similarly, the drying shrinkage values decreased with the increasing replacement of FA, MK, SF, and RHA compared to the control mix at all periods.

From the SEM analysis of different NFC mixes prepared with FA, a refinement in pore structure is observed at later ages due to the formation of higher amount of C-S-H gel. Similarly, NFC mixes prepared by replacing cement with MK show higher concentration of C-S-H gel formation leading to a dense microstructure and higher strengths at all ages. It is also well corroborated by the XRD spectrum; wherein additional C-S-H gel peaks are observed due to this consequent decrease in the peak of quartz. Similar observations are made with replacement of up to 10% of cement with SF. XRD spectrum indicates that major phases formed in NFC mixes prepared by replacement of cement with SF and RHA remain the same. But an additional peak of C-S-H gel is observed in the NFC-SF10 mix accompanied by peak of quartz. In RHA replacement, the primary phase was quartz, which does not participate in the pozzolanic activity. Microstructural analysis of NFC mixes prepared by using different gradation of natural coarse aggregates show the denser microstructure in NFC prepared with smaller sized aggregates at each curing age.

Table of Contents

Contents ***Page***

LIST OF TABLES

Table ***Page***

LIST OF FIGURES

Figure ***Page***

LIST OF ABBREVIATIONS

AASC	- Alkali-Activated Slag Cement
ACI	- American Concrete Institute
APA	- Asphalt Pavement Analyzer
ASTM	- American Society for Testing and Materials
BIS	- Bureau of Indian Standards
c/a	- Cement to aggregate ratio
CC	- Calcium Carbonate
CH	- Calcium Hydroxide
CSH	- Calcium Silicate Hydrate
EAFS	- Electric Arc Furnace Slag
EPA	- Environmental Protection Agency
FA	- Fly Ash
FM	- Fineness Modulus
HID	- High Impact Development
LID	- Low Impact Development
MK	- Metakaolin
MSWIBA	- Municipal Solid Waste Incinerator Bottom Ash
NFC	- No-Fines Concrete
OPC	- Ordinary Portland Cement
PSR	- Plastic to Soil Ratio
RHA	- Rice Husk Ash
SCMs	- Supplementary Cementitious Materials

SEM	- Scanning Electron Microscopy
SF	- Silica Fume
SP	- Superplasticizer
UHI	- Urban Heat Island
UTM	- Universal Testing Machine
VAE	- Vinyl Acetate-Ethylene
w/cm	- Water to cementitious ratio
XRD	- X-Ray Diffraction

LIST OF SYMBOLS AND UNITS

°C	- Degree Celsius
kN	- Kilo Newton
cm	- Centimeter
mm	- Millimeter
kg	- Kilogram
gm	- Gram
sec	- Seconds
m	- Meter
MPa	- Mega Pascal
cm/s	- Centimeter per second
kg/m^3	- Kilogram per cubic meter
m^2/kg	- Meter square per kilogram
cm^2	- Centimeter square
Hz	- Hertz
µm	- Micrometer
Ø	- Porosity of concrete specimen (%)
ρ	- Density of concrete specimen (kg/m^3)
K	- Water Permeability, (cm/s)
ρ_w	- Density of water (kg/m^3)

CHAPTER 1
INTRODUCTION

This chapter introduces No-Fines Concrete (NFC), its historical background and field application. It also covers the introduction of Supplementary Cementitious Materials (SCMs) with their chemical properties and main objectives of this research work are also briefed.

1.1 GENERAL

In recent decades, the fast-growing population and mass movement towards developed areas have increased, resulting in rapid urbanization, consequently leading to increased construction infrastructure (Miller et al., 2014). In the present scenario, half of the world`s population is inhabiting metropolitan areas. It is predicted that by the end of 2050, approximately 70% of the global population will start living in the built-up areas (United Nations, 2014). However, urban development is a positive indicator of advancement expected to improve humankind`s quality of life. Nevertheless, the current rapid, unplanned, and uncontrolled way it is occurring around the globe has raised concerns of various environmentalists, research scholars, urban planners, and developers about its impact on sustainability. Sustainable development can be coined as "A process of change in which the exploitation of resources, the direction of investments, the orientation of technological development, and institutional change are made consistent with the future as well as present needs" (Sustainable Development, 1987).

Over the last few years, urbanization has consumed the natural terrain at twice the human population's rate. In order to provide shelter and connectivity, the natural landscape is being turned into manmade constructions, primarily buildings and pavements (Anush K. Chandrappa and Biligiri, 2016a). The pavements cover around 20-40% of the total urbanized area, turning the naturally pervious ground into impervious ground (Anush K. Chandrappa and Biligiri, 2016a; Qin and Hiller, 2014). Because of their dense material composition, the conventional pavements are essentially impermeable to water. These pavements are currently the area of research as they are the source of two apparent changes in the environment relating to urban hydrology and the encompassing ambient temperature (Anush K. Chandrappa and Biligiri, 2016a). The impermeable land reduces the period of runoff concentration, resulting in flood-like conditions in metropolitan areas, which is currently a critical element impacting the urban people`s regular functioning. Increased runoff lowers groundwater recharge while also growing the first flush volume, necessitating the construction of large water treatment plants to clean filthy water before it is discharged into local water bodies.

Furthermore, when natural ground with a high latent heat capacity is replaced with paving materials with a lesser heat capacity, the thermal mass will store more heat. The accumulated heat is released into the atmosphere, raising the temperature of the nearby metropolitan area by roughly 2 to 8 °C above that of the adjacent countryside (Akbari et al., 2001; Anush K. Chandrappa and Biligiri, 2016a; Ferguson, 2005; Golden, 2004). The urban heat island (UHI) consist of temperature differences contrasting urban and rural conditions that harm civilized tenants' health due to thermal discomfort (Saboo et al., 2019). In addition, urbanization causes many other effects on the environment, referred to as high impact development (HID) (Anush K Chandrappa and Biligiri, 2016). To minimize the negative impacts of rapid advancement on the environment, it is necessary to concentrate on a sustainable approach to economic and social policies along with environment conservation which may contribute to low impact development (LID) (Anush K Chandrappa and Biligiri, 2016; Luck et al., 2008; Maria et al., 2020). Even though conventional concrete pavements are widely utilized due to their higher strength and relatively high durability properties, there is a need to replace them with other viable options where conventional pavements might not be necessary, such as low volume traffic congestion roads, cycle tracks, parking lots, which majorly constituents a large portion of pavement network in urban and undeveloped areas (Hesami et al., 2014; Saboo et al., 2019). No-Fines Concrete (NFC) is one such alternate solution that may solve this complex problem and which can be easily integrated by engineers, designers, research scholars, urban planners, and developers into their urban infrastructure design.

1.2 NO-FINES CONCRETE

No-Fines Concrete (NFC) is a special type of concrete in which lightweight aggregates are gap graded. This type of concrete comprises of Portland cement, uniformly graded coarse aggregate, with relatively small amount or without fine aggregates and water. The texture of NFC is rough as compared to conventional one (Deo and Neithalath, 2010). No-fines concrete is also termed as pervious concrete, porous concrete, zero slumps, gap graded concrete, and water-permeable concrete. In NFC, adequate water and cementitious materials are used to make a paste that creates a thin layer covering on aggregates but leaves a gap between them. As a result, pores are formed in the gap-graded material (Montes, 2006; Tennis et al., 2004). No-fines concrete contains a high void content to allow stormwater to penetrate through, which minimize the runoff volume. The stormwater flows through different layers of the NFC pavement system and recharges the groundwater table. (Anush K Chandrappa and Biligiri, 2016).

Furthermore, water in the NFC does not dry out instantly due to the twisted pore structure. It has a high latent heat capacity, in which the solar energy absorbed is utilized to evaporate the water layer surrounding the pore walls instead of storing the heat energy (Asaeda and Ca, 2000; Li et al., 2014). When NFC pavements are placed in relevant places such as local roads, residential streets, cycle tracks, or parking lots exposed to direct sunlight, NFC assists the high latent heat capacity of water to minimize the UHI effect. In addition, thermal properties of NFCs like specific heat, thermal diffusivity, thermal conductivity, and albedo are conducive to effectively reducing UHI impacts (Sreedhar and Biligiri, 2016). Figure 1.1 schematically demonstrates the comparison between conventional impervious concrete and pervious concrete.

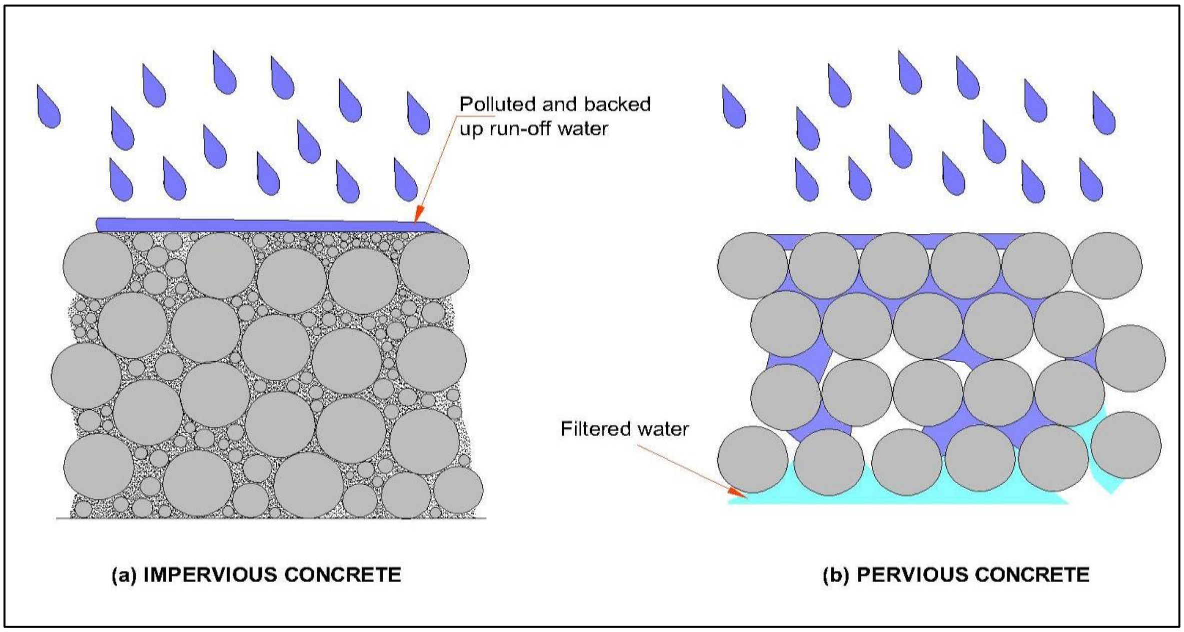

Figure 1.1. Pictorial representation of conventional impervious concrete and pervious concrete (Zhong et al., 2018)

1.3 HISTORICAL BACKGROUND OF NFC

Initially, the concept of NFC was introduced in European Countries, but soon the technology spread to developing countries like India. The initial use of NFC was in the 19th century England where mainly load-bearing walls used NFC. The concept gained popularity during Second World War as a direct response to limited availability of cement. The USA encouraged the use of NFC concrete during the 1970s, the advent of NFC in India was in year 2000. After the 1970s, the primary purpose behind using NFC was its excellent permeability rather than lower production cost (Ghafoori and Dutta, 1995).

To achieve zero emission target, researchers and scientists are well aware to develop the new sustainable construction materials and methods. This led to the popularity of NFC. This concrete has been awarded as sustainable material for its usefulness in controlling the surface runoff by absorbing the rainwater into the soil (Tennis et al., 2004). Its practical application also extends to pavement material in regions where stormwater management is the major issue. Thus, the usage of NFC as a viable alternative to conventional concrete has developed into a multi-functional tool in the construction sector, despite its sluggish start.

1.4 FIELD APPLICATIONS OF NFC

No-fines concrete can be used in many applications, but it is restricted to specific applications due to poor performance in mechanical properties. Therefore, the primary use of NFC pertains to the pavements which are subjected to limited traffic volumes. It was used as load-bearing walls in its starting ages, presently vehicular parking areas are the main places where NFC is used. Following are the potential applications of NFC as per ACI 522R (ACI Committee 522, 2010):

- Rigid drainage layers which run beneath exterior mall areas
- Greenhouse flooring which prevents any flooding of the floor area
- Structural wall applications which are directly aimed at achieving lightweight or/and better heat deterrent material,
- Pavements, floors and walls with high acoustic absorption
- The surface course for vehicular parking lots, tennis courts in urban areas, zoo areas etc.
- Decks of swimming pool
- Bridge embankments
- Beach near about structures and seawalls.

  Since of the open pore structure of the material, unreinforced NFC is often used for all of these applications because the danger of corrosion for the exposed steel is substantial.

1.5 ADVANTAGES/DISADVANTAGES OF NFC

No-fines concrete has numerous benefits, including reduced - runoff volume, pollution, need for stormwater infrastructure, flood risk, decreased heat island effect and road salt application, improved pavement noise absorption performance, and exclusion of pollution generated by asphalt pavements and sealers (Anush K Chandrappa and Biligiri, 2016; Zhong et al., 2018). The most significant benefits can be briefed as below:

- The main feature of NFC is its ability of permeation properties. No-fines concrete prevents water from accumulating on pavement surfaces and increases the quality of the groundwater under it. In addition, NFC is frequently used as shoulders alongside the conventional pavement because of its drainage characteristics.
- No-fines concrete pavements reduce the urban heat island effect. However, NFC pavements do not absorb and store heat because of their open structure before radiating it into surrounding like conventionally used asphalt surface, causing the heat island effect (Anush K. Chandrappa and Biligiri, 2016b).
- In comparison to conventional concrete, which utilizes 60-75 percent aggregate, NFC employs 50-65 percent aggregate. As a result, NFC helps to preserve natural aggregate. The United States Environmental Protection Agency (US-EPA) considers NFC environmentally friendly (Barišić et al., 2017; Tennis et al., 2004) cite report.
- No-fines concrete offers better noise absorption properties due to its increased voids and porous structure. Traffic noise on the NFC pavement is lower than the conventional cement concrete pavements and asphalt concrete pavements.

The usage of NFC also presents certain challenges such as:

- The clogging of voids in the NFC pavement. The pavement has tendency to get clogged due to deposition of dust and dirt in pores from the surrounding area of roads or from tires (Cackler E.T. et al., 2006).
- Repeated cleaning and maintenance will be required for optimum functioning of NFC pavement to maintain its permeability.
- Limited usage in heavy traffic volume areas where specialized construction practice will be required to maintain required quality.

1.6 SUPPLEMENTARY CEMENTITIOUS MATERIALS (SCMs)

In recent decades, strength and durability properties are major parameters to be focused while designing the mortar and concrete using advance technologies. Concrete comprises cement, fine aggregates, water, coarse aggregates, mineral additives, and admixtures with an estimated annual usage of up to 30 billion tons in 2020 (Monteiro et al., 2017). Because of its binding qualities, Portland cement plays a vital role in manufacturing mortar and concrete and is consequently a preferred construction material. Cement production is increasing globally in the last decade from 3300 to 4100 million tons from 2010 to 2020, which is around a 24% increase ("Mineral Commodity Summaries (USGS)," 2020, "Mineral Commodity Summaries (USGS)," 2011). Increased cement manufacturing brings with it a slew of environmental concerns, including energy and resource conservation, manufacturing costs, and greenhouse gas emissions. The cement production industry alone accounts for about 10% of CO_2 emissions worldwide. One ton of cement emits equivalent weight of CO_2 and other greenhouse gases into the atmosphere. This indicates that the cement and concrete sector will have a tough time maintaining long-term growth in the building and construction materials market. (Saboo et al., 2019; Zaetang et al., 2017).

Hence, Supplementary Cementitious Materials is the need for modern construction as a partial replacement of cement to effectively decrease the cement demand, reduce carbon emissions from cement production and additionally enhance the strength properties and also durability characteristics (Dinakar et al., 2013; Saboo et al., 2019). Portland cement is responsible for roughly 7-8 percent of world CO_2 emissions. As a result, pozzolanic materials must be employed to improve the quality of building materials in order to minimise emissions. The usage of SCMs in mortar and concrete cuts costs while also reducing disposal difficulties. In both the fresh and hardened phases, the use of SCMs increases the mechanical and durability qualities of mortar and concrete. Self-cementitious materials are pozzolanic materials that are by-products of several chemical processes and can be utilised as a replacement or addition to cement. Fly ash, rice husk ash, granulated ground blast furnace slag, metakaolin, and silica fume are some of the other minerals available. The above mentioned SCMs possesses different pozzolanic activity depending upon their mineralogical composition and particle size.

The comparison between the pozzolanic behaviour of silica fume (SF), fly-ash (FA), rice husk ash (RHA), and metakaolin (MK) in the application of NFC has been studied in present research.

1.6.1 Fly ash

Fly ash serves as a cost efficient and environmentally friendly pozzolanic material compared to conventional cement. The usage of FA as SCM proved to be more advantageous over conventional material and also, possesses adequate strength and durability properties. It is inexpensive and aids in the improvement of concrete plasticity as well as the durability and strength of hardened concrete. When pulverised coal is burnt in electric power plants, fly ash is created. Mineral impurities in coal, such as quartz, clay, and shale, stay suspended during burning and ascend with the exhaust gases above the combustion chamber. As the molten material cools, it condenses into spherical glassy particles called FA. Electrostatic precipitators collect from exhaust gases are a fine-grained, powdery particle substance. About 85-99% and 75-85% of FA can be collected from flue gases and coal ash respectively. The recovery amount depends upon the collection system, which may include mechanical, electrical precipitators, and fabric filters while the rest is separated as bottom ash or boiler slag Bottom ash doesn't exhibit pozzolanic properties. But mineralogical composition of FA shows that particles are small in size and amorphous in nature, fly ash is typically pozzolanic and, in certain cases, self-cementitious.

Large quantities of FA which is around 780 million tons are released annually by thermal plants around the globe. Enormous amount of FA is added to the environment annually by thermal plants in India which exceeds 100 million tons, with 25 percent approximately of the total cementitious material being used in concrete.

Classification of fly ash

Fly ash can be classified into three categories as per ASTM C618 (ASTM C 618, 2009).

Class C fly ash: The majority of Class C fly ashes come from low quality coal lignite. This form of FA has pozzolanic and self-cementitious characteristics in various degrees. CaO level in Class C fly ashes is known to be greater than 15%. However, a minor percentage of Class C fly ash includes CaO in the range of 10%. The principal element of this type of fly ash is calcium alumino-silca glass, which is extremely reactive. Lime, anhydrite, quartz, and cement elements such as C_3A, C_2S, and C_4A_3S are crystalline phases in this category of fly ash (Siddique, 2007; Siddique and Khan, 2011).

Class F fly ash: CaO level is relatively low in Class F fly ashes. They're made by burning anthracite or bituminous coal, both of which come within this group. This FA type has very little pozzolanic activity and essentially no self-hardening ability. They are mostly made up of non-crystalline silica (70%) which is responsible for the pozzolanic action. Quartz, magnetite, and hematite are the most common crystalline minerals found in their rocks (Siddique, 2007; Siddique and Khan, 2011).

Class N fly ash: This group includes raw or calcined natural pozzolans such as diatomaceous earths, volcanic ashes, opaline chert, shale etc. This group of pozzolans also includes calcined kaolin clay along with varying amount of laterite shale. (Siddique, 2007; Siddique and Khan, 2011).

Physical properties of fly ash

Specific gravity: The shape and chemical content of FA particles affect their specific gravity. The specific gravity of FA typically ranges from 1.3 to 4.8.

Particle morphology: Under dispersive x-ray examination, fly ash particles are clear glassy spheres with dimensions typically between 1 to 150 μm, the majority of which are smaller than 44 microns.

Fineness: One of the most important physical qualities of FA is its fineness, which is linked to its pozzolanic activity. The size of a substantial percentage of ash particles is less than 3μm.

Chemical composition of Fly ash

The major chemical components of FA are found to be silicon dioxide (SiO_2), aluminium oxide (Al_2O_3) and iron oxide (Fe_2O_3), Chemical analysis of various parameters of FA varies from source to source. Some of the chemical compositions as presented in Table 1.1.

Table 1.1 Chemical compositions of typical fly ashes

Properties	(Uma Maguesvari and Sundararajan, 2017)	(Saboo et al., 2019)	(Singh and Singh, 2020)
SiO_2 (%)	51.56	33.50	56.50
Al_2O_3 (%)	23.23	5.70	17.69
Fe_2O_3 (%)	7.15	4.40	11.10
CaO (%)	10.78	62.5	3.19
MgO (%)	2.90	2.50	5.40
SO_3 (%)	1.85	1.74	0.0
K_2O (%)	0.0	0.0	0.0
Na_2O (%)	0.0	0.0	0.0
LOI (%)	2.52	2.45	1.21
Specific gravity	-	-	2.38

1.6.2 Metakaolin

Metakaolin (MK), a de-hydroxylated form of kaolinite mineral, is obtained by calcinating a kaolinite clay from 500 °C and 800 °C. The process of obtaining starts by heating the clay initially to 100 varying up to 200 °C, at this temp pore water is removed from clay minerals. At higher heating temperature of 500 and 800 °C, kaolinite changed form to calcined through de-hydroxilization. The raw material from which Metakaolin ($Al_2Si_2O_7$) is derived is kaolin clay. Kaolin possesses a fine, white clay composition which can be used in the manufacturing of porcelain. The de-hydroxilization of kaolin is done to obtain metakaolin by the endothermic process which has high energy requirement. Kaolinite converts to metakaolin after reaching this temperature range, forming a 2-D crystal structure (Siddique, 2007; Siddique and Khan, 2011).

Physical properties of MK (Siddique, 2007; Siddique and Khan, 2011)

Specific gravity: The specific gravity of MK typically ranges from 2.5 to 2.62.

Particle size: Metakaolin is very fine in nature compared to cement. It has 99.9% of its particles lying below 16 µm and comprising of particles having average size of 3 µm. Its color is off-white.

Surface area: The average surface area of MK is very high and can vary from 12 to 30* 10^3 m^2/kg.

Chemical composition of metakaolin

Silicon dioxide (SiO_2) and alumina oxide are two important ingredients of metakaolin (Al_2O_3). Calcium oxide, ferric oxide, magnesium oxide, and other oxides are among the other ingredients. Table 1.2 shows chemical properties of MK.

Table 1.2. Typical chemical compositions of metakaolin

Properties (%)	(Gill and Siddique, 2017)	(Saboo et al., 2019)	(Singh and Singh, 2020)
SiO_2	51.10	50.85	52.10
Al_2O_3	43.80	40.15	41
Fe_2O_3	1.60	0.80	4.32
CaO	0.20	3.20	0.39
MgO	0.30	0.26	0.0
SO_3	0.05	0.0	0.0
K_2O	0.20	0.0	0.0
Na_2O	0.10	0.0	0.0

1.6.3 Silica Fume

Silica Fume (SF) is a by-product of the smelting process in the silicon and ferrosilicon industries, and an ultrafine powder with a silicon content of 75 percent and non-crystalline silica in the range of 85-95 percent. The 50 percent silicon by-product of ferrosilicon alloy manufacture has a substantially lower silica concentration. The amount of SiO_2 in SF determines the kind of alloy generated in the manufacturing unit.

Physical properties of SF (Siddique, 2007; Siddique and Khan, 2011)

Specific gravity: The specific gravity of SF varies from 2.20 to 2.30.

Particle size: Silica fume particle size is essentially less than 1 µm. It comes in two colours: grey and premium white.

Surface area: The average surface area of MK is very high and can vary from 13to 30* 10^3 m^2/kg.

Chemical composition

Non crystalline form of virgin silica is major constituent of Silica fume. The presence of vitreous silica, mostly in the form of cristobalite, is confirmed by X-ray diffraction examination of various silica gases. Amorphous silicon dioxide and extremely tiny spherical particles are abundant in silica fume. Silica fume typically comprises a high percentage of SiO_2 (about 90%). Iron, magnesium, and alkali oxides are also present in small concentrations. The chemical compositions are shown in Table 1.3.

Table 1.3. Typical chemical compositions of silica fume

Properties (%)	(Siddique et al., 2017)	(Karthikeyan and Dhinakaran, 2018)	(Wu et al., 2018)
SiO_2	91.92	97.36	98.0
Al_2O_3	1.05	0.53	0.70
Fe_2O_3	1.11	0.15	0.50
CaO	1.35	0.14	0.2
MgO	0.61	0.79	0.60
SO_3	0.0	0.51	0.0
K_2O	1.73	0.29	0.0
Na_2O	0.60	0.06	0.0

1.6.4 Rice Husk Ash

Rice husk is an agriculturally produced by-product of rice millers and constitutes about 20% of the weight of rice. This rice husk does not possess any monetary value and to dispose it off it is burnt in the open environment, which causes air pollution and disturbs soil health. When properly burnt in incinerators at a temperature range between 500 °C to 800 °C rice husk produces non-crystalline ash rich in amorphous silica, which is highly reactive. It is a highly reactive, very fine pozzolanic material with a high surface area and silica content generally above 80% of its total weight. After China, India is the world`s second-largest producer of rice, and from every 1MT of rice produced, around 200 kg of rice husk ash (RHA) is obtained.

Physical properties of RHA (Siddique, 2007; Siddique and Khan, 2011)

Specific gravity: Rice husk ash specific gravity lying in the range 2.02 to 2.23.

Particle size: Rice husk ash is a high-quality substance. RHA particles range in size from 3 to 10 μm.

Surface area: The surface area of RHA can be as high as 50,000 m^2/kg.

Chemical composition

Rice husk ash has a high concentration of silica. RHA typically has a silica concentration of more than 80%. To be used in concrete as a cement substitute, the total amount of silicon dioxide (SiO_2), iron oxide (Fe_2O_3), and aluminium oxide ($A1_2O_3$) in the ash should not be less than 70%, and the LOI should not be more than 12%. Table 1.4 shows chemical properties of rice husk ash.

Table 1.4. Typical chemical compositions of rice husk ash

Properties (%)	(Hesami et al., 2014)	(Chopra et al., 2015)	(Gill and Siddique, 2017)
SiO_2	86.02	94.0	93.50
Al_2O_3	0.36	1.2	0.55
Fe_2O_3	0.16	0.37	0.23
CaO	1.12	2.93	1.11
MgO	0.39	0.60	0.31
SO_3	-	0.30	0.07
K_2O	-	0.50	1.40
Na_2O	1.15	-	0.10

1.7 RESEARCH SIGNIFICANCE

No-fines Concrete can be utilized in many applications, although its usage is limited to some particular applications due to its poor inherent mechanical properties. The primary application of NFC is in pavements with lower traffic volumes. It was employed as load-bearing walls in its early days, but nowadays, parking lots, sidewalks, tennis courts, and zoo areas are the primary application for NFC. Increased voids also characterize No-fines concrete with limited strength properties and restricted usage. Therefore, the challenge is to study the utilization of pervious concrete in its existing form for its porous behavior without compromising its inherent properties of groundwater recharge and controlling rainwater runoff but improving its strength and retaining optimum porosity. This research effort aims to enhance the strength enhancement of NFC using SCMs as partial replacement of cement to make it more suitable for use as pavements in surface course layers in low and medium volumes traffic roads as in residential areas, sidewalks and parking lots, running tracks, etc. The most important property for designing concrete material for pavement applications is its compressive and flexural strength. The study is focused on achieving the same by adding SCMs while preparing NFC mixes. Hence, any replacement of binding material should not compromise on the porous nature of NFC, and the use of SCMs as replacement of cement and varying sizes of coarse aggregates are proposed and investigated in this research effort.

1.8 GAPS IN THE RESEARCH AREA

No-Fines Concrete (NFC) is being studied as it offers an alternate solution to surface runoff drainage and the problem of water table recharge in urban areas. It can be used in permeable pavements. Due to the construction of impervious pavements and rapid urbanization, the natural groundwater recharge capacity of the rainwater is decreasing day by day, as the rainwater cannot percolate into the ground. Therefore, the groundwater table in India is reaching an alarmingly low level, thereby destroying the natural aquifers. Also, the excess rainwater turns into floodwater collected on the pavements, eventually destroying the pavement surface. Hence, the construction of pavements with NFC offers a potential solution to these problems. Until now, most of the research work has been carried out on the effect of replacing coarse aggregates and the addition of fibers on NFC, but limited work has been reported on the impact of the SCMs in NFC. Therefore, further research is required to investigate the influence of SCMs and also different sizes and gradations of coarse aggregates on the NFC.

1.9 OBJECTIVES OF THIS RESEARCH WORK

No-fines concrete has found its usage as a primary material in building construction related applications before this concept was extended to pavement construction. However, its application was relatively limited due to its low-strength properties. The principal focus of this study is to remedy the problem of strength characteristics of NFC so that its performance may be enhanced and it may be used in structures and less-volume traffic pavements. In this research work, the literature review and specific standard tests were conducted on NFC. In addition, to increase the mechanical strength of NFC, SCMs were used as a replacement for cement without compromising its permeation properties.

The objectives of the proposed work can be outlined as:

- Effect of supplementary cementitious materials on the mechanical and permeation properties of No-Fines Concrete.
- Effect of coarse aggregates on the mechanical and permeation properties of No-Fines Concrete.
- Microstructural analysis of No-Fines Concrete.

1.10 SCOPE OF THE PRESENT STUDY

- A comprehensive assessment of the literature to better understand current research trends in NFC and identify relevant research gaps.
- Procurements of materials for the preparation of NFC specimens of various geometries.
- Production of NFC mixes with varying SCMs replacement levels and varying sizes of coarse aggregates.
- Casting of NFC control specimens as well as SCMs concrete mixes.
- Investigation of strength and permeation properties of NFC control specimens and SCMs specimens.
- Studying the flow of water through the porous matrix of the NFC while paying attention to the pore structure.
- Investigation of permeation properties of NFC control and SCMs samples.

1.11 OUTLINE OF THE THESIS

The thesis is comprised of five chapters. Description of chapters is discussed below:

Chapter-1 Serves as the preamble of the study, introducing the objective of the research and the scope of the work.

Chapter-2 presents a comprehensive literature review discussing various research studies carried out on NFC and the influence of different SCMs on its strength and durability properties. A brief review of the replacement of coarse aggregates in NFC is also reviewed in this chapter.

Chapter-3 This chapter explains the different materials and procedures of test methods used in this study and laboratory tests conducted to determine the properties of NFC mixes.

Chapter-4 This chapter deals with the test results of the strength and permeation properties of NFC mixes. In addition, this chapter also depicts the analysis of Scanning Electron microscopes and phase identification of hardened concrete samples done by using X-ray Diffraction.

Chapter-5 Summarizes the various research outcomes from the experiments performed in this research study and the scope of future research.

CHAPTER 2
LITERATURE REVIEW

This chapter deals with a detailed literature review on use of different types of Supplementary Cementitious Materials (SCMs) and the various types of coarse aggregates on properties of the prepared NFC mixes.

2.1 GENERAL

The various research documents covering different features of NFC were reviewed and published to comprehend NFC as a suitable paving material and appreciate its advantages. A plethora of literature is available on No-Fines Concrete (NFC). The properties of compressive strength, splitting tensile strength, flexure strength, abrasion resistance, permeability, porosity, and freezing-thawing have been reported. Although some quality research work has already been undertaken on NFC in recent years, still some further research needs to be done for its practical applications in civil engineering structures.

Due to a reduced amount of cement, cost efficiency was the key motivation for the usage of NFC in 1800s as construction material for load bearing walls. Due of the paucity of cement following WWII, it became more practical throughout Europe (Ghafoori and Dutta, 1995). In India, it became popular in 2000. In this chapter, the review has been done in two ways. In the first part, a review of various NFC prepared using different types of aggregates or mix proportions, or water-cement ratios is discussed. The second part presents a property-wise review of works done on NFC by replacing cement with different SCMs.

2.2 NFC CONCRETE

Parasivamurthy et al. (2010) prepared the pervious cement concrete from the recycled aggregates obtained from crushed concrete wastes to investigate the properties of pervious concrete. Two different mix proportions with water-cement ratios of 0.45 and 0.40 for both recycled aggregate concrete and natural aggregate concrete were made as per IS 10262-1982. The results showed that crushed concrete debris had a 3 percent to 11 percent lower compressive strength after 28-day than pervious concrete prepared with natural aggregates. When compared to concrete constructed with natural aggregates, crushed concrete waste had a 12 percent to 20% lower flexural strength. When compared to concrete constructed with natural aggregates, crushed concrete waste displayed an improvement in porosity of 8% to 18%. They suggested that recycling crushed concrete wastes in pervious concrete is a viable solution to the challenges of dumping hundreds of thousands of tons of waste and a scarcity of natural aggregates.

Lian et al. (2011) established a mathematical model to investigate and relate the relationship among porosity and compressive strength for porous concrete by evaluating theoretical derivations and empirical results. Two groups of samples were used to prepare the porous concrete. Only cement, coarse aggregates, and water were used to make the first group. The second group was prepared with quarry sand as fine aggregates and silica fume (7%) and superplasticizer (0.8%) by weight of cement. Existing models were evaluated, and a new model was created as a consequence. The newly presented model was based on Griffith's theory, matched the experimental results for porous concrete better.

Agar Ozbek et al. (2013) performed the dynamic experiments using a drop-weight impact test setup and Laser Doppler velocimetry to take the porous concrete measurements. In this study, two different types of aggregates, i.e., river gravel and crushed basalt, two binders such as silica fume and cement, three different aggregates grading, and two compaction levels, were used to prepare porous concrete. Nine different design mixes were cast with different gradation and different types of aggregates along with other binders. The impact strength of different kinds of porous concretes was calculated in correlation with their mixture composition and production technique. The results found that the main factors that influence the dynamic performance of porous concretes are the compactive effort and the properties of the aggregates.

Kevern (2013) developed the mix design for pervious concrete and its effect on the strength and durability property of pervious concrete relating to free-thaw in cold weather climates. There were two stages to the mixed design. Phase I of the study examined how the aggregate size and cement content affect the Portland cement pervious concrete (PCPC) void ratio and strength. After achieving the desired void ratio and strength, Phase II was carried out to find the effects of sand latex as a binder and silica fume on the PCPC characteristics. The results indicated that using a single-sized aggregate showed increased porosity but decreased compressive strength. Increased cement concentration resulted in lower concrete porosity above a certain point but did not affect concrete strength. With the usage of sand and latex together improved the workability of PCPC remarkably and even resulted in higher strength and appropriate permeability. The freeze-thaw results showed less than 6% mass loss up to 180 cycles for all mixes.

.

Ibrahim et al. (2014) presented the hydrological and mechanical characteristics of Portland cement pervious concrete. Twenty-four different concretes were prepared with different water-cement ratios. Two different sizes of crushed limestone were used to prepare the design mix. They found that the single-size aggregate was not ideal for the mix as the compressive strength reduced by 75% compared to the highest value acquired. The average density was approximately 1716 kg/m^3 with a porosity value of 37%. They also found that the density of pervious concrete increased, the permeability and porosity decreased. Linear regression showed the good relationships between permeability and porosity, porosity, and density.

Chang et al. (2016) used the Alkali-Activated Slag Cement (AASC) and Electric Arc Furnace Slag (EAFS) to find the characteristics of pervious concrete. In comparison to OPC, they found that the combination created using EAFS and AASC was the best. The water permeability was higher than 0.49 cm/s and the compressive strength was 35 MPa at 28-day testing. Furthermore, to evaluate low-frequency sound waves, the sound absorption ratio increased for the pervious concrete containing AASC along with EAFS, with a value of 0.94. (125 Hz). They also discovered that the porous character of EAFS played a key role in achieving a better interlinking effect.

Wu et al. (2016) performed freeze-thaw test of the concrete to evaluate resistance of concrete to cold conditions in field and laboratory on Portland cement pervious concrete. Three mix designs of open-graded limestone with grain sizes of 4.75 to 9.5 mm were created for this test. In addition, the concrete mix included vinyl acetate-ethylene (VAE), copolymer latex, polypropylene fibre, and polycarboxylate superplasticizer (SP). The results of the tests revealed that even in a saturated state, the PCPC might be damaged by freezing and thawing. In comparison to other combinations, latex-modified mixtures showed greater freeze-thaw resistance due to enhanced cementitious matrix and bonding strength among aggregate particles.

Nguyen et al. (2017) investigated the durability of pervious concrete with crushed seashells. Three types of crushed seashells were used to prepare the pervious concrete. The conclusion of the study showed a low freeze-thaw resistance of seashell pervious concrete as compared to control pervious concrete. The compressive strength decreased for each type of crushed shells. This was due to the reason that crushed shells have higher fragility. The tensile strength seemed to closely follow the results observed in compressive strength. The observed values were adequate and could find its application in surface layer for pavement structures.

Singh and Singh (2020) prepared the pervious concrete with coarse aggregates which were recycled from previous concrete (RCA). Mixes were made by replacing natural aggregates with RCA at various amounts of replacement and adding fly ash and metakaolin to the concrete mix. They came to the conclusion that increasing RCA replacement levels decreased strength, whereas adding metakaolin increased the strength qualities.

2.3 MECHANICAL PROPERTIES OF NFC

No-fines concrete is a material with many beneficial qualities that achieves a good balance of structural and functional properties. Compressive strength and flexural strength are significant structural properties in the design and selection of NFC mixes. Split tensile strength and density, in addition to these parameters, are significant in comprehending the structural behavior of NFCs.

2.3.1 Compressive Strength

The most common quality control metric for evaluating the integrity of conventional concrete and NFC is compressive strength. No-fines concrete has compressive strength that is typically lower than conventional concrete used in pavement construction due to higher porosity, typically in the range of 15-40 percent. Although, the compressive strength obtained by NFC is adequate for low-volume road traffic. The variation of compressive strength in no-fines concrete stands at around from 3 - 28 MPa and hence can be used in various of applications (Tennis et al., 2004; Wang et al., 2006). This value highly dependent upon factors such as mixed proportions, the individual properties (physical and chemical) of the material used.

Effect of replacement of cement with FA

Fly ash is made up of microscopic spherical particles with a diameter of 0.2 to 10 µm that are created from mineral impurities that bind together during coal burning (Chindaprasirt et al., 2005). Fly ash, due to its chemical composition and fine particle size is good pozzolanic material which can also act self-cementitious in some cases.

Chen et al. (2013) considered two types of pervious concrete, polymer-modified pervious concrete along with supplementary cementitious material -modified pervious concrete (SPC), to investigate the strength and fracture of pervious concrete. SCM replaced the cement and two different granite aggregate sizes to prepare the concrete mix. They concluded that SPC and PPC achieved higher strength at 28-day, but later the strength decreased. The compressive strength decreased as cube size increased due to an increase in flaw size. The rate of SPC and PPC strength development was unaffected by porosity.

Anderson and Dewoolkar (2015) prepared the pervious concrete by replacing cement with FA at different replacement levels with different quantity of concentrations of salt. They found that higher replacement levels of FA showed greater damage in freezing and thawing test with salt solutions than control mix. The 28-day of compressive strength decreased with an increased percentage replacement of FA (Table 2.1).

Sata et al. (2016) observed the effect of pervious concrete which incorporated fly ash (high quantity of calcium). Three different water to binder ratios were compared along with FA replacements of 10, 20, and 30% with cement along with water reducing agent type F superplasticizer were used in this study (Table 2.1). The findings revealed that using FA as a partial replacement of OPC had a positive impact. Fly ash helps to enhance the workability of cement paste providing a more consistent mix, therefore less quantity of superplasticizer was required in the mixture.

According to the aforementioned compressive strength investigations, as the percentage of FA replaced with cement increases, compressive strength decreases when compared to the reference mix. This may be because the pozzolanic reaction of FA at young ages is slower than the cement hydration process.

Table 2.1. Compressive strength (MPa) at different replacement levels of FA

Research reported by	**Age (days)**	**Fly Ash (%)**			
		0	**10**	**20**	**30**
Anderson and Dewoolkar (2015)	28	11.03	10.76	9.45	9.02
(Sata et al., 2016)	28	20.2	17.5	18.3	17.8

Chen et al. (2019) studied the engineering properties, economic cost and energy, and environmental impacts of pervious concrete with the incorporation of FA and slag and compared it with regular pervious concrete. The three types of mix design with and without SCMs were prepared. They determined that the pervious concrete with FA and slag showed lower mechanical strength but had the same freeze-thaw resistance as compared to regular pervious concrete. The pervious concrete mixture with fly ash resulted in substantially higher energy and environmental impact with the mass allocation approach.

Saboo et al. (2019) investigated pervious concrete prepared with different replacement levels of the combination of FA and MK with different curing conditions and different water-cement ratios. The interaction graphs revealed that adding MK considerably increased the density and decreased the porosity. The compressive strength was lower when porosity increased. In addition to this, curing conditions had no considerable impact on the pervious concrete characteristics.

Effect of replacement of cement with rice husk ash

Hesami et al. (2014) found the effect of rice husk ash on the strength properties of pervious concrete pavement. Coarse aggregate sizes 2.36 mm to 19 mm were used as per ASTM C33. The water-cement ratio was constant at 0.27 in this study, as shown in Table 2.2. Different types of fibers, including steel, glass, and polyphenylene sulfide (PPS), were used. Rice husk ash was used as a pozzolanic material to improve cement paste in this study, and the effect of different replacement levels of RHA with cement on the mechanical properties of concrete mixtures was tested.

Talsania et al. (2015) observed the influence of RHA on the properties of pervious concrete. This study aimed to introduce RHA in place of OPC 53-grade cement. The mix proportion selected for control mix concrete was 1:4, and further, three different water-cement ratios were selected for this study as shown in Table 2.2. The effect of inclusion of RHA along with cement in the concrete mixture was studied. The optimum replacement of mixture content of rice husk ash with cement was 10%, beyond the value of compressive strength decreased.

Based on experimental investigation relating to compressive strength of concrete, the following correlation are made that higher w/c ratio provides improved strength. With the increasing amount of RHA percentage (replacing cement), the strength reduces for a lower water-cement ratio but slight increase was found for higher w/c ratios. Compared to the controlled mix, slight enhancement in the compressive strength value was observed when 10% RHA replaced the cement. It may be because RHA as a pozzolan reacts with calcium hydroxide in the hydration process, improves aggregate-paste connectivity, and reduces transition zone thickness between aggregate and cement paste.

Table 2.2. Test results of compressive strength (MPa) at different replacement levels of RHA

Research Reported By	Age (days)	w/c ratio	Rice Husk Ash (%)							
			0	2	4	6	8	10	12	20
Hesami et al. (2014)	28	0.27	13.8	14	14.9	16.1	17.8	16.9	15	−
Talsania et al. (2015)	7	0.30	6.72	−	−	−	−	7.29	−	6.42
		0.35	7.13	−	−	−	−	8.38	−	6.82
		0.40	8.57	−	−	−	−	9.11	−	7.91
	14	0.30	7.40	−	−	−	−	8.00	−	7.10
		0.35	8.20	−	−	−	−	9.20	−	8.10
		0.40	9.40	−	−	−	−	10.05	−	8.50
	28	0.30	8.02	−	−	−	−	8.83	−	7.86
		0.35	9.42	−	−	−	−	10.05	−	9.19
		0.40	10.35	−	−	−	−	10.98	−	9.78

Effect of silica fume and superplasticizer

Yang and Jiang (2003) introduced silica fume (SF), superplasticizer (SP), and smaller-sized aggregate in the pervious concrete to increase the strength properties. The four different sizes of gravel and sand were used along with SF and different types of additives to prepare the pervious concrete mixes. The smaller aggregate tends to provide maximum compressive strength. The compressive strength tends to improve over the addition of SF and SP dosage rates at 28-day. The organic polymer also enhanced the compressive strength but decreased the water penetration coefficient.

Adil et al. (2020) investigated the rheology and strength characteristics of pervious concrete with variation of SF and different mineral admixtures along with different types of coarse aggregates. The water to cementitious ratio was between 0.27 and 0.32, and the cementitious to aggregate ratio of 0.24 for every pervious concrete mixture. The rheological testing revealed that a 5.5% SF substitute for cement was preferable for workability. The compressive strength was decreased as the percentage replacement of SF was beyond 5% but increased the void content inside concrete mix. The unwashed coarse aggregate improved compressive strength, but SF with rough limestone aggregate did not affect the abrasion resistance considerably.

Effect of macro synthetic fibers content

Kevern et al. (2015) studied the effect of macro synthetic fibres on the compressive strength of pervious concrete. In a single mixture, the effects of two lengths of fibre (38 mm and 56 mm) were examined at three dosages (1.5, 3.0, and 4.5 kg/m^3). A control mixture without fibres was also used in this study to assess the influence of fibres and non-fibres conventional mixtures on compressive strength. It was observed from Figure 2.1 that with the different dosage levels of macro synthetic fibres, the compressive strength results were unaffected with any type of treatment. When compared to controlled concrete, there was a little improvement in compressive strength.

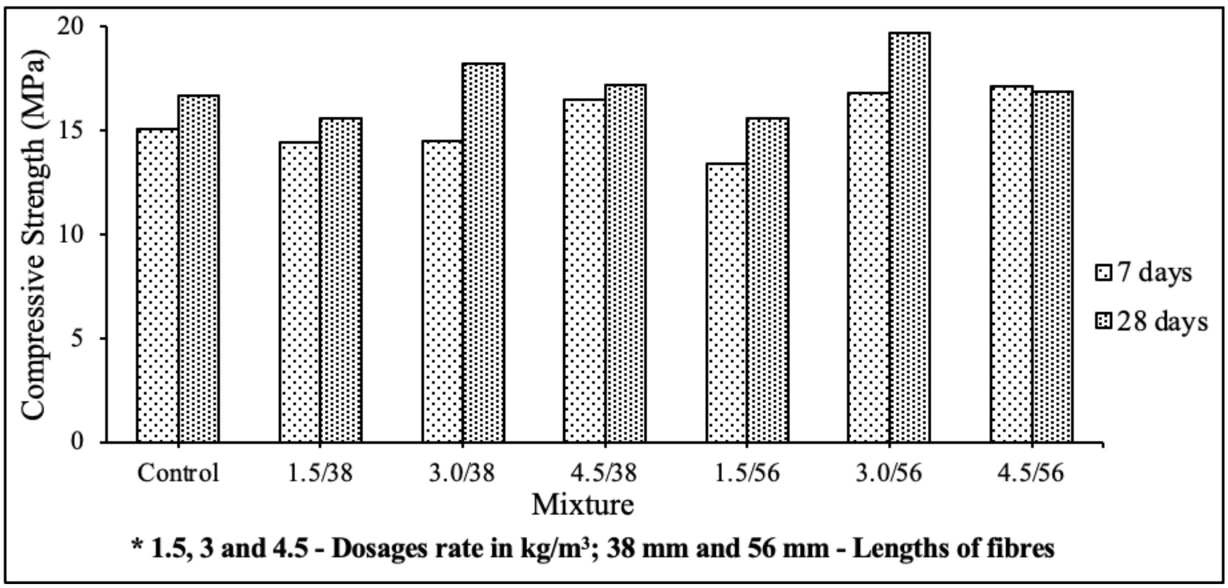

Figure 2.1. Effect of fibres of different lengths on compressive strength (Kevern et al., 2015)

Effect of different types of aggregates (substitution/without substitution)

The observations of different researchers regarding the compressive strength of different materials at different ages are summarized:

- *Effect of lightweight aggregates*

Deo and Neithalath (2010) studied the compressive behavior of pervious concrete and made a model to analyze the stress-strain response and its relation to most of the pore structures features. The pervious concrete was prepared by using OPC and different gradation sizes of limestone aggregates. The water-cement ratio was 0.33, whereas the aggregate-cement ratio was taken 5 to prepare the concrete mix. They found that larger-sized aggregates show higher strength than smaller ones. When the pore volume percentage was increased by 10%, the compressive strength was reduced by about 50%.

Maguesvari and Narasimha (2013) studied the effect of different grading sizes of coarse aggregate and fine aggregate incorporated in pervious concrete. The control mix was made with four different aggregate sizes and fine aggregate content ranging from 0% to 50%. For pervious concrete mixes, the w/c proportion was 0.34, and the aggregate-cement ratio was 4.75:1. The compressive strength of the concrete improved when the aggregate size dropped, and the addition of sand increased the small aggregate contact area and made the concrete denser. For 7 to 28-day, the average increase in compressive strength was 27%, for 28 to 56 days, it was 24%.

Zaetang et al. (2013) presented research about implementation of lightweight aggregates to achieve a low-weight pervious concrete (LWPC). Diatomite (DA), Pumice (PA) and Recycled LWA from auto-claved aerated concrete (RA) were added as natural LWAs in pervious concretes. Three cement paste contents of by volume were used to compare the findings. It was observed from Figure 2.2 that the compressive strengths up to 28-day of DA were better than those of PA and RA. The pozzolanic property of DA was improved by calcining it to remove clay minerals, which improved the strength of its concrete.

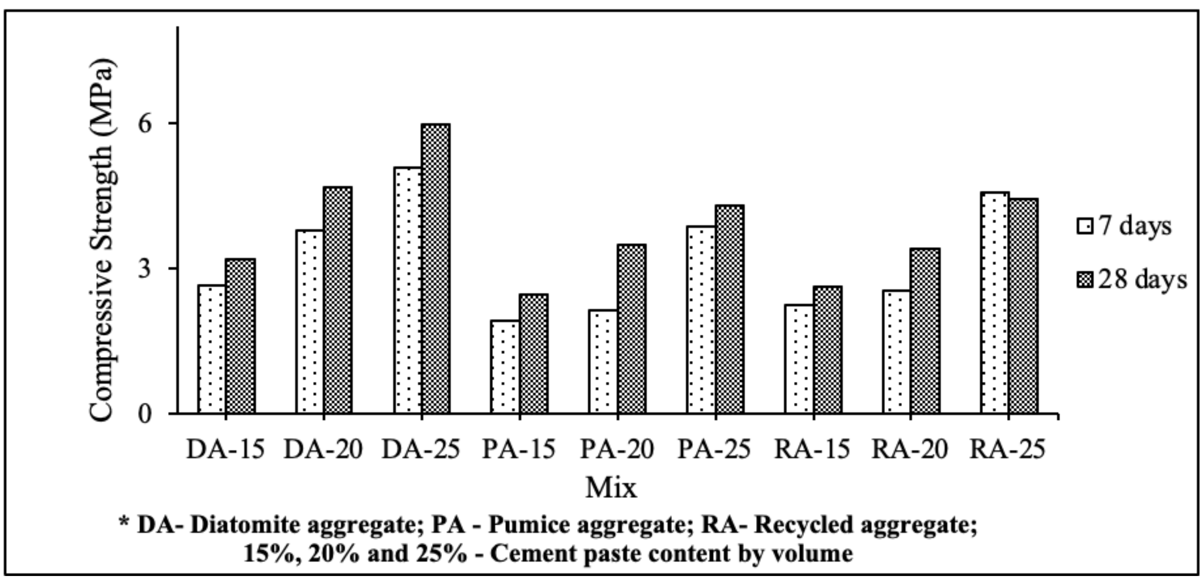

Figure 2.2. Effect of lightweight aggregates on compressive strength (Zaetang et al., 2013)

Sun et al. (2018) used the three types of binders, i.e., Alkali-Activated Slag (AAS), Metakaolin Geopolymer (MKG), and Metakaolin Ground Granulated Blast Furnace Slag Geopolymer (MGG), for mix design of pervious concrete. Three different sizes of natural gravel coarse aggregates were used. The aggregate to binder proportion was kept 8 for every pervious concrete mixes. The compressive strength was decreased by 28% and 44% for AAS, 32% and 41% for MKG, and 29% and 40% for MGG at 7-day. The density was decreased by 14% and 23% for AAS, 17% and 23% for MKG, and 16% and 22% for MGG at 7-day. The maximum compressive strength was attained with MGG compared to MKG and AAS using the same aggregate size.

- *Effect of recycled aggregate*

Bhutta et al. (2013) observed the characteristics of porous concrete which include recycled aggregate. In comparison to regular aggregate, recycled aggregate pervious concrete has a lower strength at the same void ratio. This could be related to a decrease in aggregate-cement paste bonding. To increase the strength of the mixes, styrene-butadiene rubber-based redispersible polymer powder (RPP) and latex were added. It is was observed from Figure 2.3 that at polymer-cement ratios of 3% and 5% for RPP, the compressive strength of porous concrete improved for normal aggregate and recycled aggregate. The compressive strength of conventional and recycled aggregate was also improved by employing latex with the same P/C ratios.

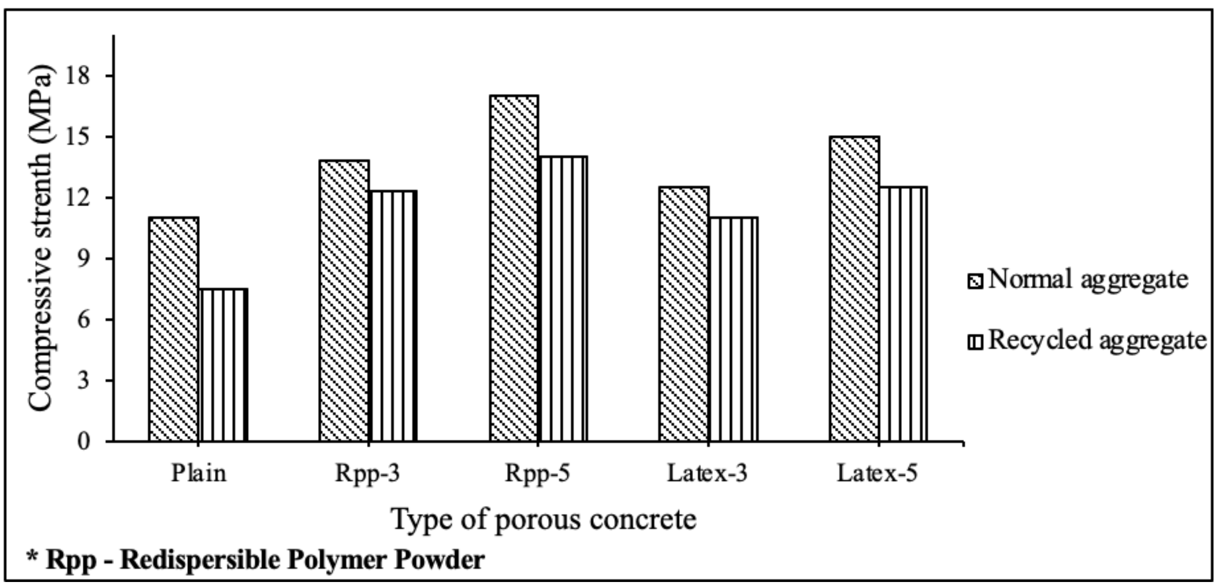

Figure 2.3. Influence of polymer and recycled aggregate on compressive strength (Bhutta et al., 2013)

Kou and Poon (2013) studied the strength and durability characteristics of concrete made with different replacement levels of FA along varying percentage of recycled aggregate concrete. The recycled aggregate concrete was developed by using FA as different percentage replacement levels with cement. They found that recycled aggregate concrete lowered the compressive strength and Young's modulus of concrete compared to control mix, whereas FA improved such properties of concrete.

- *Effect of palm oil clinker*

Ibrahim and Abdul Razak (2016) replaced coarse aggregate with palm oil clinker (POC) in pervious concrete. The palm oil clinker pervious concrete (POCPC) was studied at different percentages of natural aggregate replacement with POC aggregate, ranging from 0% to 100%. Figure 2.4 demonstrates that at 28-day, the compressive strength of the POCPC was 9.5 MPa and 3.4 MPa at 0% and 100% replacement, respectively, whereas at 7-day, the compressive strength was 8.3 MPa and 3.0 MPa at 0% and 100% replacement, respectively. As the percentage of natural aggregate substituted with POC grew, the rate at which the concrete gained strength increased. Increase in replacement level, on the other hand, resulted in a loss of strength. The usage of POC significantly lowered the concrete's compressive strength. Because failure occurs through the aggregates, the interfacial zone of the aggregates has a noteworthy influence on compressive strength of pervious concrete.

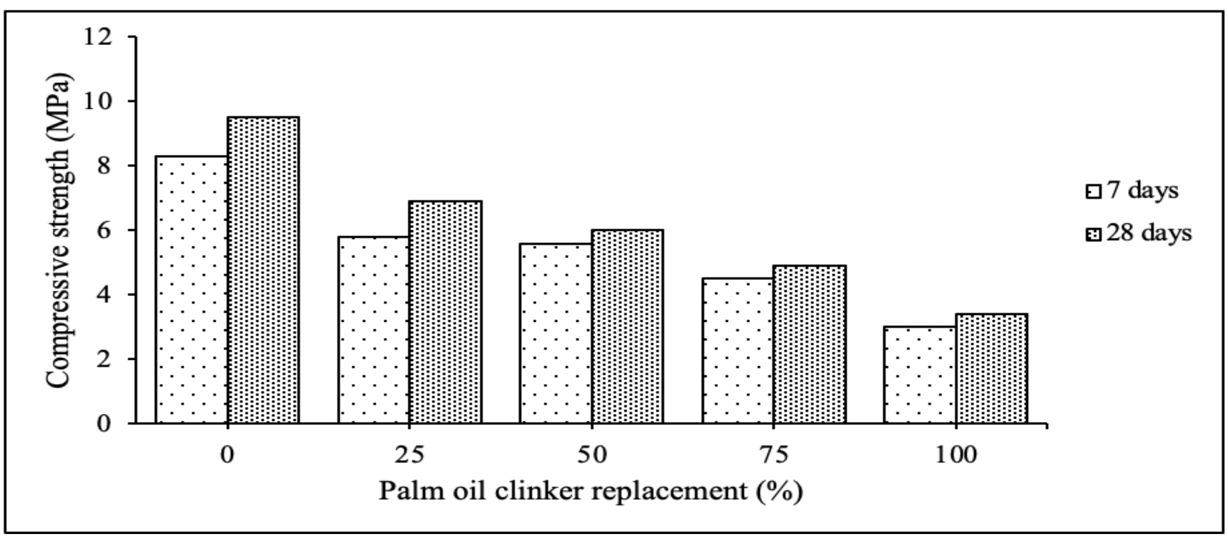

Figure 2.4. Influence of palm oil clinker replacement on compressive strength (Ibrahim and Abdul Razak, 2016)

2.3.2 Split Tensile Strength

Effect of aggregate size and fibres

Huang et al. (2010) analyzed the laboratory evaluation on splitting tensile strength of polymer-modified pervious concrete. The testing was performed to see if integrating the latex polymer into pervious concrete could increase its strength properties. For improving the strength characteristics of pervious concrete, natural sand and fibre were added in addition to latex. Split tensile strength was shown to be higher in concrete formulations with smaller particle sizes. The addition of fibre to the control mix seems to boost splitting tensile strength significantly (Table 2.3). The splitting tensile strength of pervious concrete mixes incorporating sand along with latex was unaffected by the inclusion of fibre.

Table 2.3. Splitting tensile strength of different fibers and aggregate size

Research Reported by	Mixture	Aggregate Size (mm)	28-day Splitting tensile strength (MPa)
Huang et al. (2010)	Reference mix	12.5	0.6
		9.5	1.1
		4.75	1.2
	Mix with fiber	12.5	1.2
		9.5	1.3
		4.75	1.90
	Mix with fiber and sand	12.5	0.65
		9.5	0.80
		4.75	0.95

Zaetang et al. (2013) used lightweight aggregates in Pervious concrete. This research looked at how lightweight aggregate (LWA) may be used to make lightweight pervious concrete (LWPC). Three different cement paste concentrations were used. When the cement paste content was in the range of 15% to 25%, the strength characteristics were improved. The splitting tensile strength of LWPC with RA increased from 0.58 to 0.93 MPa. A similar trend was followed by DA and PA (Table 2.4).

Kevern et al. (2015) presented an influence of macro-synthetic fibers on pervious concrete characteristics. In a single mixture, the effects of two different fibre lengths (38 mm and 56 mm) were studied at three different dosages. The effect of fibres and non-fibers conventional mixtures on split tensile strength after 28-day was compared in this study using a control mixture without fibres. The results have shown in Table 2.4 that split tensile strength was not affected in any appreciable quantity by the addition of macro synthetic fibers.

Table 2.4. Split tensile strength of different aggregate sizes and fibers

Research Reported by	**Mixture**	**28-Day Split Tensile Strength (MPa)**
Zaetang et al. (2013)	Diatomite (DA)-15	0.57
	Diatomite (DA)-20	0.71
	Diatomite (DA)-25	0.93
	Pumice (PA)-15	0.47
	Pumice (PA)-20	0.75
	Pumice (PA)-25	0.99
	Recycled (RA)-15	0.58
	Recycled (RA)-20	0.67
	Recycled (RA)-25	0.93
Kevern et al. (2015)	Control	1.70
	1.5/38	1.75
	3.0/38	2.15
	4.5/38	2.45
	1.5/56	2.00
	3.0/56	2.31
	4.5/56	2.50

Note: 1.5, 3.0, and 4.5 - Dosages rate in kg/m^3; 38 mm and 56 mm – Lengths of fibres.

The use of latex polymer greatly enhanced the strength of pervious concrete, according to split tensile strength testing. The inclusion of fibres had no effect on the tensile strength because the fibres weren't thoroughly disseminated and irregularly distributed during mixing, the mixes containing fibres only showed a small improvement in splitting tensile strength.

Effect of oil palm kernel shell as replacement of coarse aggregate

Khankhaje et al. (2016) investigated the properties of oil palm kernel shell in place of coarse aggregate in a sustainable pervious concrete. This study demonstrated the development of a lightweight pervious concrete by usage of kernel shell of sized 4.75–6.30 mm (KPC4, KPC5, KPC6, and KPC7) and 6.30–9.50 mm (KPC4, KPC5, KPC6, and KPC7) (KPC1, KPC2, KPC3, and KPC7). Oil palm kernel shell partially replaced limestone (from 25 to 75 percent by mass) in order to generate a lightweight pervious concrete that is sustainable. The tensile strength was dependent on the size of the OPKS: the larger the OPKS, the lower the tensile strength. The KPC4, KPC5, and KPC6 mix designs had a 7%, 41%, and 61 percent loss in tensile strength, respectively, when compared to the reference mix. Figure 2.5 shows how a smaller OPKS might fit inside the pores, reducing the amount of free space. The larger OPKS (6.30-9.50 mm), on the other hand, disrupted the granular arrangement, resulting in lower mechanical strength.

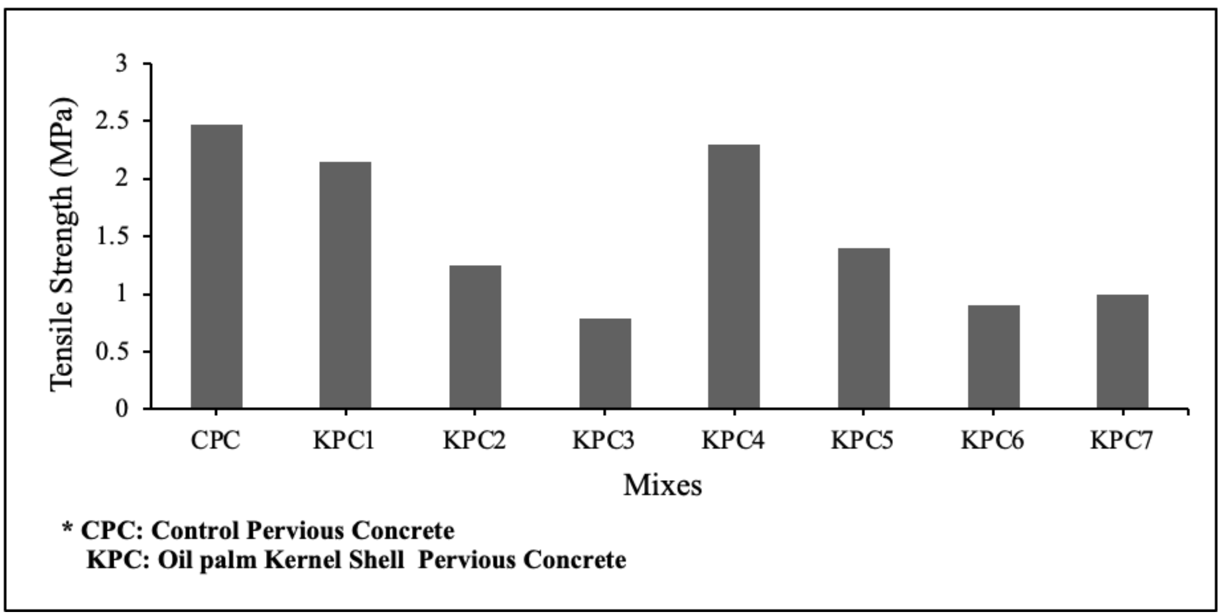

Figure 2.5. Split tensile strength at 28-day (Khankhaje et al., 2016)

Effect of high calcium fly ash

Tho-In et al. (2012) presented research about the pervious geopolymer with fly ash concrete. Using lignite fly ash, sodium silicate, NaOH solution pervious geopolymer concretes (PGCs) were created. The PGC mix proportions were 1:8 FA to coarse aggregate by weight, 0.50 constant NS/NH ratio, 0.35, 0.40, and 0.45 alkaline liquid/FA (L/A) ratios, and different NaOH concentrations. The splitting tensile strengths of PGCs ranged from 0.7 to 1.4 MPa, according to Table 2.5. This was most likely owing to a better interfacial transition zone surround the aggregates and the geopolymer matrix than the conventional Portland cement matrix.

Table 2.5. Split tensile strength of high calcium fly ash (Tho-In et al., 2012)

Mix	28-Day Splitting Tensile Strength
35PGC10	1.0
35PGC15	1.3
35PGC20	0.7
40PGC10	1.1
40PGC15	1.3
40PGC20	1.4
45PGC10	1.1
45PGC15	1.2
45PGC20	1.2

Note: PGC- Pervious Geopolymer Concrete

2.3.3 Flexural Strength

The flexural strength of NFC is essential since it is used to calculate the thickness of rigid pavements and evaluate fatigue life. The NFC has a lower flexural strength than pavement quality concrete (PQC), ranging from 0.43 to 6.1 MPa (Chen et al., 2013; Ibrahim et al., 2014; Wang et al., 2006; Yang and Jiang, 2003).

Effect of fibers and replacement of cement with RHA

Hesami et al. (2014) tried to investigate the combined effect of different fibres and RHA at various amounts of cement replacement on the strength characteristics of pervious concrete pavements (PVC). The influence of fibre type on the flexural strength of pervious concrete was explored in this study, which included different fibres along with varying amount of RHA. With higher rate of cement replacement with RHA, the flexural strength first increases, but then falls after a time.

Talsania et al. (2015) revealed the influence of RHA on pervious concrete properties. OPC was replaced by RHA by weight of cement for varying water/cement ratio. It was generally observed from Table 2.6 that as the amount of cement replacement with RHA particle increases, the flexural strength also increases first, but it decreases after the replacement level increases.

Table 2.6. Test results on flexural strength

Research reported by	**Age (days)**	**Mix**	**w/c ratio**	**Rice Husk Ash (%)**							
				0	**2**	**4**	**6**	**8**	**10**	**12**	**20**
Hesami et al. (2014)	28	Glass fiber	0.27	2.90	2.70	3.25	3.80	4.15	4.20	4.10	−
		Steel fiber		2.80	3.00	3.60	4.25	4.50	4.40	4.35	−
		PPS fiber		2.80	2.98	3.40	3.70	4.30	4.32	4.30	−
		Glass fiber	0.33	2.90	2.91	3.50	4.05	4.70	4.65	4.50	−
		Steel fiber		2.90	3.10	3.60	4.15	4.70	4.65	4.70	−
		PPS fiber		2.99	3.20	3.80	4.40	4.90	5.00	4.95	−
		Glass fiber	0.40	2.45	2.60	3.10	3.30	3.85	3.90	3.88	−
		Steel fiber		2.55	2.70	3.15	3.50	3.90	4.00	4.00	−
		PPS fiber		2.65	2.80	3.35	3.90	4.00	4.00	3.95	−
Talsania et al. (2015)	7	−	0.30	1.14	−	−	−	−	1.55	−	1.10
			0.35	1.40	−	−	−	−	1.88	−	1.31
			0.40	1.89	−	−	−	−	2.41	−	1.80
	14	−	0.30	1.30	−	−	−	−	1.65	−	1.15
			0.35	1.58	−	−	−	−	2.02	−	1.55
			0.40	2.15	−	−	−	−	2.70	−	2.20
	28	−	0.30	1.49	−	−	−	−	1.87	−	1.32
			0.35	1.85	−	−	−	−	2.38	−	1.75
			0.40	2.43	−	−	−	−	3.05	−	2.40

Effect of replacement of cement by fly ash

Sata et al. (2016) tested pervious concrete containing high-calcium fly ash. The result showed that usage of fly ash as an alternative to OPC improved the cement paste by forming a uniform mix. At 28-day, fly ash replacement in the pervious concrete had little effect on flexural strength due to constrained pozzolanic reaction at an early stage. The results of this research work were shown in Table 2.7. It was generally observed from the above flexural strength studies that by replacing cement with fly ash, flexural strength decreases with respect to reference mix.

Table 2.7. Test results of flexural strength (MPa) of different replacement levels of fly ash

Research Reported By	**Age (days)**	**Fly Ash (%)**			
		0	**10**	**20**	**30**
Sata et al. (2016)	28	3.31	3.22	3.18	3.09

Effect of recycled aggregates

Bhutta et al. (2013) verified the properties of pervious concrete which incorporated recycled aggregate. They came to the conclusion that the best mix proportions were used to make pervious concrete with both conventional and recycled particles. Table 2.8 shows that using recycled aggregate in pervious concrete reduces flexural strength as compared to using conventional aggregate, while using polymer modification increases flexural strength in all pervious concretes.

Ćosić et al. (2015) provided research on the effects of aggregate type and size on pervious concrete qualities. A dense concrete mixture and four pervious concrete mixtures were developed using different aggregate types and different proportions of aggregate fractions. For all mixes, the w/c ratio was 0.33. The studies demonstrated that increasing the ratio of small aggregate in concrete mixtures increased flexural strength. Concrete mixtures containing dolomite had higher flexural strength than those containing slag, as shown in Table 2.9.

Table 2.8. Test results of flexural strength of recycled aggregates (Bhutta et al., 2013)

Types of Porous Concrete	Polymer-Cement (P/C) ratio (%)	Classification of Aggregate	28-Day Flexural Strength (MPa)
Plain	–	Normal	2.60
		Recycled	1.90
Redispersible Polymer Powder (RPP)	3	Normal	3.40
		Recycled	2.70
	5	Normal	3.95
		Recycled	3.15
Latex	3	Normal	3.10
		Recycled	2.36
	5	Normal	3.60
		Recycled	2.75

Table 2.9. Effect of different mixtures on flexural strength (Ćosić et al., 2015)

Mixture	28-Day flexural strength (MPa)
M1	9.70
M2	4.90
M3	4.00
M4	4.00
M5	2.80

Note: M1- Reference mixture made entirely from dolomite (fractions of 0-4, 4-8, and 8-16 mm);
M2 and M4- Prepared from coarse dolomite aggregate (fractions of 4-8 and 8-16 mm);
M3 and M5- Prepared from coarse steel slag aggregate (fractions of 4-8 and 8-16 mm).

2.3.4 Abrasion Resistance

No-fines concrete is a coarse-grained pavement material that experiences abrasive forces due to tire-pavement interaction. Due to such interactions, the cement paste-coated aggregates will be sensitive to de-bonding, resulting in functional failure and lowering the pavement's serviceability. As a result, in order to increase serviceability, it is essential to comprehend the abrasion phenomena, and various studies have contributed to the understanding of abrasion properties of NFC materials. Using tail grinding equipment, a wheel tracker, a Los Angeles abrasion machine, and a surface abrasion tester, the abrasion resistance of NFC can be examined (Dong et al., 2013; Ghafoori and Dutta, 1995).

Zaetang et al. (2013) presented research on the impact of aggregate and their size on pervious concrete properties. Four pervious concrete mixtures were made with varied aggregate types and different amounts of aggregate fractions. All of the mixtures had a 0.33 water to cement ratio. The researchers discovered that increasing the ratio of small aggregate in concrete mixtures increased flexural strength. It was observed from Table 2.10 that the surface abrasion of LWPC containing DA was higher than those of PA and RA due to its denser texture.

Table 2.10. Test results of surface abrasion loss (Zaetang et al., 2013)

Mix	Surface abrasion weight loss (g)
Diatomite (DA)-15	13.2
Diatomite (DA)-20	10.2
Diatomite (DA) -25	8.2
Pumice (PA)-15	17.8
Pumice (PA)-20	12.3
Pumice (PA)-25	10.2
Recycled (RA)-15	17.0
Recycled (RA)-20	14.7
Recycled (RA)-25	9.7

Gesoğlu et al. (2014) investigated the effects of particle size along with the quantity of tire crumb rubber on pervious concrete. A consistent w/c ratio of 0.27 and a cement content of 450 kg/m^3 were used in the experiment. Figure 2.6 illustrates that raising the rubber component from 0% to 20% increased abrasion resistance in a systematic manner. Fine crumb enhanced the abrasion resistance of pervious concrete compared to crumb rubber. Sample wear decreased from 0.91% to 0.17% percent when fine crumb rubber replaced 20% of the natural aggregate, exhibiting abrasion resistance. The wear was significantly reduced when the other types of rubber were used. When compared to control concrete, abrasion of pervious concrete containing fine crumb rubber was reduced by around 59 percent and 81 percent at 10% and 20% replacement levels, respectively.

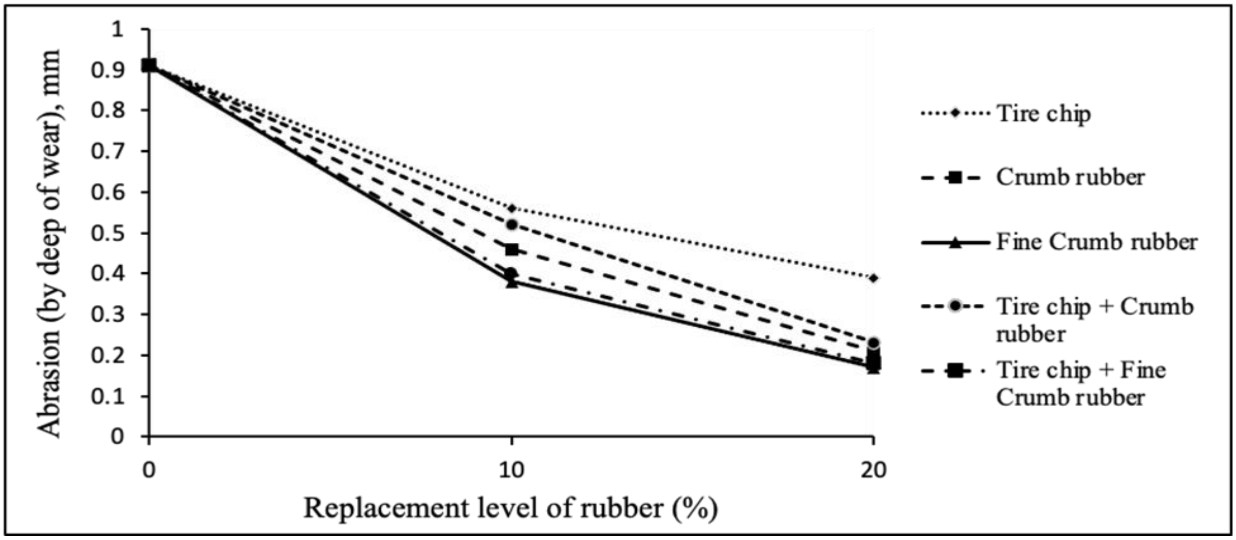

Figure 2.6. Abrasion resistance of pervious concretes versus rubber content (Gesoğlu et al., 2014)

Kevern et al. (2015) reported on the relation of macro synthetic fibres on the characteristics of pervious concrete. The mix proportion selected for control mix concrete was 1:3.79. In a single mixture, the effects of two fibre length i.e., 38 mm and 56 mm, were examined at different dosage rate. In comparison to the control, all fibre doses reduced abrasion. The longer 56 mm fibres, on the other hand, showed no trend. Figure 2.7 shows that the 38 mm fibre lost much less mass than the longer 56 mm fibres at the 1.5 kg/m^3 and 4.5 kg/m^3 dosing rates. Abrasion resistance did not show any patterns as a function of dose rate or fibre length.

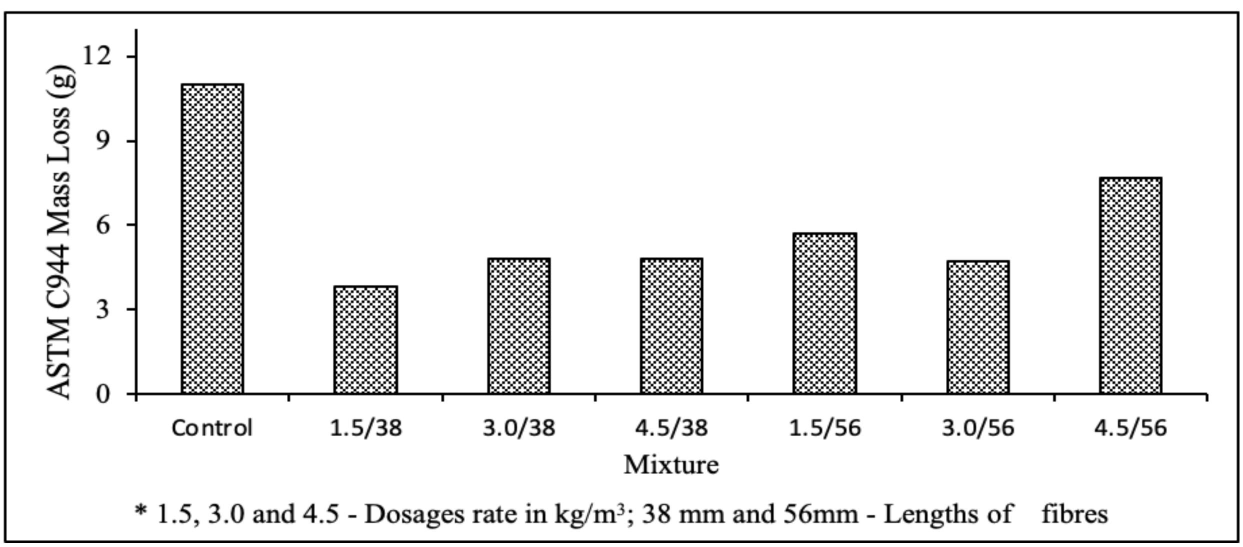

Figure 2.7. Surface abrasion results from ASTM C944 (Kevern et al., 2015)

2.4 PERMEATION PROPERTIES OF NO-FINES CONCRETE

Permeation characteristics are parameters that aid in quantifying a material's interior macro-pore structure. Water permeability, porosity, and infiltration capacity are essential pore parameters that influence functional properties.

2.4.1 Permeability

Permeability can be explained as the flow of water through porous material. Hydraulic conductivity, also known as permeability, is based on Darcy`s law and measured with a constant head permeameter and falling head permeameter. In the case of NFC, the permeability lies in the range of 0.1 to 5 cm/sec, which is primarily dependent on the porosity, and the relationship may be best fitted using the power function (Ghafoori and Dutta, 1995; Kuang et al., 2011).

Huang et al. (2010) reported the perviousness and strength of polymer-modified pervious concrete. They found that all of the pervious mixtures had permeability values of 10 to 20 mm/s. The permeability was not consistently influenced by aggregate gradation. The permeability values of the mixtures prepared with three different sizes of aggregates were similar. According to Table 2.11, the usage of sand and latex was able to reduce permeability.

Table 2.11. Test result of permeability with different aggregate sizes and fibers

Research Reported by	Mixture	Aggregate Size (mm)	Permeability (cm/s)
Huang et al. (2010)	Control Mix	12.5	19.0
		9.5	17.5
		4.75	19.0
	Mix with Fiber	12.5	16.5
		9.5	15.0
		4.75	12.5
	Mix with Fiber and Sand	12.5	15.0
		9.5	15.0
		4.75	13.0
	Mix with Fiber, Latex and Sand	12.5	14.5
		9.5	12.0
		4.75	13.0

Hesami et al. (2014) Hesami et al. (2014) investigated the combined effect of various fibre types and RHA at various amounts of cement replacement on the properties of pervious concrete pavement (PVC). RHA was utilised to enhance pozzolanic cement paste and the effects of varied RHA replacement levels with cement in concrete mixtures were investigated. In addition, 0.2 percent V_f glass, 0.5 percent V_f steel, and 0.3 percent V_f polyphenylene sulphide (PPS) fibres were employed. The permeability ranged between 0.08 and 0.48 cm/s, making it suitable for use as a drainage layer in the pavement. Fiber has no discernible influence on permeability at various w/c ratios, as seen in Table 2.12, whereas RHA causes a quick drop in permeability. When RHA is increased to 8–10%, however, permeability declines, while it increases with higher RHA amounts.

Table 2.12. Influence of fibers and RHA on permeability (cm/s) in different w/c ratios (Hesami et al., 2014)

w/c ratio	Types of fibres	Replacement level of Rice Husk Ash (RHA) (%)						
		0	2	4	6	8	10	12
0.27	Glass Fibre	0.24	0.22	0.19	0.17	0.145	0.2	0.25
0.33		0.19	0.16	0.13	0.14	0.1	0.08	0.24
0.40		0.48	0.45	0.39	0.33	0.37	0.39	0.47
0.27	Steel Fibre	0.25	0.22	0.186	0.16	0.12	0.23	0.28
0.33		0.21	0.19	0.17	0.14	0.12	0.09	0.23
0.40		0.41	0.37	0.33	0.3	0.26	0.21	0.32
0.27	PPS Fibre	0.25	0.202	0.18	0.165	0.14	0.108	0.26
0.33		0.21	0.18	0.19	0.15	0.12	0.095	0.21
0.40		0.45	0.41	0.38	0.35	0.3	0.36	0.38

Gao et al. (2014) studied the permeability coefficient of pervious concrete mixed with polypropylene split fibre (PPSF). The w/c was 0.30, and the mix proportion was set at 1:5.26. A1, A2, and D1 were three mixture samples that were composed of different grades of cement. Figure 2.8 shows that, when compared to A1, the permeability coefficient of mixture D1 decreased with the addition of a certain amount of PPSF. This was due to the monofilament fibre wrapped effectively by cement paste being able to enhance compaction of the cementation layer, resulting in a lower permeability coefficient when compared to A1 and A2 mixtures.

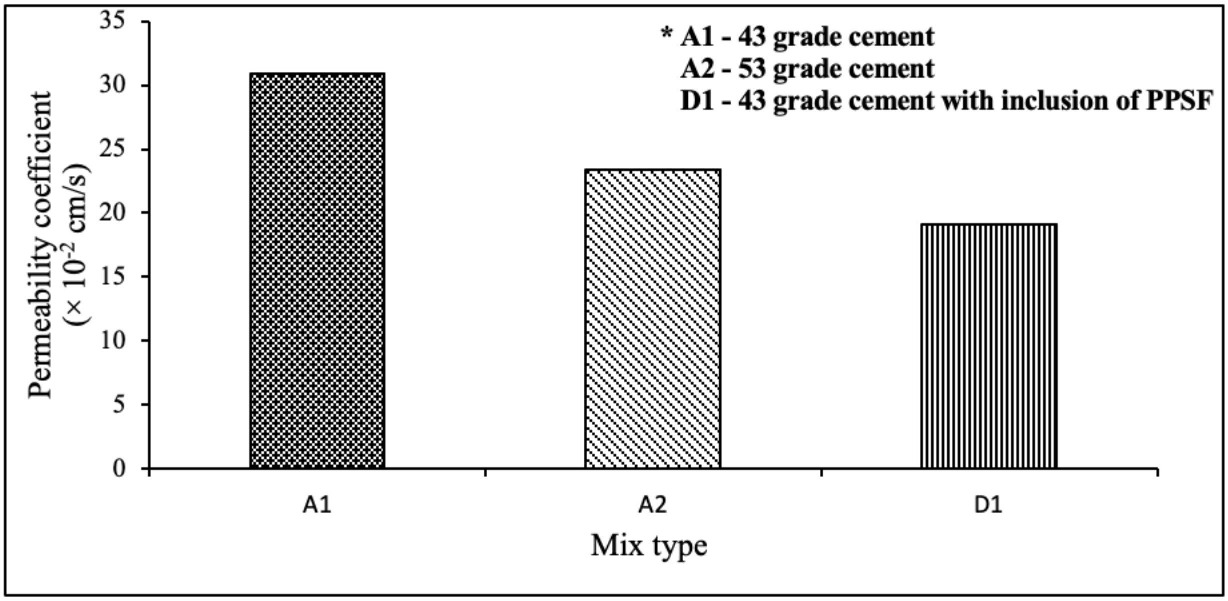

Figure 2.8. Comparison of permeability coefficient results (Gao et al., 2014)

Kevern et al. (2015) inspected the role of macro synthetic fibres on the characteristics of pervious concrete. The effects of two distinct lengths of fibre were tested at three different dosages in a single mixture. Fibres had a lower permeability than the control when compared to the control. There were no permeability-related variations in the dosage rate for the shorter fibres (38 mm). Permeability reduced as the number of fibres increased for the longer fibres, 56 mm, as indicated in Table 2.13. The permeability was reduced when macro synthetic fibres were added. The lower dosages of the longer fibres, 0.33 and 0.49 percent, showed the most dramatic reductions. The addition of fibres to pervious concrete reduced the permeability of the material, as demonstrated in Table 2.13.

Table 2.13. Test result of permeability with different lengths of fibers

Research Reported by	Mixture	Permeability (cm/s)
Kevern et al. (2015)	Control	1.19
	1.5/38	0.78
	3.0/38	0.83
	4.5/38	0.82
	1.5/56	1.07
	3.0/56	0.32
	4.5/56	0.31

Note: 1.5, 3.0, and 4.5 - Dosages rate in kg/m^3; 38 mm and 56 mm – Lengths of fibres.

2.4.2 Porosity

Hesami et al. (2014) examined the combined effect of various fibre types and RHA at various amounts of cement replacement on the mechanical properties of pervious concrete pavement (PVC). The effect of different RHA replacement levels with cement in concrete mixtures was explored in this study. Glass (0.2 % V_f), steel (0.5 % V_f), and polyphenylene sulphide (PPS) fibres (0.3 percent V_f) were also used. As shown in Figure 2.9 to Figure 2.11, it was observed that with different w/c ratios, fibers didn't have any substantial impact on the porosity, while using RHA causes porosity to decrease.

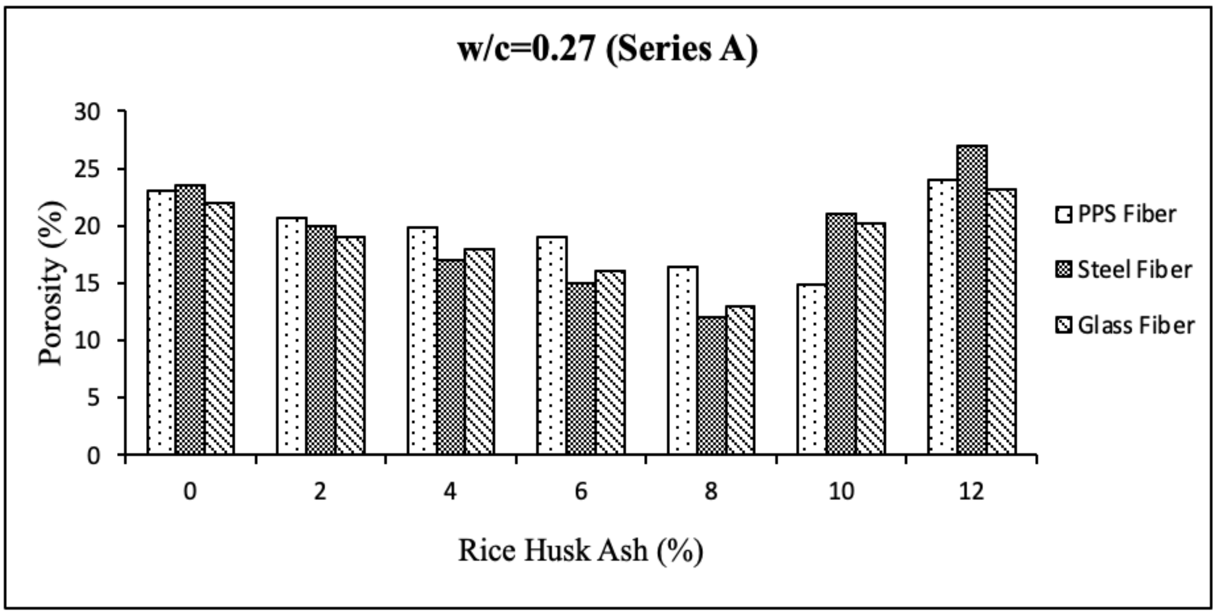

Figure 2.9. Porosity pervious concrete containing RHA and fibers with w/c ratio = 0.27 (Series A) (Hesami et al., 2014)

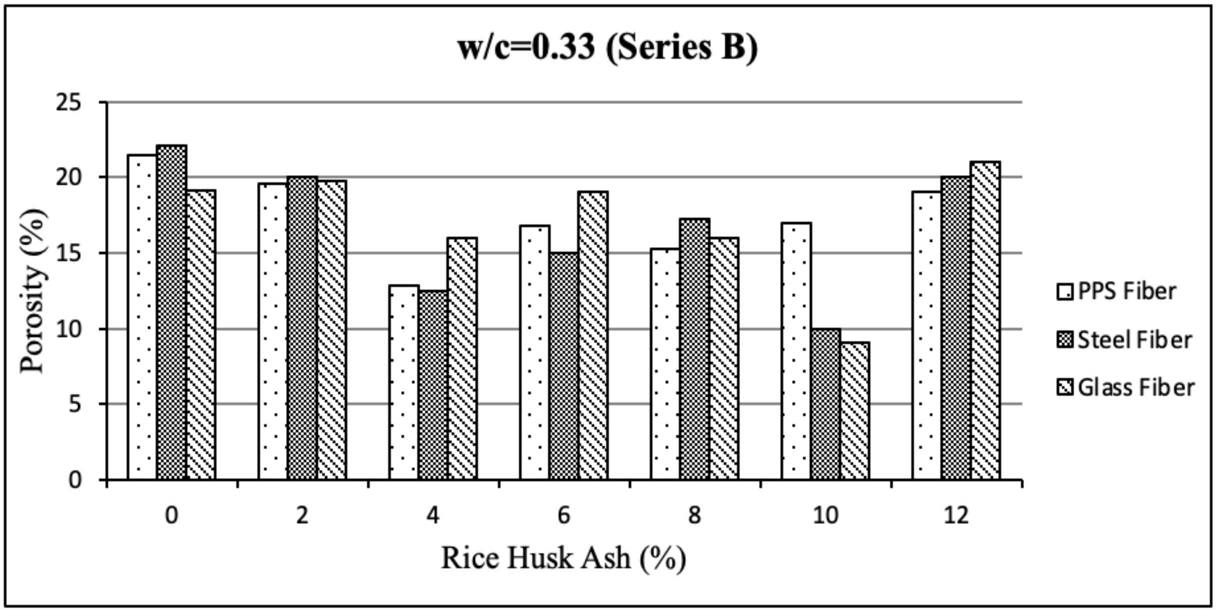

Figure 2.10. Porosity pervious concrete containing RHA and fibers with w/c ratio = 0.33 (Series B) (Hesami et al., 2014)

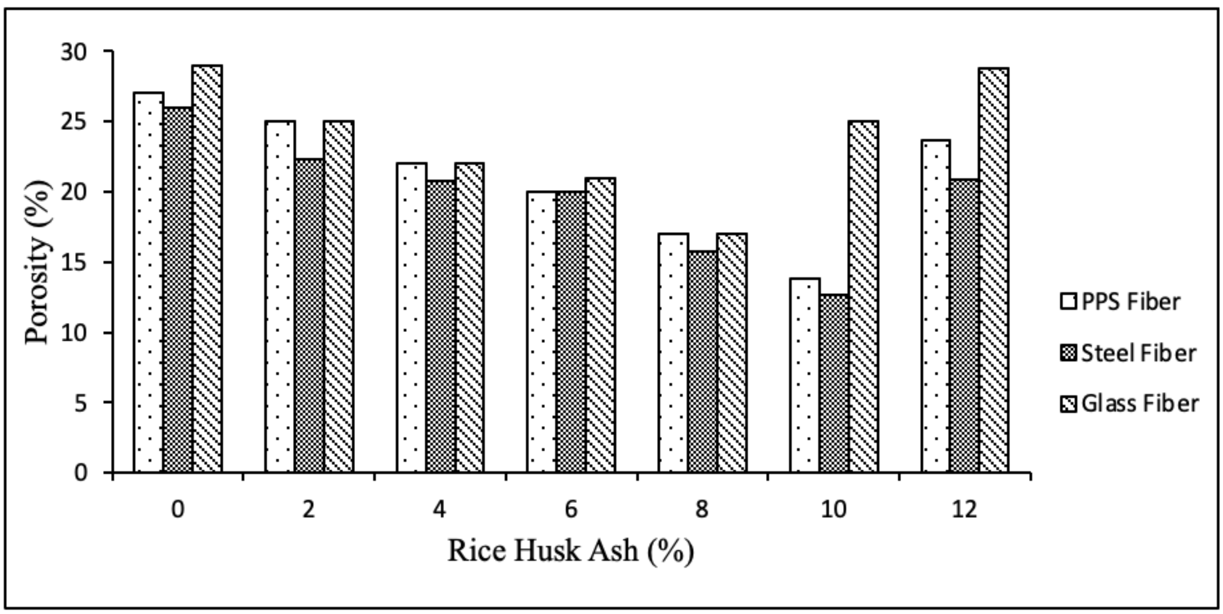

Figure 2.11. Porosity pervious concrete containing RHA and fibers with w/c ratio = 0.4 (Series C)"(Hesami et al., 2014)

Ibrahim and Abdul Razak (2016) revealed the use of POC as coarse aggregate in the production of pervious concrete (PC). OPC Type I coarse aggregate with a nominal size of 10 mm was employed. Various mixtures with a set water-cement ratio of 0.3 were produced as a result of this. The palm oil clinker pervious concrete (POCPC) was investigated at various amounts of natural aggregate replacement with POC aggregate, ranging from 0% to 100%. For five POCPC mixes, a total of 15 samples were examined, with three samples each combination.

Figure 2.12 below shows the effect of POC replacement on the porosity for all the mixes. The obtained porosity values ranged from 23.9% to 35.18%, which is within an acceptable range of 15–35%, as stated in ACI 522. The porosity of the concrete increased as the amount of POC included into the mix increased. The flaky and rough surface of POC coarse aggregate could be the reason.

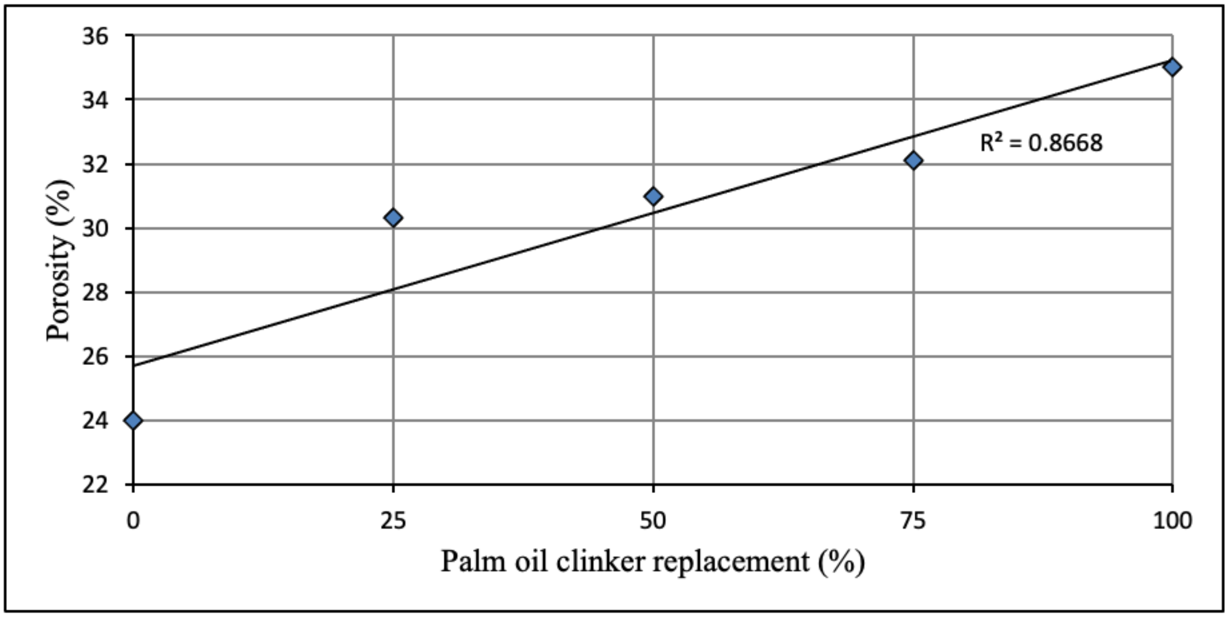

Figure 2.12. Effect of palm oil clinker (POC) replacement on porosity (Ibrahim and Abdul Razak, 2016)

Zhou et al. (2016) investigated the performance of polymer-induced pervious concrete (PPC) which might be employed in infrastructure base courses. For single-sized aggregate mixes, three aggregate sizes were used. They used 0.32 w/c ratio and a 1:6 cement-to-aggregate ratio. Figure 2.13 shows that the effective porosity rises as the aggregate size increases from PPC-27.5 to PPC-37.5 mm. It's possible that this is because when the aggregate size is smaller, the initial porosity after packing is lower.

As a result, with pervious concrete built with smaller size aggregates, the remaining porosity was lesser when the volume percent of filled voids remains the same. The porosity of the PPC was found to be between 25% and 32%, according to the findings. As the aggregate size increased, the porosity increased and the flexural strength decreased. They also discovered that, when compared to other mixes, PPC-27.5 mm performed best in terms of fatigue characteristics.

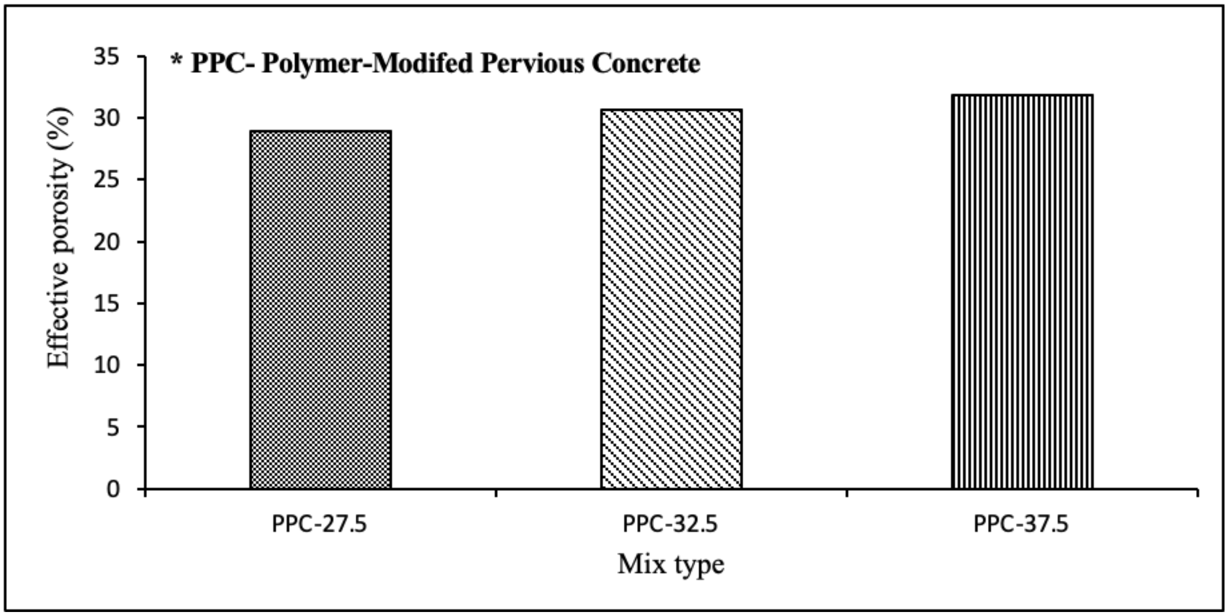

Figure 2.13. Comparison of effective porosity results (Zhou et al., 2016)

2.4.3 Freezing and Thawing

Anderson and Dewoolkar (2015) presented research about the freezing-and-thawing durability of fly ash pervious concrete. Cement was replaced with fly ash to make pervious concrete. The specimens were frozen and thawed once a day for 100 days in a drained condition using NaCl solutions containing 0, 2, 4, 8, and 12% sodium chloride. They showed that the 12% salt and no-salt specimens had the least damage, with only 2% difference between the two groups. The mass loss from the 12% solution, which was predicted to be quite harmful, was insignificant. Freezing and thawing tests revealed that replacing 10% and 20% of cement with the fly ash increased durability for all salt solution concentrations. Specimens exposed to 30% fly ash suffered higher damage than those exposed to 0% fly ash.

Kevern et al. (2015) presented an effect of macro synthetic fibres on pervious concrete properties. In a single mixture, the effects of two different lengths of fibre were examined at three dosages. The mass and dynamic modulus criteria correlated well with freeze-thaw durability. It was observed from Table 2.14 that the shorter 38 mm fibres had no appreciable effects on performance at the lower of the two dosage rates and only provided an improvement at the 4.5 kg/m^3 dosage rate.

Table 2.14. Test results of freeze-thaw durability of fibres of different lengths (Kevern et al., 2015)

Mixture	Durability Factor (Mass)	Durability Factor (RDM)
Control	53	14
1.5/38	38	12
3.0/38	53	7
4.5/38	85	21
1.5/56	89	40
3.0/56	91	41
4.5/56	96	44

Note: 1.5, 3.0, and 4.5 - Dosages rate in kg/m^3; 38 mm and 56 mm – Lengths of fibres

2.4.4 Drying shrinkage

Brooks and Megat Johari (2001) studied the effect of metakaolin in controlling creep character tics along with shrinkage. MK replaced cement up to 15%. The water to binder ratio and content of the superplasticizer was constant for all the concrete mixes. They reported that the drying shrinkage values were lower with the increasing replacement of metakaolin compared to the reference concrete.

Güneyisi et al. (2012) studied the effect on strength, permeability, and shrinkage cracking of silica fume and metakaolin concretes. The two series of control mixtures with water to cement ratios of 0.25 and 0.35 were designed. The Portland cement was replaced with 5% and 15% of metakaolin and silica fume for both the series. They observed that the difference between the drying shrinkage inclusion of metakaolin and silica fume values was significantly equal throughout the time period. It was noted that the values of drying shrinkage decreased at 15% replacement of metakaolin and silica fume compared to control concrete. They showed that the increasing replacement of metakaolin and silica fume decreased the drying shrinkage.

Hassan et al. (2012) presented an effect of metakaolin and silica fume on the durability properties of self-consolidating concrete. Seven mixtures were prepared by replacing cement with 3%, 5%, 8%, 11%, 15%, 20%, and 25% of metakaolin and four mixes were prepared with 3%, 5%, 8%, and 11% of silica fume. They found that the drying shrinkage values with the replacement of metakaolin varied from 0.042% to 0.066% and 0.052% to 0.069% with the replacement of silica fume after 400 days of a time period. The shrinkage values decreased from 8% to 22% when the replacement level of metakaolin increased from 0% to 11%. Similarly, the shrinkage values decreased from 5% to 28%, increasing silica fume replacement from 0% to 11%. The lowest values were noted at 15%, 20%, and 25% metakaolin replacement.

Limbachiya et al. (2012) used the recycled concrete aggregate in fly ash concrete. The concrete was prepared by 30% replacement of fly ash in place of cement. In addition to this, the natural aggregate was replaced by 30%, 50%, and 100% of recycled aggregate. They reported that replacing 30% FA in natural aggregate concrete decreased the drying shrinkage up to 37% compared to the control mix. In comparison, the concrete prepared with recycled aggregates increased the drying shrinkage as compared to normal concrete. They also found that 30% recycled aggregate replacement did not show any significant results in both the concrete types (PC and PCFA).

Khassaf et al. (2014) examined the properties of conventional concrete with the inclusion of RHA to reduce the seepage in canals. For this study, the concrete was prepared by replacing cement with 10%, 20%, and 30% of rice husk ash. The test results of drying shrinkage depicted that high amount of drying shrinkage were observed at an early age. The drying shrinkage values declined with the growing percentage replacement of RHA. The shrinkage values were maximum decreased at 30% replacement of rice husk ash.

Mohseni et al. (2016) studied the effect of polypropylene fiber reinforced cement mortars having rice husk ash and nano-alumina. In this study, twenty-six mixtures were made with different amounts of rice husk ash and nano-alumina. The water to binder ratio was kept constant at 0.49 for all the mixtures, and the amount of superplasticizer was varied from 0.2% to 15 by weight of the binder. They revealed that the drying shrinkage values containing rice husk ash ranged from 801 to 843 micro-strains at 90-day. The concrete containing RHA showed lower shrinkage than the control mix after 90-day. They also found that the drying shrinkage was decreased by 5% to 12%, with the increasing percentage replacement of RHA.

Zhang et al. (2020) reported the shrinkage effect by using fly ash (FA) in concrete mixtures in lieu of fine aggregate. The concrete was prepared by replacing cement with 15%, 25%, 35%, and 45% fly ash. They concluded that with the increasing replacement of FA, drying shrinkage values decreased. The replacement level of 25% fly ash decreased the shrinkage by 20.81%. The concrete mixture containing 15% replacement of fly ash in place of fine aggregates showed a lower shrinkage rate.

2.5 CLOSING REMARKS

This chapter presents an elaborate review of literature of the recent/latest works done in the area of NFC/Pervious Concrete.

CHAPTER 3

EXPERIMENTAL PROGRAM & METHODOLOGY

This chapter discusses the testing methodology adopted for the present study to characterize the materials used in producing NFC and assess the effect of SCMs and varying sizes of natural coarse aggregates on the properties of the NFC.

3.1 GENERAL

The investigational program includes lab tests on the strength and permeation properties of NFC. the methodology follows the concrete casting, curing and specimens testing to assess the impact of SCMs as replacement of cement and impact of variation in sizes of coarse aggregates. The adopted methodology is demonstrated in Figure 3.1 and the designation of different SCMs is outlined in Table 3.1.

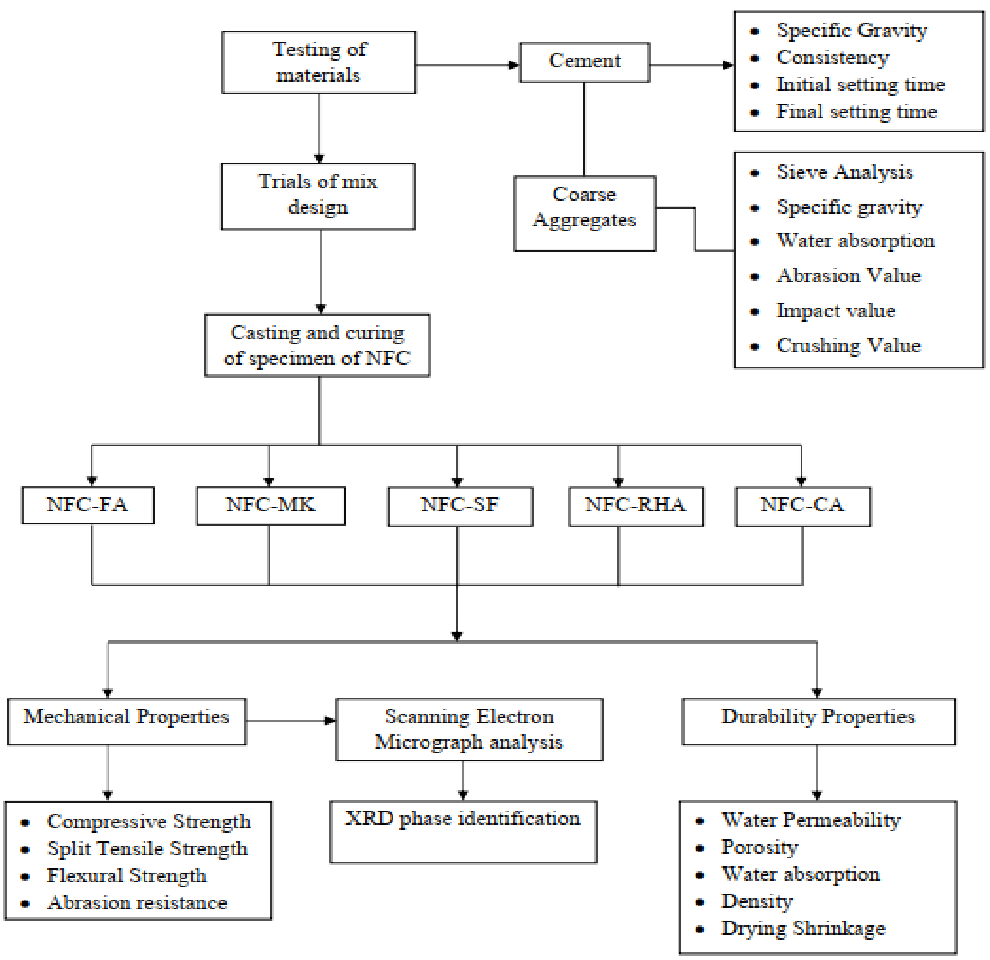

Figure 3.1 Schematic of the experimental program

Table 3.1. Designation of different concrete mixes.

Designation	Constituents
NFC-FA	No-Fines Concrete containing Fly Ash
NFC-MK	No-Fines Concrete containing Metakaolin
NFC-SF	No-Fines Concrete containing Silica Fume
NFC-RHA	No-Fines Concrete containing Rice Husk Ash
NFC-CA	No-Fines Concrete containing gradation of aggregates

3.2 MATERIALS

3.2.1 Cement

Ordinary Portland Cement (OPC) 43 grade conforming to BIS: 8112 (2013) was used. The following physical properties of cement, were calculated as per BIS: 4031 (1988).

- Consistency
- Initial and final setting time
- Compressive strength

Specific gravity

Specific gravity is defined as “The ratio mass of a given volume of material to an equal volume of water at the same temperature”. The pycnometer apparatus was used to determine the specific gravity as per BIS: 4031 (Part 11) (1988). Kerosene is used as a liquid rather than water because it does not react with cement, and due to its addition, cement does not set.

Standard consistency

The standard consistency of cement paste is defined as “The consistency that will allow the Vicat plunger to ingress to a height of 5 to 7 mm from the bottom of the Vicat mould.” The standard consistency was evaluated at BIS: 4031 (Part 4) (1997). The cement paste was molded into a 500-gm ball and inserted in the mould. The upper surface of the mould was smoothed with a single palm movement, and the mould was softly shaken to evacuate air. Place the mould and a non-pervious plate beneath the plunger-attached rod. Lower down the plunger until it touches the paste's top surface, then instantly release it, allowing it to sink into the paste. Prepare the trial pastes with various percentages of water until you've found the right amount of water to achieve the desired consistency.

The reason to be performed this test is to determine how much water should be added to the cement for attaining a consistent paste, and also cement paste consistency may change setting time.

Setting time

Initial and final setting time of cement was calculated as per BIS: 4031 (Part 5) (1988) guidelines., Prepare a cement paste by mixing the cement with 0.85 times the water essential to provide a consistent paste. Fill the Vicat mould with prepared cement paste and level it with the help of a trowel. With the needle, place the mould and a non-porous plate beneath the rod-bearing. Lower the plunger until it touches the paste's top surface, then instantly release it to allow it to enter the paste. Repeated the technique until the needle was unable to pierce the sample for a distance of around 5 mm measured from the mold's bottom.” The first setting time was estimated as the time between adding water to the cement and the needle failing to puncture the test block at a depth of around 5 mm measured from the bottom of the mould.

The needle of the Vicat apparatus was altered via annular attachment in order to calculate the ultimate setting time. When the attachment leaves no impression on the paste's surface but the needle does, the cement is said to be fully set. The final setting time was measured from when water was added to the cement until the needle made an impression on the top surface of the test block

Compressive strength

The compressive strength of cement was determined by casting the size of the cubes with side of 7.06 cm as per procedure given in BIS: 4031 (Part 6) (1988). The standard sand confirming to BIS: 650 (1991) was used to prepare the mixture of cement and sand in the proportion of 1:3 by mass. The quantities of cement and sand are as follows:

Amount of cement used (W_1) = 200 gm

Amount of standard sand used (W_2) = 600 gm

$$\text{Water} = \left(\frac{P}{4} + 3\right) \%\ \text{of the } (W_1+W_2), \qquad \textbf{(3.1)}$$

where P = % of water for standard consistency.

Compaction of the assembled cubes is performed on a vibrating machine, placed for 2 minutes. De-mold the cube after completing vibrations at about 24 hours and submerged it in water at a controlled temperature of 27 °C. The cubes were tested for compressive strength after 3,7 and 28-day of curing. The cube specimens were loaded at a stress rate of 35 N/mm^2/minute rate in a compression testing machine (CTM). The physical properties of OPC cement are shown in Table 3.2 and have satisfied the requirements of BIS: 8112 (2013).

Table 3.2. Physical characteristics of OPC43 cement

Properties	**BIS Code used**	**BIS value specified by BIS: 8112-2013**	**Test Result**
Compressive Strength (MPa)	(BIS: 4031 (Part 6), 1988)	-	-
3-day		> 23.0	25.4
7-day		> 33.0	38.9
28-day		> 43.0	46.2
Initial setting time (minutes)	(BIS: 4031 (Part 5), 1988)	> 30.0	75
Final setting time (minutes)		< 600.0	230
Consistency (%)	(BIS: 4031 (Part 4), 1997)	-	29
Specific gravity	(BIS: 4031 (Part 11), 1988)	-	3.02

3.2.2 Coarse Aggregates

Crushed river gravel was sourced from a quarry near Pathankot, Punjab, for the study's coarse aggregates. To make the concrete mix, a 65:35 ratio of 20 mm and 10 mm sized particles was used. The aggregates were cleaned and dried to surface dry conditions after being washed to remove dirt and dust.

Sieve analysis

Sieve analysis measures coarse aggregates particle size distribution and is called the gradation test. Fineness modulus is defined as "The empirical factor calculated by adding the total percentage of aggregates retained on each sieve set and dividing the sum by 100." Table 3.3 and Table 3.4 shows the sieve analysis results of aggregates having maximum size of 20 mm and 10 mm, respectively.

Table 3.3. Sieve analysis of 20 mm coarse aggregates

Total mass of sample taken = 3000 gm					
Sr. No	**IS-Sieve (mm)**	**Wt. Retained (gm)**	**% retained**	**% finer**	**Cumulative % retained**
1	40	0.00	0.00	100.00	0.00
2	20	178.00	5.93	94.07	5.93
3	10	2052.00	68.40	25.67	74.33
4	4.75	320.00	10.67	15.00	85.00
5	Pan	450.00	15.00	0.00	100.00
	Total	**3000.00**		**SUM**	**165.26 + 500 = 665.26**
				FM =	*6.65*

Table 3.4. Sieve analysis of 10 mm coarse aggregates

Total mass of sample taken = 3000 gm					
Sr. No	**IS-Sieve (mm)**	**Wt. Retained (gm)**	**% retained**	**% finer**	**Cumulative % retained**
1	20	0.00	0.00	100.00	0.00
2	12.5	114.00	3.80	96.23	3.80
3	10	670.00	22.33	73.87	26.13
4	4.75	1925.00	64.17	9.70	90.30
5	Pan	291.00	9.70	0.00	100.00
	Total	**3000.00**		**SUM**	**120.23 + 500 = 620.23**
				FM =	*6.20*

Water absorption capacity and Specific gravity

The water absorption capacity and specific gravity were determined as per guidelines given in BIS: 2386 (Part 3) (1963).The 3.0 kg coarse aggregate was soaked in water for 24 hours. The sample was then dried at room temperature until no free surface moisture could be seen. First, a saturated surface dry aggregate sample was weighed (weight X). The coarse aggregate was then weighed in a basket filled with water (weight Y). Remove the aggregates from the basket, place them in the oven to dry for 24± 1 hours at 110 °C, and then weigh them (weight Z). The physical properties of coarse aggregates used in the study are shown in Table 3.5. Water absorption and specific gravity were determined as follows:

$$\text{Specific gravity} = \frac{\mathrm{Z}}{(\mathrm{X}-\mathrm{Y})} \tag{3.2}$$

$$\text{Water absorption} = \frac{[100\,(X-Z)]}{Z} \tag{3.3}$$

where,

X = mass of saturated surface dry aggregate in air, gm

Y = mass of saturated aggregate in water, gm

Z = mass of oven-dry aggregate in air, gm.

Impact value

Aggregate toughness refers to their ability to resist impact. The impact value was measured as per BIS: 2386 (Part 4) (1963). The impact load imposed by vehicle movement on the pavement aggregates should be sufficient to avoid aggregate splitting. As a result, the aggregate impact value denotes toughness or resistance to sudden impact instead of its efficiency under a uniformly increasing compressive load. The impact value of the aggregate mix was obtained as 12% and can be measured by the following equation:

$$\text{Impact Value} = \frac{\mathrm{X}}{\mathrm{Y}} \times 100 \tag{3.4}$$

where,

X = weight of fraction passing through IS Sieve 2.36 mm

Y = weight of the oven-dried sample.

Table 3.5. Physical characteristics of coarse aggregates

Properties	Coarse aggregates		BIS Code used
	10 mm	20 mm	
Water Absorption (%)	0.97	0.99	(BIS: 2386 (Part 3), 1963)
Specific Gravity	2.690	2.704	

Abrasion value

Los Angeles test was used to determine the abrasion resistance of aggregates and was carried out as per BIS: 2386 (Part 4) (1963). The abrasion value indicates the abrasion and toughness properties. Therefore, any procedure in the aggregate's manufacturing, stockpiling, and placement production, as well as compaction, should have adequate crushing strength to prevent disintegration and deterioration. The Los Angeles abrasion value of aggregates was 21.48% and was calculated as follows:

$$\text{Abrasion Value} = \frac{\text{X}}{\text{Y}} \times 100 \qquad \textbf{(3.5)}$$

where,

X = Difference between the initial and final weight of the sample

Y = Initial weight of the sample.”

Crushing value

The crushing value was determined by consistently applying compressive loads and was evaluated as per BIS: 2386 (Part 4) (1963). The output values provide the crushing resistance of aggregates. The crushing value was obtained as 22% and was evaluated from the following formula:

$$\text{Crushing value} = \frac{\text{X}}{\text{Y}} \times 100 \qquad \textbf{(3.6)}$$

where,

X = weight of fraction passing through IS Sieve 2.36 mm

Y = weight of the surface dry sample.

3.3 SUPPLEMENTARY CEMENTITIOUS MATERIALS (SCMs)

The SCMs of Fly Ash (FA), Metakaolin (MK), Silica Fume (SF), and Rice Husk Ash (RHA) were used in present study. Fly ash was procured from the nearest thermal power plant at Rajpura in Punjab and belonged to Class F fly ash as per BIS 3812 (2013). The specific gravity of FA was 2.04. The SEM image of the procured FA shows spherical-shaped particles with a glassy and spongy appearance Figure 3.2 (a). Metakaolin was supplied by Kaomin Industries Gujarat, India. The specific gravity of MK was 2.41. SEM image reveals irregular-shaped particles randomly distributed over the surface Figure 3.2 (b). Silica fume was supplied by Haryana Ceramic & Allied Products Ind. situated at Village Devi Nagar, Ambala City, India. The specific gravity of SF was 2.19. The SEM image for silica fume depicts angular particles and irregular shapes Figure 3.2 (c). Rice husk ash was procured from Ludhiana, Punjab. The specific gravity of RHA was 2.07. SEM analysis shows that RHA is multilayered and has a microporous surface Figure 3.2 (d). The chemical compositions of cement and different SCMs such as FA, MK, SF, and RHA were listed in Table 3.6.

Table 3.6. Chemical composition of cement, fly ash, metakaolin, silica fume, and rice husk ash used

Constituents (%)	Cement	Fly Ash	Metakaolin	Silica Fume	Rice Husk Ash
CaO	63.44	0.32	0.29	0.25	0.34
SiO_2	26.34	57.40	58.20	99.41	93.97
Al_2O_3	3.65	39.95	41.40	0.21	0.14
FeO	2.16	1.05	0.38	0.14	0.76
SO_3	1.62	0.0	0.0	0.0	0.0
MgO	1.28	0.33	0.13	0.13	0.50
K_2O	0.82	0.85	0.29	0.06	0.94
Na_2O	0.68	0.10	0.12	0.02	0.20

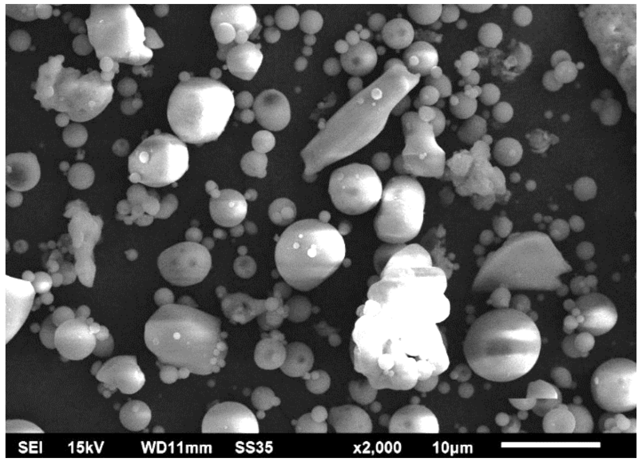

(a) SEM image of FA used

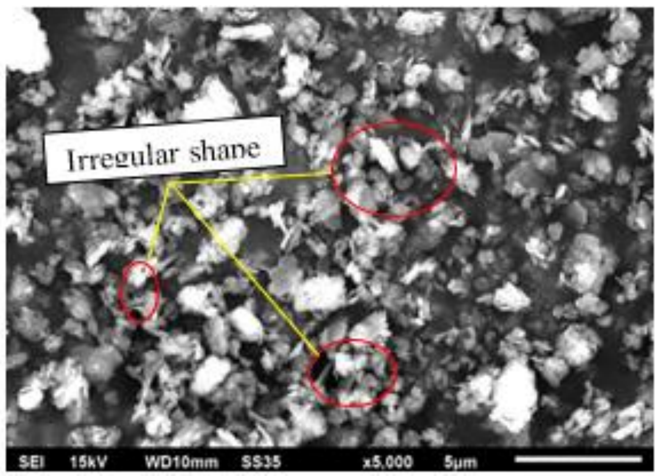

(b) SEM image of MK used

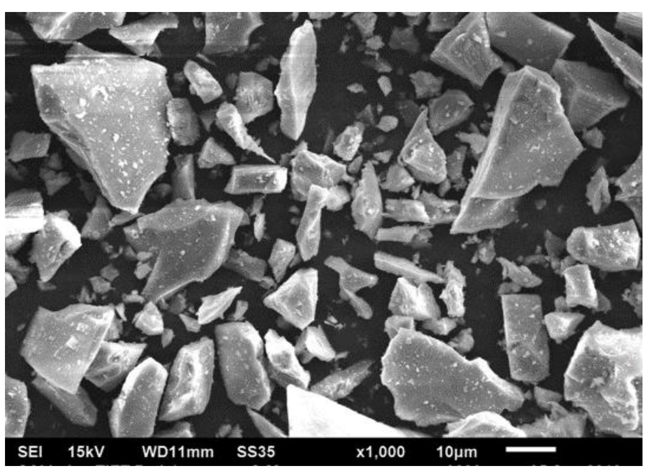

(c) SEM image of SF used

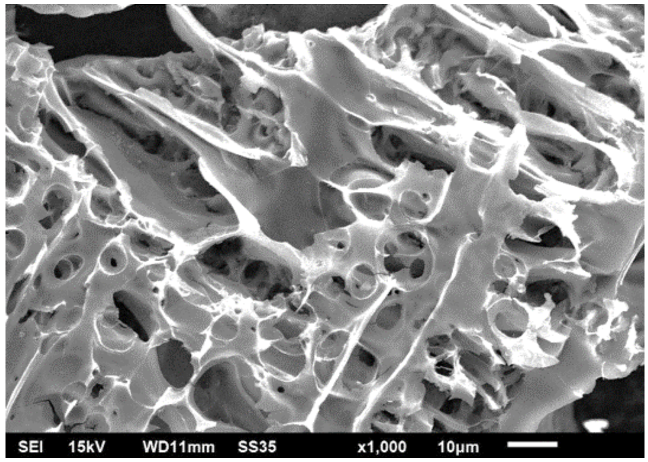

(d) SEM image of RHA used

Figure 3.2. Physical characteristics of constituents used

3.4 CONCRETE MIX DESIGN

The control mix is designed by using the materials with properties as described above. NFC is prepared from the same materials as conventional concrete but eliminates the fine aggregates that make it porous. In addition to the high permeability, the grading of coarse aggregates is to be kept low to achieve the appropriate mechanical properties. BIS:12727 (1989) only applies to NFC as a brick masonry substitute if damping removal is necessary. It has no information concerning the use of NFC on pavements. American Concrete Institute (ACI) published ACI Committee 522 (2010), a report on no-fines concrete and pavement application. This report provides the technical aspects of the no-fines application, design methodologies, materials used, properties, construction methods, mixture proportioning, inspection, and testing. ACI Committee 522 (2010) specifies the standard ranges of the material extent used to prepare NFC as shown in Table 3.7.

Table 3.7. Typical ranges of material proportions in NFC (ACI Committee 522, 2010)

Material	Proportions (kg/m^3)
Cementitious materials	270 to 415
w/cm ratio	0.27 to 0.38
Aggregate: cement ratio	4:1 to 4.5:1
Fine: coarse aggregate ratio	0 to 1:1

Control NFC mix proportions per m^3 were prepared after several trial mixes as per ACI Committee 522 (2010), as shown in Table 3.8 and Table 3.9.

Table 3.8. Quantities of materials used to prepare a control mix

Material	Quantity (kg/m^3)
Cementitious material	403
Water	153
w/cm ratio	0.38
Aggregate: cement ratio	4.5:1

Table 3.9. Design mix proportions of No-Fines Concrete (NFC) mixes prepared (w/cm ratio= 0.38; cement aggregate (c/a) ratio= 1:4.5 for all mixes)

Mix	Cement (kg/m^3)	Aggregates (kg/m^3)		Fly Ash (kg/m^3)	Metakaolin (kg/m^3)	Silica Fume (kg/m^3)	Rice Husk Ash (kg/m^3)
		10 mm	20 mm				
NFC-0	403.2	740.88	1375.92	0	0	0	0
NFC-5FA	383.0			20.2	–	–	–
NFC-10FA	362.8			40.4	–	–	–
NFC-15FA	342.7			60.5	–	–	–
NFC-20FA	322.6			80.6	–	–	–
NFC-5MK	383.0			–	20.2	–	–
NFC-10MK	362.8			–	40.2	–	–
NFC-15MK	342.6			–	60.5	–	–
NFC-20MK	322.6			–	80.6	–	–
NFC-5SF	383.0			–	–	20.2	–
NFC-10SF	362.8			–	–	40.2	–
NFC-15SF	342.7			–	–	60.5	–
NFC-20SF	322.6			–	–	80.6	–
NFC-5RHA	383.0			–	–	–	20.2
NFC-10RHA	362.8			–	–	–	40.2
NFC-15RHA	342.7			–	–	–	60.5
NFC-20RHA	322.6			–	–	–	80.6

3.5 CASTING AND CURING OF SPECIMENS

First, the aggregates were added with a small amount of measured water and then cement to the wet aggregates. The mixing was continued until the cement was evenly disseminated. The remaining water was then added and mixed for around 1.5 minutes, or until the mixture was uniformly colored. Before casting the specimens, all of the molds were well lubricated. The fresh mixture was divided into relatively equal halves, then each half was placed into the mould and compacted with 25 blows per layer using a tampering rod. The first layer was scraped somewhat before compacting the second layer to improve bonding between the two layers. Excess material was scraped off with a spatula after the second layer was compacted and leveled the surface. However, it wasn't easy to get a smooth surface, unlike conventional concrete specimens (ASTM C1688-14a, 2014). Moreover, over-finishing the surface will cause the pores to close.

Figure 3.3. Casting of NFC specimens

The compressive strength of NFC mixes was found using cubes of size 150 mm. Cylindrical specimens of size 300 mm height and 150 mm diameter were cast to determine the split tensile strength. The flexural strength was conducted on the beam of size 100 mm × 100 mm × 300 mm. NFC cylindrical specimens of dimensions 200 mm height and 100 mm diameter were prepared to determine the water permeability, porosity, density, and abrasion resistance parameters. Three replicates for each NFC mix for all strength and permeability tests were cast and tested to ensure repeatability for each curing age, and the error bars have been plotted to report the same. Prism samples of 75 mm × 285 mm were used to determine the length change during air drying. The freshly prepared specimens were placed in the mold for 24 hours without being disturbed and de-molded. The NFC concrete specimens were provided with appropriate labels and stored in the curing tanks for the specified period. The NFC specimens used for evaluating the mechanical properties are shown in Figure 3.3.

3.6 TESTING PROCEDURE

3.6.1 Compressive Strength

The compressive strength of NFC was calculated as per BIS: 516 (1959). At the prescribed curing age, surface water and grit were scraped off the cube specimens as soon as they were removed from the water. The cube was placed in the Universal Testing Machine (UTM) of 1000 kN capacity, as shown in Figure 3.4. The cube was positioned so that the load was applied to the cube's opposite sides, rather than the top and bottom, while it was casted. The load was applied without shock and progressively increased at a rate of 5 kN/sec until the cube's resistance to the rising load broke down and it could sustain no additional load. The maximum load on the cube was then measured, and three cubes for each percentage ratio of NFC blends were tested. The compressive strength of the NFC cube specimen was calculated by dividing the maximum load applied by the cross-sectional area of the cube specimen. The average of three values calculated the compressive strength of the NFC mixes by using the following formula.

$$f_{ck} = \frac{P}{A} \tag{3.7}$$

where,

P = maximum applied load, kN

A = cross-sectional surface area of a cube of size 150 mm × 150 mm × 150 mm

Figure 3.4. Strength test of NFC Sample in progress in the UTM

3.6.2 Split Tensile Strength

The split tensile strength of NFC cylindrical specimens was measured as per BIS: 5816 (1999). The specimen was kept so that load was applied over the entire length. The cylindrical specimen was placed in the compression testing machine of capacity 5000 kN shown in Figure 3.5, and the load was applied without any shock and increased continuously at a rate of 1.2 N/(mm^2/min.) to 2.4 N/(mm^2/min.). Maintain the rate, once adjusted, until failure. The maximum applied load was recorded for each NFC cylindrical specimen. The average of three values calculated the split tensile strength of the NFC mixes by using the following formula.

$$f_{ct} = \frac{2P}{\pi l d} \quad \textbf{(3.8)}$$

where,

P = maximum load applied to the specimen, kN

l = length of the specimen, mm

d = cross-sectional dimension of the specimen, mm.

Figure 3.5. Experimental set up for split tensile strength test

3.6.3 Flexural Strength

The NFC beams flexural strength was determined as per BIS: 516 (1959) in the UTM of capacity 1000 kN, as shown in Figure 3.6. The beam specimen was placed in the machine to apply the load along two lines 13.3 cm apart to the highest surface as cast in the mould. In this test, the applied load is evenly distributed between the two loading rollers. All of the rollers are positioned in such a way that the load is applied axially and without torsional stresses. For the 10.0 cm specimen, the load was applied without any shock and increased at a constant rate of 180 kg/min. Three beams were tested for each percentage ratio of NFC mixtures, and the maximum stress on the beam was measured. The flexural strength of the specimen is also expressed as modulus of rupture f_b, will be calculated by the following formula:

$$f_b = \frac{p \times l}{b \times d^2} \tag{3.9}$$

where,

b = measured width of the specimen (in cm),

d = measured depth of the specimen at the point of failure (in cm),

p = maximum load in kN applied to the specimen, and

l = length of the span on which the specimen was supported (in cm).

Figure 3.6. Experimental set up for the flexural strength test

3.6.4 Measurement of Porosity and Density

The porosity (∅) and density (ρ) influence the structural and functional properties of NFC. The test was performed according to ASTM C1754 (2012). The cured cylindrical specimens having 100 × 200 mm were placed inside oven at a temperature of 50 °C for seven days, and their weight was noted to determine density. The weight of the specimen was monitored every 24 hours, and when the percentage change in mass between two successive cycles was less than 0.5%, the final dry weight was measured. The specimens were kept submerged in water for computing the porosity, and the submerged weight was calculated. The relationship between oven-dried weight and submerged weight is used in ASTM C1754 (2012) to determine the percentage of porosity. The evaluation of submerged mass and specimens placed in an oven are illustrated in Figure 3.7.

Calculate the porosity and density of the specimen by the following formula:

$$\text{Porosity } (\emptyset) = \left[1 - \left(\frac{\mathrm{K} \times (\mathrm{A}-\mathrm{B})}{\rho_{\mathrm{w}} \times \mathrm{D}^2 \times \mathrm{L}}\right)\right] \times 100 \qquad \textbf{(3.10)}$$

$$Density\ (\rho) = \frac{K \times A}{D^2 \times L} \qquad \textbf{(3.11)}$$

where,

A = dry mass of the specimen (in gm),

B = submerged mass of the specimen (in gm),

ρ_w = density of water at a temperature of the water bath (in kg/m^3),

V = volume of the specimen (in m^3),

D = average diameter of the specimen (in mm),

L = average length of the specimen (in mm), and

K = 1 273 240 in SI units or 2200 in [inch-pound] units.

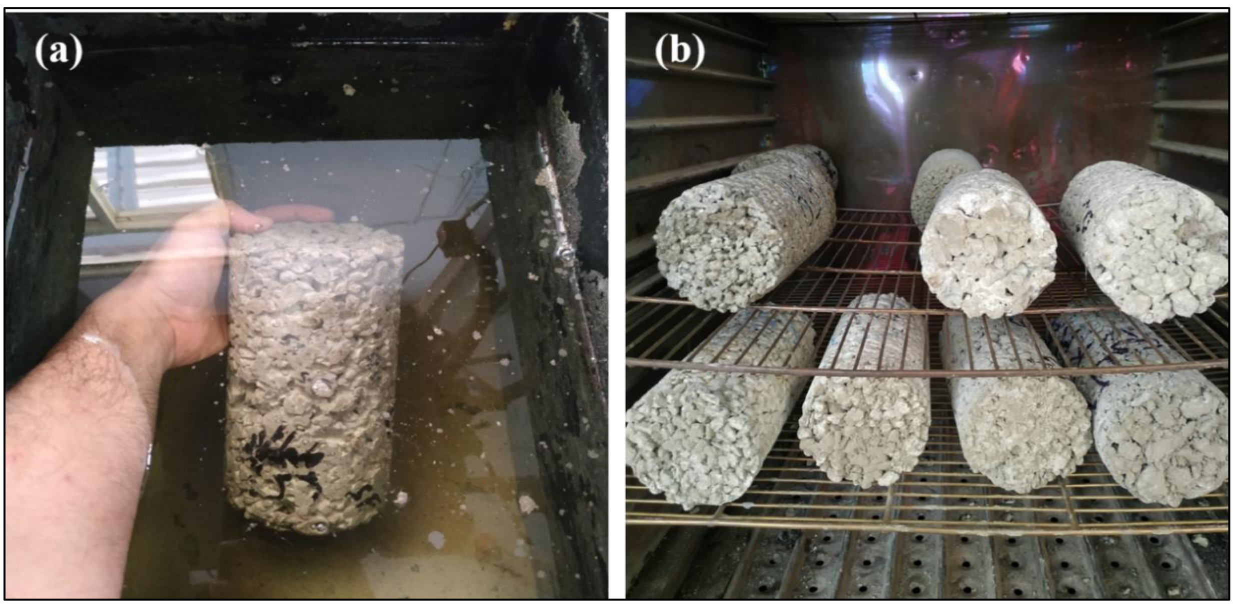

(a) Agitating the NFC sample to remove air bubbles; (b) Oven drying the NFC samples

Figure 3.7. Density and Porosity measurement

3.6.5 Measurement of Permeability

The water permeability test was conducted as per JIS A 5371 (2016) to evaluate the permeability coefficient. For this, the sides of cylindrical specimens of 200 mm height and 100 mm diameter were tightly covered with duct tape to prevent any water leakage. The water can only enter from the top surface and exit only from the bottom surface of the water cylindrical specimens. The specimens were placed inside the standpipe, and silicone gel was used to prevent any leakage between the specimens and the standpipe, as shown in Figure 3.8 (a). This test was performed after the flow was steady or saturated. The permeability coefficient of the average of three NFC specimens was calculated with Darcy Law using equation below.

$$K = \frac{Q}{AT\frac{H}{L}} \quad \textbf{(3.12)}$$

where,

K = water permeability coefficient in cm/sec;

Q = water quantity in mm permeating within the whole test period after the steady-state has been reached;

A = specimen area in cm^2;

T= time in seconds over which Q is measured;

H = pressure head; and

L = thickness of the specimen.

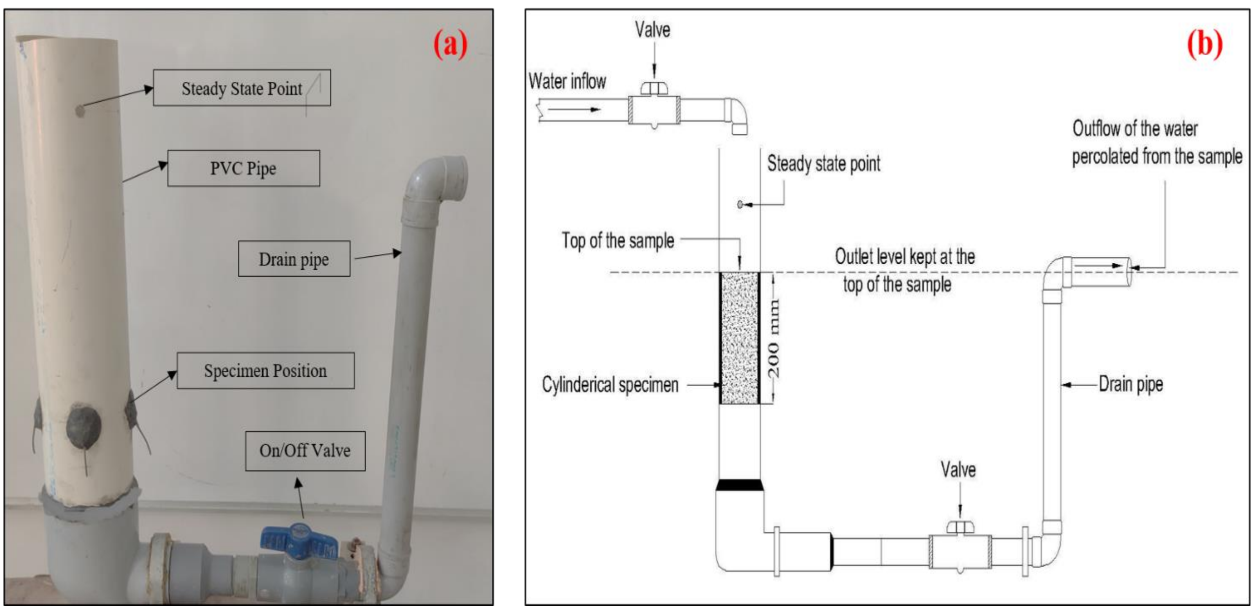

Figure 3.8. (a) Constant head permeability test apparatus (b) Schematic of PVC mold used

3.6.6 Measurement of Water Absorption

The water absorption test is an indicator of the perviousness of the material and was performed as per ASTM C642 (2013). This test was conducted based on oven-dry mass and saturated mass. The initial mass of cured specimens was measured on a cylindrical core size of 50 mm height and 100 mm in diameter after 28-day of curing. The specimens were placed in an oven at 100 to 110 °C for 24 h. Further, extract each specimen from the oven, put it in dry air at room temperature, and measure its mass. Now, submerge the specimen after drying, cooling, and determines its mass in the water at a temperature of 21 °C for 48 h. The following formula was used to calculate the water absorption of NFC specimens.

$$\text{Absorption after immersion, \%} = [(B - A)/A] \times 100 \quad \textbf{(3.13)}$$

where,

A = mass of oven-dried sample in the air (in gm),

B = mass of surface dry sample in the air after immersion (in gm).

3.6.7 Drying Shrinkage

Drying shrinkage is caused by the loss of water during drying of the concrete. It was determined as per ASTM C157/C157M (1999). Three specimens were utilized in this test. The length of the specimen was noted as the initial comparator to readings after 28-day of curing. The comparative values were taken after 4, 7, 14, and 28-day of air storage, as well as 8, 16, 32, and 64 weeks as shown in Figure 3.9. The following formula calculated the length change at any age after the initial reading.

$$\Delta L_x = \frac{CRD - \text{Initial } CRD}{G} \times 100 \quad \textbf{(3.14)}$$

where,

ΔL_x = specimen length change at any age (%),

CRD = Difference between the specimen comparator reading and reference bar at any age,

G = the gauge length (250 mm).

Figure 3.9. Experimental set up of measuring length gauge

3.6.8 Abrasion Resistance

The abrasion resistance of NFC was determined as per ASTM C1747/C1747M (2015) on cylindrical specimens of 100 × 200 mm. The three cylindrical specimens pre-determined mass was initially measured before testing and placed in the abrasion apparatus, as shown in Figure 3.10 (a). The test is executed by subjecting the three cylindrical specimens to 500 revolutions at 33 revolutions per minute in the Los Angeles abrasion machine without steel balls surcharge. After subjecting them to abrasion, the material was sieved through a 25 mm sieve. The mass of material retained over the sieve was measured. The percentage of mass loss after abrasion was calculated as the ratio of mass loss original mass and multiplied by 100.

Figure 3.10. (a) Experimental set up of abrasion resistance (b) NFC specimens prepared for abrasion testing

3.6.9 Scanning Electron Microscopy (SEM)

The concrete microstructure comprises hydrated cement paste, aggregate, and ITZ. In order to determination the microstructure of concrete, scanning electron microscopy (SEM) plays a pivotal part. Materials can be analyzed topographically and compositionally by using SEM. The SEM's application improves the ability to portray the microstructure of concrete and assist in determining the factors that influence concrete's mechanical and durability properties. The concrete microstructure is an integrated system that consists of calcium silicate hydrate (CSH) gel, calcium carbonate, calcium hydroxide, and calcium sulfoaluminate hydrate (ettringite and monosulfate), coarse aggregate, and interfacial transition zone between cement paste and aggregates. Calcium silicate hydrate has a morphology that ranges from fibrous to uneven grains, forming a complicated network. The most common morphology of CSH structure at the early age of cement hydration is fibrous; however, a reticular network can also occur. As the cement hydrates, the equant grain shape of CSH appears. Calcium silicate hydrates have a dimpled form with either closely packed or regular pores equant grains. The calcium carbonate appears to be in the shape of an octagonal plate crystal. Flat plate-type crystals and thin elongated crystals are all examples of calcium hydroxide. Ettringites and monosulfate are two morphologies of calcium sulfoaluminate. Monosulfate looks like hexagonal plate crystals, while ettringite looks like needle-like crystals.

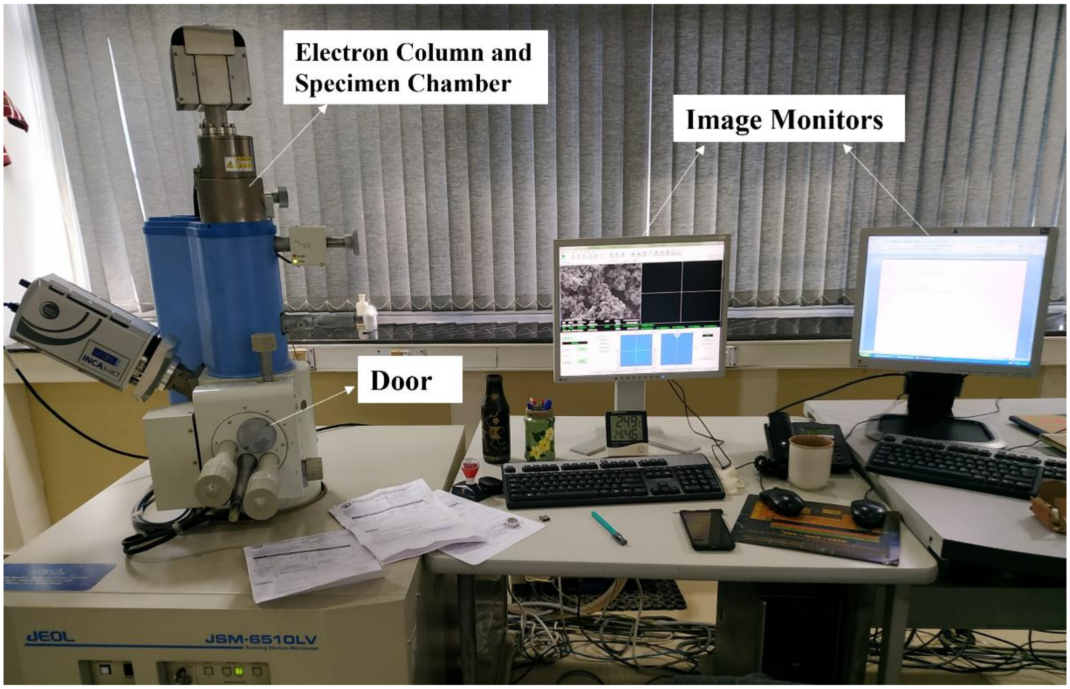

Figure 3.11. Experimental set up of Scanning Electron Microscope

SEM micrographs were taken of the ruptured fragments of NFC samples produced from the compressive strength test. NFC specimens were scanned using a scanning electron microscope at 28 and 90-day after curing. Before being placed on the scanning electron microscopy stem, the specimens were coated with a fine layer of gold to make them electrically conductive. The secondary electron was used to capture SEM images of concrete samples. Secondary electrons are the low-energy particles produced when a primary beam electron collides with an outer electron of the testing sample by inelastic collision mechanism. Surface topography images are formed when secondary electrons formed near the surface escape. The chemical analysis of concrete samples was carried out with energy dispersive spectroscopy. The experimental setup for SEM is shown in Figure 3.11.

3.6.10 X-Ray Diffraction (XRD) Analysis

It is a valuable technique for determining the crystalline and amorphous phases in concrete. Low-intensity peaks are caused by the microstructure of concrete`s interfacial transition zone. X-ray diffraction analysis of concrete also shows the peaks of hydration products. The identification of hydration phases present in concrete is limited by the weak diffraction peaks from poorly crystalline calcium silicate hydrate phase of concrete and interference from diffraction peaks of minerals present in aggregate. The diffraction peak of calcium hydroxide tends to be overwhelmed the weak diffraction peaks of calcium silicate hydrate. The diffraction picture of each crystalline phase is unique. The diffractogram is made up of a series of diffraction maximum points, with the diffracted radiation intensity plotted on the ordinate and angle 2θ plotted on the abscissa. The XRD technique was utilized to determine different phases in hardened NFC as well as control concrete from 28 and 90-day. This data was compared with the standard peaks of compounds in the diffraction database released by the International Center for Diffraction Data (ICDD). Figure 3.12 illustrates the X-Ray Diffraction (XRD) instrument.

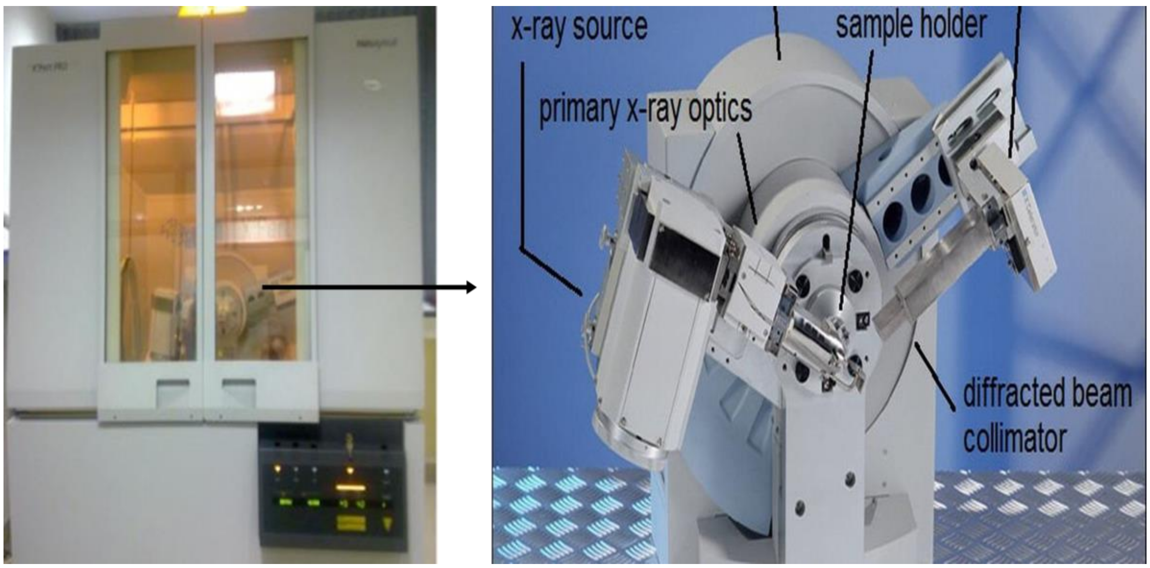

Figure 3.12. Typical X-Ray Diffraction (XRD) instrument

3.7 CLOSING REMARKS

The chapter presented the various materials and methods utilized in this study to investigate several properties and characteristics related to NFC mixes. However, there are currently no standard test methods for NFC except for identifying the basic properties such as porosity, density, and abrasion in the laboratory. Most of the test methods formulated for conventional concrete assessment were used for other properties. The procedures used to prepare samples of various geometrics and experimental methodologies and determine the various properties of NFC were thoroughly detailed in this chapter. The destructive methods mainly included: compressive strength, split tensile strength, flexural strength, and abrasion resistance tests. The permeation properties included: water permeability, porosity, density, drying shrinkage, and water absorption. This chapter included the experimental methodology used to investigate the properties of NFC.

CHAPTER 4
RESULTS AND DISCUSSIONS

4.1 INTRODUCTION

This chapter examines the strength along with permeation properties of prepared NFC mixes by replacing cement content by varying percentages of FA, MK, SF, and RHA from 5-20%. Mechanical properties of compressive, split tensile, and flexural strength of the prepared NFC mixes were measured at 7, 28, 90, and 365-day of curing and permeation properties of water permeability, water absorption, density, and porosity tests at 28, 90, and 365-day of curing were investigated. Three replicates for each NFC mix for all strength and permeability tests were cast and tested to ensure repeatability for each curing age, and the error bars have been plotted to report the same. Microstructural analysis of SEM and phase identification using XRD are represented in this chapter also. This research focusses on strength and permeation properties of samples prepared with SCMs and varying sizes of coarse aggregates.

4.2 STRENGTH PROPERTIES

4.2.1 Compressive Strength

Effect of replacement by fly ash (FA)

Compressive strength results of different NFC mixes containing FA with varying percentage replacement of cement at 7, 28, 90, and 365-day were presented in Figure 4.1. Three samples were evaluated for every mix, and the outcomes were presented as the average of three. The compressive strength value of the NFC control mix was 11.14 MPa at 7-day which improved to 15.05 MPa at 365-day. A nominal decrease in compressive strength was observed on substituting cement with FA with highest value at 20% replacement in NFC at 7 and 28-day of curing. At 7-day of control mix (11.14 MPa), the compressive strength decreased by 1.16%, 2.11%, 2.92%, and 5.29% and by 0.92%, 1.52%, 4.86% and 9.41% at 28-day as compared to controlled sample mix (12.43 MPa) at 5, 10, 15, and 20% replacement level of FA respectively. Comparable results were reported by (Anderson and Dewoolkar, 2015; Sata et al., 2016) in NFC. They have presented that the compressive strength of NFC with FA was decreased by approximately 11% to 18% than NFC control mix at 28-day. This was because the FA has delayed pozzolanic reaction compared to cement (Sata et al., 2016; Siddique, 2004; Tangpagasit et al., 2005). But an improvement in compressive strength was observed at 90-day up to 1.07%, 2.06%, 2.34%, and 3.09% at 5%, 10%, 15%, and 20% for FA content in the mix, when compared with control NFC mix (12.62 MPa). Similarly, at 365-day, the compressive strength was increased up to 0.38%, 0.53%, 1.02%, and 1.73% at 5%, 10%, 15%, and 20% for FA content in the mix in comparison to control NFC mix (15.05 MPa) (Figure 4.1). At 90 and 365-day, FA's fineness and pozzolanic activity lead to an overall improvement in the quality of cement matrix and enhancement in the microstructure of the transition zone existing between the aggregate and the binder material. Moreover the continuous process of pore refining, the strength at later ages was increased due to the incorporation of FA hydration products into the concrete (Hadi et al., 2018; Siddique, 2004; Siddique et al., 2012; Tang and Lo, 2009; Tangpagasit et al., 2005). The above presented findings were well supported by pore-refinement structure at increasing replacement levels of cement by FA in the SEM images of different mixes of NFC.

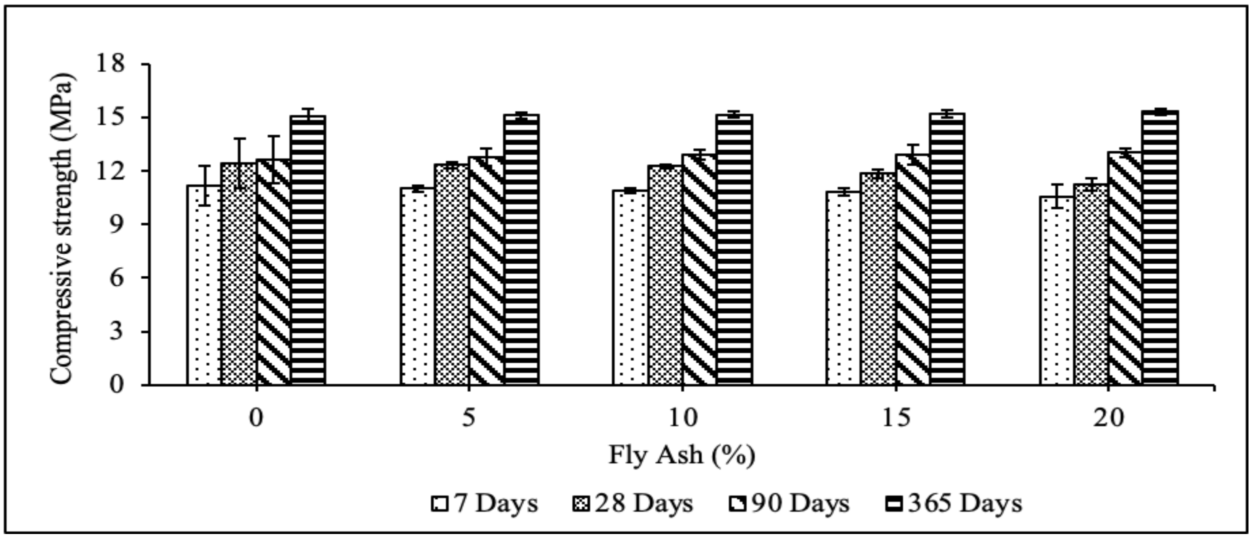

Figure 4.1. Compressive strength of NFC mixes with varying replacement of FA

Effect of replacement by metakaolin (MK)

The compressive strength results of several NFC mixes containing MK at varying levels of cement at 7, 28, 90, and 365-day were shown in Figure 4.2. It has been observed that on increasing the percentage of MK from 5% to 20%, compressive strength consistently increased compared to the control mix at different curing ages. At 7-day of control mix (11.14 MPa), an increase in compressive strength was observed as 2.24%, 18.22%, 29.22%, and 40.80 % at 5%, 10%, 15%, and 20% replacement of cement with MK, respectively. Similarly, at 28-day of curing of controlled mix (12.43 MPa), there was corresponding increase in compressive strength of 10.86%, 16.65%, 32.02%, and 41.11% was observed at 5%, 10%, 15%, and 20% replacement of cement with MK, respectively. Similar results and trends were observed at 90-day with a maximum increase of 46% with 20% replacement level of MK. At 90-day of control mix (12.62 MPa), the compressive strength increase was 18.46%, 26.27%, 39.89%, and 46% at 5%, 10%, 15%, and 20% replacement of cement with MK. Similarly, at 365-day, the value of compressive strength increases by 8.97%, 18.45%, 21.11%, and 31.47% compared to the control mix (15.05 MPa). Hence, the results indicate a consistent and regular increase in compressive strength with increasing MK levels up to 20% at all curing ages. Similar results were reported by (Patel et al., 2018; Rawat et al., 2021; Siddique and Kadri, 2011; Wild et al., 1996) by experimental investigations on conventional or normal concrete, increasing approximately 14.8% to 17.53% in compressive strengths was reported by 15-20% replacement of cement by MK. The increased mechanical strength in NFC with increasing MK replacement of cement can be credited to the higher pozzolanic activity of MK and pore structure refinement at increasing replacement levels. Moreover, the addition of MK improved the interfacial transition zone connecting aggregate to cement paste that arrests crack propagation from cement to aggregate, which provides strength to the NFC mixes (Güneyisi et al., 2012; Khatib and Hibbert, 2005; Singh and Singh, 2020). The major constituents of MK, i.e., silicon dioxide and aluminium oxide, react with CaOH in cement paste and generate more C-S-H gel products, which helps increase the compressive strength by increasing replacement percentage compared to the control NFC mix. This is also well corroborated by dense microstructure with increasing replacement of cement percentage with MK in SEM images of different mixes of NFC.

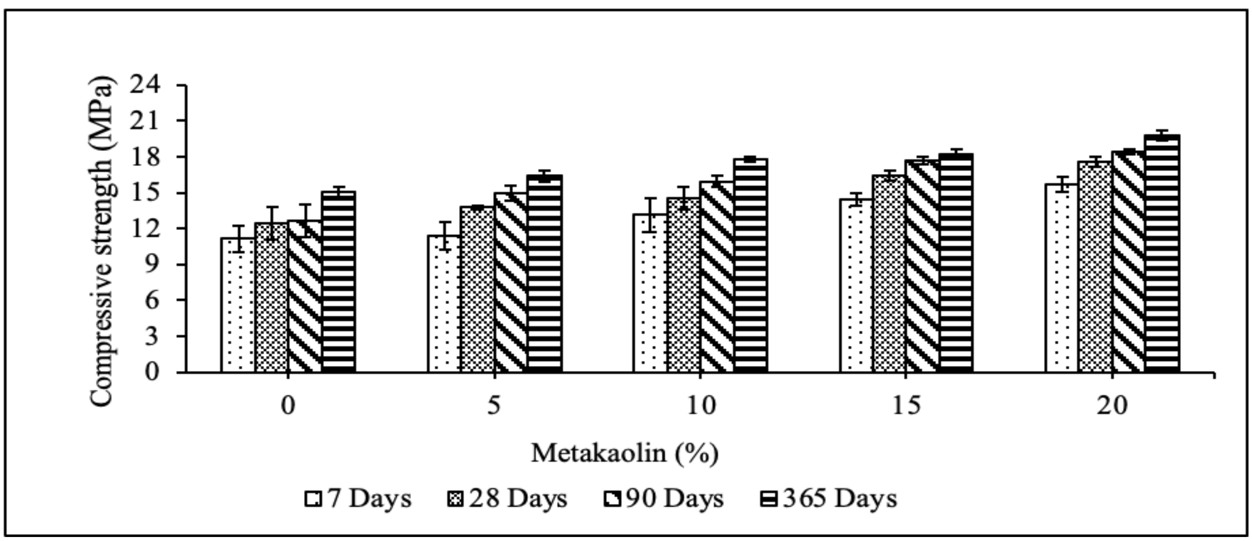

Figure 4.2. Compressive strength of NFC mixes with varying replacement of MK

Effect of replacement with silica fume (SF)

The compressive strength results of the NFC containing SF at different percentage replacement levels of cement at testing ages of 7, 28, 90, and 365-day were illustrated by Figure 4.3. The compressive strength (7-day) for NFC with 5% and 10% SF replacement increased by 13.91% and 15.08%, respectively, but at 15% and 20% replacement levels, a decrease in strength was noticed to be 21.99% and 22.26%, respectively. Similar trends were observed at 28-day, wherein the compressive strength for NFC with 5% and 10% SF replacement increased by 15.93% and 17.70%, respectively, but the strength decreased by 1.36% and 16.49% at 15% and 20% replacement. Similarly, at 90-day, with increases of 15.84% and 16.40% at 5 and 10% SF, but the strength results decreased to 0.95% and 9.11% at 15 and 20% replacement, respectively. Similarly, at 365-day, the compressive strength value increased by 0.60% and 1.13% at 5 and 10% SF and decreased by 16.27% and 17.47% at 15 and 20% replacement. The strength increase at lower replacement levels of 5%-10% with SF was due to very fine nature of highly amorphous silica, which increases the pozzolanic reaction by reacting with calcium hydroxide resulting from primary hydration and increases the compressive strength (Mehta and Ashish, 2019; Yue et al., 2018). An increase in SF content beyond 10% because of its smaller size than cement causes the cement grains to move apart, leading to unpacking of the system and poor dispersion of SF particles in the concrete mix. Excess precipitated silica particles do not take part in the chemical reaction of cement hydration causes a reduction in strength, as confirmed later in EDS plots (Shannag, 2000).

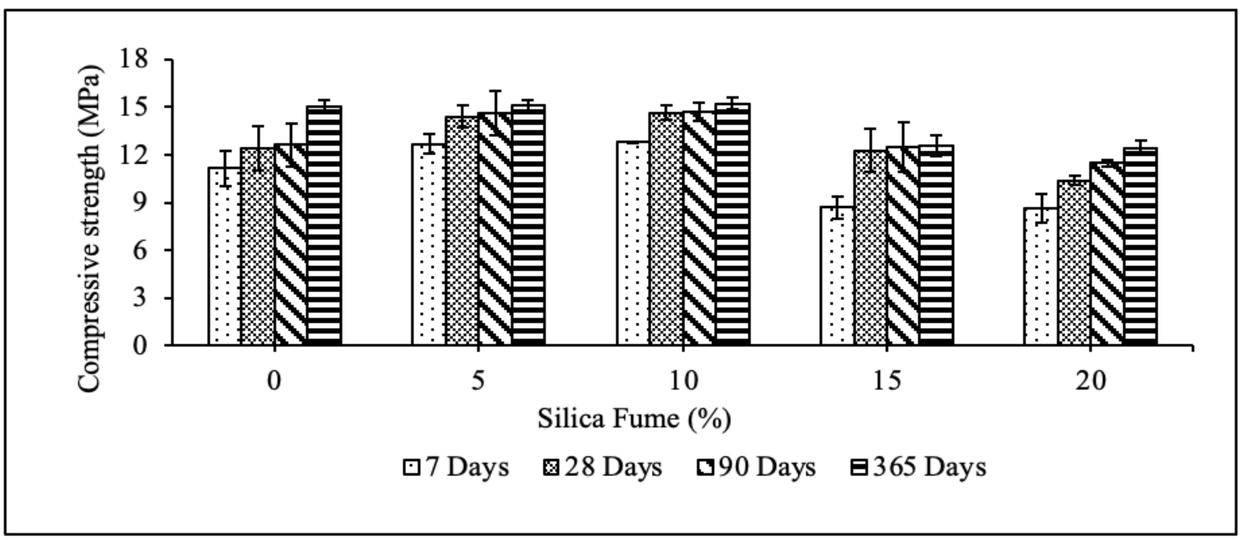

Figure 4.3. Compressive strength of NFC mixes with varying replacement of SF

Effect of replacement by rice husk ash (RHA)

The compressive strength results of the NFC containing RHA at different percentage replacement levels of cement at testing ages of 7 to 365-day were represented in Figure 4.4. Compressive strength test results had a different trend by replacing cement with RHA in NFC, as shown in Figure 4.4. At early ages of 7-day, compressive strength decreased by 21.54%, 21.83%, 28.09%, and 29.80% at 5%, 10%, 15%, and 20% replacement level with RHA, respectively. Similarly, at 28-day, strength reduced by 10.53%, 12.79%, 25.82% and 26.14% at 5%, 10%, 15%, and 20% replacement level with RHA. The decrease in strength was mainly due to fact that RHA absorbs a high volume of water, and non-uniform distribution of ash decreases the compaction amount of the fresh mix, causing more voids leading to strength loss at an early age (Le et al., 2014; Van Tuan et al., 2011). However, at the subsequent ages of 90 and 365-day, compressive strength first increased with the increase in replacement level up to 5% and then decreased with further increase in percentage replacement level to 10% and 20%, but overall compressive strength values were higher than that of control mix at all percentage replacement levels. At 90-day, the strength increased by 25.04%, 15.77%, 2.77%, and 1.11% as compared to control NFC mix (12.62 MPa). Similarly, at 365-day, strength increased by 6.80%, 3.03%, 1.55%, and 0.66% in comparison to control mix (15.05 MPa) but decreases beyond 5% replacement (Figure 4.4). This is due to the fact that RHA, as a pozzolan, reacts with CaOH in the hydration and improves the aggregate paste connectivity but reduces the transition zone thickness connecting aggregate to cement matrix because of the precipitation of CaOH crystals on the surface of the grains (Hesami et al., 2014).

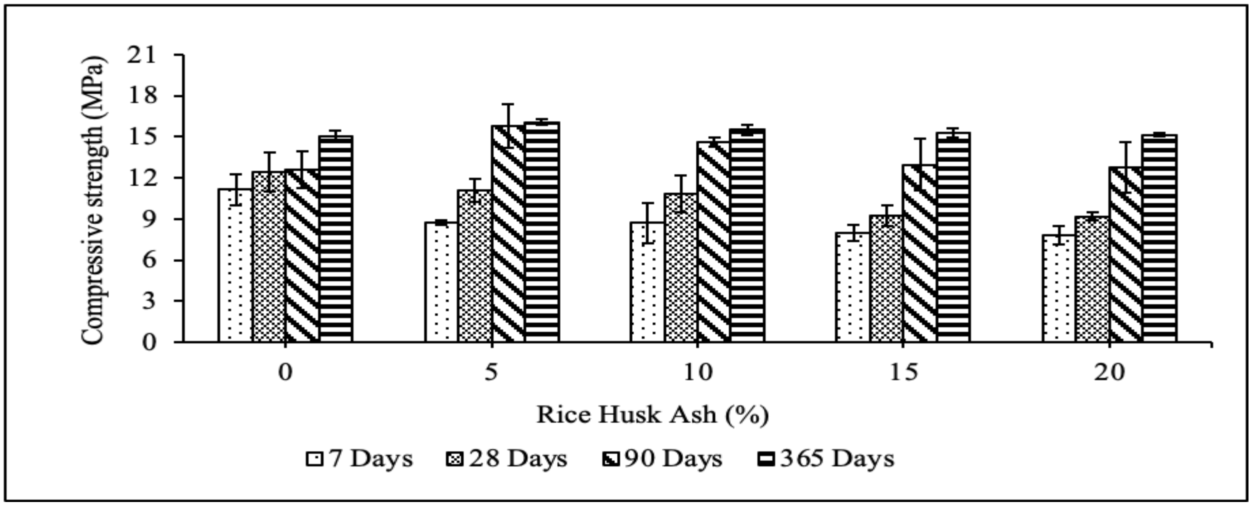

Figure 4.4. Compressive strength of NFC mixes with varying replacement of RHA

From the compressive strength results, the compressive strength increases with increasing percentage replacement of MK with cement up to 365-day of curing age. Maximum enhancement in strength is seen with 15-20% replacement which can be taken as a reasonably optimum replacement level in NFC for strength improvement. On the other hand, with the increasing replacement of FA, early age strengths (7 and 28-day) do not significantly improve. Maximum strength is reported at 20% replacement at 365-day. However, it can be concluded that increasing percentage replacement of cement with SF in the NFC mixes is highly beneficial up to 10% and results in strength enhancement by 17.70% and 16.40% at 28 and 90-day, respectively.

On the other hand, optimal replacement of RHA in NFC mixes up to 5% also increased compressive strength by 25.04% at 90-day. The increased compressive strengths with minor modification in the form of SCMs in NFC mixes enhances the applicability of NFC for vast infrastructural applications such as low- to medium-traffic pavements and meets the compressive strength requirements of ACI 522R (ACI 2010) and IRC:44 (IRC 2017) guidelines. This is well supported by the microstructural analysis in SEM, EDS, and XRD images of control mixes and various NFC mixes, as discussed in "Microstructural Analysis."

Effect of different gradation of coarse aggregates

The experiment outcomes for compressive strength of different NFC mixes containing different single-sized coarse aggregates at 7, 28, 90, and 365-day of testing was presented in Figure 4.5. It was seen that compressive strength increases with increasing curing ages in all NFC mixes, irrespective of the size of aggregates used. An important observation was that the compressive strength of various NFC mixes made with aggregates of increasing size from 4.75 mm, 6.3 mm, 8 mm, and 9.5 mm decreases at all curing durations of up to 365-day. At 28-day, the compressive strength with NFC-9.5, NFC-8, NFC-6.3, and NFC-4.75 aggregate size of concrete was 8.84 MPa, 9.19 MPa, 9.62 MPa and 10.01 MPa, respectively. The maximum percentage increase in strength is 13.23 % at 28-day and 15.18 % at 365-day for NFC-4.75 compared to the NFC-9.5 mix. The average percentage increase of compressive strength was 12% to 16%, and similar results have been reported by (Elango and Revathi, 2017; Fu et al., 2014; Huang et al., 2010; Lian et al., 2011; Lian and Zhuge, 2010; Wu et al., 2011). It was evident from the results that the NFC made with smaller size aggregates displayed better compressive strength in relation to previous concrete with larger size aggregates. It was because aggregates of smaller sizes reduce voids due to efficient packing making the NFC mix denser (Elango and Revathi, 2017; Yahia and Kabagire, 2014). Also, smaller size aggregates increase the surface area and, therefore, increase the binding area, making a better bond with cement matrix and providing better strength to the NFC mixes (Elango and Revathi, 2017; Kevern et al., 2010; Wang et al., 2006).

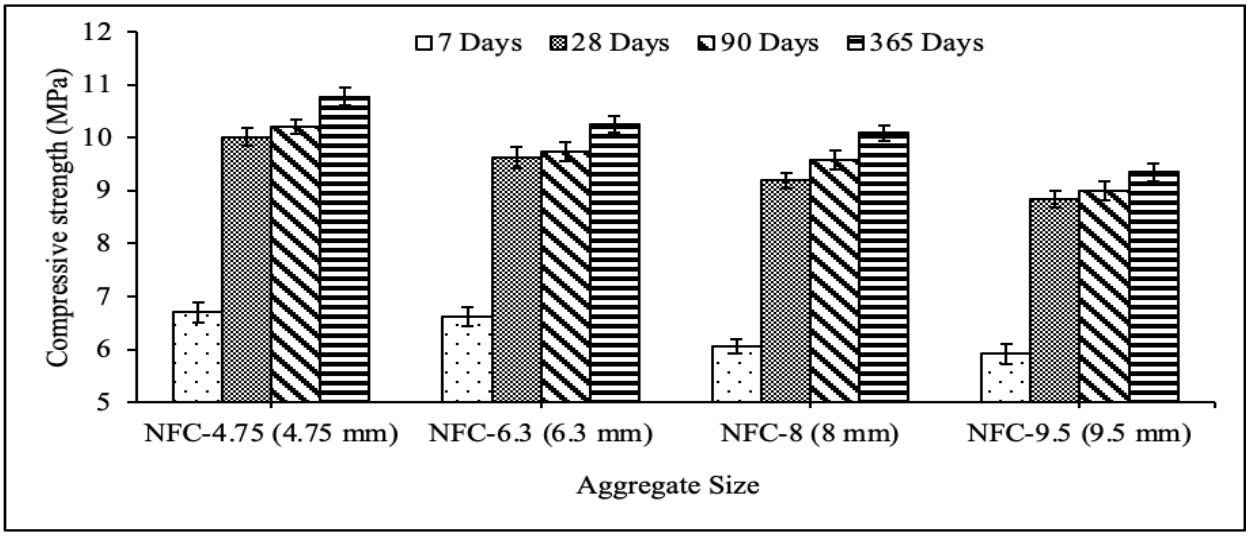

Figure 4.5. Compressive strength of NFC mixes with different gradations of coarse aggregates

4.2.2 Split Tensile Strength

Effect of replacement by fly ash (FA)

The split tensile strength of NFC mixes prepared containing varying replacement levels of FA at 7, 28, 90, and 365-day as presented in Figure 4.6. On replacing cement with FA, split tensile strength decreases at 7 and 28-day as compared to control NFC mix having average split tensile strength 1.65 MPa and 1.90 MPa, respectively (Figure 4.6). The split tensile strength decreased by 9.39%, 14.14%, 20.61%, and 24.24% at 5, 10, 15, and 20% replacement levels of FA for tests performed at 7-day, respectively. Similarly, at 28-day, the strength decreased by 5.52%, 9.21%, 20.26%, and 28.94% at 5, 10, 15, and 20% replacement of FA, respectively. But at 90-day, an improvement in split tensile strength was 2.63%, 6.58%, 10.53%, and 15.79% at 5, 10, 15, and 20% replacement levels of FA, respectively. Comparable results and trends were observed at 365-day where an increase in strength was 1.80%, 3.92%, 6.13%, and 12.75% at 5%, 10%, 15%, and 20% replacement of FA. Hence, it can be concluded that no significant contribution by FA replacement in compressive and tensile strength is observed at early ages as it requires a longer curing period to reach strength comparable to cement. A decrease in hydration rate with FA addition was observed, resulting in a slower rate of hardening and reduced strength of NFC at early ages. But at 90 and 365-day, the later age strength improves due to finesses and increased pozzolanic reaction of FA with hydration products of cement, leading to a continuous process of pore refining (Siddique, 2004; Tangpagasit et al., 2005).

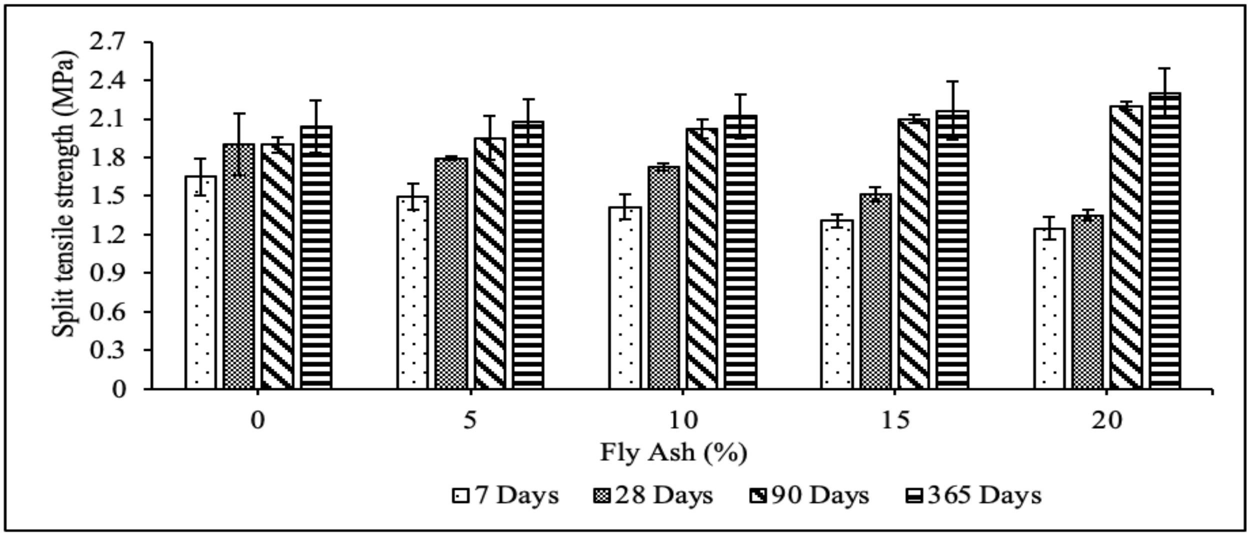

Figure 4.6. Split tensile strength of NFC using FA

Effect of replacement by metakaolin (MK)

The split tensile strength of the NFC comprising MK at different percentage replacement levels of cement up to 365-day were shown in Figure 4.7. It was seen that with increasing replacement level of MK, the split tensile strength increases at different curing ages. At 7-day of curing age, the strength increased by 4.24%, 9.09%, 16.97%, and 26.67% at 5%, 10%, 15%, and 20% replacement of MK in comparison to control mix (1.65 MPa). At 28-day, the split tensile strength increased by 6.84%, 23.68%, 43.68%, and 50.26% at 5%, 10%, 15%, and 20% replacement respectively in comparison to reference NFC mix with split tensile strength 1.9 MPa. Similarly, at 90-day, the percentage increase in strength was 13.16%, 33.68%, 58.16%, and 67.37% at 5%, 10%, 15%, and 20% replacement of MK as compared to the control mix of 1.90 MPa. At 365-day of control mix (2.04 MPa), the strength increased by 7.11%, 27.70%, 51.96%, and 58.33% at varying percentage replacement of MK. Related result was stated by Güneyisi et al. (2012) in his previous study of high-performance concrete. An approximate percentage increase of split tensile strength was 12.55% at 28-day by 15% cement replacement by MK. The strength increase is due to MK's filling effect and the pozzolanic reaction with calcium hydroxide to produce C-S-H gel, which increased strength (Güneyisi et al., 2012; Wild et al., 1996). Hence, from this study, it was established that the best replacement level for MK is 15-20% in the NFC.

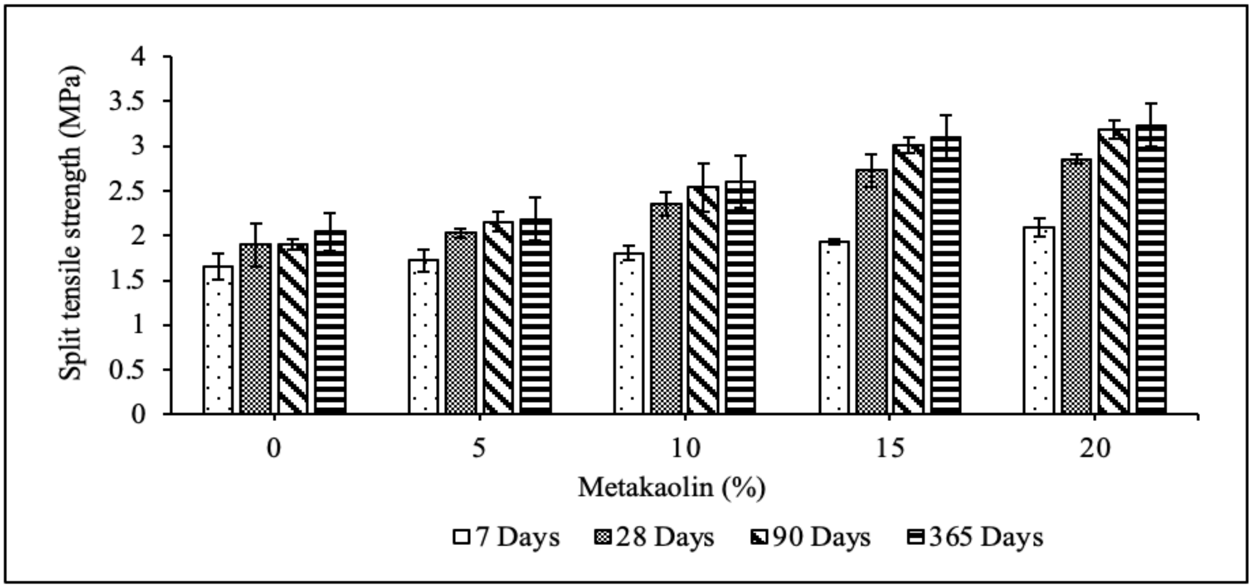

Figure 4.7. Split tensile strength of NFC using MK

Effect of replacement by silica fume (SF)

The split tensile strength of the NFC comprising SF at different percentage replacement levels of cement at 7, 28, 90, and 365-day was illustrated in Figure 4.8. The tests demonstrated that use of SF in NFC mixes resulted in an improvement of split tensile strength up to 12%, 8%, and 9% for 7, 28, and 90-day with replacement level of 10%, but at higher replacement levels, tensile strength decreases compared to control mix. At 7-day, the split tensile strength for NFC with 5% and 10% SF replacement increased by 2.42% and 12.12%, respectively, but at 15% and 20% replacement levels, a fall in strength was witnessed by 23.63% and 44.24% respectively compared to control mix (1.65 MPa). At 28-day of control mix (1.90 MPa), the strength increased by 0.52% and 7.89% at 5% and 10% replacement of SF but 15% and 20% replacement, split tensile strength decreased by 33.68% and 50.53%. Similar results and trends were observed at 90 and 365-day. At 365-day, the strength increased by 1.96% and 6.86% at 5% and 10% replacement of SF but decreased by 9.80% and 15.19% at 15% and 20% replacement of SF compared to the control mix (2.04 MPa). This may be ascribed to the high amount of reactive amorphous silica and high fineness of SF, which improves the rate of pozzolanic reaction with the CaOH produced from cement hydration. The finer size of SF also helps to improve Interfacial Transition Zone (ITZ) between the aggregates and cement paste with up to 10% SF replacement (Shannag, 2000). Beyond 10% replacement, due to the non-uniform dispersion of fine particles of SF, resulting in weak zones in the NFC mix decreased the strength (Karthikeyan and Dhinakaran, 2018).

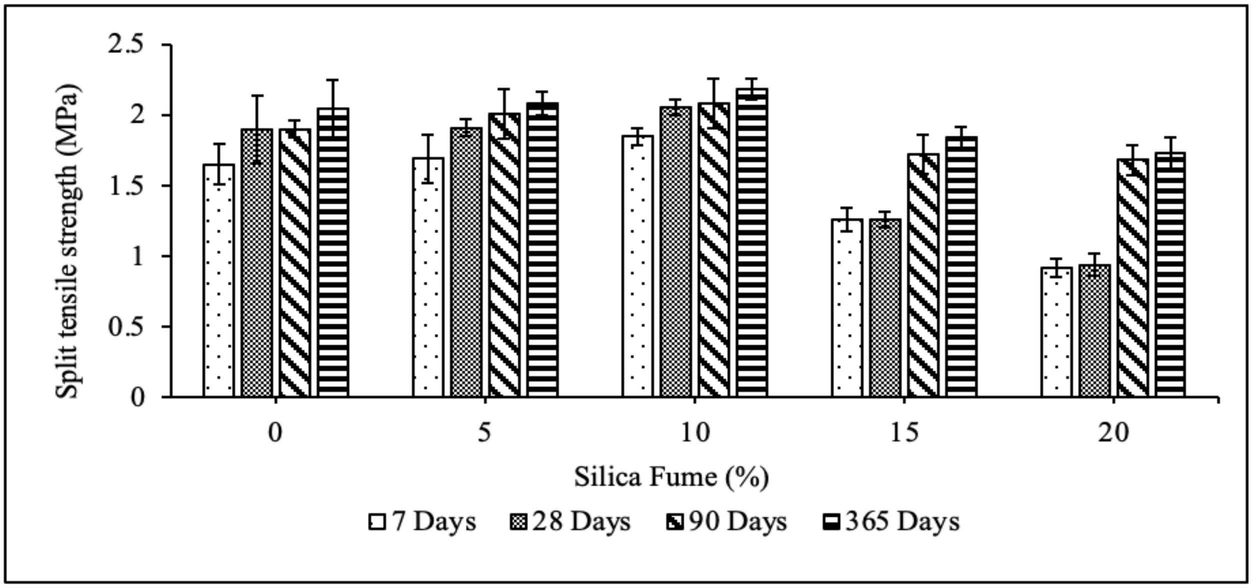

Figure 4.8. Split tensile strength of NFC using SF

Effect of replacement by rice husk ash (RHA)

The split tensile strength of the NFC comprising RHA at different percentage replacement levels of cement at 7, 28, 90, and 365-day were shown in Figure 4.9. when replacing cement with RHA, the split tensile strength decreased continuously as the percentage replacement level increased from 0 to 20%, and similar results were reported by (Padhi et al. 2018). The split tensile strength decreased by 35%, 16%, and 2% at 7, 28, 90-day at 5% replacement level. At 7-day of control mix (1.65 MPa), the strength decreased by 35.15%, 36.97%, 40%, and 58.79% at 5%, 10%, 15%, and 20% replacement of RHA. At 28-day, the strength decreased by 15.79%, 44.74%, 47.89%, and 62.10% at 5%, 10%, 15%, and 20% replacement of RHA as compared to reference mix (1.90 MPa). Similarly at 90-day of control mix (1.90 MPa), the strength decreased by 2.10%, 6.32%, 26.84%, and 56.84% at 5%, 10%, 15%, and 20% replacement of RHA. At 365-day, the strength decreased by 6.86%, 12.52%, 19.60%, and 31.86% at 5%, 10%, 15%, and 20% replacement of RHA as compared to reference mix (2.04 MPa). Increasing the percentage replacement of RHA further decreased the strength due to the non-uniform distribution of RHA and the porous nature, which weakened the concrete matrix (Le et al., 2014).

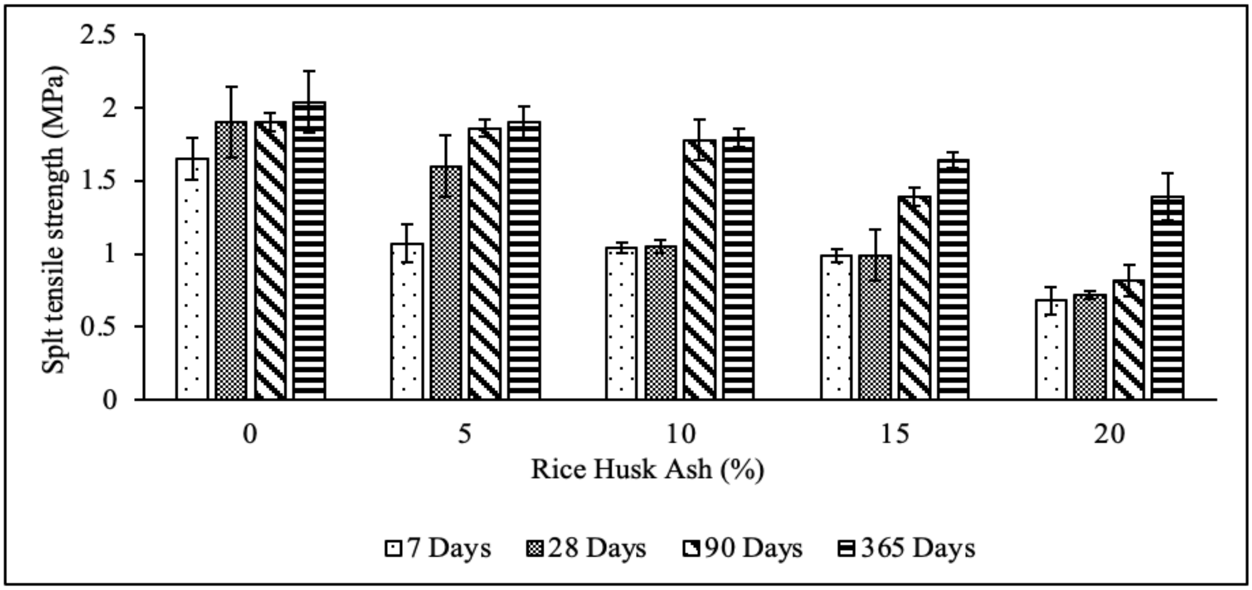

Figure 4.9. Split tensile strength of NFC using RHA

Effect of different gradation of coarse aggregates

The split tensile strength of the NFC mixes comprising different gradations with single-size natural coarse aggregates at different curing ages was presented in Figure 4.10. It was noticed that the split tensile strength of NFC mixes increased with increasing size of aggregates along with the increasing age of curing. The split tensile strength of NFC-4.75, NFC-6.3, NFC-8, and NFC-9.5 mixes is 0.75 MPa, 0.71 MPa, 0.68 MPa, and 0.65 MPa respectively at 28-day. The highest percentage increase in split tensile strength was 15.38 % at 28-day and 17.33 % at 365-day of curing for NFC-4.75 compared to the NFC-9.5 mix. Comparable results have been previously reported by (Elango and Revathi, 2017; Fu et al., 2014; Huang et al., 2010; Lian and Zhuge, 2010; Wu et al., 2011). The NFC mix prepared with smaller-sized aggregates shows better split tensile strength than the NFC mixes made with larger ones. This can be ascribed to the non-uniformity of the paste material and crack propagation taking place along with the weakest link in mixes prepared with larger-sized aggregates (Fu et al., 2014). Therefore, the compact size of smaller aggregate resists the initial crack at the loading surface, improving the bond strength and contact area between the aggregates and cement (Deo and Neithalath, 2011; Elango and Revathi, 2017; Yang and Jiang, 2003). Hence, the smaller-sized aggregates are more effective in NFC mixes and provide more strength than mixes with larger aggregates.

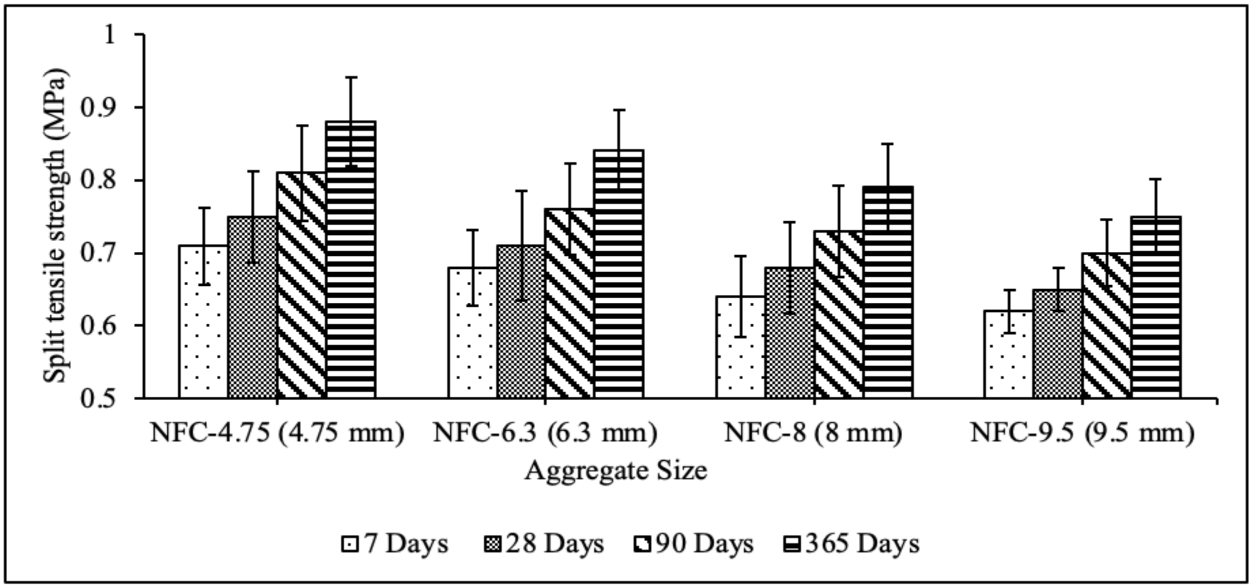

Figure 4.10. Split tensile strength of NFC mixes with different gradations of coarse aggregate

4.2.3 Flexural Strength

Effect of replacement by fly ash (FA)

The flexural strength result of NFC containing FA at different replacement levels of cement at 7, 28, 90, and 365-day of curing was presented in Figure 4.11. on replacing cement with FA, a decrease in flexural strength of 10.37%, 17.22%, 29.63%, 33.70% at 7-day of control mix (2.70 MPa) and 1.98%, 3.61%, 10.28%, and 19.13% at 28-day as compared to control mix (2.77 MPa) with 5, 10, 15, and 20% replacement level of FA was observed (Figure 4.11). The strength decrease was due to the lower pozzolanic reaction of FA at an early age (Park et al., 2009; Sata et al., 2016). But at 90-day, the strength increased by 2.67%, 4.80%, 10.14%, and 11.74% at 5, 10, 15, and 20% replacement level of FA of control mix (2.81 MPa), respectively. Similarly at 365-day of control mix (3.50 MPa), the flexural strength increased by 2.67%, 6.10%, 9.24%, and 10.29% at 5%, 10%, 15%, and 20% replacement of FA. With the addition of FA, the rate of hydration decreases, resulting in a slower rate of hardening and lesser strength of NFC at an early age. However, due to finesses and improved pozzolanic reactivity of FA with hydration products of cement, the later age strength improves at 90 and 365-day.

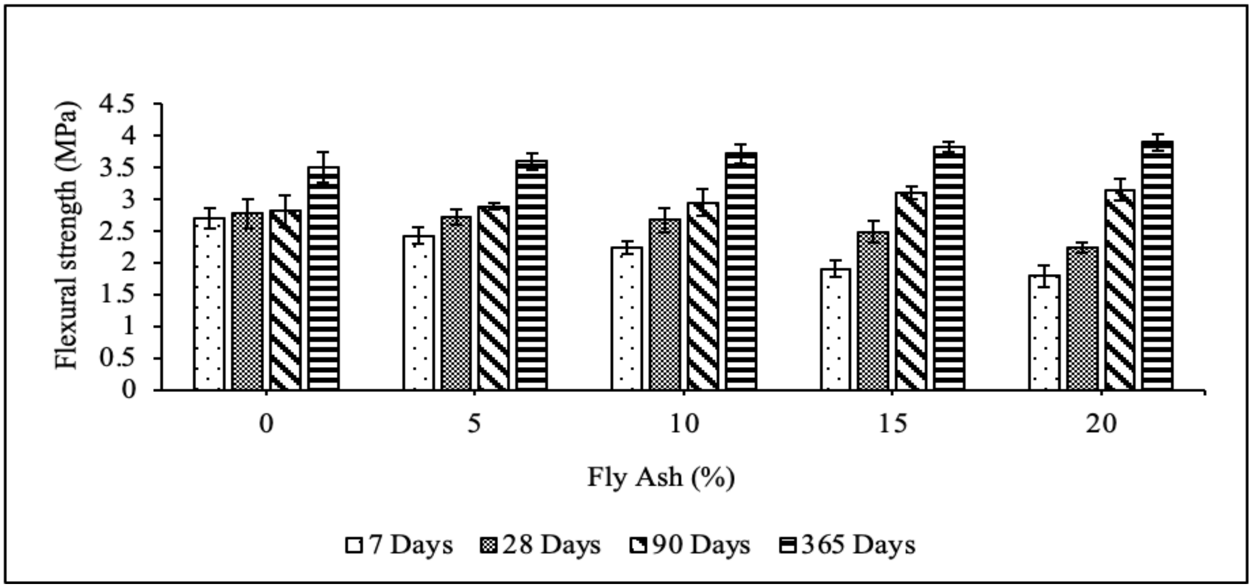

Figure 4.11. Flexural strength of NFC containing FA

Effect of replacement by metakaolin (MK)

The flexural strength result of NFC containing MK at different replacement levels of cement at 7, 28, 90, and 365-day of curing was presented in Figure 4.12. It has been observed that on increasing the replacement level of MK, flexural strength increases in comparison to the control NFC mix. At 7-day, the strength increased by 2.96%, 5.74%, 7.41%, and 9.44% at 5%, 10%, 15%, and 20% replacement of MK. A strength increases of 6.13%, 11.73%, 17.51%, and 22.92% at 28-day and 9.43%, 13.70%, 19.22%, and 22.91% with 90-day was observed at 5, 10, 15, and 20% replacement levels of MK respectively in NFC mixes. Similarly, at 365-day, strength increased by 3.14%, 6.95%, 10.29%, and 13.81% at 5%, 10%, 15%, and 20% replacement of MK. Metakaolin particles help refine the inter-transition zone due to finer size and higher reactivity than cement, which leads to improved flexural strength (Khatib and Hibbert, 2005).

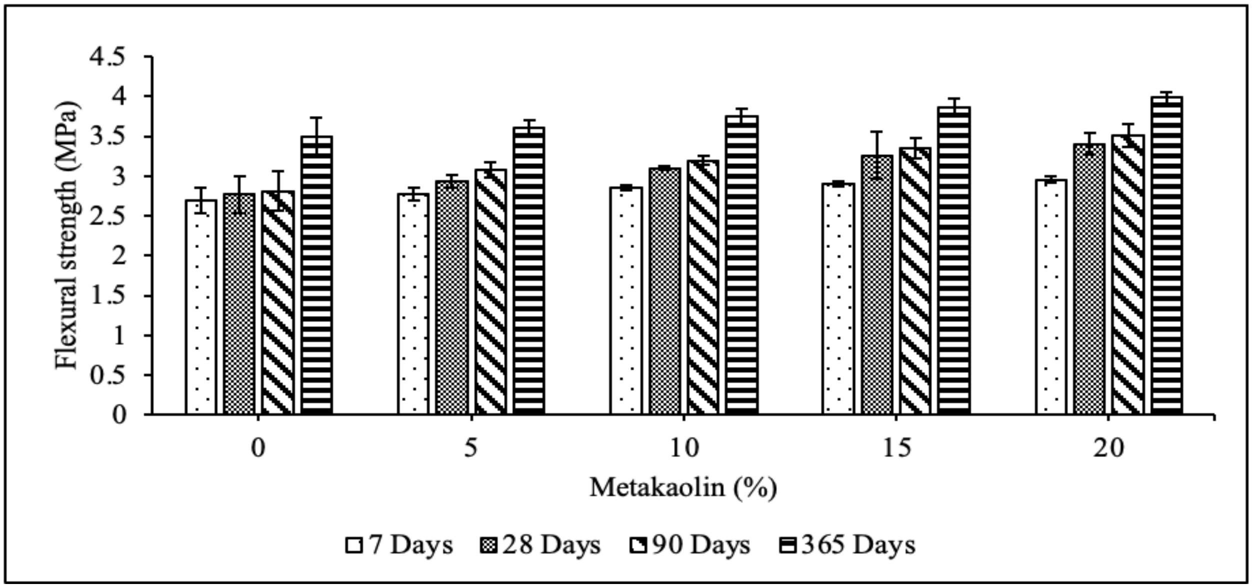

Figure 4.12. Flexural strength of NFC containing MK

Effect of replacement by silica fume (SF)

The flexural strength result of NFC containing SF at different replacement levels of cement at 7, 28, 90, and 365-day of curing was presented in Figure 4.13. Similar results were found in flexural testing of NFC containing SF as SCMs as split tensile strength. The flexural strength increases by 7.77%, 14%, and 28% at 7, 28, and 90-day with 10% replacement compared to the control mix, but beyond 10% replacement, flexural strength decreased. At 7-day, the strength increased by 6.67% and 7.78% at 5% and 10% replacement of SF, but at 15% and 20%, the strength decreased by 10.74% and 14.44%, respectively. At 28-day, the flexural strength increased by 7.58% and 14.40% at 5% and 10% replacement of SF but decreased by 2.17% and 4.33% at 15% and 20% replacement. Similarly, at 90-day, at 5% and 10% replacement of SF, the strength increased by 10.68% and 28.11%, but at 15% and 20%, the strength decreased by 1.07% and 3.56%. At 365-day, the strength increased by 12.29%, 15.43%, 8.29%, and 0.57% at 5%, 10%, 15% and 20% replacement of SF as compared to control mix (3.50 MPa). A large amount of reactive amorphous silica in SF and its fineness improves the rate of pozzolanic reaction with calcium hydroxide formed during cement hydration. The finer size of SF also helps to improve Interfacial Transition Zone (ITZ) between the aggregates and cement paste (Shannag, 2000).

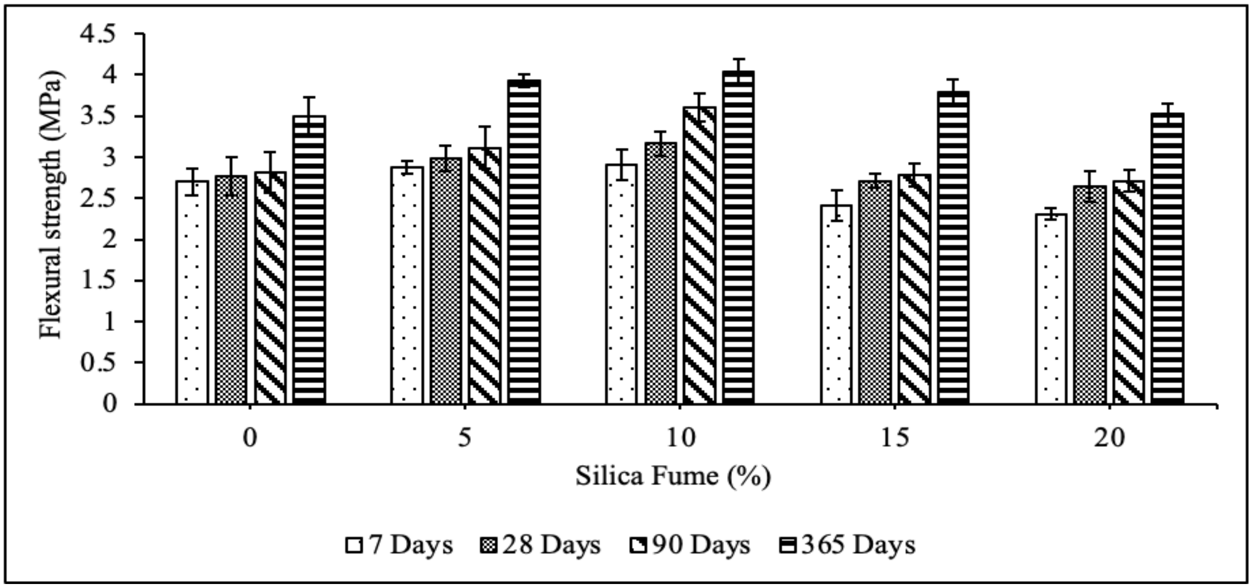

Figure 4.13. Flexural strength of NFC containing SF

Effect of replacement by rice husk ash (RHA)

The flexural strength result of NFC containing RHA at different replacement levels of cement at 7, 28, 90, and 365-day of curing was presented in Figure 4.14. The flexural strength decreased by 2.52%, 13.35%, 24.18%, and 32.13% as the percentage replacement increased from 5 to 20% in increments of 5% at 28-day. Similar results were obtained at 90-day (3.55%, 12.81%, 21.7%, 29.89% decrease) with increasing replacement of RHA. At 365-day, the strength decreased by 6.28%, 3.66%, 6.96%, and 14.97% at 5%, 10%, 15%, and 20% replacement of RHA. The results of flexural strength followed similar trends as split tensile strength. The non-uniform distribution of RHA and the porous nature of the concrete matrix reduced the concrete matrix as the percentage replacement of RHA was increased (Le et al., 2014). The inclusion of unreactive silica in the concrete mix, which does not participate in the pozzolanic cement hydration reaction, was also attributed to the lower strength.

Hence, the flexural strength results and split tensile strength results closely follow compressive strength results indicating that increasing the replacement level of MK from 15-20% and with FA up to 20% with cement in NFC mixes is a significant improvement in strength is observed. The most important property for designing concrete material for pavement applications is its compressive strength. By adding SCMs, the compressive strength increases by 39-46% with MK (15-20%) and 3.09% with FA at replacement of 20%. The addition of SF in NFC can be beneficial up to 10% replacement for improved flexural strength, whereas with RHA replacement, no significant change in split tensile strength or flexure strength is obtained, and an optimal replacement of 5% RHA is advantageous with a significant increase in compressive strength. This indicates that NFC made with Supplementary Cementitious Materials like MK, FA, and SF in small proportions would result in NFC with increased compressive, flexural, and split tensile strength, which makes NFC more suitable for pavements in surface course layers in low as well as medium volumes traffic roads as in residential areas, sidewalks, and parking lots, running tracks, etc. Pavement design for parking lots, pedestrian trails, walkways requires adequate flexure strength, a more important parameter than compressive strength (Shen et al., 2013). The results from the experiment showed that NFC mix containing SCMs like MK, FA, SF, and RHA satisfies the minimum strength criteria for flexural strength in NFC pavements (ACI 522R 2010; (NRMCA) 2004). This conclusion was well corroborated by microstructural analysis in the form of SEM, EDS, and XRD images of control mix and various NFC mixes, as discussed in the following section.

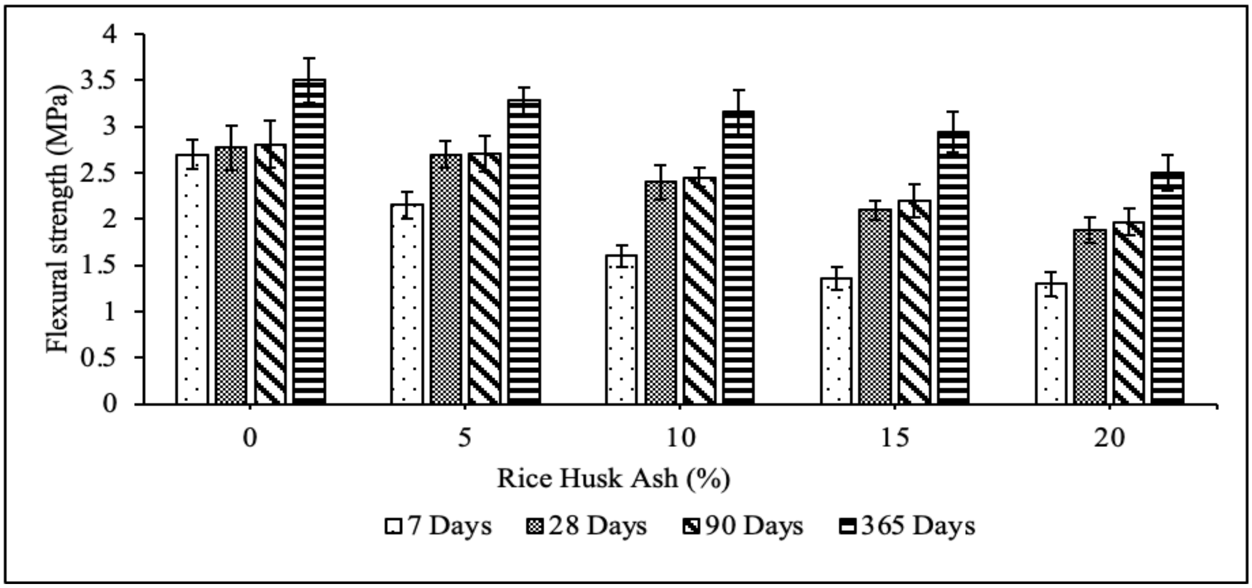

Figure 4.14. Flexural strength of NFC containing RHA

Effect of different gradation of coarse aggregates

The flexural strength at 7, 28, 90, and 365-day of different NFC mixes consisting of different single-size natural coarse aggregates is illustrated in Figure 4.15. The flexural strength value for NFC-4.75, NFC-6.3, NFC-8, and NFC-9.5 aggregate size concrete was 1.57 MPa, 1.51 MPa, 1.45 MPa, and 1.37 MPa, respectively, at 28-day the age of curing. The percentage increase in flexural strength was 14.59 % in the NFC-4.75 mix at 28-day and 16.56 % at 365-day of curing compared to the NFC-9.5 mix. The above results relate well to the findings of (Fu et al., 2014; Wu et al., 2011). The trends of flexural strength were similar to compressive and split tensile strength results of NFC mixes with different aggregates sizes such that the smaller size aggregates perform better than larger sized aggregates in NFC mixes. The reason for the above results was that by using smaller-sized aggregates, the number of aggregate particles per unit volume of concrete increases leading to a higher surface area of aggregates providing more binding area for cement mix, hence, increasing the strength of the NFC mixes (Fu et al., 2014; Wu et al., 2011; Yang and Jiang, 2003).

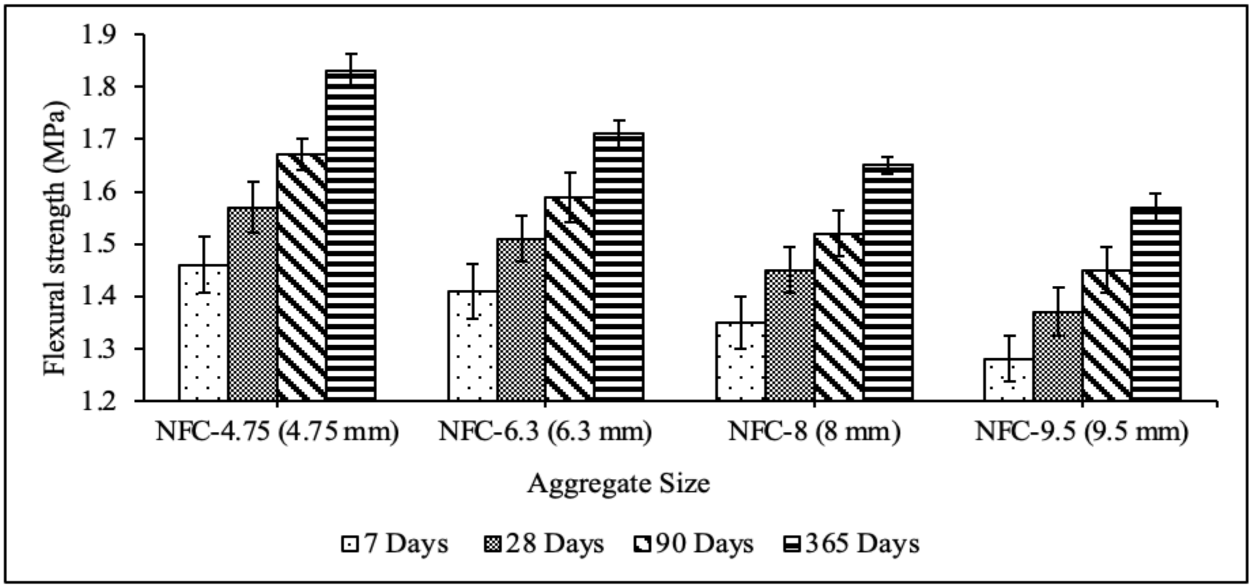

Figure 4.15. Flexural strength of NFC mixes with different gradations of coarse aggregates

4.2.4 Abrasion Resistance

In the abrasion test, the samples were examined after subjecting them to 500 revolutions to demonstrate the percentage mass loss. Abrasion resistance test is an efficient test to evaluate the performance of no-fines concrete for pavement applications, especially in low-medium traffic conditions as in parking lots, decks of swimming pool, tennis courts, zoo areas, sidewalks, etc. (ACI Committee 522, 2010). To resist the skidding, breaking friction, and sliding of vehicles, the rough surface of the NFC pavements is appropriate, and a higher abrasion resistance value means preferable pavement concrete. From Figure 4.16 (b), it can be observed that the edges of the cylindrical specimen have become rounded, and its shape has changed to spherical.

Figure 4.16. (a) NFC specimens before abrasion test and (b) NFC specimens after abrasion test

Effect of replacement by fly ash (FA)

The abrasion resistance test of NFC mix containing FA at 7 and 28-day was shown in Table 4.1. The abrasion resistance in terms of mass loss was determined at the age of 7-day and 28-day. As the FA replacement increased, the percentage mass loss decreased, and the abrasion resistance increased. The percentage mass loss decreased from 36% (control mix) to 25% at 7-day and from 31% (control mix) to 20% at 28-day for 5% to 20% replacement of FA. Similar findings were reported by (Sata et al., 2016; Woo et al., 2011; Yen et al., 2007). This can be attributed to the pozzolanic activity and filler effect of FA, resulting in increased abrasion resistance (Siddique and Khatib, 2010).

Table 4.1. Abrasion results of NFC mix using FA

Mix	**Mass loss in FA samples (%)**	
	7-day	**28-day**
NFC-0	36	31
NFC-5	34	27
NFC-10	32	25
NFC-15	29	22
NFC-20	25	20

Effect of replacement by metakaolin (MK)

The abrasion resistance test of NFC mix containing MK at 7 and 28-day was presented in Table 4.2. It was observed that with increasing replacement level of MK, percentage mass loss decreased compared to the control mix. The percentage mass loss decreased from 33% to 23% for 5 to 20% replacement level of MK respectively at 7-day. Similarly, at 28-day, the percentage mass loss decreased from 29% to 20% for the 5 to 20% replacement level of MK compared to the control mix. This can be explained by MK proving beneficial for internal structure, making it denser (Rashad, 2013).

Table 4.2. Abrasion results of NFC mix using MK

Mix	**Mass loss in MK samples (%)**	
	7-day	**28-day**
NFC-0	36	31
NFC-5	33	29
NFC-10	31	26
NFC-15	26	24
NFC-20	23	20

Effect of replacement by silica fume (SF)

The abrasion resistance property of NFC mix with SF incorporation at 7 and 28-day was listed in Table 4.3. It was observed that up to 10% replacement with SF, abrasion resistance was comparable with that of control mix, but beyond 10%, the abrasion resistance was affected adversely, as indicated by the significant increase in percentage mass loss.

Table 4.3. Abrasion results of NFC mix using SF

Mix	**Mass loss in SF samples (%)**	
	7-day	**28-day**
NFC-0	36	31
NFC-5	39	38
NFC-10	37	30
NFC-15	47	40
NFC-20	49	46

Effect of replacement by rice husk ash (RHA)

NFC mixes containing RHA, percentage mass loss consistently increased with increasing replacement increased with RHA, causing a decrease in abrasion resistance was represented in Table 4.4. This was probably due to the non-uniform dispersion of ash, which reduces the degree of compaction, resulting in the presence of voids. Concrete`s abrasion resistance is relative to its compressive strength (Li et al., 2006; Siddique et al., 2016). Optimal replacement of cement in NFC with 5% RHA and 10% SF gave encouraging results in terms of strength.

Table 4.4. Abrasion results of NFC mix using RHA

Mix	**Mass loss in RHA samples (%)**	
	7-day	**28-day**
NFC-0	36	31
NFC-5	43	40
NFC-10	44	43
NFC-15	44	43
NFC-20	47	46

Effect of different gradation of coarse aggregates

The abrasion resistance of NFC mixes with the different gradation sizes of coarse aggregates at 7 and 28-day was shown in Table 4.5. The results show that the weight loss was more in 9.5 mm size aggregate concrete than the 4.75 mm size aggregate concrete. Similar results were reported by (Elango and Revathi, 2017; Wu et al., 2011). The abrasion resistance seemed to be directly related to the compressive strength of concrete as they followed a similar trend (Elango and Revathi, 2017; Li et al., 2006; Siddique et al., 2016). Results specify that higher compressive strength achieved by using smaller-sized aggregates was a significant factor in influencing the abrasion resistance of concrete. The use of smaller-sized aggregates in NFC resulted in higher strength due to increased surface area for the cement to cover the aggregates and higher packing efficiency, making the NFC denser and compact, leading to lower weight loss (Sata et al., 2016).

Table 4.5. Abrasion results of NFC mix with different gradations of coarse aggregates

Name of concrete mix	Mass loss (kg) = original mass-final mass		Mass loss (%)	
	7-day	28-day	7-day	28-day
NFC-4.75	3.420	3.466	40	38
NFC-6.3	4.426	3.938	48	45
NFC-8	4.732	4.278	55	49
NFC-9.5	5.182	4.848	59	55

From the above results, it can be concluded that NFC made with smaller-sized aggregates (NFC-4.75) showed better performance in strength properties and abrasion resistance than NFC-9.5. The increased strength of smaller-sized aggregates enhances the applicability of NFC for vast infrastructural applications such as parking lots, walkways, surface courses for tennis courts and parks. The low traffic pavement requires adequate flexural strength, a more significant parameter than compressive strength (Shen et al., 2013). NFC prepared using different was indeed able to satisfy the flexure strength criteria. The smaller-sized aggregates also showed higher abrasion resistance which is preferable for pavement concrete. The above results from the experiments show that NFC can fulfill the minimum strength criteria for pavements and can be a viable option for pavement construction based on strength characteristics (ACI Committee 522, 2010; National Ready Mixed Concrete Association, 2004) for applications in low-medium traffic applications as specified above.

4.3 PERMEATION PROPERTIES

4.3.1 Water Permeability

Water permeability is the most important property to determine the field performance of NFC in terms of their capability to drain stormwater runoff. The future permeability performance is mainly dependent on the water permeability of the NFC.

Effect of replacement by fly ash (FA)

The results of the water permeability test of NFC comprising FA at varying percentage replacement levels of cement at 7, 28, 90, and 365-day were shown in Figure 4.17. On replacing cement with an increasing percentage of FA in NFC, the strength of the mixes decreased, whereas water permeability increased. The water permeability values of control mix were 0.70 cm/s at 7-day, 0.44 cm/s at 28-day, 0.32 cm/s at 90-day, and 0.30 cm/s at 365-day of curing. The water permeability results of NFC at 7-day were in the ranges of 0.37 cm/s to 0.54 cm/s for 5% to 20%, whereas at 28-day, permeability values were in the ranges of 0.44 cm/s to 0.55 cm/s. Similarly, at 90-day, the permeability was between 0.32 cm/s to 0.51 cm/s. At 365-day, the water permeability values were in the range of 0.29 cm/s to 0.66 cm/s for 5% to 20% replacement of FA. From the results, it was found that water permeability decreases at 7-day at all replacement levels of FA, but after 7-day, the water permeability values increase as the percentage replacement increases from 5% to 20% for an increment of 5%. This was because water permeability was related to pore size distribution, presence of continuous voids, and pore roughness, and FA addition helped improve the factors mentioned above (Sata et al., 2016). Water permeability values fall within the recommended values of 0.14 cm/s to 1.22 cm/s as suggested by ACI 522R (ACI Committee 522, 2010) for NFC to be used in pavements for drainage purposes (Bhutta et al., 2012; Lang et al., 2019; Nguyen et al., 2013).

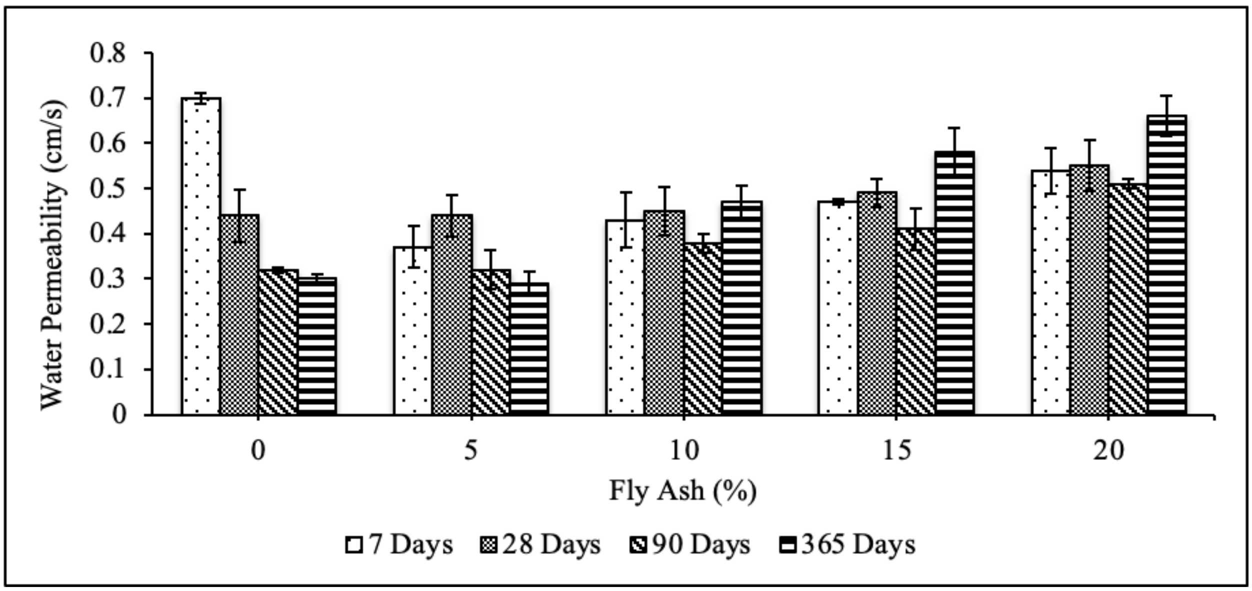

Figure 4.17. Water permeability of NFC containing FA

Effect of replacement by metakaolin (MK)

The results of the water permeability test of NFC comprising MK at varying percentage replacement levels of cement at 7, 28, 90, and 365-day were presented in Figure 4.18. It has been observed that as the percentage replacement level of MK increases from 5-20%, water permeability decreases at different curing days. Water permeability reduced from 0.70 cm/s (reference mix) to 0.39 cm/s at 7day, from 0.44 cm/s (reference mix) to 0.34 cm/s for 28-day, and from 0.32 cm/s (reference mix) to 0.25 cm/s at 90-day at different percentage replacement of MK. Similarly, at 365-day, the water permeability values decreased from 0.30 cm/s (reference mix) to 0.20 cm/s (Figure 4.17), which falls well within the recommended values of 0.14 cm/s to 1.22 cm/s as suggested by ACI 522R (ACI Committee 522, 2010) for NFC for drainage purposes (Bhutta et al., 2012; Lang et al., 2019; Nguyen et al., 2013). This was due to the densification of mixes with increased C-S-H gel formation, pore reduction, and transition zone thickness with increasing content of MK in NFC mixes.

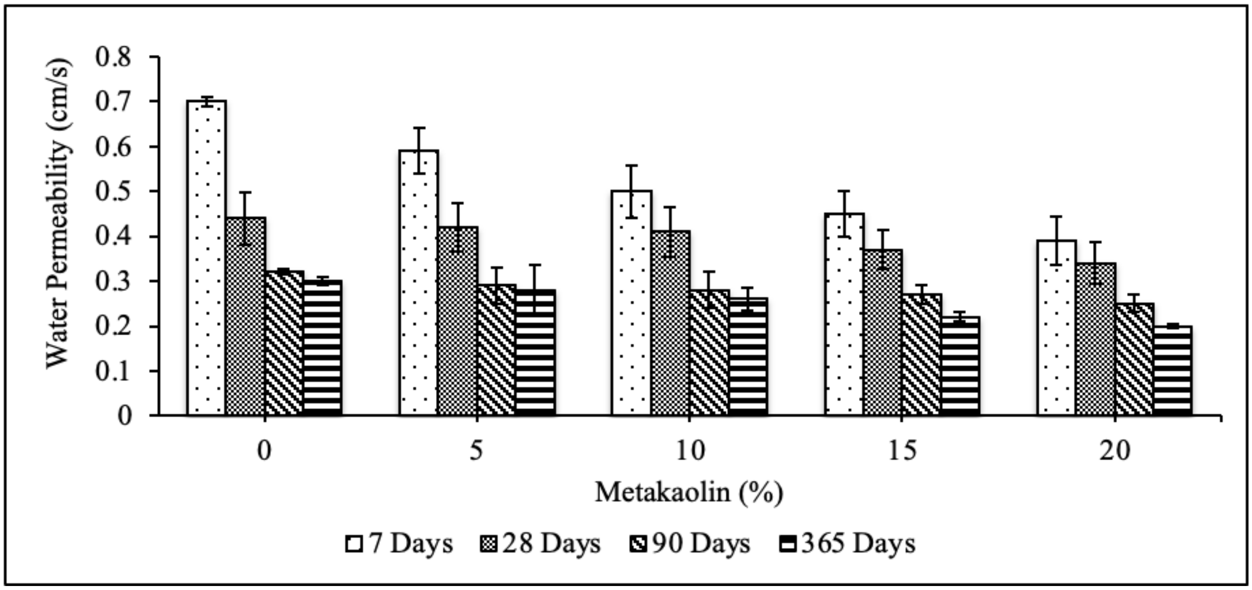

Figure 4.18. Water permeability of NFC containing MK

Effect of replacement by silica fume (SF)

The water permeability test results of NFC with SF at different percentage replacement levels of cement at 7, 28, 90, and 365-day were represented in Figure 4.19. It was observed that permeability decreased by as much as 5% and then increased with increasing replacement levels at each curing age. At proposed optimum level of 10% replacement, water permeability reduced from approximately 0.7 cm/s (control mix) to 0.68 cm/s at 7-day, 0.44 cm/s (control mix) to 0.41 cm/s of SF at 28-day, 0.32 cm/s (control mix) to 0.31 cm/s at 90-day, 0.30 cm/s (control mix) to 0.28 cm/s at 365-day, which is quite suitable for drainage purposes in NFC (Bhutta et al., 2012; Grubeša et al., 2018; Lang et al., 2019; Nguyen et al., 2013).

The water permeability result trends were opposite to the strength results due to the pore-size refinement and matrix densification, reduction in calcium hydroxide content, and cement paste aggregate interfacial refinement. Water permeability at 7-day was relatively higher at 28, 90, and 365-day as shown in Figure 4.19. At higher SF replacement levels of 15% and 20%, the permeability improved marginally compared with that of the control mix but the overall compressive, flexural, and split strengths were compromised at higher SF levels, which is undesirable.

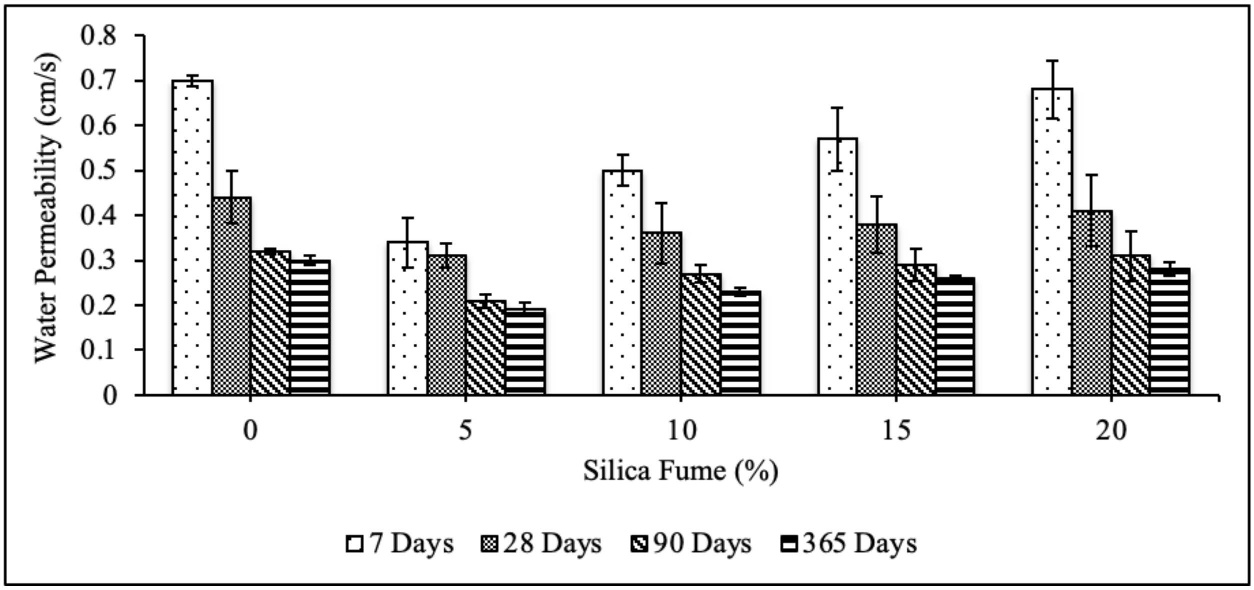

Figure 4.19. Water permeability of NFC containing SF

Effect of replacement by rice husk ash (RHA)

The water permeability test results of NFC with RHA at different percentage replacement levels of cement at 7, 28, 90, and 365-day were shown in Figure 4.20. The water permeability of NFC mixes containing RHA continuously decreased as the percentage replacement level increased. The value of permeability was roughly between 0.7 cm/s-0.07 cm/s at 7-day, 0.44 cm/s-0.06 cm/s at 28-day, 0.32 cm/s-0.02 cm/s at 90-day, and 0.30 cm/s-0.02 cm/s at 365-day at 5%-20% replacement levels. From the results, it was observed that the values of water permeability decreased at all the percentage replacement of RHA increased at all curing ages. This was due to the contraction in the thickness of the transition zone with increasing RHA content and finer RHA particles that improve the particle packing density of the resulting NFC.

Hence, it can be concluded that water permeability, in general, marginally reduces with optimum FA (5%), MK (20%), SF (10%), and RHA (5%) replacement level, but the permeability of resulting NFC mixes is well within the values appropriate as recommended the range of 0.14 cm/s to 1.22 cm/s by ACI Committee 522 (ACI Committee 522, 2010, 2006) for the drainage purposes in pavements utilizing NFC.

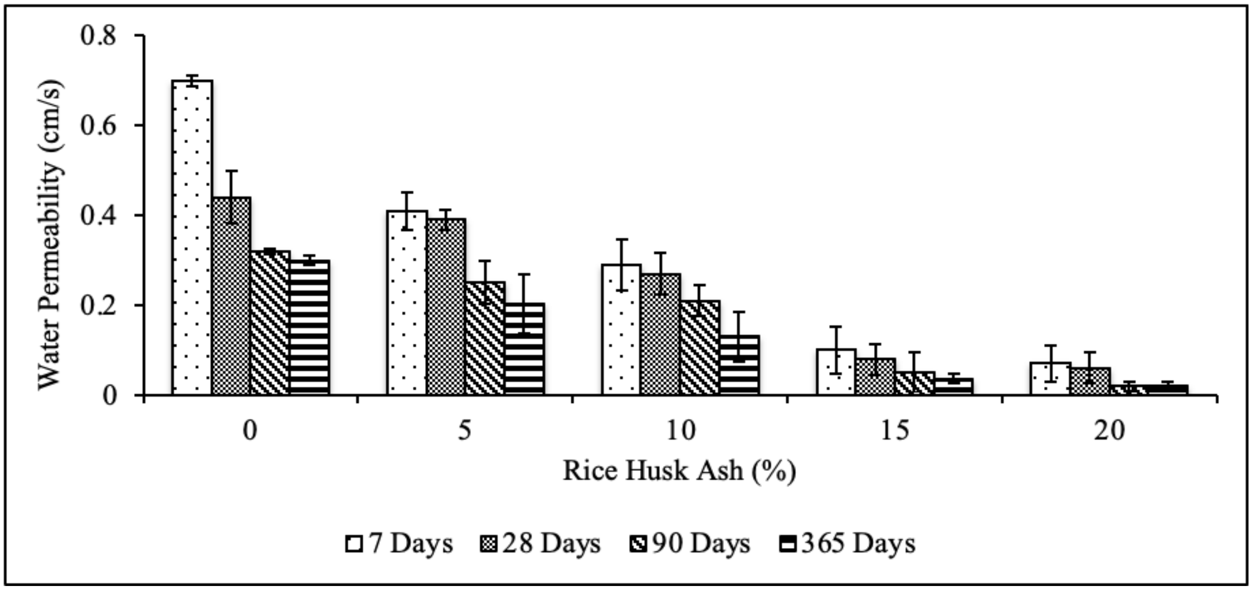

Figure 4.20. Water permeability of NFC containing RHA

Effect of different gradation of coarse aggregates

The important property for assessing the field performance of NFC in terms of its ability to drain stormwater runoff is water permeability. The permeation properties are mainly dependent on the water permeability of NFC. The test results of water permeability of different NFC mixes utilizing different single-sized aggregates at 7, 28, 90, and 365-day were shown in Figure 4.21. It has been observed from the results that the water permeability increased with the increase in aggregate size in NFC mixes at different ages of curing. The value of water permeability of NFC with aggregate size of NFC-9.5, NFC-8, NFC-6.3, NFC-4.75 is 1.97 cm/s, 1.6 cm/s, 1.27 cm/s and 0.98 cm/s respectively at 28-day, which is sufficient enough for the purposes of drainage in NFC (Elango and Revathi, 2017; Fu et al., 2014; Jain et al., 2011). The recommended values of 0.14 to 1.22 cm/s as suggested by ACI 522R (ACI Committee 522, 2010). Various researchers (Elango and Revathi, 2017; Fu et al., 2014; Jain et al., 2011; Maguesvari and Narasimha, 2013; Mrakovčić et al., 2014) reported similar results. The rate of flow of water from the NFC is more affected by pore sizes than the total porosity in the concrete section. NFC prepared with the larger aggregate size formed larger pores in size, which causes an increase in their water permeability (Elango and Revathi, 2017; Fu et al., 2014; Maguesvari and Narasimha, 2013). Water permeability values are well within the acceptable limits vis-à-vis drainage in pavement applications when small-sized

4.75 mm aggregates are used. The increased structural and acceptable drainage aspects were well taken care of when no-fine concrete was prepared using small-sized aggregates.

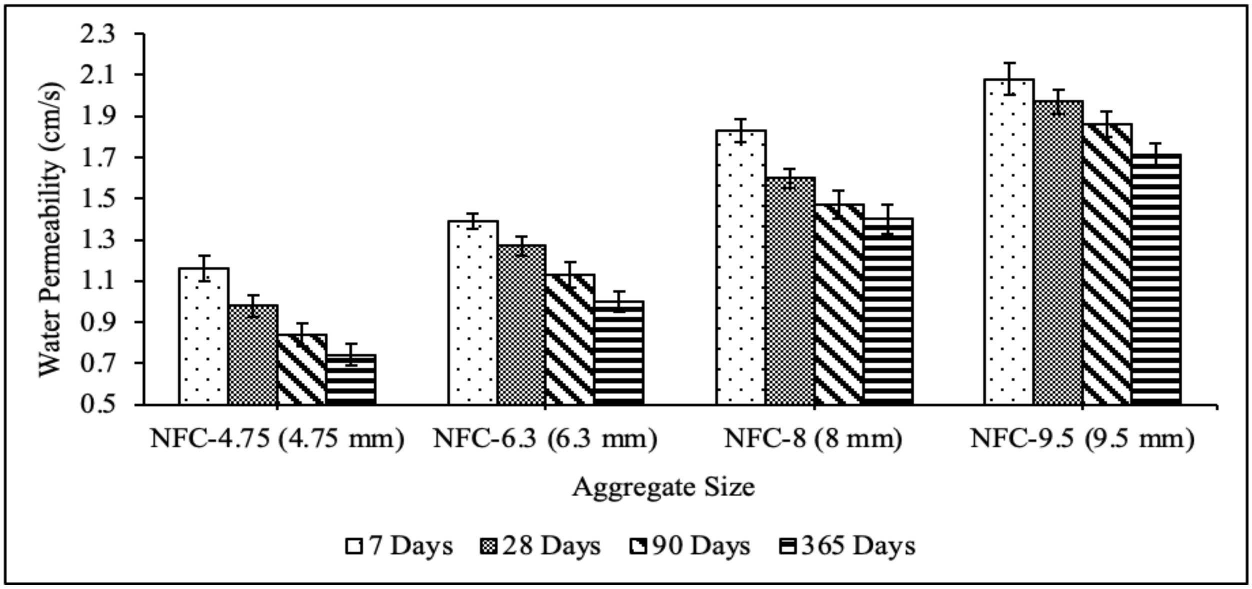

Figure 4.21. Water permeability of NFC mixes with different gradations of coarse aggregates

4.3.2 Porosity

Effect of replacement by fly ash (FA)

The porosity of NFC mixes prepared using an increasing percentage of FA at 7, 28, 90, and 365-day was illustrated in Figure 4.22. The porosity of NFC mixes with increasing FA content shows similar increasing trends as in water permeability tests. The porosity values decreased up to 5% replacement level of FA, but beyond 5%, the values increased. The porosity values were 18.15%, 18.40%, 18.50%, and 18.62% at 5%, 10%, 15, and 20% replacement of FA. At 28-day, the values of porosity were 17.56%, 17.67%, 17.8%, and 18.1% at 5%-20% replacement of FA. The porosity values were 17.35%, 17.51%, 17.59%, and 17.83% at different replacement of FA at 90-day. Similarly at 365-day, the porosity values were 17.27%, 17.38%, 17.53%, and 17.74% at 5%, 10%, 15%, and 20% replacement of FA. The average porosity values lie in the range of 17.5-18.5 % with FA replacement at 7, 28, 90, and 365-day of curing, which is sufficient for better drainage purposes in the pavement made of NFC (Hesami et al., 2014) and lies within the acceptable range of porosity of 15 to 35% for NFC as per ACI (ACI Committee 522, 2010).

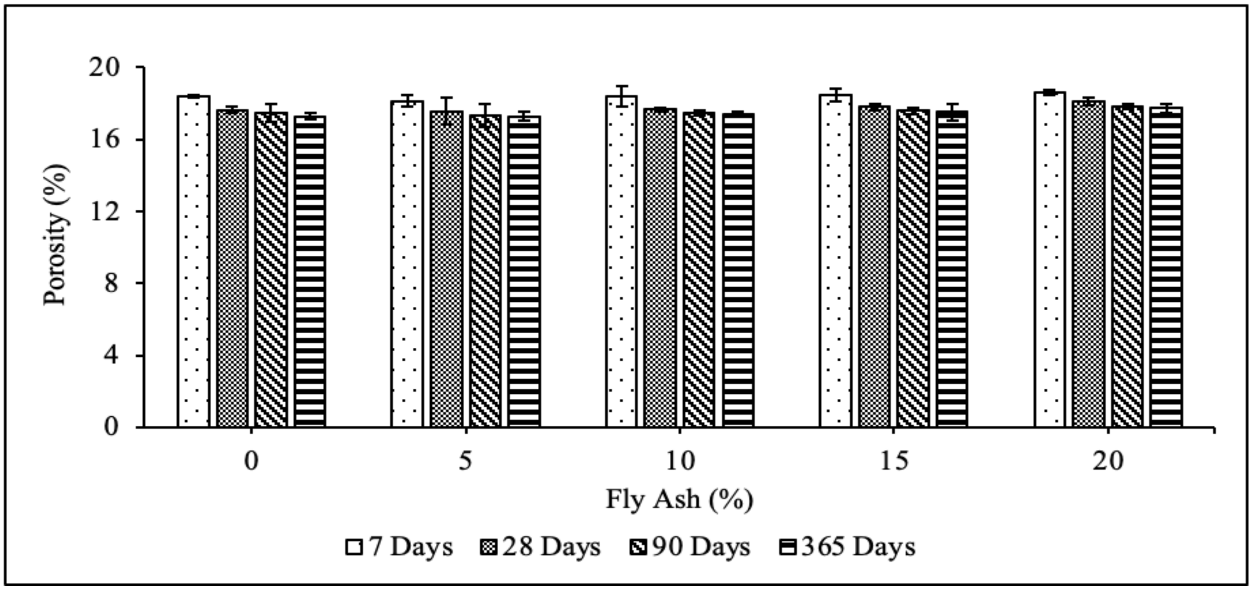

Figure 4.22. Porosity of NFC containing FA

Effect of replacement by metakaolin (MK)

The porosity of NFC mixes prepared using an increasing percentage of MK at 7, 28, 90, and 365-day was presented in Figure 4.23. The trend observed was similar to water permeability results since they directly relate to each other (ACI Committee 522, 2006). The porosity value decreased with an increase in the percentage replacement level of MK. The values of porosity were 18.15%, 18.1%, 17.8%, and 17.16% at 5%, 10%, 15%, and 20% replacement of MK at 7-day of curing. At 28-day, the values were 17.55%, 17.35%, 17.13%, and 16.83% at 5%-20% replacement of MK. Similarly at 90-day, the porosity values were 17.3%, 17.2%, 17.05%, and 16.6%, and at 365-day, the porosity values were 16.94%, 16.75%, 16.34%, and 16.15% at 5%-20% replacement of MK. The observed average porosity values were in the range of 16.6 to 18.4%, and the values are well within the recommended ranges of 15 to 35% as recommended by ACI (ACI Committee 522, 2010), which is sufficient for drainage purposes in pavements made with NFC (Hesami et al., 2014). It has been observed that porosity at 7-day is higher than that at 28 and 90-day, respectively, in the NFC mixes.

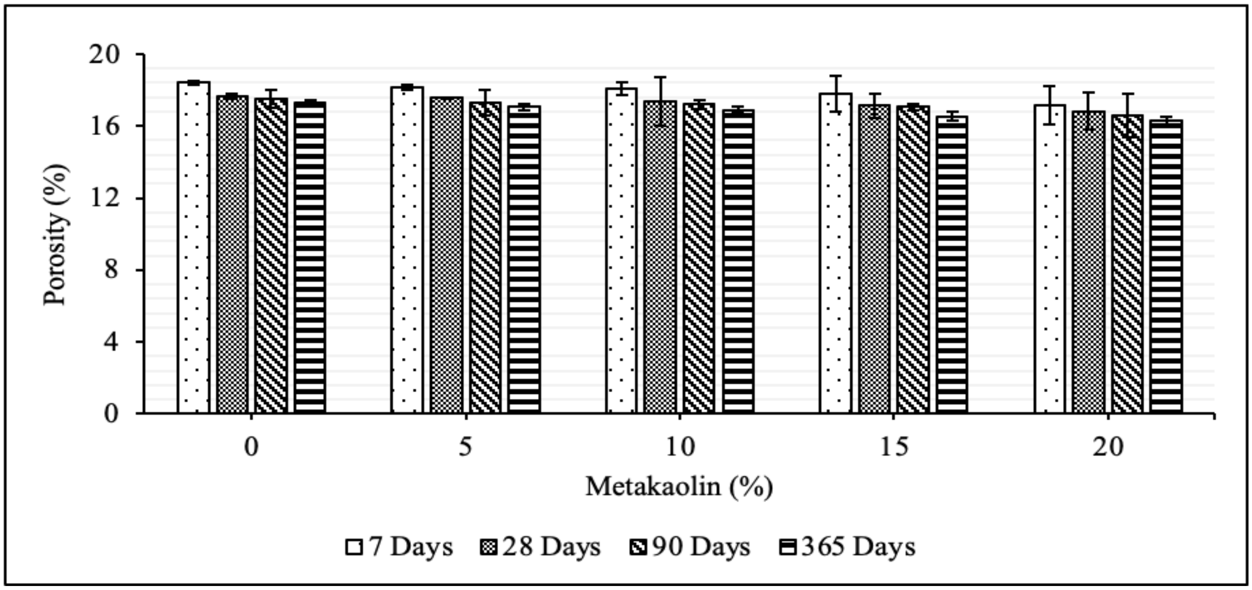

Figure 4.23. Porosity of NFC containing MK

Effect of replacement by silica fume (SF)

The porosity of NFC mixes containing SF at different percentage replacement levels of cement at 7, 28, 90, and 365-day was shown in Figure 4.24. The porosity results followed a similar trend as those of water permeability results. An increase in porosity indicates more voided space which increases the permeation of water in NFC (Grubeša et al., 2018). Both permeability and porosity decrease up to 5% SF replacement, and the trend reversed for SF replacement above 5%, with the values of porosity increasing up to 20% replacement with SF in the NFC mix. The porosity values were 17.85%, 17.95%, 18.05%, and 18.2% at 5%, 10%, 15%, and 20% replacement of SF at 7-day. At 28-day, the values were 16.5%, 16.95%, 17.1%, and 17.37% at 5%-20% replacement. Similarly at 90-day, the porosity values were 16%, 16.53%, 17%, and 17.3% and at 365-day, the porosity values were 15.83%, 16.37%, 16.67%, and 16.87% at 5%, 10%, 15%, and 20% replacement of SF. The average value of porosity containing SF in the range of 16 to 20% at different percentage levels and curing ages was suitable for drainage purposes in NFC pavements (Hesami et al., 2014).

Effect of replacement by rice husk ash (RHA)

The porosity of NFC mixes containing RHA at different percentage replacement levels of cement at 7, 28, 90, and 365-day was represented in Figure 4.25. NFC mixes with an increasing amount of RHA, the porosity value trend was similar to water permeability results, wherein porosity reduced with increasing RHA at different replacement levels and different testing ages. The values of porosity decreased by 18.05%, 16.5%, 15.1%, and 13.75% at 5%, 10%, 15%, and 20% replacement of RHA. At 28-day, the porosity value was 17.35%, 16.35%, 12.85%, and 11.35% at different replacement levels of RHA. Similarly, at 90-day, the values were 17%, 15.85%, 12.7%, and 10.63% and at 365-day, the values were 16%, 14.4%, 12%, and 10.5% at 5%-20% replacement of RHA. The average porosity values were in the range of 12.70% to 18.4% and were well within the suggested range of 15-35% by ACI (ACI Committee 522, 2010).

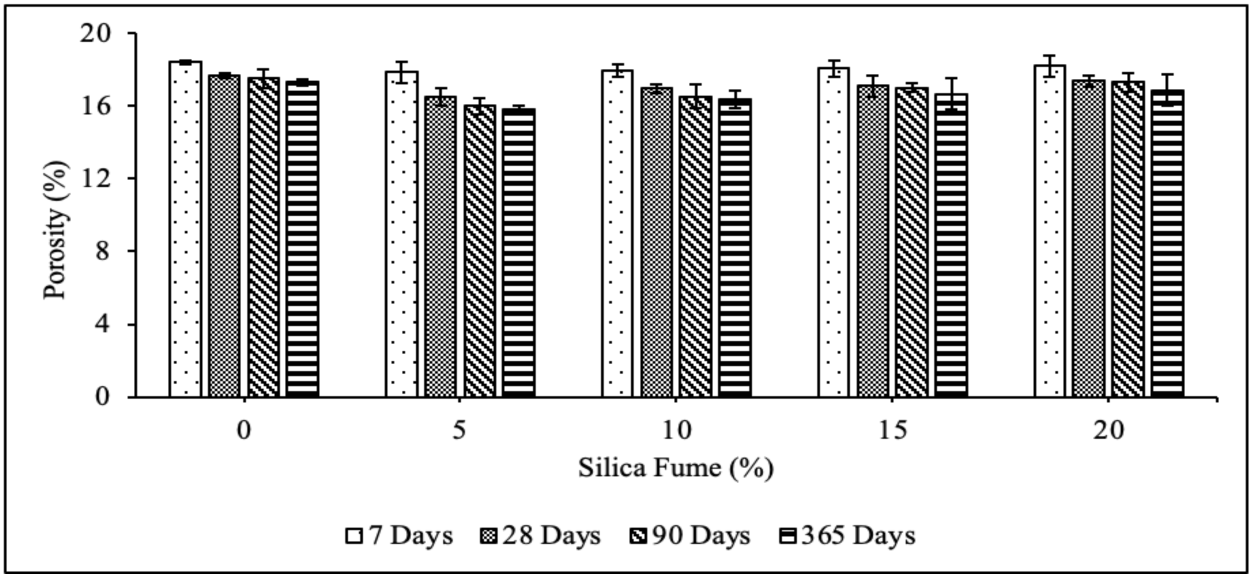

Figure 4.24. Porosity of NFC containing SF

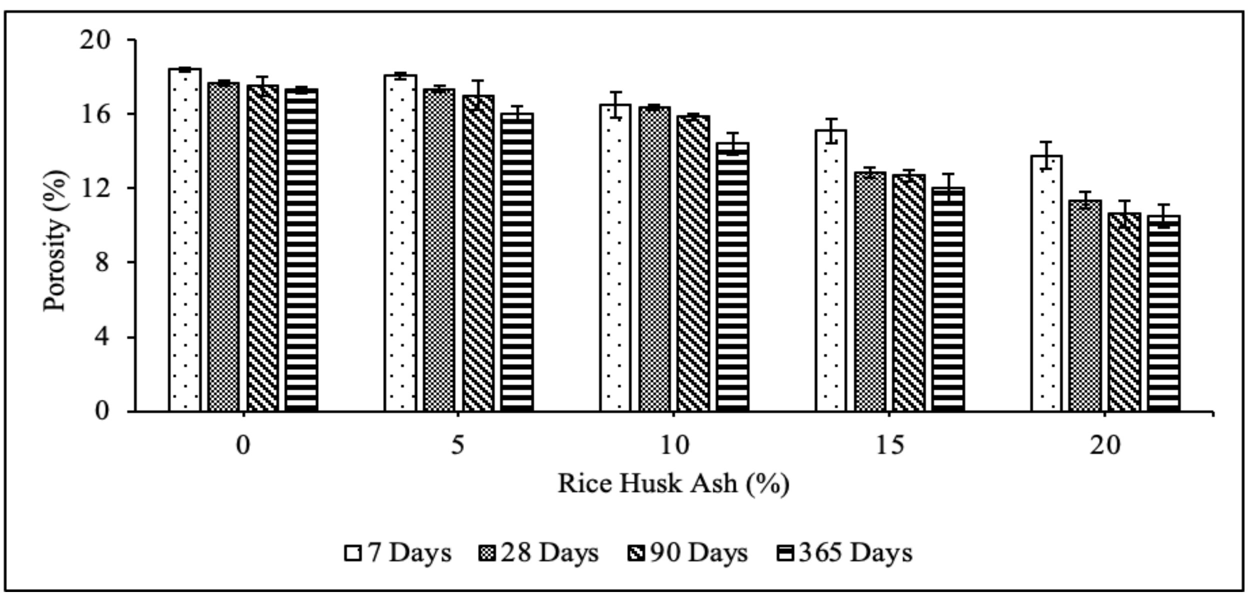

Figure 4.25. Porosity of NFC containing RHA

Effect of different gradation of coarse aggregates

The porosity of different NFC mixes prepared using different single-size natural coarse aggregates at 7, 28, 90, and 365-day was shown in Figure 4.26. It can be observed that porosity increased with the increase in aggregate size concrete at different curing ages and followed a trend similar to water permeability since they are directly related to each other (ACI Committee 522, 2006). The porosity of NFC-9.5 mm, NFC-8 mm, NFC-6.3 mm and NFC-4.75 mm aggregate size of concrete is 28.93%, 27.50%, 27% and 26.5% at 28-day respectively. The average value of porosity lies in the range of 24 to 30%. It was well within the suggested range of 15-35% by ACI 522R (ACI Committee 522, 2010) using different sizes of coarse aggregates at all different curing ages (Figure 4.26). Porosity is an indirect indicator of drainage and permeation properties of no-fines concrete. For NFC pavement applications, the use of smaller-sized aggregates (4.75mm) leads to a 9.17 % decrease in porosity at 28-day. The achieved average porosity value of approximately 26.5% is acceptable as per ACI guidelines and would not compromise their drainage properties in field applications.

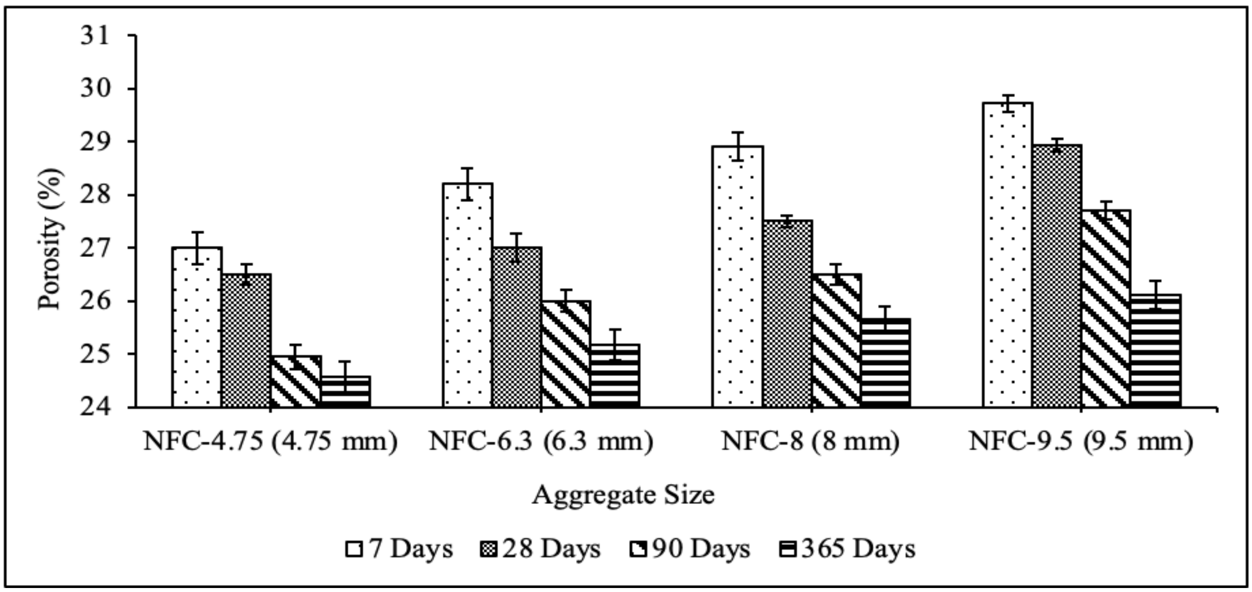

Figure 4.26. Porosity of NFC mixes with different gradations of coarse aggregates

4.3.3 Density

Effect of replacement by fly ash (FA)

The density of the NFC mixes was measured as the average of three cylindrical specimens of 100 mm in diameter and 200 mm in height at different ages of curing. The density of NFC mixes prepared using an increasing percentage of FA at 7, 28, 90, and 365-day was illustrated in Figure

4.27. With increasing replacement level of FA, density decreased but remained well within the acceptable limits of 1600 to 2000 kg/m^3 (Tennis et al., 2004). At 7-day, density decreased from 2075 kg/m^3 (reference mix) to 1947 kg/m^3. Similarly, at 28-day, the values decreased from 2088 kg/m^3 (reference mix) to 2018 kg/m^3. But at 90-day, density increased from 2105 kg/m^3 (reference mix) to 2127 kg/m^3. Similarly, at 365-day, the density increased from 2114 kg/m^3 (reference mix) to 2137 kg/m^3. The variation in density with FA mixes was due to the combined effect of varying degrees of compaction and the presence of low-density FA compared to cement.

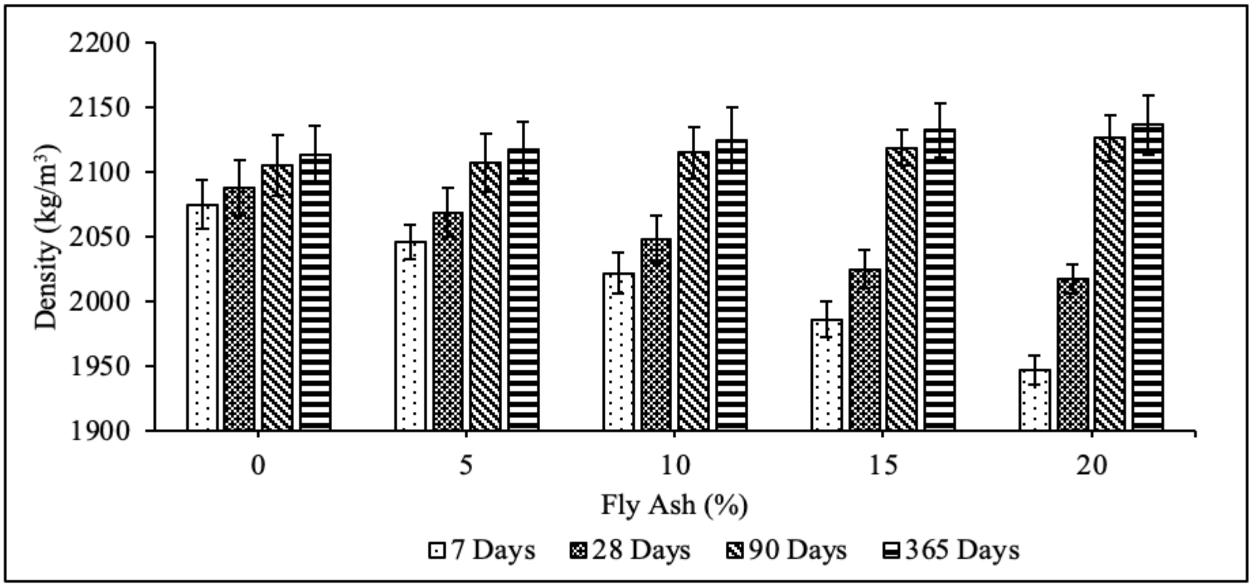

Figure 4.27. Density of NFC containing FA

Effect of replacement by metakaolin (MK)

The density of NFC depends on the void content of the concrete mix. The density of NFC mixes prepared using an increasing percentage of MK at 7, 28, 90, and 365-day was presented in Figure 4.28. The density values increased from 2075 kg/m^3 (reference mix) to 2143 kg/m^3 at 7-day. At 28-day, the density values increased from 2088 kg/m^3 (reference mix) to 2166 kg/m^3. Similarly, the density values increased from 2105 kg/m^3 (reference mix) to 2188 kg/m^3 at 90-day. At 365-day, the density values increased from 2114 kg/m^3 (reference mix) to 2202 kg/m^3. The average density values for different replacement levels of MK range from 2075 kg/m^3 to 2200 kg/m^{3,} which is an acceptable limit since the density values of NFC reported by various researchers have been estimated to lie between 1600 kg/m^3 to 2000 kg/m^3 (ACI Committee 522, 2010; National Ready Mixed Concrete Association, 2004; Tennis et al., 2004). It has been noticed that the density increased as MK's replacement level increased compared to the control NFC mix.

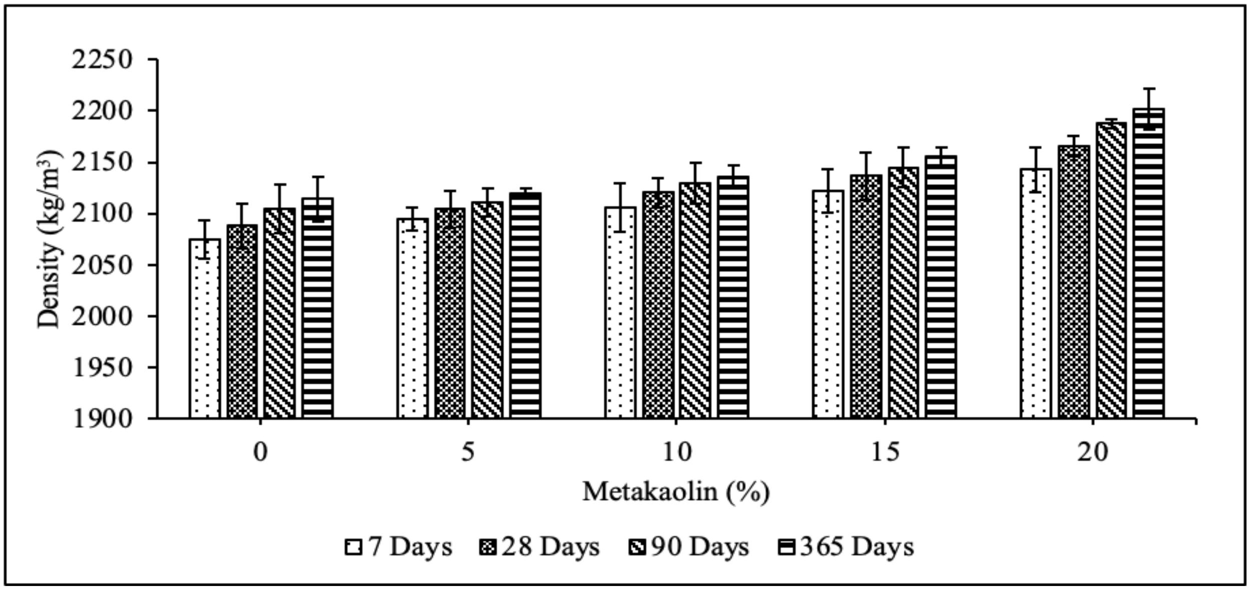

Figure 4.28. Density of NFC containing MK

Effect of replacement by silica fume (SF)

The density of NFC mixes containing SF at different percentage replacement levels of cement at 7, 28, 90, and 365-day was shown in Figure 4.29. The average values of density measured in different replacement levels of SF ranged from 2018 to 2163 kg/m^3 and agreed with the results of previous studies (Tennis et al., 2004). In general, density values observed at different curing ages were marginally less than the values of control mixes at all replacement levels except 5% and 10% replacement, at which porosity increased at all curing ages. The density increased from 2075 kg/m^3 (reference mix) to 2101 kg/m^3 and 2120 kg/m^3 at 5% and 10% replacement of cement by SF, respectively, but decreased marginally at 15% and 20% replacement of cement by SF at 7-day. Similar trends in density values were observed at 28, 90, and 365-day of curing. The dense microstructure can explain the increase in density at 5 and 10% replacement due to high silica content, which increases the rate of pozzolanic reaction with calcium hydroxide. In general, the porosity marginally reduced with increasing SF above 10% due to very fine particles of SF, which tend to segregate and cannot distribute uniformly in the concrete mix.

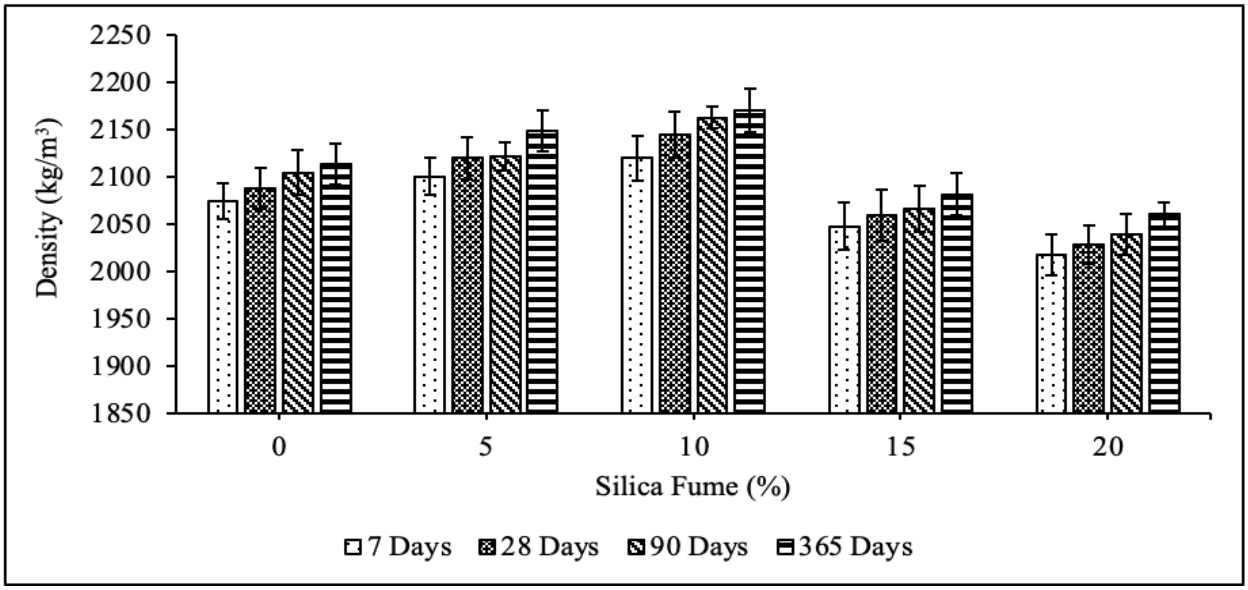

Figure 4.29. Density of NFC containing SF

Effect of replacement by rice husk ash (RHA)

The density of NFC mixes containing RHA at different percentage replacement levels of cement at 7, 28, 90, and 365-day was represented in Figure 4.30. The density marginally decreased with increasing percentage replacement levels of RHA and ranged from 2005 kg/m^3 to 2122 kg/m^{3,} specifically at higher replacement levels. At suggested optimum replacement of 5% RHA, density of the resulting NFC mixes marginally improved from 2075 kg/m^3 (reference mix) to 2088 kg/m^3 at 7-day, 2088 kg/m^3 (reference mix) to 2118 kg/m^3 at 28-day, from 2105 kg/m^3 (reference mix) to 2122 kg/m^3 at 90-day, and 2114 kg/m^3 (reference mix) to 2133 kg/m^3 at 365-day. Density decreased with increasing RHA beyond 5% levels due to lower specific gravity of RHA as compared to cement which plays a major role in density reduction of the resulting hybrid NFC-RHA mixes. The preceding results agree with previous research (Olutoge and Adesina, 2019; Padhi et al., 2018).

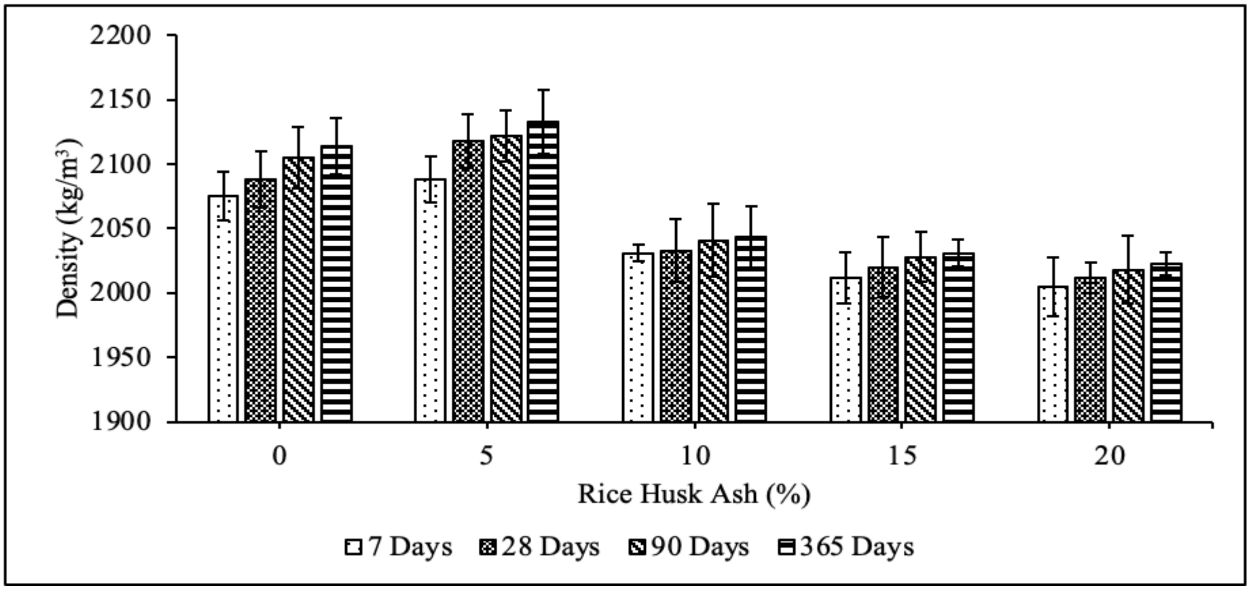

Figure 4.30. Density of NFC containing RHA

Effect of different gradation of coarse aggregates

The density of NFC mix depends relatively on the aggregate used, however, concrete with a density of less than 2000 kg/m^3 may be considered lightweight concrete (Gesoğlu et al., 2014; Ibrahim and Abdul Razak, 2016; Tennis et al., 2004). The density of the NFC mixes was measured as the average of three cylindrical specimens of 100 mm in diameter and 200 mm in height at different ages of curing. The average density values for NFC-4.75 were 1810 kg/m^3 at 7-day, 1836 kg/m^3 at 28-day, 1867 kg/m^3 at 90-day, and 1891 kg/m^3 at 365-day of curing. It falls well within the desired range of 1768 kg/m^3 to 1920 kg/m^3 (ACI Committee 522, 2010; National Ready Mixed Concrete Association, 2004; Tennis et al., 2004) (Figure 4.31). It was noted that the value of density decreases with an increase in aggregate size in various NFC mixes at different ages of curing. Maximum density was observed in NFC mix prepared using 4.75mm aggregate, leading to improved compressive strength properties. The lowest density of NFC concrete prepared with 9.5 mm aggregate was observed at all curing ages and lies in the typical range of 1600 kg/m^3 to 2000 kg/m^3 (Tennis et al., 2004; Wang et al., 2006).

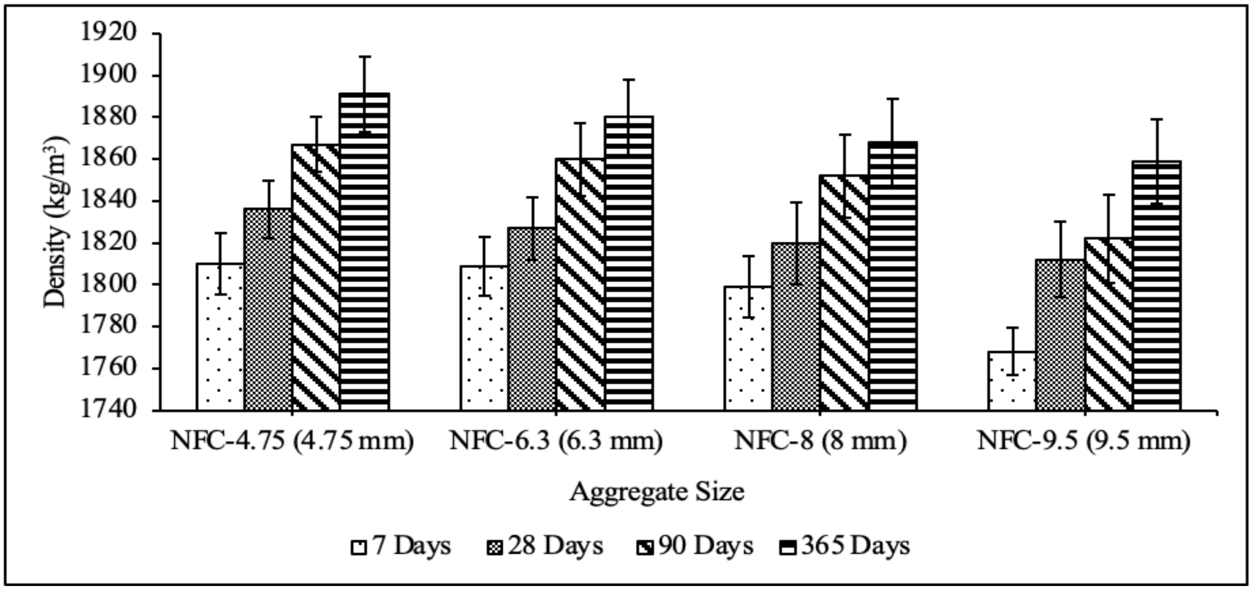

Figure 4.31. Density of NFC mixes with different gradations of coarse aggregates

4.3.4 Water Absorption

Effect of replacement by fly ash (FA)

The water absorption results of NFC using FA at 28-day, 90-day, and 365-day of curing were listed in Table 4.6. It was observed from the results that there was a minor drop in water absorption values with increasing FA replacement of cement in NFC mixes at 28 and 90-day. Water absorption values decreased from 5.22% to 4.90% at 28-day. Similarly, the water absorption value decreased from 5.67 % to 4.89% at 90-day and from 5.79% to 4.86% at 365-day compared to the control mix. This was probably because FA is an amorphous material having slow reactivity during cement hydration, causing a drop in water absorption values due to the pozzolanic effect. The overall effect of the decrease in water absorption in NFC with FA is that it leads to improvement in the permeability of NFC.

Table 4.6. Water absorption of NFC mixes using FA

Mix	**Water absorption of FA (%)**		
	28-day	**90-day**	**365-day**
NFC-0	5.22	5.74	5.79
NFC-5	5.01	5.00	4.97
NFC-10	4.96	4.96	4.92
NFC-15	4.94	4.92	4.88
NFC-20	4.90	4.89	4.86

Effect of replacement by metakaolin (MK)

The water absorption results of NFC using MK at 28-day, 90-day, and 365-day of curing were listed in Table 4.7. It can be seen that water absorption values decreased with an increase in curing ages and with increasing replacement levels of 5, 10, 15, and 20% of MK as compared to the control NFC mix. Water absorption is generally a surface phenomenon, and it indicates the perviousness of the material. The decrease in water absorption values may be due to the small size of MK particle size (3µm), which is very small as compared to cement leading to compact structure for lower water ingress and may be due to the formation of a denser hydration phase (Khatib and Clay, 2004). The minimum water absorption value was observed with a 20% MK replacement level at 28-day 4.90%, at 90-day, the absorption value was 4.85% and was 4.83% at 365-day.

Table 4.7. Water absorption of NFC mixes using MK

Mix	Water absorption of MK (%)		
	28-day	**90-day**	**365-day**
NFC-0	5.22	5.74	5.79
NFC-5	5.15	5.15	5.10
NFC-10	5.09	5.07	5.04
NFC-15	4.98	4.93	4.89
NFC-20	4.90	4.85	4.83

Effect of replacement by silica fume (SF)

The test results of water absorption of NFC containing SF at different curing ages, i.e., at 28, 90, and 365-day were listed in Table 4.8. The control mix's water absorption value at 28, 90, and 365-day is 5.22%, 5.74%, and 5.79%, respectively. It can be seen from Table 4.8, the water absorption of the NFC sample containing SF decreased with the increase in the percentage replacement as compared to the control mix. The water absorption decreases nearby 5% at 28-day for all percentage replacement levels. The decrease in water absorption is due to the fine nature of SF particles filling the pores in the bulk paste and the interfacial transition zone between cement paste and aggregates, leading to the reduction in capillary pores and, hence, reduction in water absorption. The minimum water absorption value was observed with a 20% SF replacement level at 28-day 4.69%. Similarly, at 90-day, the absorption value was 4.67% and was 4.66% at 365-day at 20% replacement of SF.

Table 4.8. Water absorption of NFC mixes using SF

Mix	Water absorption of SF (%)		
	28-day	90-day	365-day
NFC-0	5.22	5.74	5.79
NFC-5	5.02	4.97	4.89
NFC-10	4.85	4.85	4.81
NFC-15	4.78	4.78	4.76
NFC-20	4.69	4.67	4.66

Effect of replacement by rice husk ash (RHA)

The test results of water absorption of NFC containing RHA at different percentages of replacement (0-20%) in NFC mixes, the water absorption results were listed in Table 4.9. Water absorption values decreased by 5.21%, 5.00%, 4.94%, and 4.86% at 28-day, and 5.46%, 5.25%, 4.88%, and 4.73% at 90-day for 5 to 20% replacement levels of RHA in NFC mixes. The test results indicated that the higher quantity of RHA resulted in marginally lower water absorption values than the control mix because RHA is finer than cement. The small particles of RHA improved the particle density of the resulting NFC-RHA mixes, leading to a reduced in the volume of pores and hence reduction in water absorption values (Ganesan et al., 2008; Sanusi et al., 2014). The minimum water absorption value was observed 4.86% at 28-day, 4.73% at 90-day, and 4.69% at 365-day at 20% replacement of RHA.

Table 4.9. Water absorption of NFC mixes using RHA

Mix	Water absorption of RHA (%)		
	28-day	90-day	365-day
NFC-0	5.22	5.74	5.79
NFC-5	5.21	5.46	5.49
NFC-10	5.00	5.25	5.28
NFC-15	4.94	4.88	4.85
NFC-20	4.86	4.73	4.69

4.3.5 Drying Shrinkage

Volume variations in concrete occur even when no loads are applied because of the hydration processes, drying, wetting and drying, and heat difference. The distortion of cementitious samples caused by moisture interaction with the external environment is drying shrinkage. Drying shrinkage is a significant phenomenon that causes time-dependent deformations under normal field conditions and is also referred to as creep under zero loads.

Effect of replacement by fly ash (FA)

The test results of drying shrinkage of NFC containing FA at different drying period was calculated. Figure 4.32 illustrates the drying shrinkage behavior of NFC containing FA and control mix. It was observed that with the increasing amount of FA, the drying shrinkage decreased compared to the control mix. The drying shrinkage values of 5% FA showed approximately similar values to the control mix. The drying shrinkage value was decreased by 29.73% at 20% replacement of FA as compared to the control mix. At 448 days, the shrinkage rate for 20% replacement of FA was 1.56×10^{-3} % compared to the control NFC mix (2.22×10^{-3} %). The reduction in shrinkage rate was because of usage of FA that produces hydrated $CaCO_3$ and hydraulic calcium aluminate, that is responsible for filling the water holding voids and prevent shrinkage. Fly ash has small-sized spherical particles that are uniformly distributed in the concrete. These particles occupy the capillary cavities in the slurry, considerably improving the internal density of the concrete and minimizing shrinking to some degree (Kothari, 2017; Qing-Xin et al., 2009; Yang et al., 2017; Zhang et al., 2020, 2019). Similar drying shrinkage results were reported by (Limbachiya et al., 2012; Mehta, 2004; Zhang et al., 2020). They witnessed that the shrinkage rate of concrete lessened with the increasing percentage of replacement of FA compared to control mix of conventional concrete or high-performance concrete.

Effect of replacement by metakaolin (MK)

Drying shrinkage results of NFC containing MK at different drying periods were presented in Figure 4.33. The shrinkage rate fell with the increase in percentage replacement of MK as compared to the control NFC mix. At 20% replacement of MK, the drying shrinkage value was decreased by 42.34% when compared with NFC control mix. The shrinkage rate for 20% MK was 1.28×10^{-3} % compared to the NFC control mix (2.22×10^{-3} %) at 448 days. This may be ascribed to the addition of MK as a cement replacement material that improved the pore structure significantly, and MK modified concrete exhibited significantly lower shrinkage strain when compared to control concrete. Drying shrinkage results from replacement of MK were well compared with (Brooks and Megat Johari, 2001; Güneyisi et al., 2012, 2008; Hassan et al., 2012). They reported that with the increasing replacement of MK, the drying shrinkage values decrease compared to conventional or self-consolidating concrete's control mix.

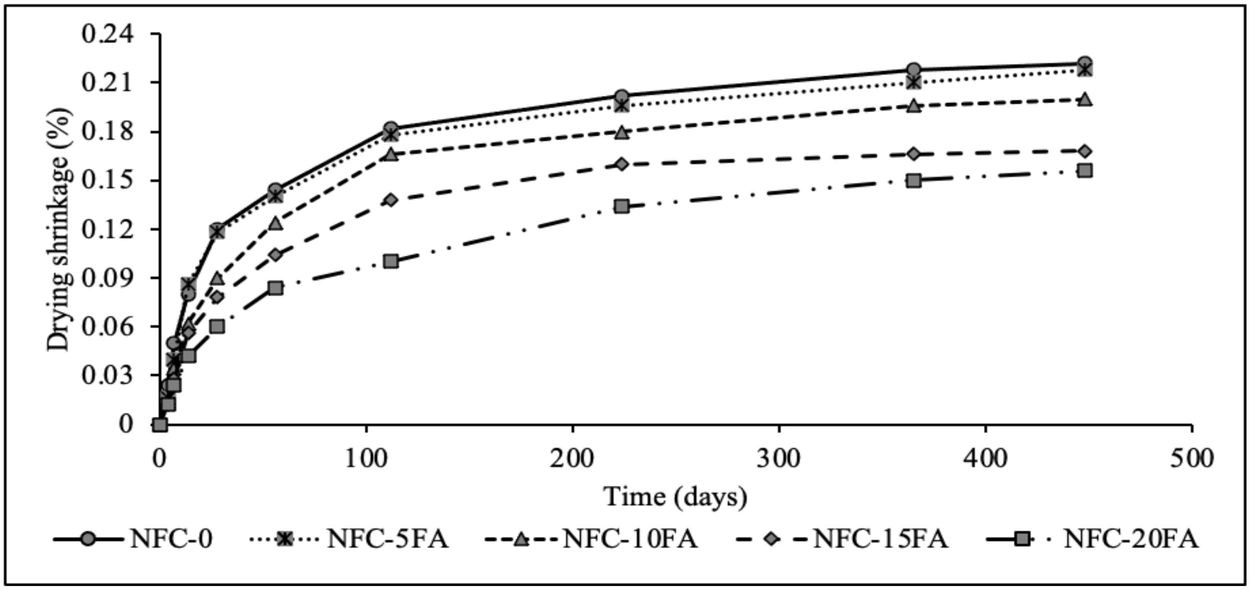

Figure 4.32. Drying shrinkage of NFC containing FA

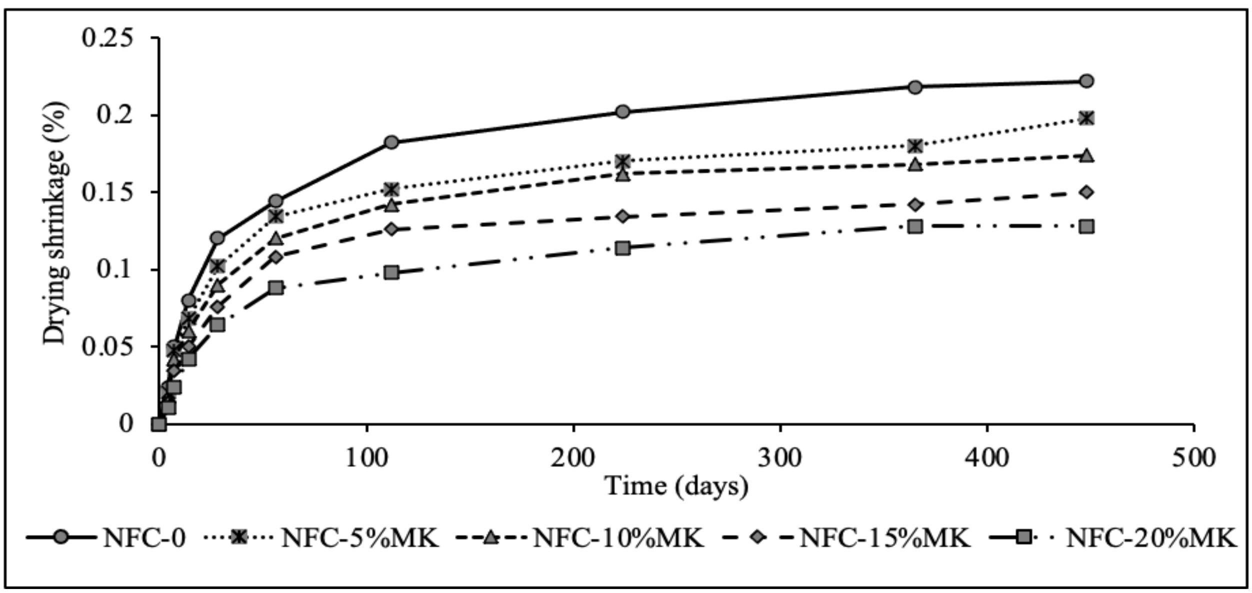

Figure 4.33. Drying shrinkage of NFC containing MK

Effect of replacement by silica fume (SF)

The test results of drying shrinkage of NFC containing SF at different drying periods were presented in Figure 4.34. With the increasing amount of SF, the shrinkage values decreased in comparison to NFC control mix. The 15% replacement of SF and 20% replacement of SF showed approximately similar results. In comparison to the control NFC mix, drying shrinkage value with 15% SF and 20% SF decreased by 31.53% and 35.14%, respectively. The shrinkage rate for 15% SF was 1.52×10^{-3} %, and for 20% replacement of SF was 1.44×10^{-3} % at 448 days compared to the control NFC mix (2.22×10^{-3} %). This can be explained by the fact that SF can significantly improve cement hydration and the amount of AFt crystal hydrates (which represents the ettringite) and C–S–H gel hydrates giving hardened concrete a tougher structure and increased resistance to deformation.

Furthermore, SF may fill microscopic pores and gaps in concrete that damage the structure. That could be the mechanism via which SF reduces the concrete drying shrinkage. These results were compatible with (Güneyisi et al., 2012; Hassan et al., 2012). They discovered that the drying shrinkage decreased by increased percentage replacement of SF compared to the control mix of conventional or self-consolidating concrete.

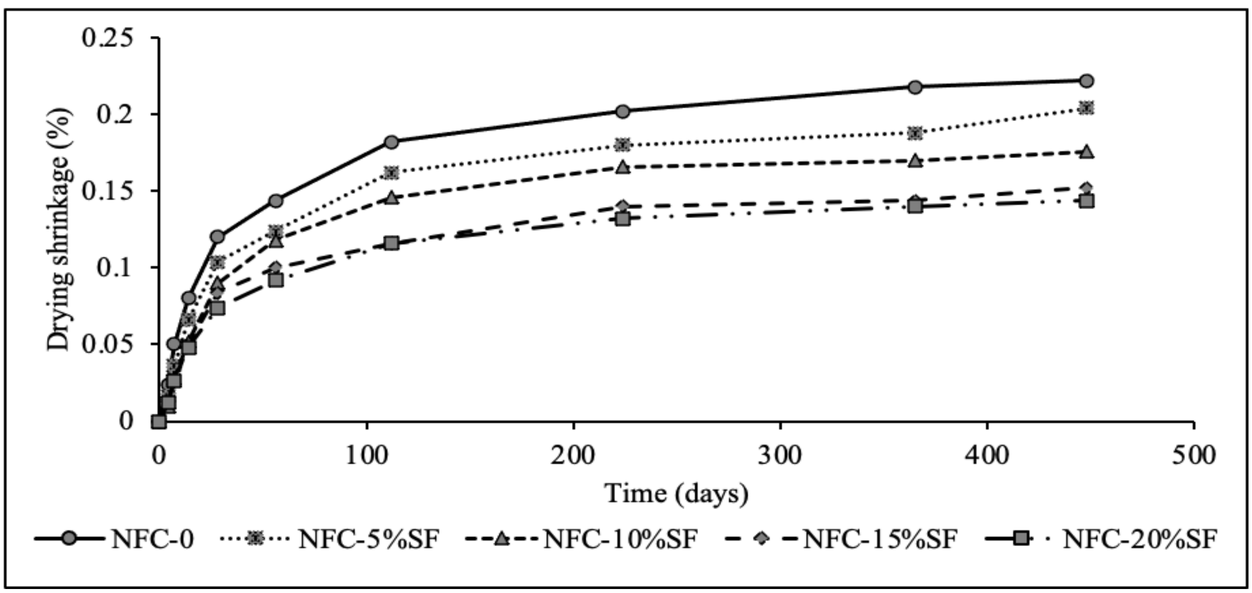

Figure 4.34. Drying shrinkage of NFC containing SF

Effect of replacement by rice husk ash (RHA)

The test results of drying shrinkage of NFC containing RHA at different drying period was presented in Figure 4.35. The shrinkage rate declined with the increase in replacement level of RHA compared to control NFC mix. At 20% replacement of RHA, the drying shrinkage value was decreased by 49.55% compared to the control NFC mix. The shrinkage rate for 20% RHA was 1.12×10^{-3} % compared to the NFC control mix (2.22×10^{-3} %) at 448 days. This could be due to the RHA having a greater surface area than cement; fineness of RHA leads to more water absorption, resulting in lower water content. Additionally, pore size and grain size refining processes improve mechanical interlocking in the transition zone; as a result, drying shrinkage was reduced. The drying shrinkage results were similar to the former studies (Khassaf et al., 2014; Mohseni et al., 2016). They observed that lower drying shrinkage rate of conventional concrete prepared with rice husk ash.

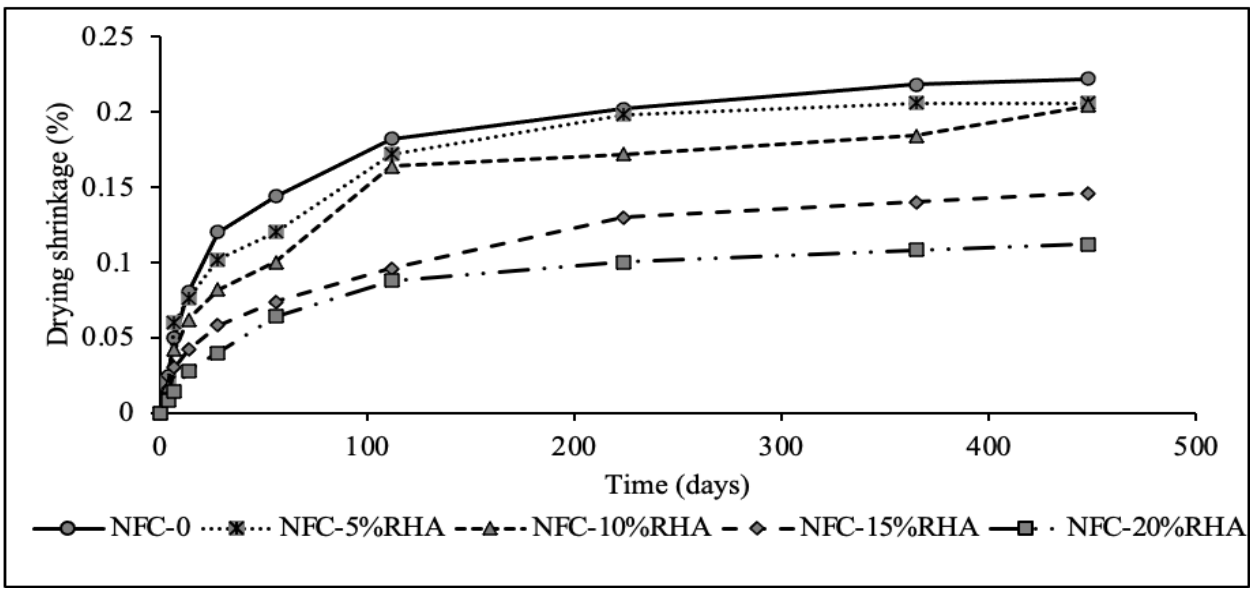

Figure 4.35. Drying shrinkage of NFC containing RHA

4.4 MICROSTRUCTURAL PROPERTIES OF CONCRETE

The concrete strength properties are determined by its inherent microstructure. Factors involving hydration period, water-cement ratio, mineral additive addition, and kind of cement used for preparation of concrete significantly impact the microstructure features. Concrete's microstructure included an aggregate, water bound cement paste, and a transition zone at interface. Scanning Electron Microscopy (SEM) is essential for resolving concrete microstructure. The fissured pieces of concrete from compression test were placed on the SEM stub, for receiving images from secondary electron (SE) image mode in this research.

4.4.1 Effect of replacement by fly ash

Scanning electron micrographs of NFC control mix and NFC containing FA were shown in Figure 4.36 to Figure 4.43. Figure 4.36 shows the dense, compact and uninterrupted CSH gel formation along with crystals of calcium hydroxide (Portlandite) obtained in the cement paste of the NFC control mix. No-fines concrete containing 5% FA, as shown in Figure 4.37, shows the formation of calcium carbonate (Calcite) evenly dispersed across the entire image. Figure 4.38 and Figure 4.39 show the non-uniform distribution of FA reduced the degree of compaction of the mix. The decrease in compressive strength of NFC mix containing different replacement levels of FA at 28-day can be explained by the difference in the microstructure of FA specimen obtained from NFC control mix because of delayed pozzolanic reaction of FA as compared to cement. Figure 4.40 to Figure 4.41 shows the more compacted, denser, continuous CSH gel, calcium hydroxide, and calcium carbonate deposited over the entire image. Moreover, needle-like crystals representative of ettringite (E) were also observed in Figure 4.41. In Figure 4.43, more needle crystals representing ettringite were observed, which is a constituent of cement hydration and can fill the voids or cracks and hence provides strength to the concrete. With increasing replacement levels, due to the formation of a higher amount of C-S-H gel, strength increases due to the higher rate of pozzolanic reaction, which improves the transition zone microstructure between the aggregate and the binder material. Figure 4.36 and Figure 4.37 shows the EDS spectrum and morphology of calcium hydroxide (CH) (Portlandite), CSH gel, and calcium carbonate (CC) (calcite).

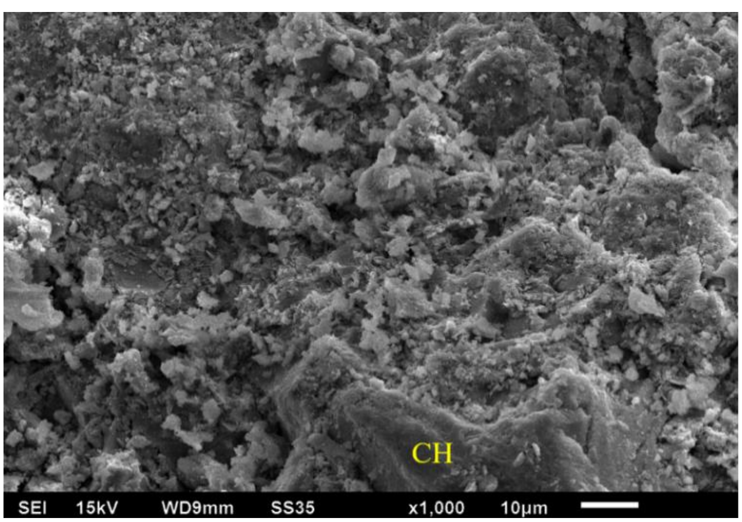

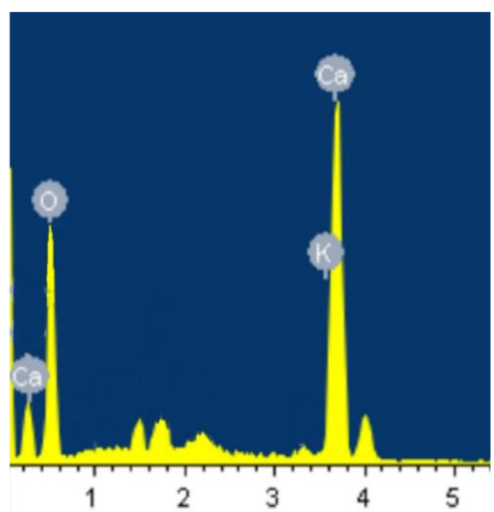

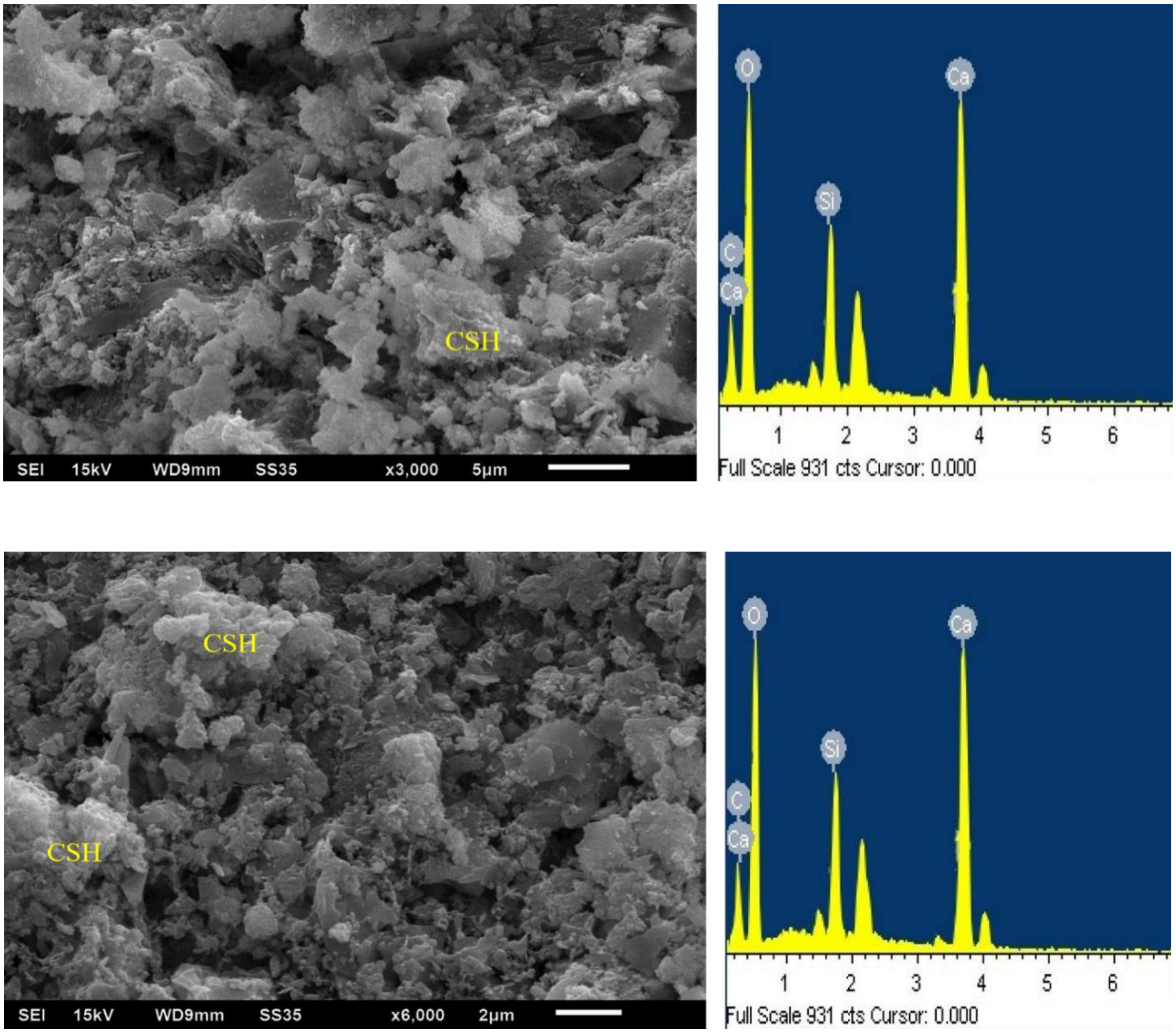

Figure 4.36. SEM micrographs and EDS spectrum of NFC-0% (control mix) at 28-day

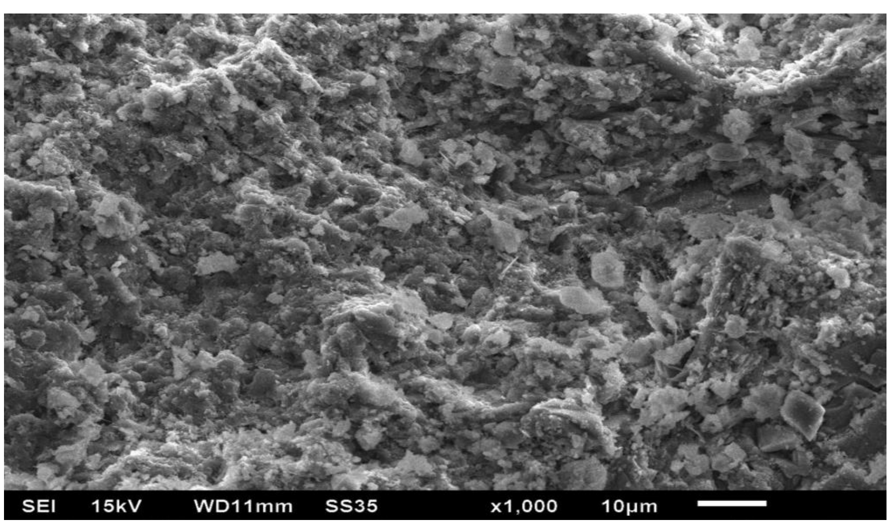

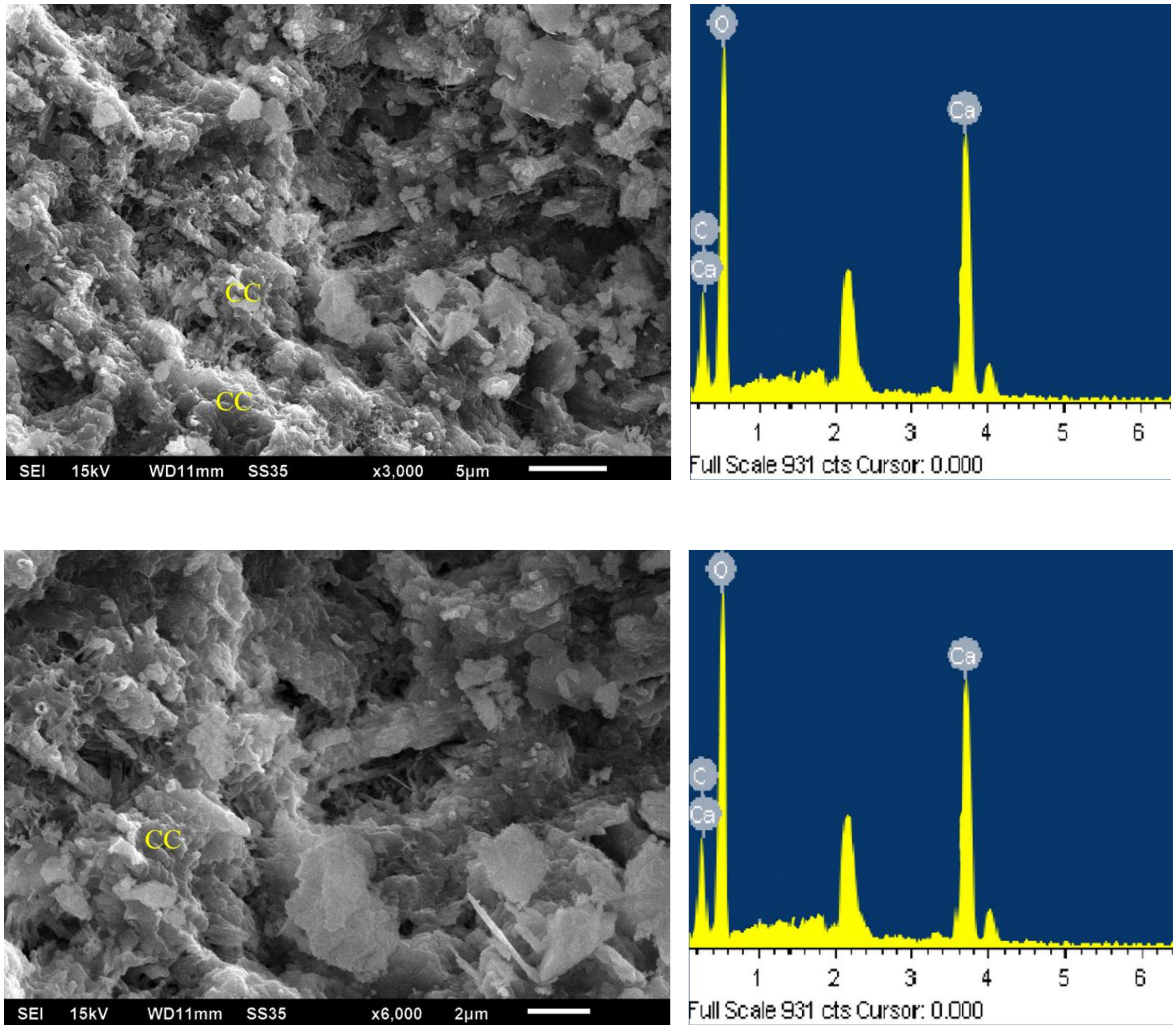

Figure 4.37. SEM micrographs and EDS spectrum of NFC-5% FA at 28-day

Figure 4.42 and Figure 4.43 of NFC mix containing 10% and 20% FA shows more uniformly and dense CSH gel and lesser voids than Figure 4.38 and Figure 4.39. Whereas Figure 4.38 and Figure 4.39 show FA's non-uniform dispersion, which reduced the degree of compactness. At 90-day, CSH gel was evenly distributed in FA mixtures in comparison to the 28-day. The pozzolanic activity of FA leads to an overall improvement in the quality of cement paste and the enhancement in the microstructure of the transition zone existing between the aggregate and the binder material after 28-day.

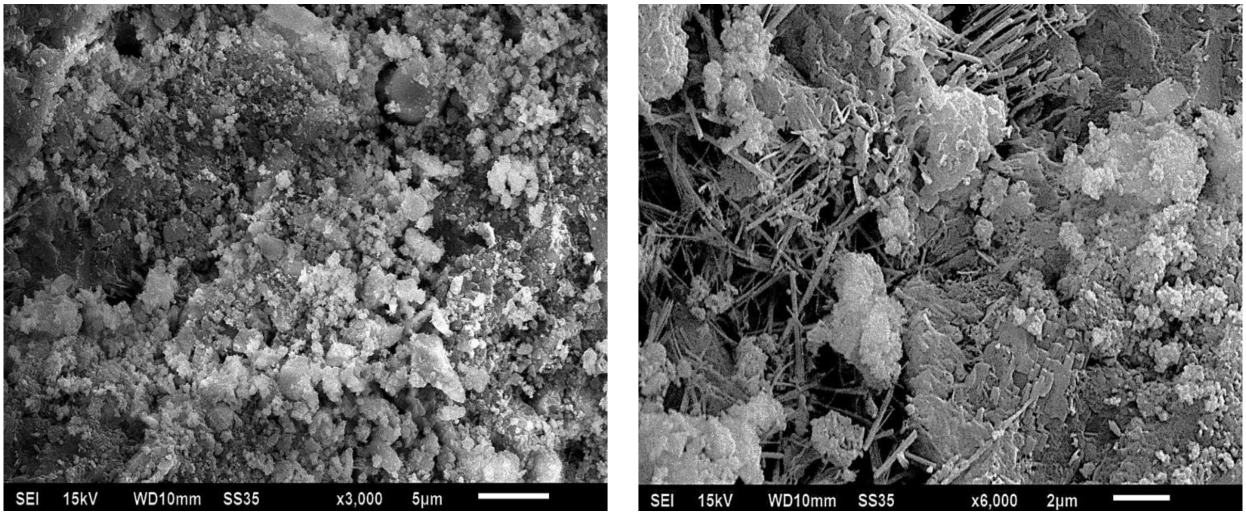

NFC-10% FA (x 3000) NFC-10% FA (x 6000)

Figure 4.38. SEM micrographs of NFC-10% FA at 28-day

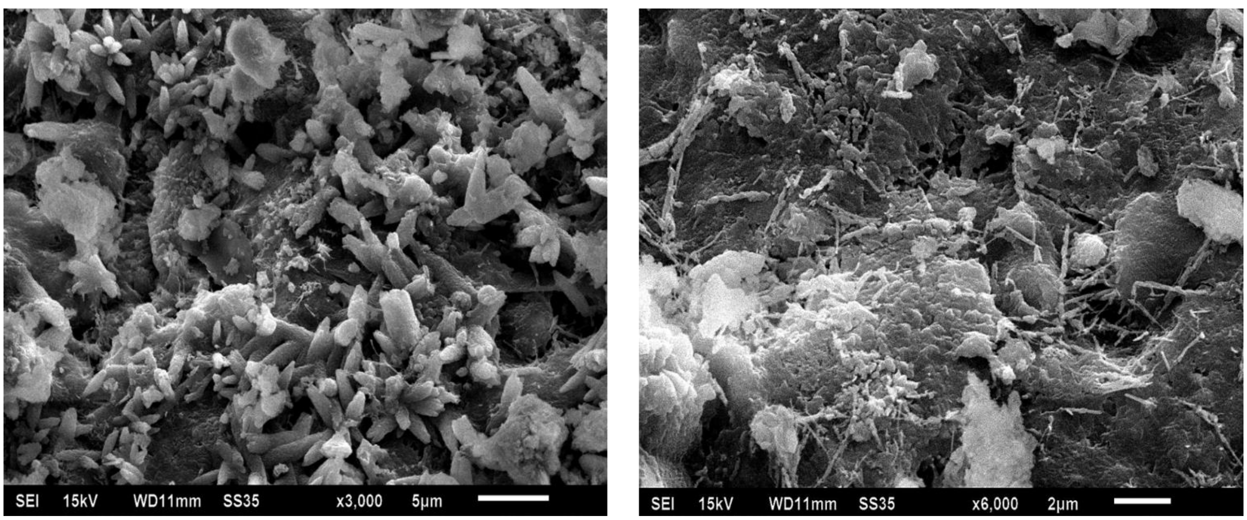

NFC-20% FA (x 3000) NFC-20% FA (x 6000)

Figure 4.39. SEM micrographs of NFC-20% FA at 28-day

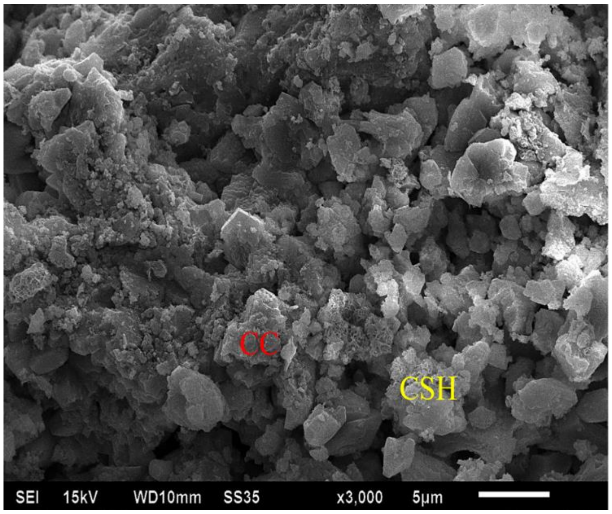

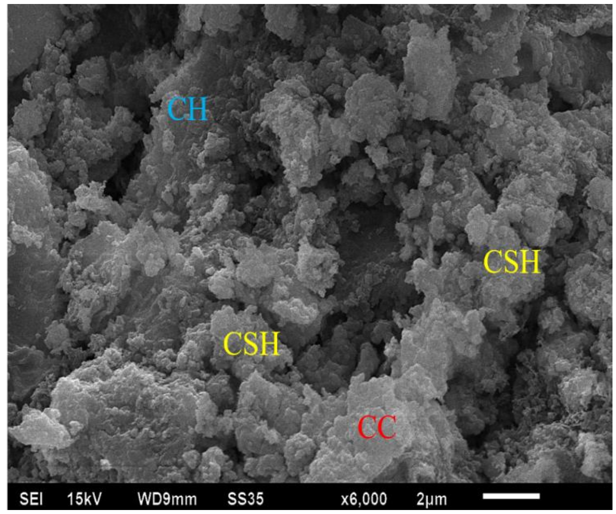

NFC-0% (x 3000) NFC-0% (x 6000)

Figure 4.40. SEM micrographs of NFC-0% (control mix) at 90-day

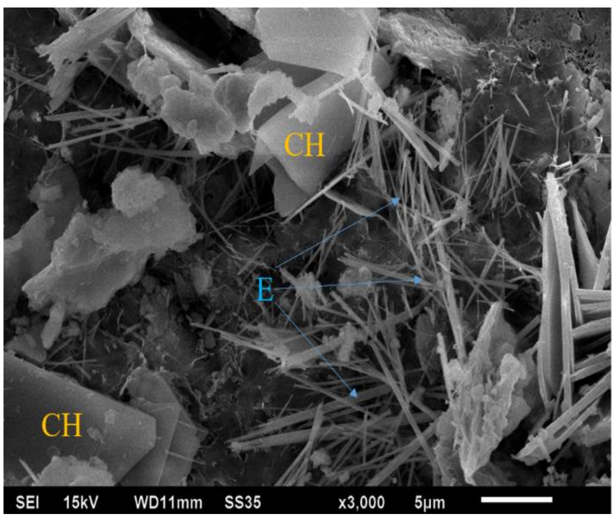

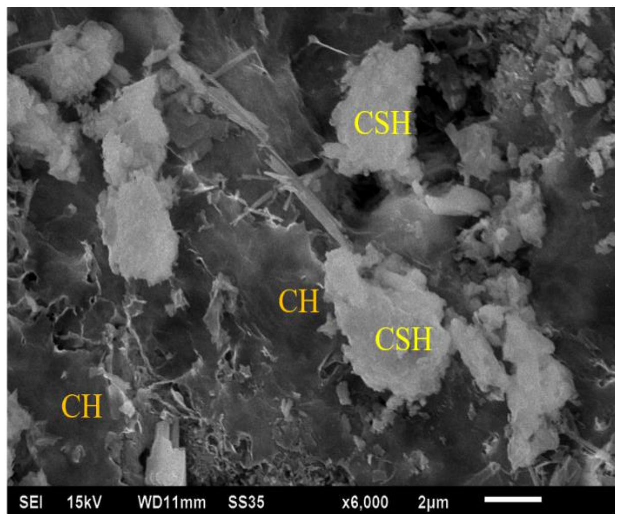

NFC-5% FA (x 3000) NFC-5% FA (x 6000)

Figure 4.41. SEM micrographs of NFC-5% FA at 90-day

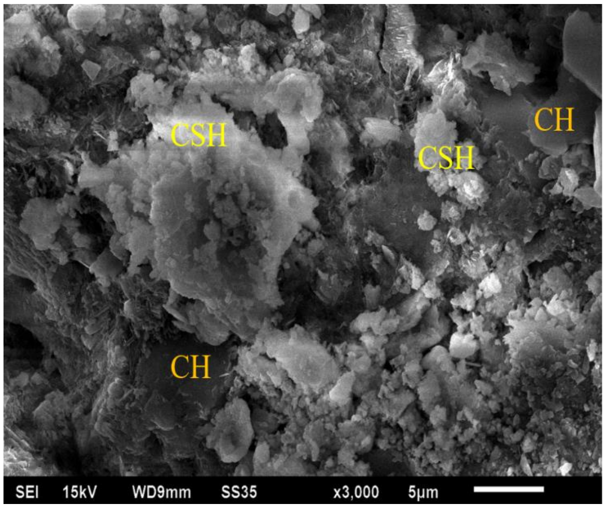

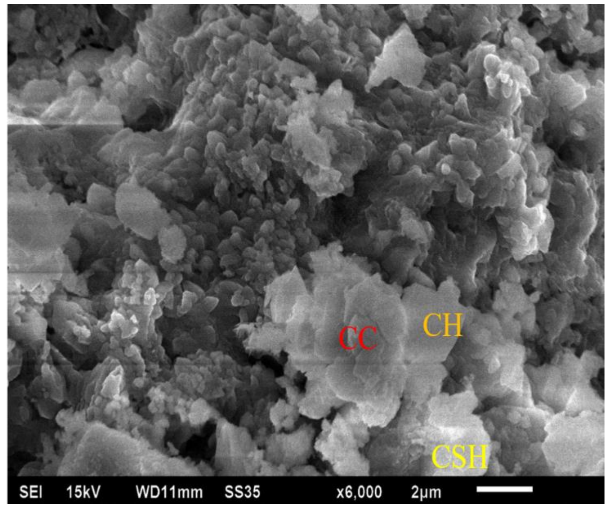

NFC-10% FA (x 3000) NFC-10% FA (x 6000)

Figure 4.42. SEM micrographs of NFC-10% FA at 90-day

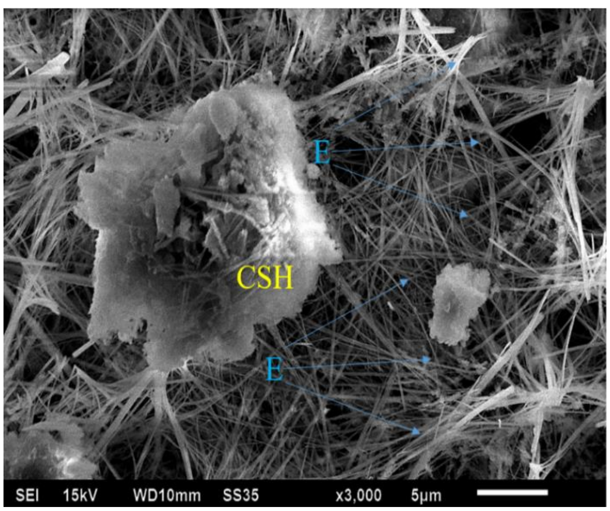

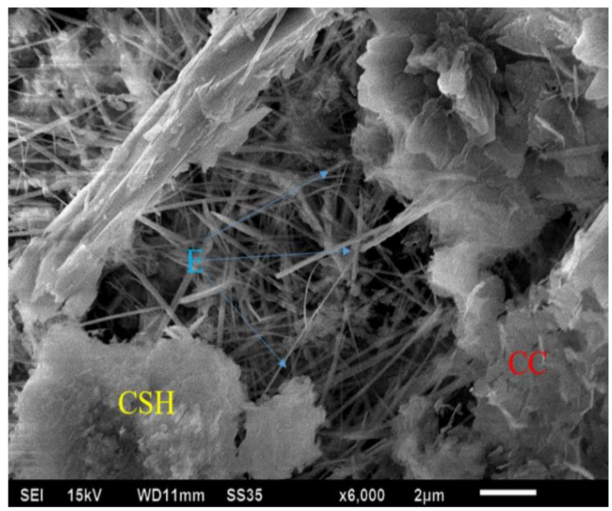

NFC-20% FA (x 3000) NFC-20% FA (x 6000)

Figure 4.43. SEM micrographs of NFC-20% FA at 90-day

4.4.2 Effect of replacement by metakaolin (MK)

Figure 4.44 to Figure 4.49 presented the SEM micrographs of NFC containing MK at different replacement levels. The SEM micrographs of increasing replacement of MK show dense and compacted CSH gel and lesser voids. All the micrographs clearly show the formation of CSH gel, calcium hydroxide (CH) (Portlandite), calcium carbonate (CC) (Calcite), and ettringites (E) in NFC mixes with increasing MK replacement levels, as seen in Figure 4.44 to Figure 4.49. It can be conferred from SEM images that 20% replacement by MK causes densification of the mix at

28-day and 90-day. It can be related to the additional formation of C-S-H gel due to the reaction of calcium hydroxide (CH) in the presence of silica. It was also due to the additional formation of calcium carbonate from carbon dioxide of air which reacts with the calcium hydroxide to provide mechanical strength to concrete. In Figure 4.47, needle crystals that represent the ettringite were observed. The major constituents of MK, i.e., silicon dioxide and aluminium oxide, react with CH in cement paste to create more C-S-H gel products, which helps increase the compressive strength with increasing level of replacement compared to the control NFC mix at higher curing age.

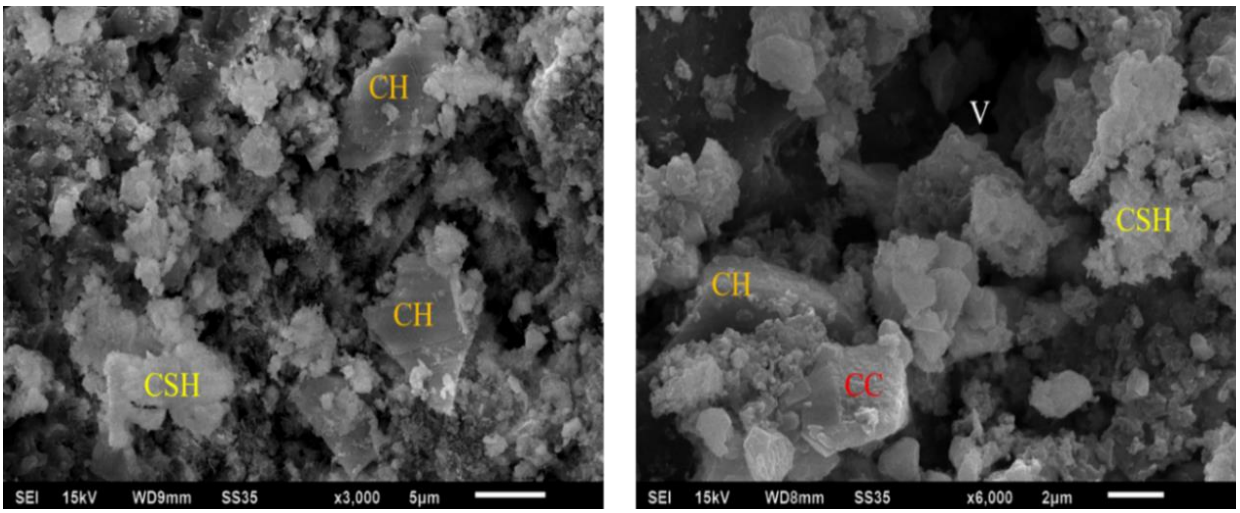

NFC-5% MK (x 3000) NFC-5% MK (x 6000)

Figure 4.44. SEM micrographs of NFC-5% MK at 28-day

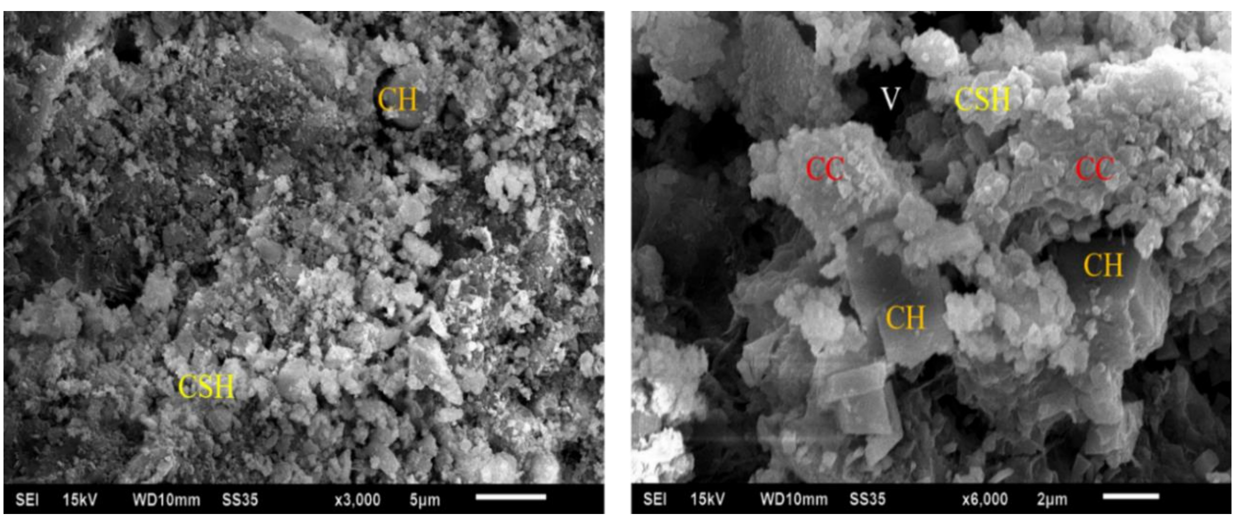

NFC-10% MK (x 3000) NFC-10% MK (x 6000)

Figure 4.45. SEM micrographs of NFC-10% MK at 28-day

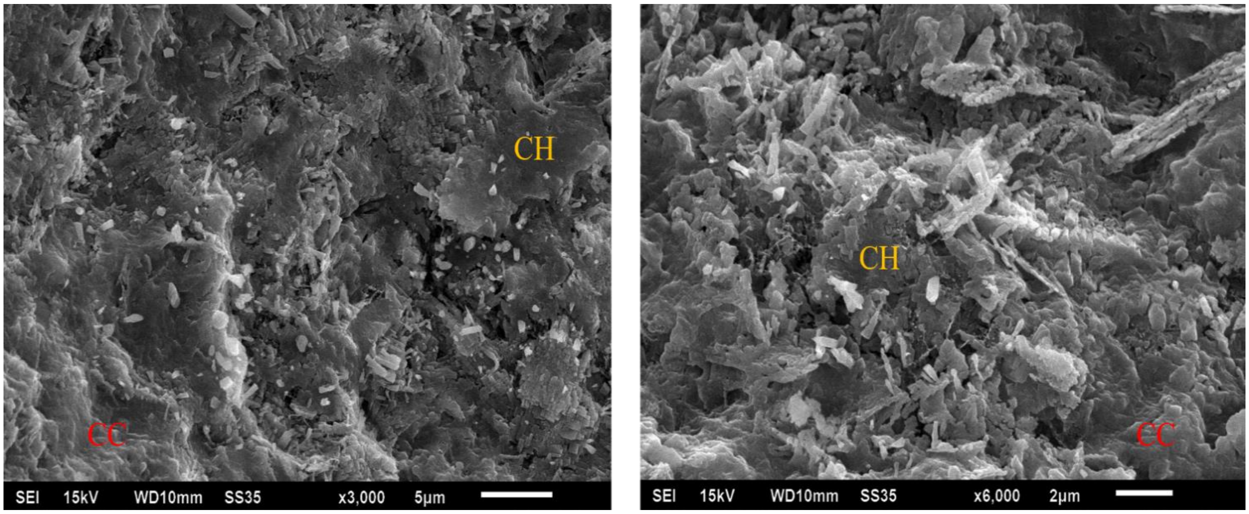

NFC-20% MK (x 3000) NFC-20% MK (x 6000)

Figure 4.46. SEM micrographs of NFC-20% MK at 28-day

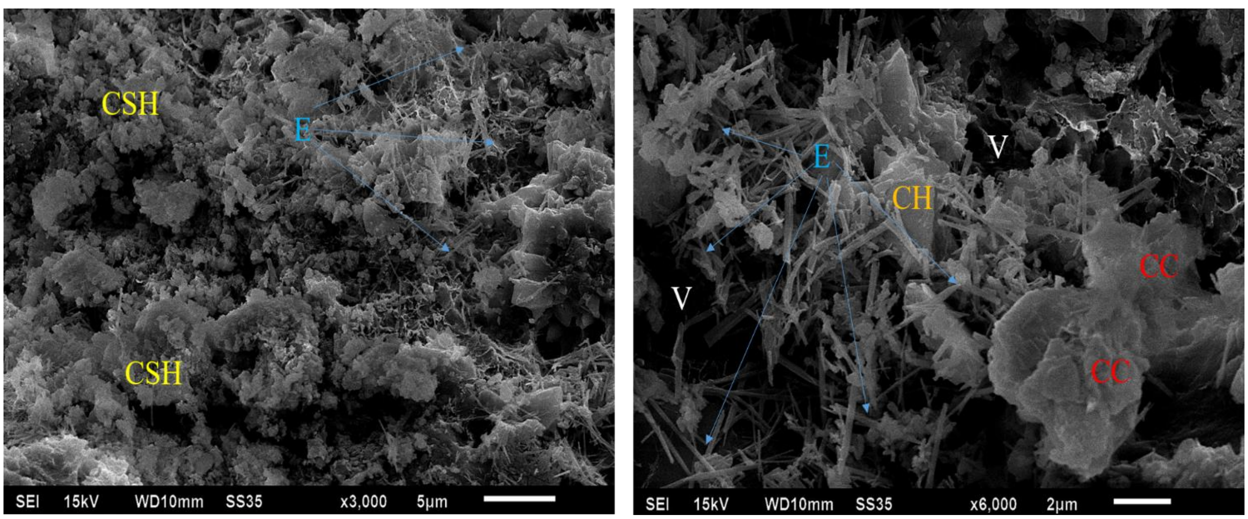

NFC-5% MK (x 3000) NFC-5% MK (x 6000)

Figure 4.47. SEM micrographs of NFC-5% MK at 90-day

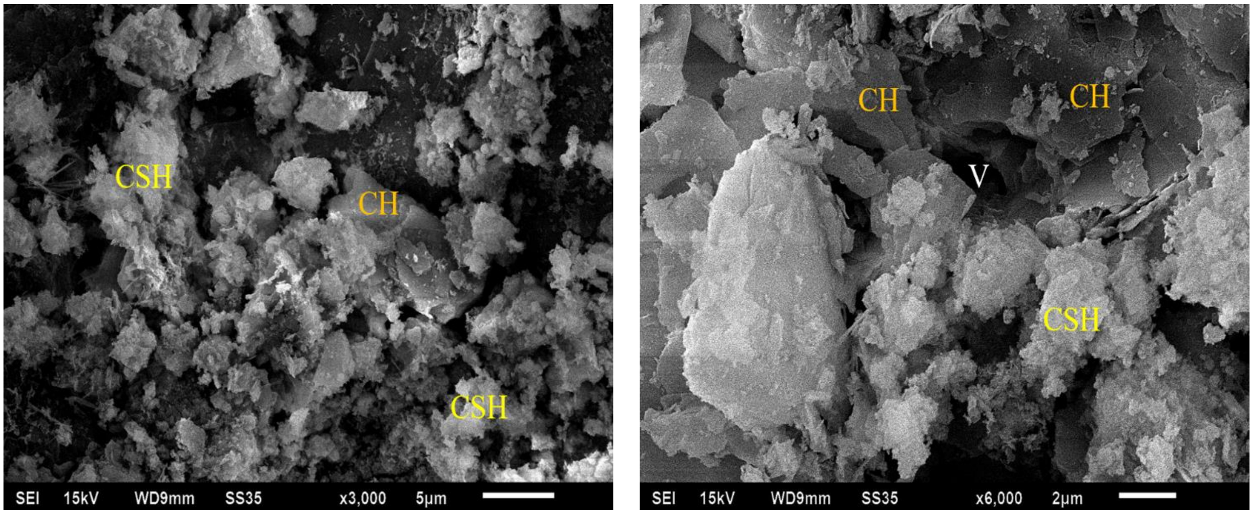

NFC-10% MK (x 3000) NFC-10% MK (x 6000)

Figure 4.48. SEM micrographs of NFC-10% MK at 90-day

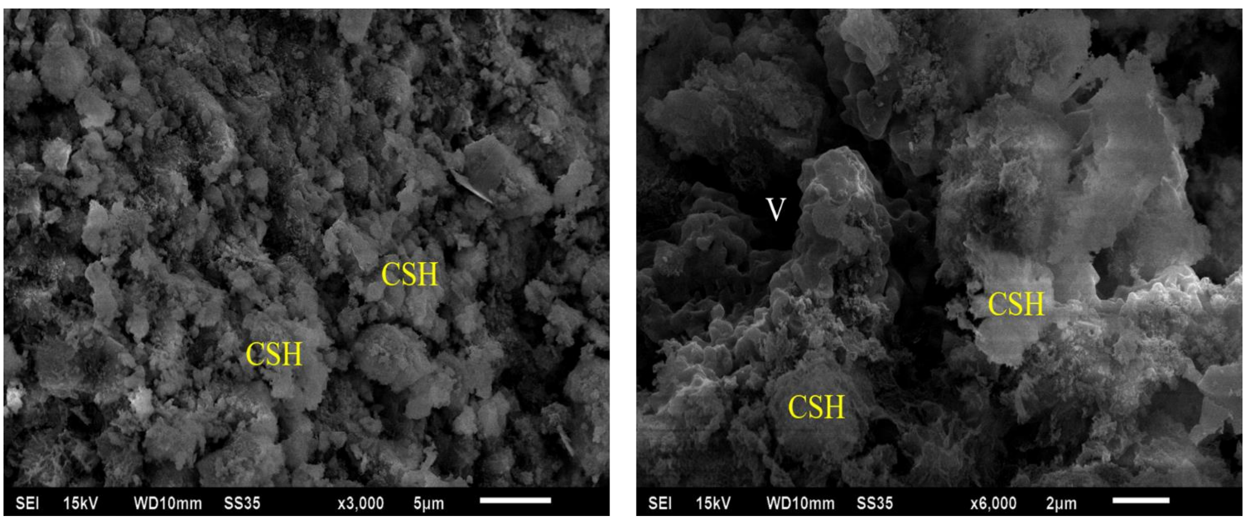

NFC-20% MK (x 3000) NFC-20% MK (x 6000)

Figure 4.49. SEM micrographs of NFC-20% MK at 90-day

4.4.3 Effect of replacement by silica fume (SF)

Scanning electron micrographs of the different NFC mixes with SF replacement of 5%, 10%, and 20% at 28 and 90-day were presented in Figure 4.50 to Figure 4.55. SEM images clearly displayed the growth of CSH gel, calcium hydroxide (CH) (Portlandite), and calcium carbonate (CC) (Calcite) in all mixes. The dense microstructure can be seen in Figure 4.54 due to the C-S-H gel formation at 10% replacement of SF with cement compared to the control mix (Figure 4.36). This can be attributed to the higher specific area, extreme fineness, and high amorphous silica content in SF, which increases the pozzolanic reaction by reacting with calcium hydroxide resulting from primary hydration leading to dense C-S-H gel, which can fill the pores and reduce the porosity of cement hydration which enhances the strength of the cement matrix. But increasing replacement to 20% SF, poor dispersion of excess SF particles occurs in the concrete mix compared to NFC-5 SF, which do not take part in the chemical reaction of cement hydration, resulting in reduced strength at higher replacement levels. In Figure 4.52 and Figure 4.54, the existence of needle crystals (Ettringite) was observed. The SEM micrographs of NFC containing 5% and 10% SF show dense microstructure, and CSH gel was more evenly dispersed in concrete mixtures at 90-day compared to 28-day SEM micrographs.

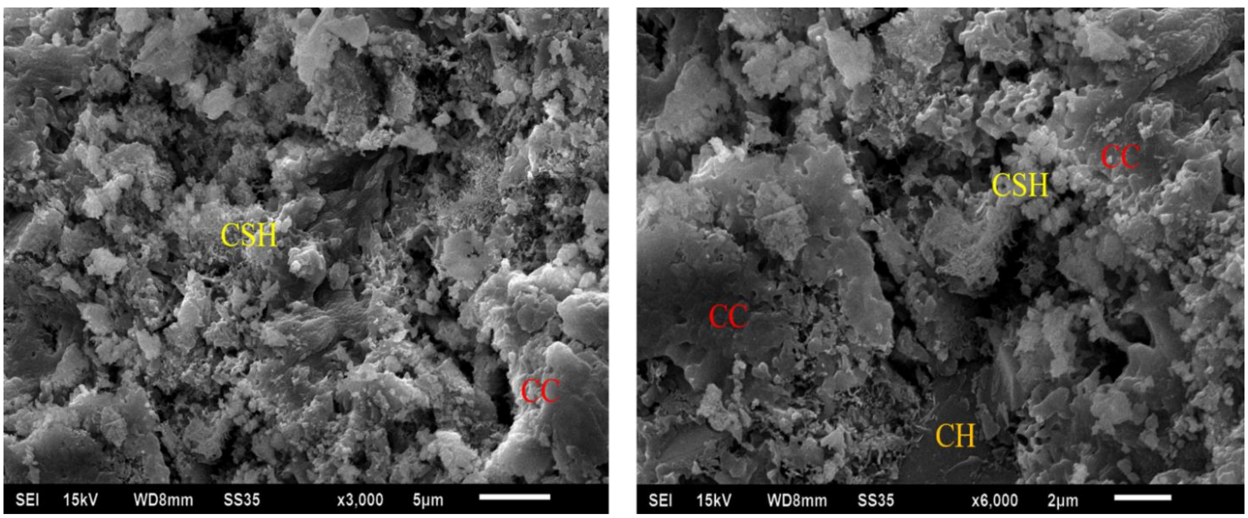

NFC-5% SF (x 3000) NFC-5% SF (x 6000)

Figure 4.50. SEM micrographs of NFC-5% SF at 28-day

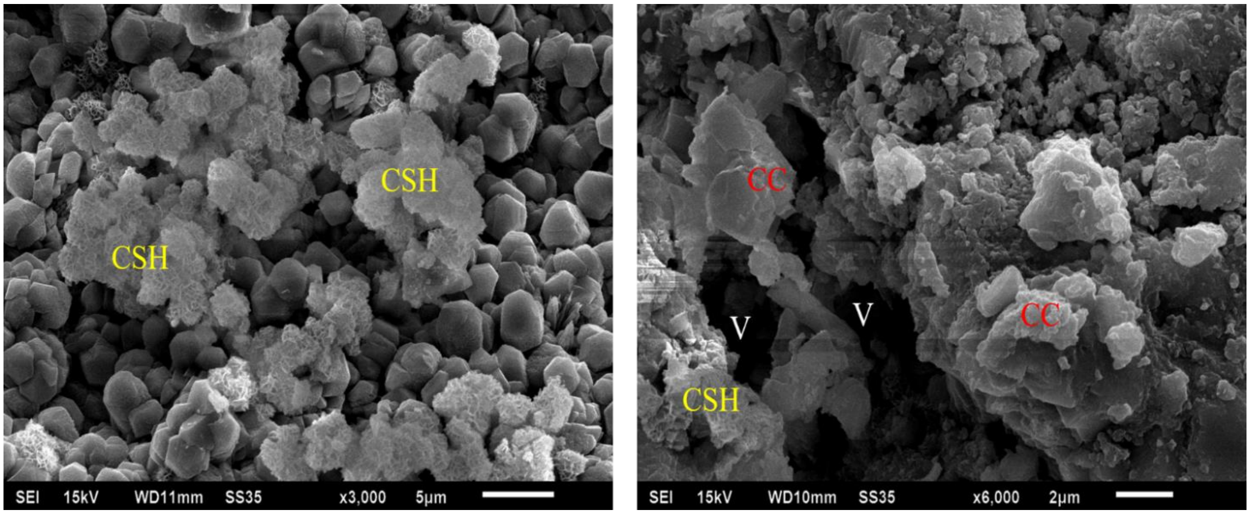

NFC-10% SF (x 3000) NFC-10% SF (x 6000)

Figure 4.51. SEM micrographs of NFC-10% SF at 28-day

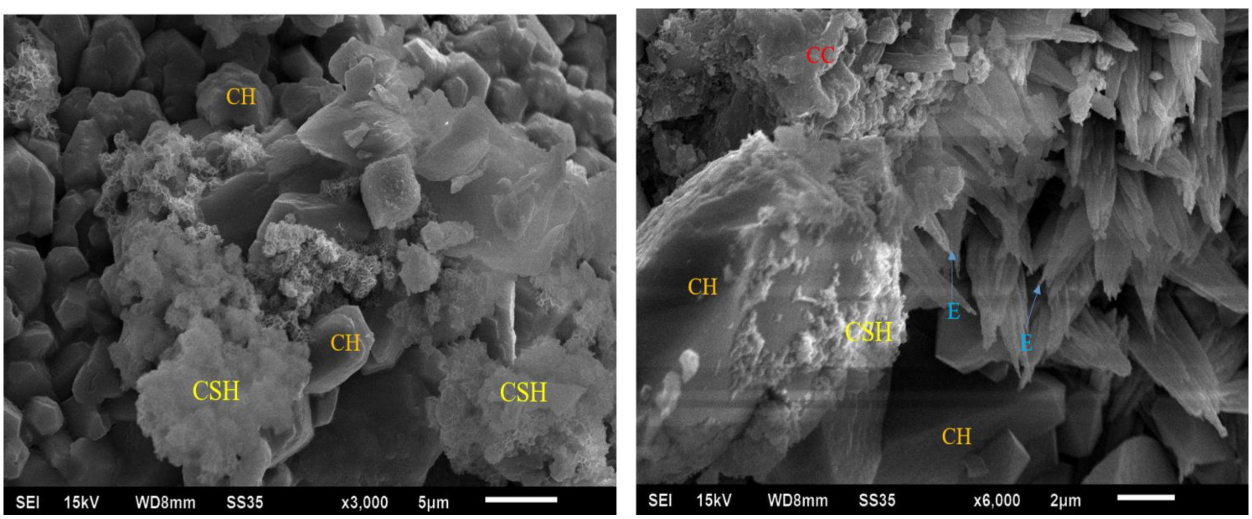

NFC-20% SF (x 3000) NFC-20% SF (x 6000)

Figure 4.52. SEM micrographs of NFC-20% SF at 28-day

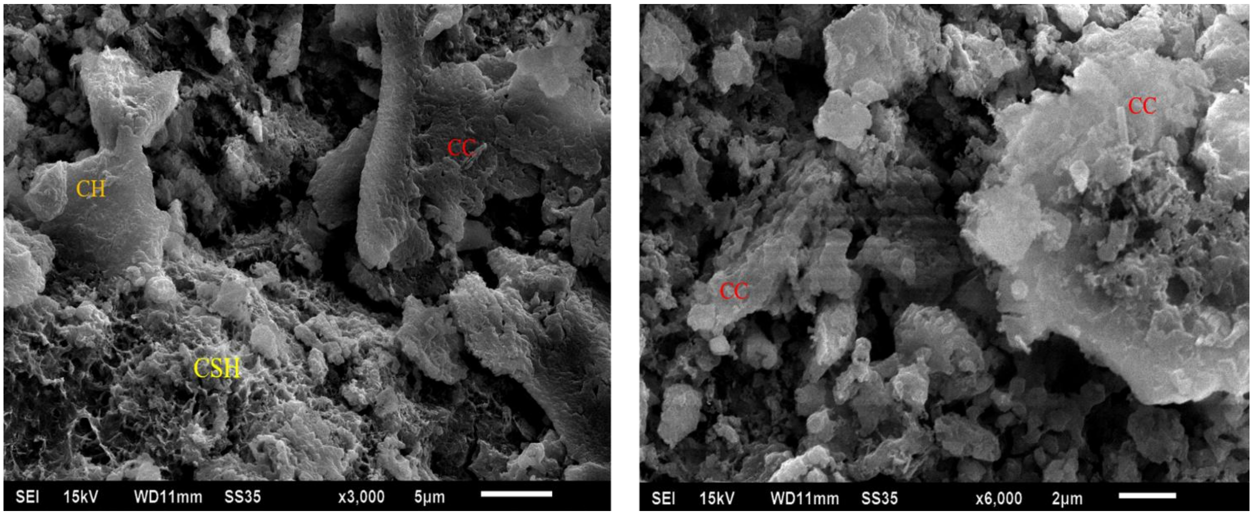

NFC-5% SF (x 3000) NFC-5% SF (x 6000)

Figure 4.53. SEM micrographs of NFC-5% SF at 90-day

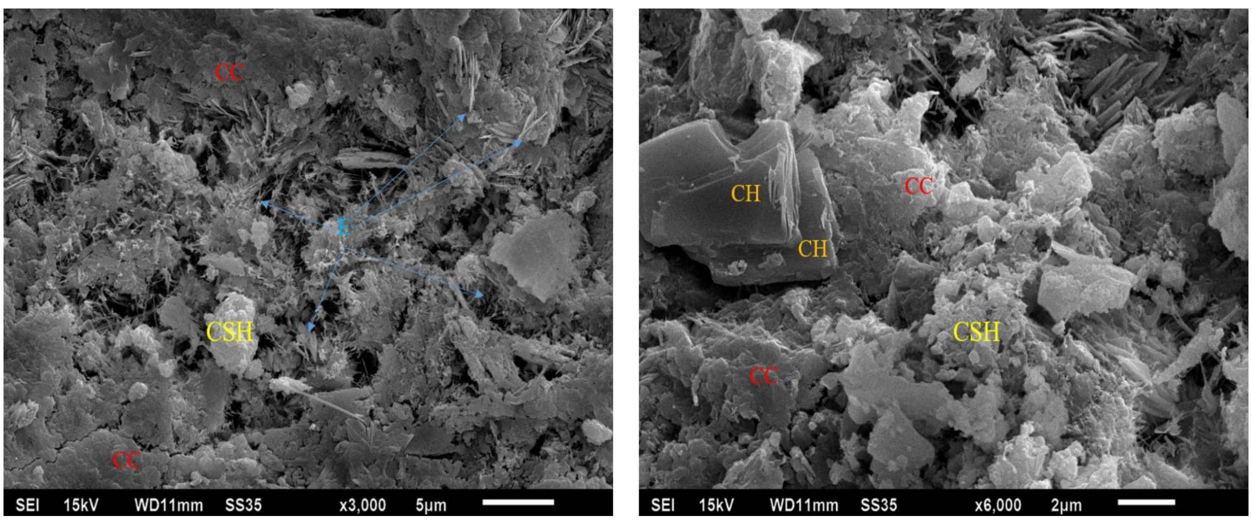

NFC-10% SF (x 3000) NFC-10% SF (x 6000)

Figure 4.54. SEM micrographs of NFC-10% SF at 90-day

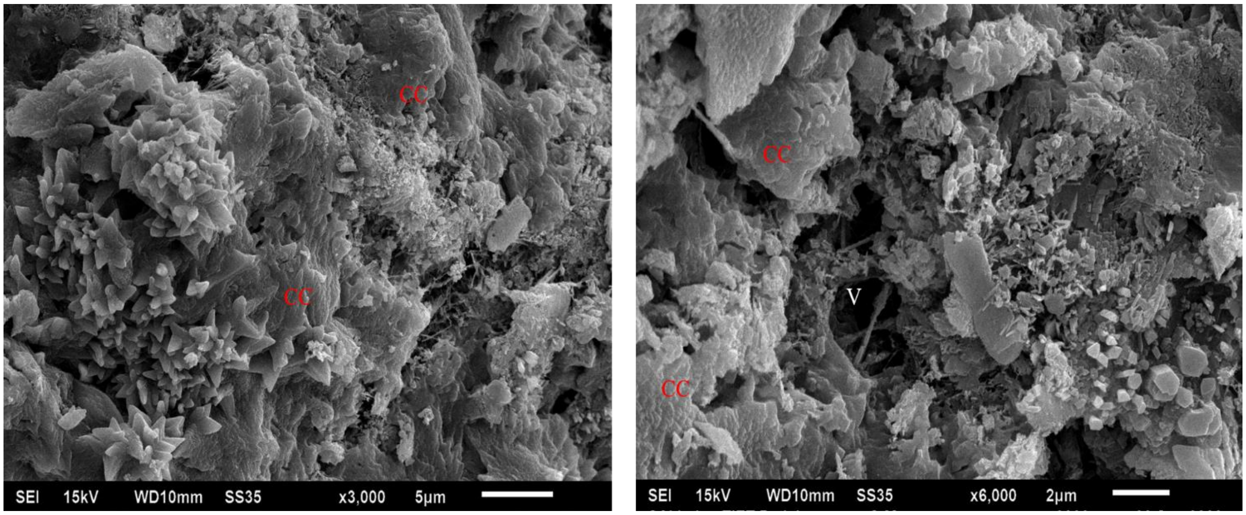

NFC-20% SF (x 3000) NFC-20% SF (x 6000)

Figure 4.55. SEM micrographs of NFC-20% SF at 90-day

4.4.4 Effect of replacement by rice husk ash (RHA)

Figure 4.56 to Figure 4.61 shows the SEM morphology of NFC mixes containing different replacement levels of RHA, i.e., 5%, 10%, and 20% at 28-day and 90-day. The dense microstructure was observed at 5% replacement of RHA at 90-day (Figure 4.59). It was because RHA acts as a pozzolan that reacts with calcium hydroxide in the hydration process and improves the aggregate paste connectivity, and reduces the transition zone thickness between aggregate and cement paste due to the precipitation of calcium hydroxide crystals on the surface of the grains (Hesami et al., 2014). In Figure 4.56 and Figure 4.59, crumpled sheets were observed at 5% replacement of RHA. The presence of ettringite in the shape of needle crystals inside the voids was seen at a higher replacement level of RHA than the NFC control mix. At 20% replacement level of RHA with cement, the non-uniform distribution of ash reduces the degree of compaction of the mix and the presence of unreactive silica in the concrete mix as compared to 5% replacement of RHA, which does not take part in the pozzolanic reaction of the cement hydration leads to increase in voids resulting in fall in compressive strength. A significant amount of unreacted calcium hydroxide was observed which reduced the strength properties (Figure 4.57). It was observed from SEM micrographs at higher replacement levels of RHA as shown in Figure 4.58, Figure 4.60, and Figure 4.61 that voids increased significantly with the curing age.

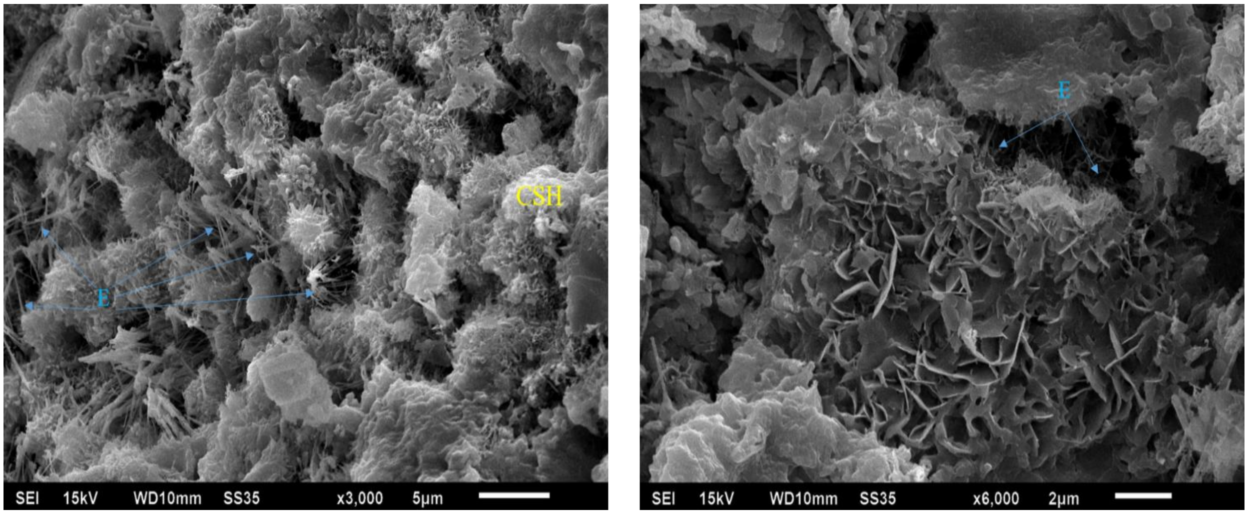

NFC-5% RHA (x 3000) NFC-5% RHA (x 6000)

Figure 4.56. SEM micrographs of NFC-5% RHA at 28-day

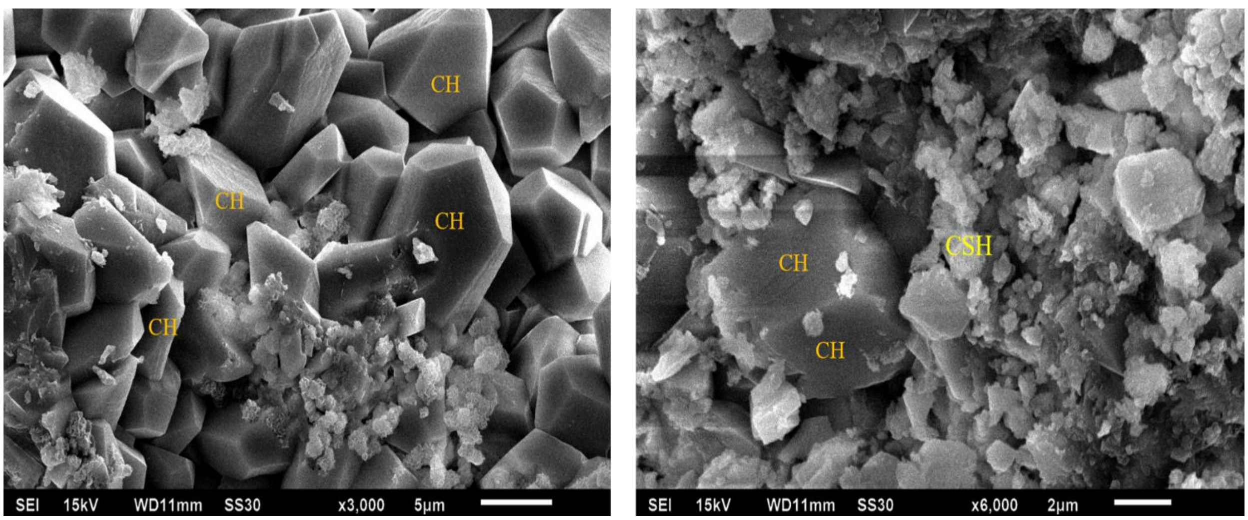

NFC-10% RHA (x 3000) NFC-10% RHA (x 6000)

Figure 4.57. SEM micrographs of NFC-10% RHA at 28-day

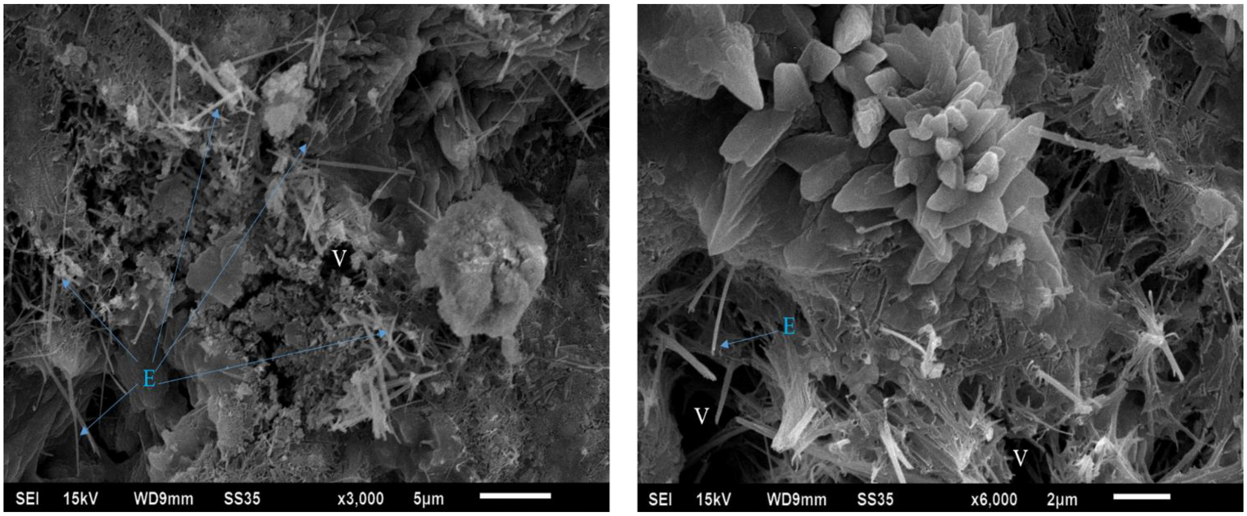

NFC-20% RHA (x 3000) NFC-20% RHA (x 6000)

Figure 4.58. SEM micrographs of NFC-20% RHA at 28-day

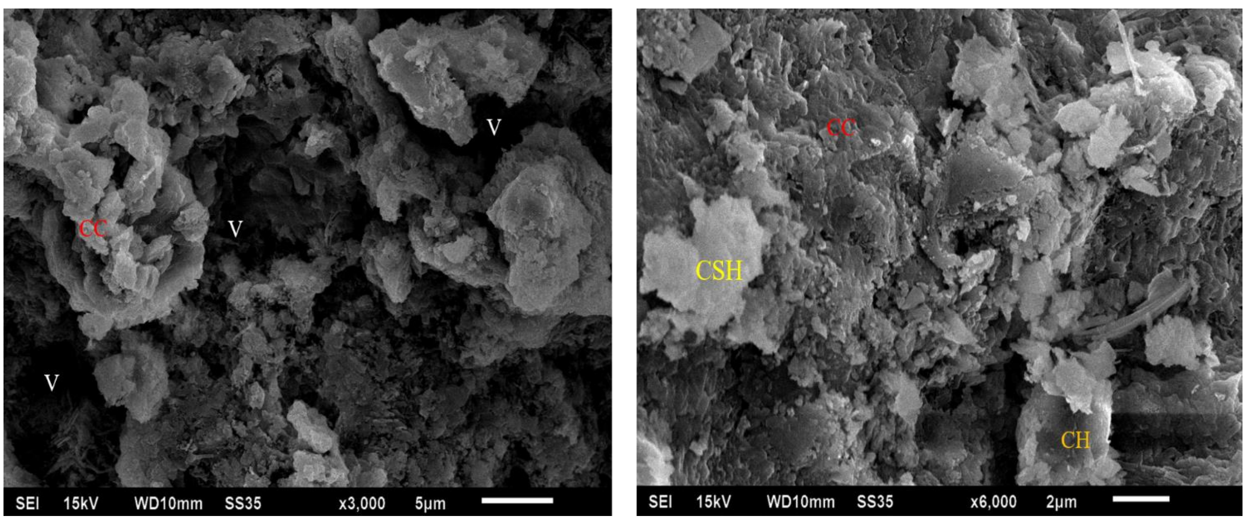

NFC-5% RHA (x 3000) NFC-5% RHA (x 6000)

Figure 4.59. SEM micrographs of NFC-5% RHA at 90-day

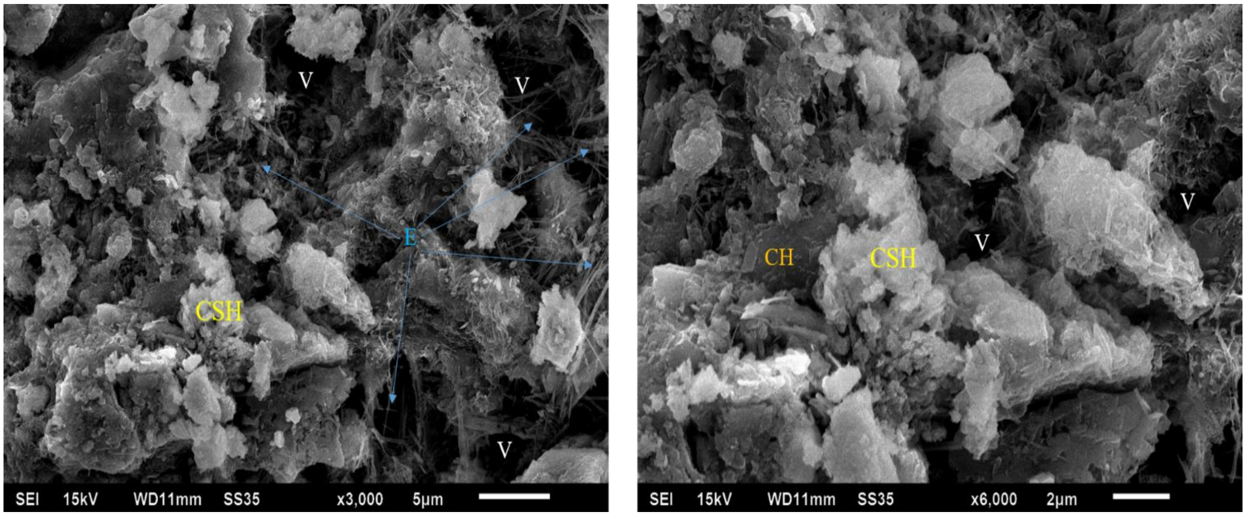

NFC-10% RHA (x 3000) NFC-10% RHA (x 6000)

Figure 4.60. SEM micrographs of NFC-10% RHA at 90-day

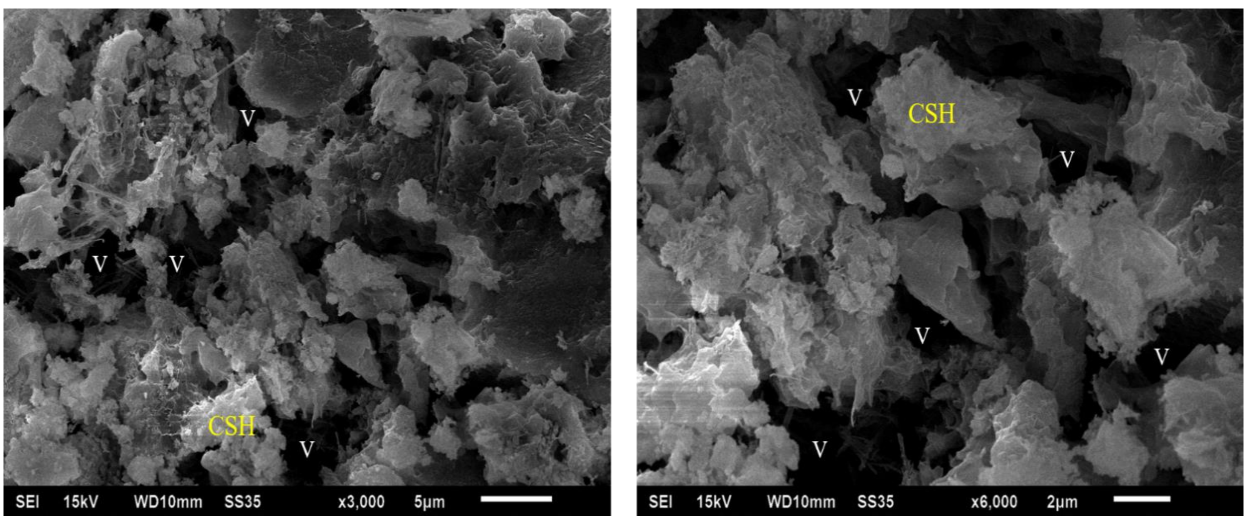

NFC-20% RHA (x 3000) NFC-20% RHA (x 6000)

Figure 4.61. SEM micrographs of NFC-20% RHA at 90-day

4.4.5 Effect of different gradation of coarse aggregates

Scanning Electron Microscopy (SEM) was used to validate the results further. Figure 4.62 (a) of NFC-4.75 at 28-day shows the porous Interfacial Transition Zone (ITZ) along with cement matrix and aggregates. Figure 4.62 (b) of NFC-4.75 at 365-day shows the denser ITZ and good intermolecular bond between cement and aggregates. Higher packing efficiency and the surface area directly lead to enhancement in the strength of the NFC mixes prepared with smaller size aggregates. On the other hand, Figure 4.62 (c) of NFC-9.5 at 28-day shows stretched hairline cracks extending all-around the surface of the aggregates-cement matrix, and Figure 4.62 (d) shows the non-uniformity of the cement matrix and aggregates of NFC-9.5 at 365-day leading to lesser strength as compared to the NFC-4.75.

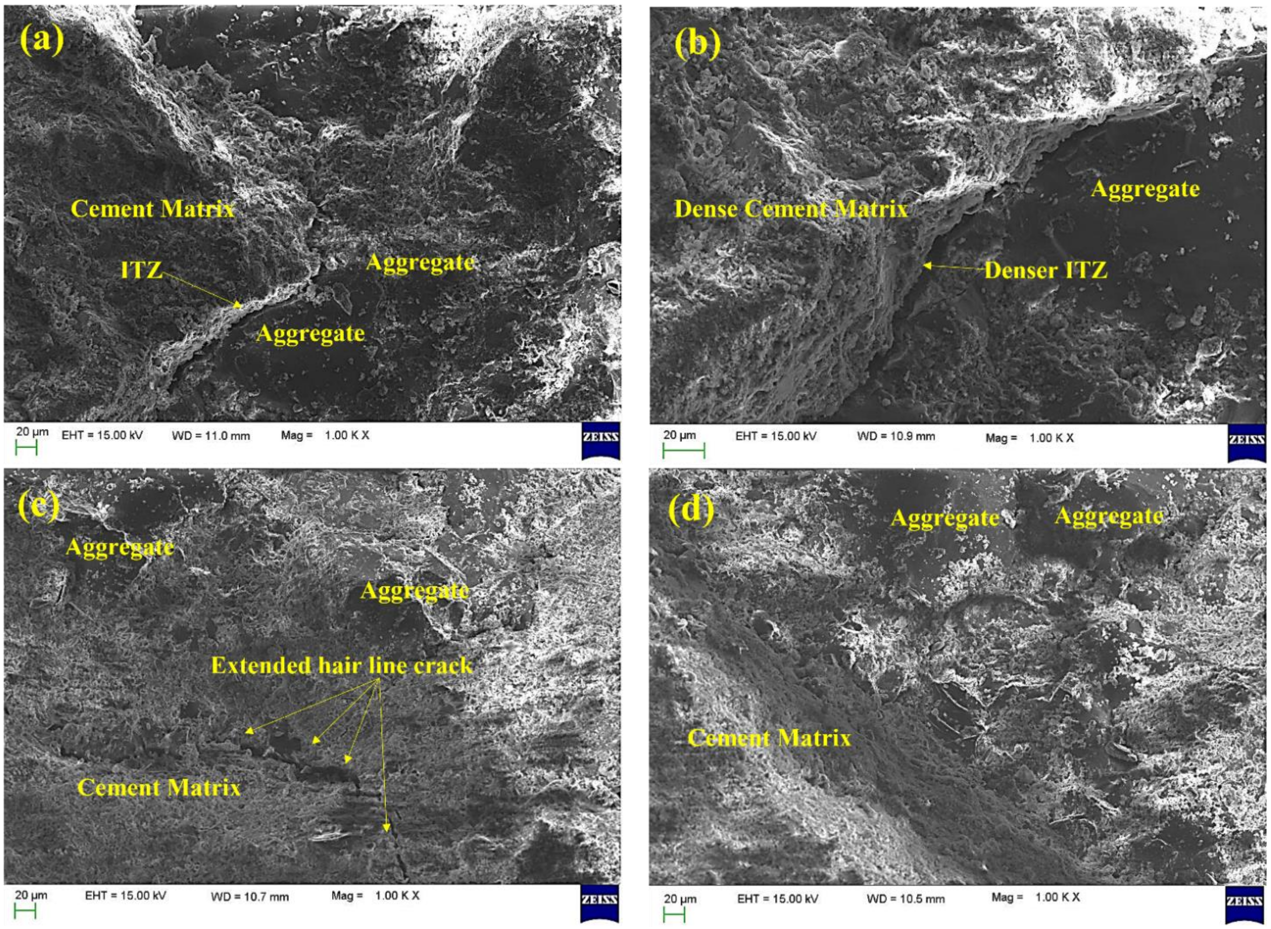

Figure 4.62. SEM micrographs of (a) NFC-4.75 at 28-day (b) NFC-4.75 at 365-day (c) NFC-9.5 at 28-day (d) NFC-9.5 at 365-day

4.5 XRD PHASE ANALYSIS

The interfacial transitional zone of concrete has a different microstructure than bulk cement paste. Identifying the hydration phase present in concrete is hindered by the weak diffraction peaks of the amorphous CSH gel phase of concrete and the interference of diffraction peaks of phases present in the sample. The diffraction peaks from portlandite tend to overcome the weak diffraction peaks of calcium silicate hydrate. At 28 and 90-day, the X-ray technique was utilized to identify the various stages present in hardened concrete of different NFC mixes and control NFC mix. The cement pastes were sieved through 90 sieves after being extracted from the concrete samples. The XRD experiments were carried out at diffraction angle 2θ ranging from 5° to 80° in steps size of 0.013°, and scan speed was 4° per minute.

4.5.1 Effect of replacement by fly ash (FA)

The XRD diffractogram of powder cement paste of NFC control mix and NFC mix containing different replacement levels of FA, i.e., 5%, 10%, and 20%, were illustrated in Figure 4.63 and Figure 4.64. All the peaks were matched with International Center for Diffraction Data (ICDD). The diffraction data analysis revealed that existence of hydrated phases like calcium hydroxide (α), silicon dioxide (β) (quartz), calcium carbonate (δ), calcium silicate hydrate (χ), and gismondine (G) which is also known as calcium aluminosilicate hydrate. XRD analysis of NFC mixes with FA (Figure 4.63 and Figure 4.64) indicates that the major phase of silicon dioxide along with calcium hydroxide and calcium carbonate was formed in the control mix. At a 5% replacement level of FA, the primary phase is silicon dioxide, which does not participate in the pozzolanic concrete activity. Carbon dioxide present in the surrounding air reacts with calcium hydroxide to form the calcium carbonate, which helps in increasing the mechanical strength. At the 20% replacement level of FA, a chemical reaction between silicon dioxide in hydrated products in a matrix of cement results in the formation of C-S-H gel, which gives strength to the concrete mix. At 90-day, the pozzolanic activity of FA leads to an overall improvement in the quality of cement paste and an enhancement in the strength compared to 28-day of the curing period.

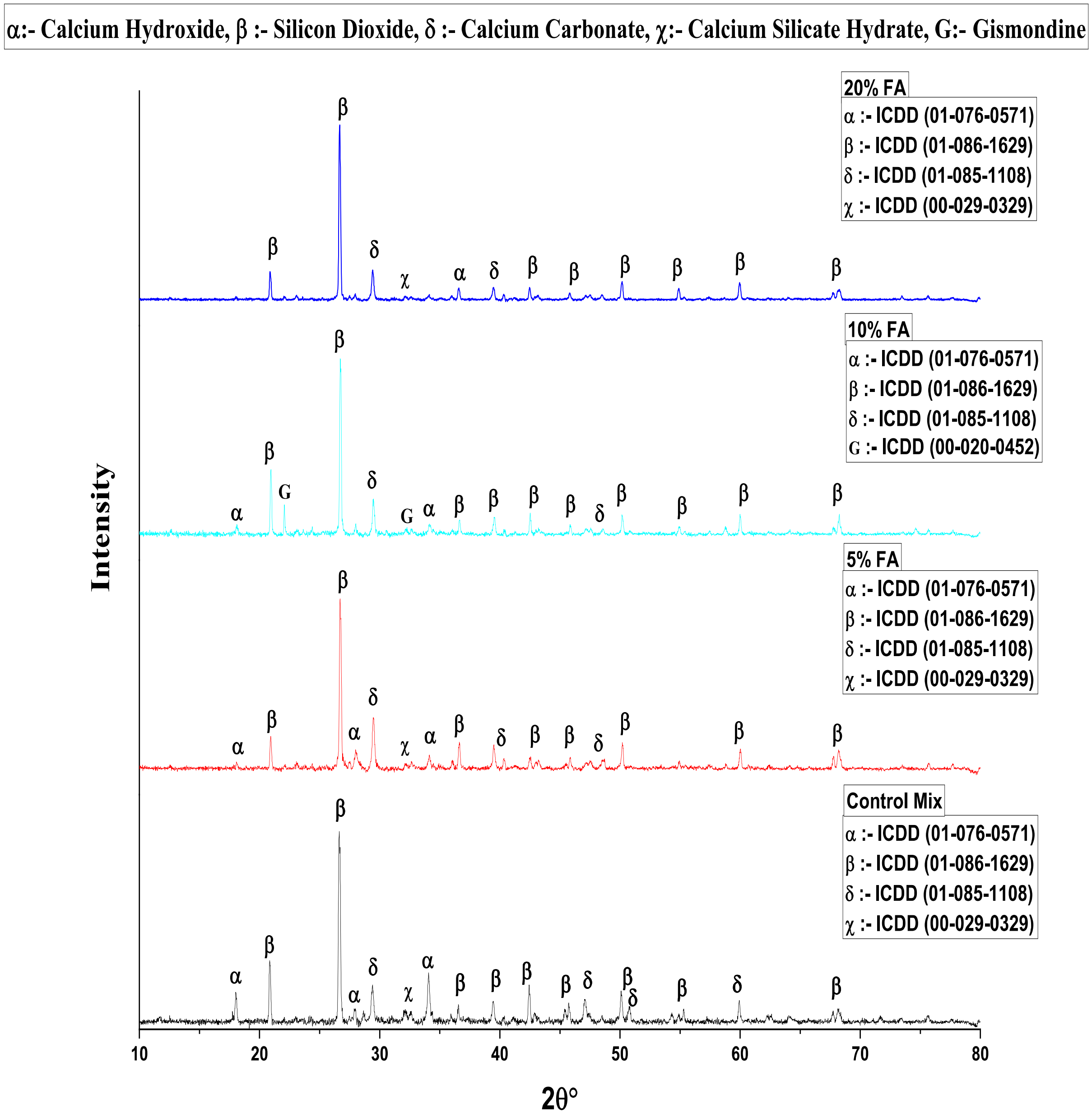

Figure 4.63. XRD image of NFC mixes using FA at 28-day

4.5.2 Effect of replacement by metakaolin (MK)

The XRD analysis of different NFC mixes prepared with different replacement levels of MK at the age of 28-day and 90-day was illustrated in Figure 4.65 and Figure 4.66. All the peaks were matched with International Center for Diffraction Data (ICDD). The diffraction pattern revealed the existence of hydrated phases like calcium hydroxide (α), silicon dioxide (β) (quartz), calcium carbonate (δ), calcium silicate hydrate (χ), and gismondine (G). It indicated that the major phase present in the control mix was silicon dioxide and calcium hydroxide, which take part in a chemical reaction. At increasing cement replacement with MK, the major phases of silicon dioxide (β peaks) take part in a chemical reaction with calcium hydroxide (α peaks). The production of gismondine (G) (calcium aluminosilicate hydrate) and calcium carbonate (δ) was obtained by the transformation of calcium hydroxide (α) (Araújo et al., 2019). The chemical reaction between unreacted amorphous silica in hydrated products in cement matrix results in the formation of C-S-H (χ peaks) and Gismondine (G peaks), providing an increase in strength at higher replacement levels of cement by MK (Macedo et al., 2020).

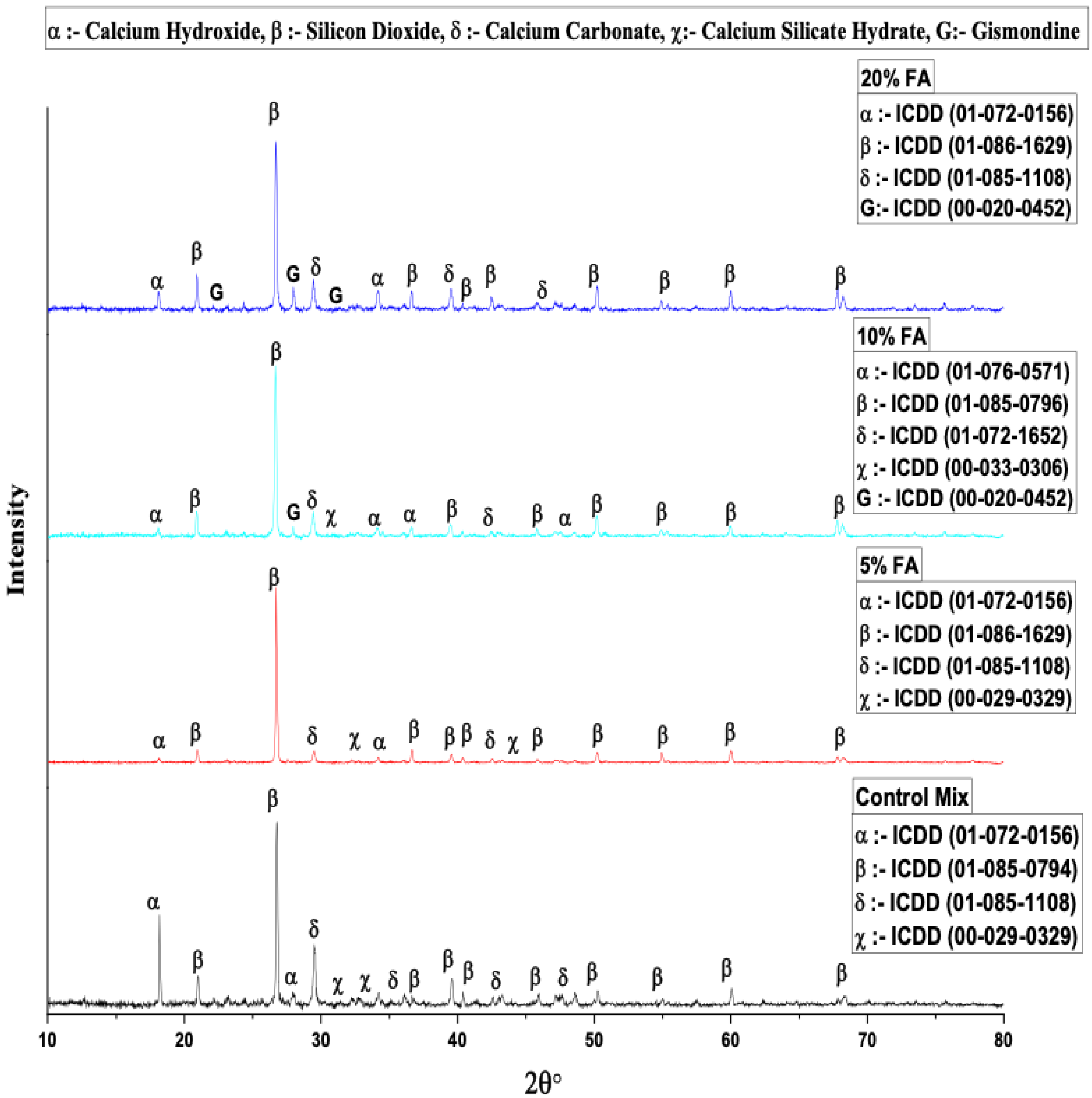

Figure 4.64. XRD image of NFC mixes using FA at 90-day

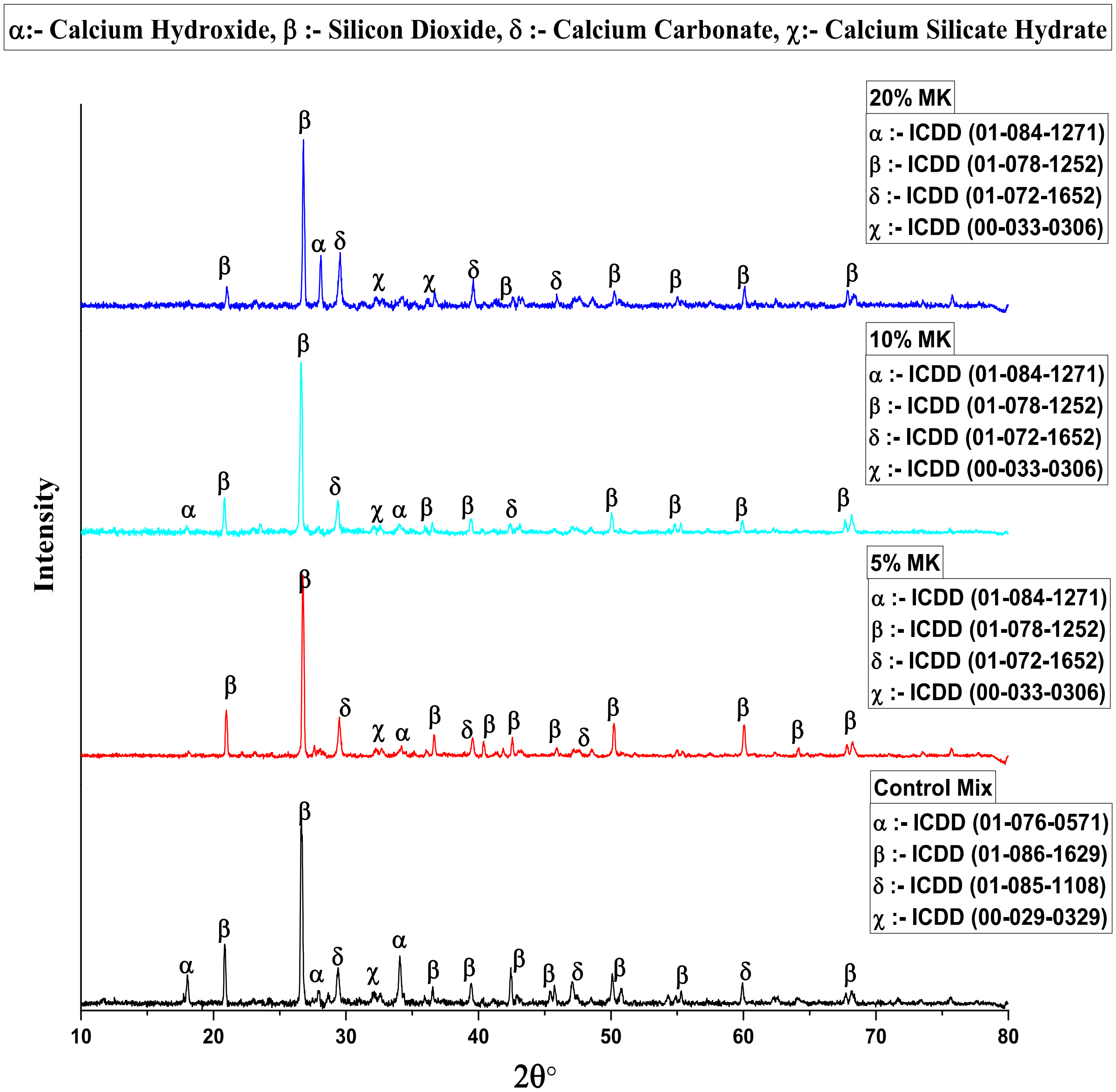

Figure 4.65. XRD image of NFC mixes using MK at 28-day

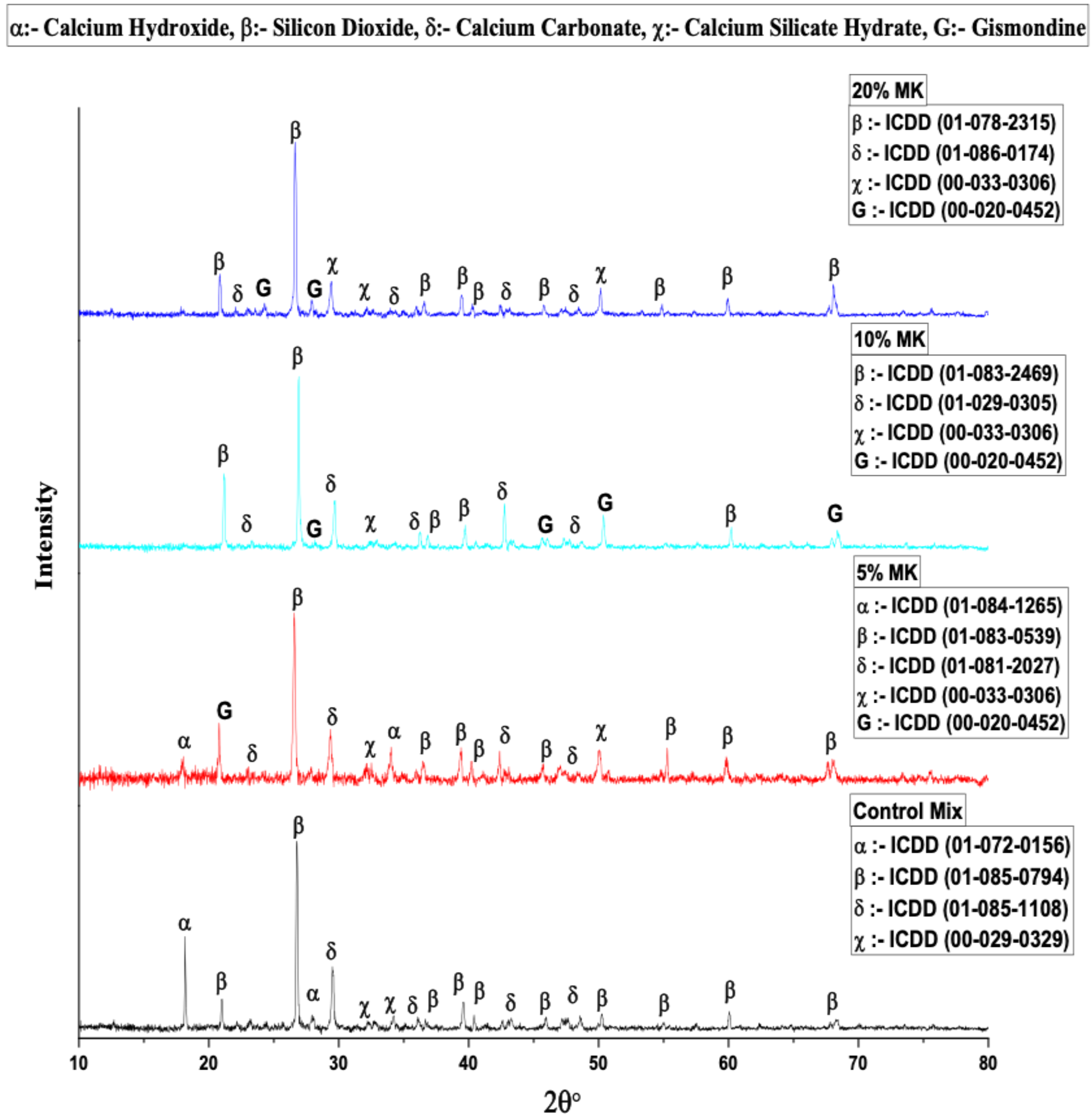

Figure 4.66. XRD image of NFC mixes using MK at 90-day

The microstructural analysis in SEM and XRD of different NFC mixes prepared using FA and MK corroborates the mechanism of strengthening NFC using optimal 20% FA at later ages and 20% MK as cement replacement.

4.5.3 Effect of replacement by silica fume (SF)

The XRD analysis of different NFC mixes prepared with different replacement levels of SF at the age of 28-day and 90-day was illustrated in Figure 4.67 and Figure 4.68. All the peaks were matched with International Center for Diffraction Data (ICDD). The major phases present in the control mix are silicon dioxide [SiO_2] (γ) along with calcium hydroxide [$Ca(OH)_2$] (ϕ), that takes part in a chemical reaction. At lower replacement levels of 5 and 10% of cement by SF, the major phases of high amorphous silica content (γ peaks) are obtained, which increases the pozzolanic reaction by reacting with calcium hydroxide (ϕ), resulting in the formation of calcium carbonate (η) and C-S-H gel (λ), which increases the mechanical strength. But at higher 20% cement replacement by SF, poor dispersion of silica particles in the concrete mix occurs. The excess silica particles which do not take part in the chemical reaction of cement hydration are precipitated as quartz peaks (γ) and reduced C-S-H gel (λ) peaks, causing a drop in strengths at higher SF replacement levels.

4.5.4 Effect of replacement by rice husk ash (RHA)

The XRD spectrums of NFC concrete at the age of 28-day and 90-day using RHA at different replacement levels were shown in Figure 4.69 and Figure 4.70. All the peaks were matched with International Center for Diffraction Data (ICDD). The control NFC mix shows the primary phase of silicon dioxide (γ) along with calcium hydroxide (ϕ) and calcium carbonate (η). At 5% cement replacement by RHA, the primary phase of silicon dioxide and calcium hydroxide (ϕ) and ettringites (μ) was formed. Silicon dioxide participates in the pozzolanic activity of concrete. Also, carbon dioxide from the air reacts with the calcium hydroxide to form the calcium carbonate, which helps in increasing the mechanical strength. But at a higher replacement level of RHA of 20%, excess silicon dioxide does not take part in a chemical reaction, leading to a decrease in strength.

Hence, microstructural analysis in the form of SEM and XRD of different NFC mixes prepared using SF and RHA corroborate the mechanism of strengthening of NFC using optimal 10% SF and 5% RHA as cement replacement.

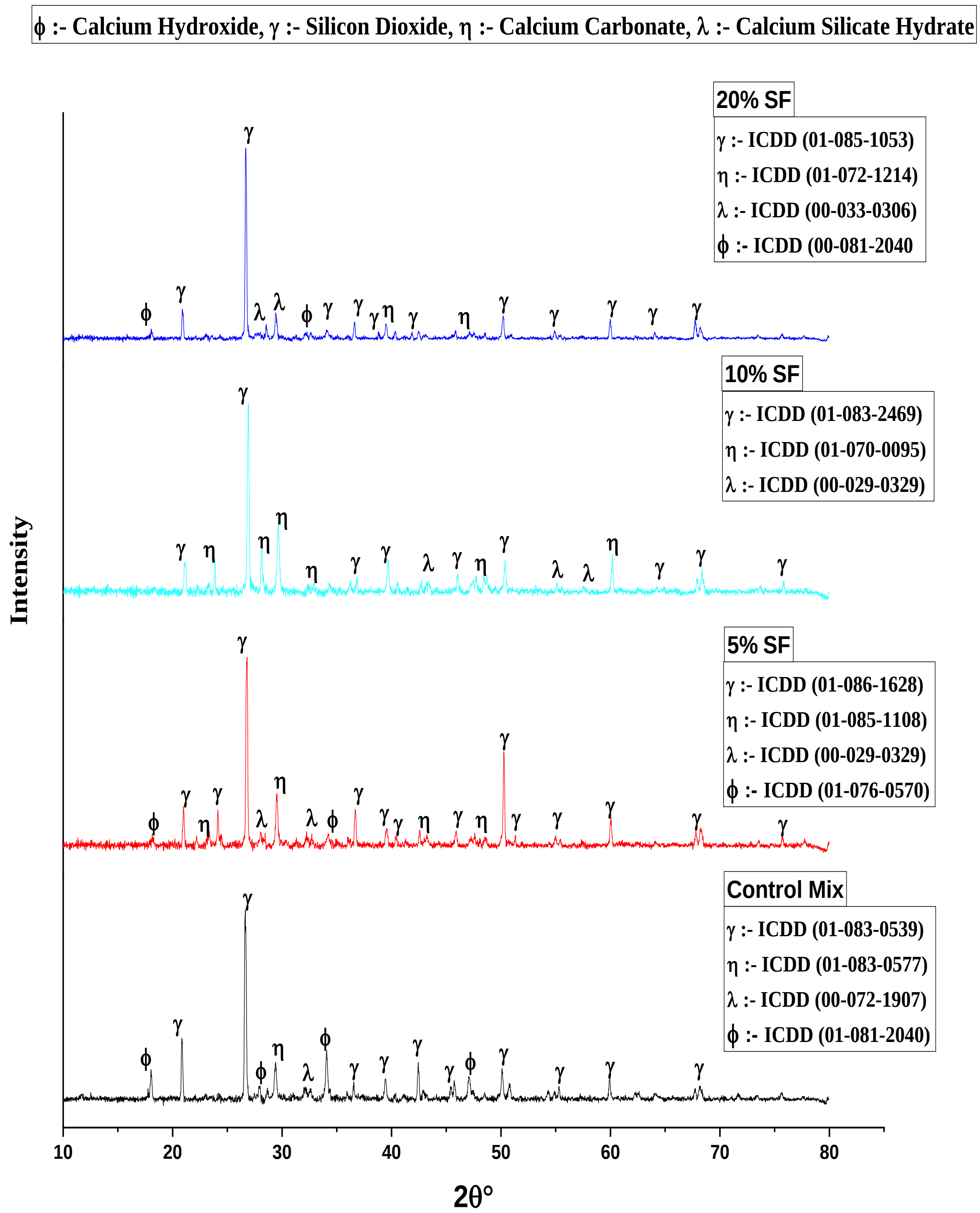

Figure 4.67. XRD image of NFC mixes using SF at 28-day

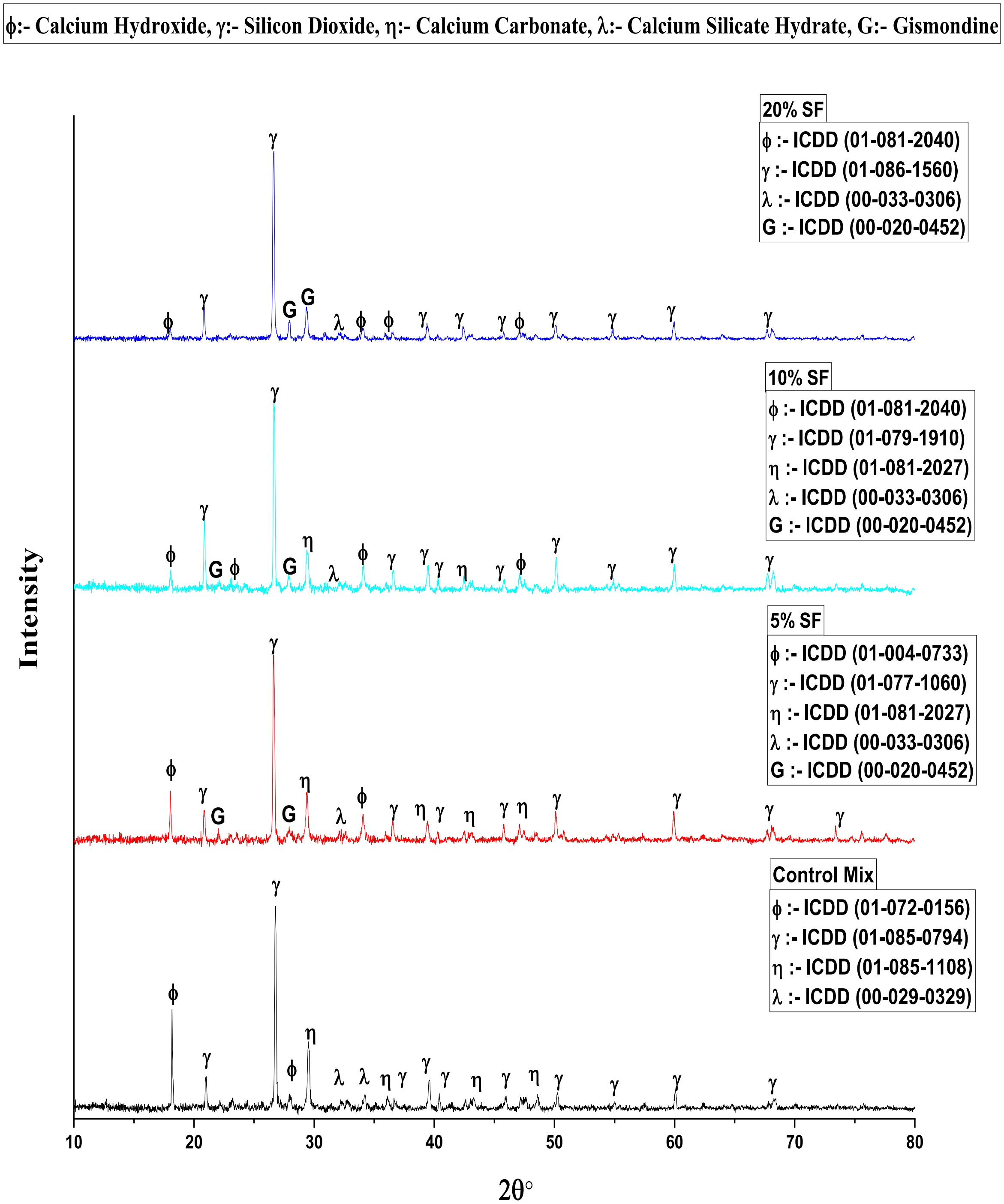

Figure 4.68. XRD image of NFC mixes using SF at 90-day

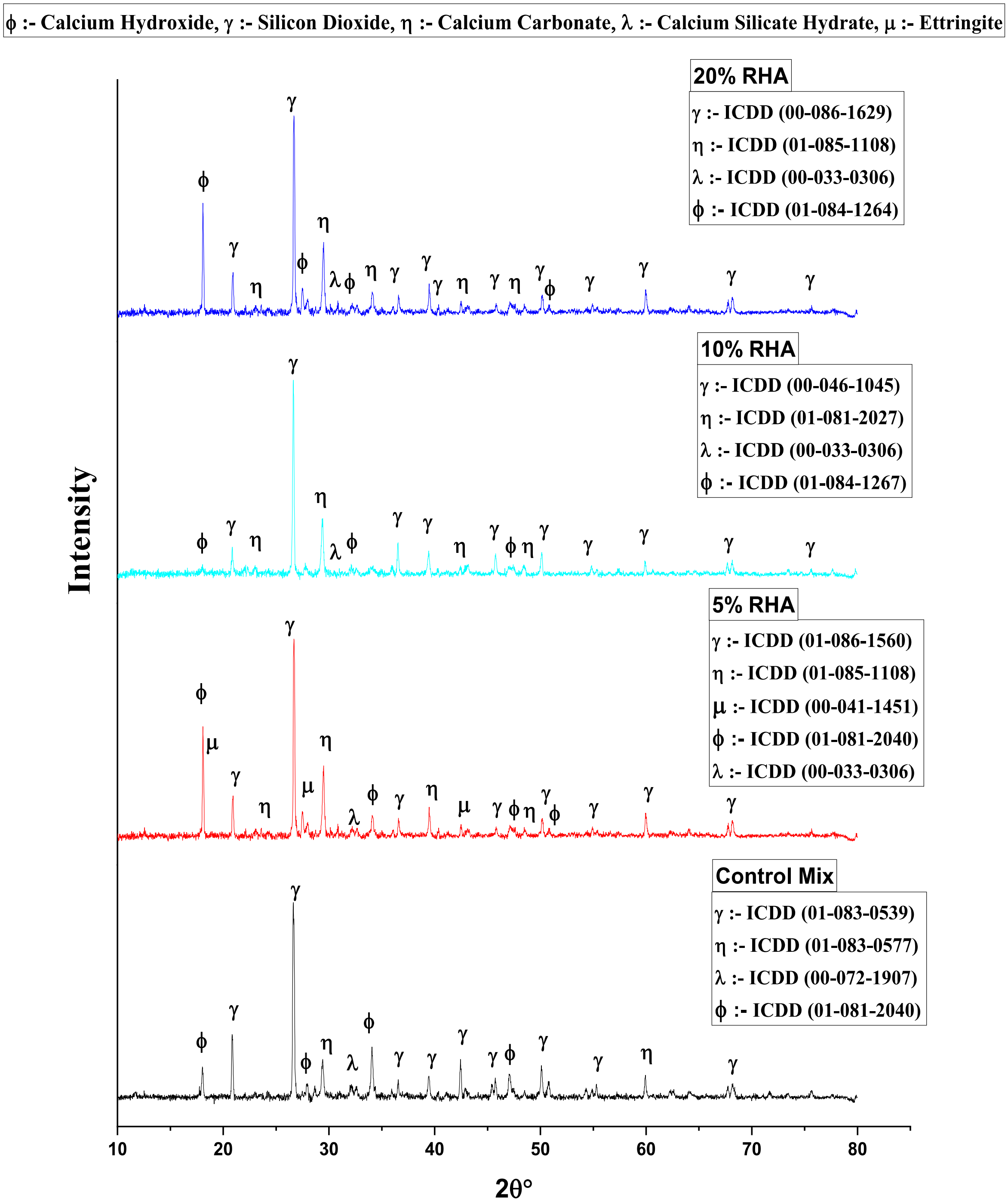

Figure 4.69. XRD image of NFC mixes using RHA at 28-day

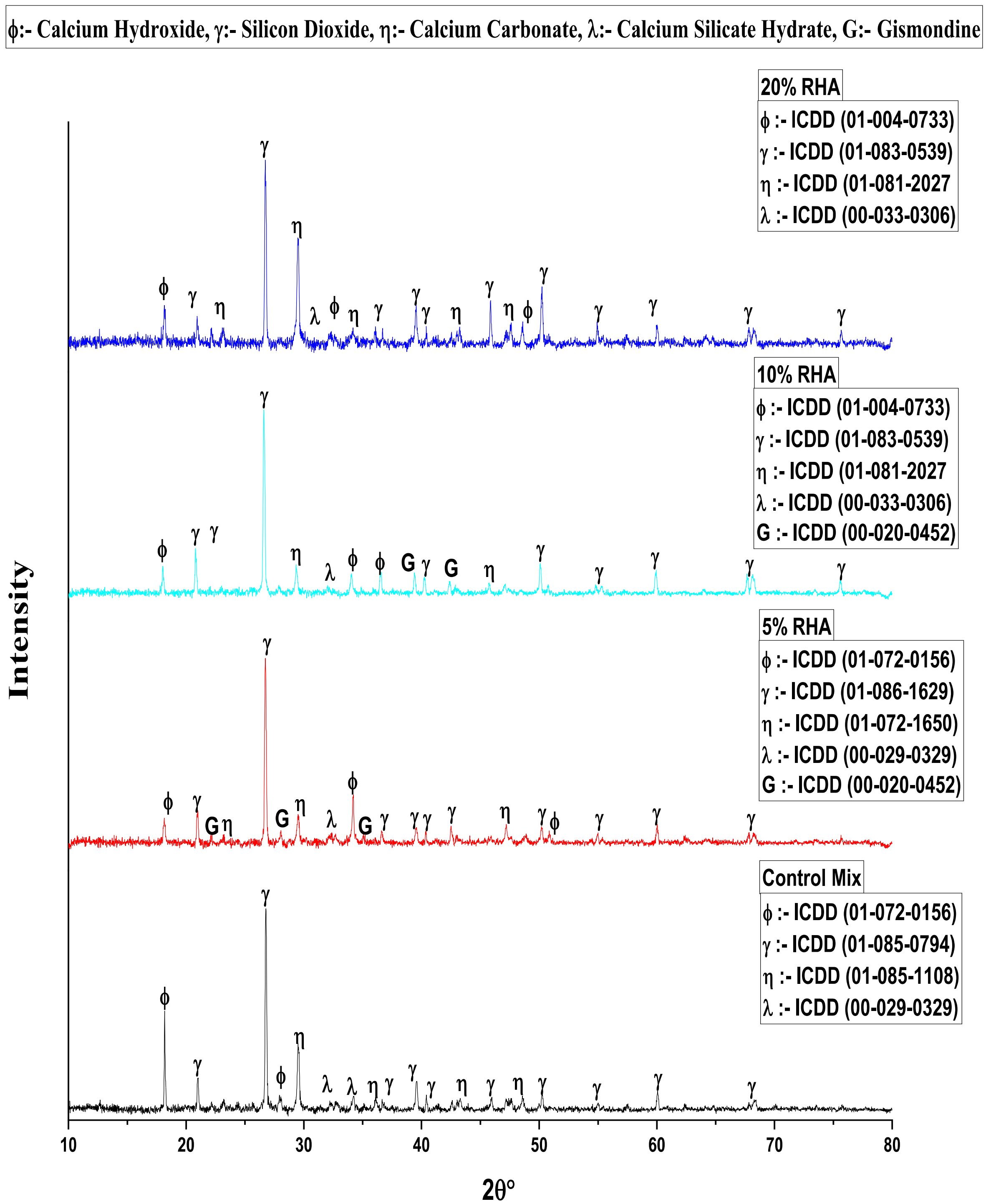

Figure 4.70. XRD image of NFC mixes using RHA at 90-day

CHAPTER 5
CONCLUSIONS

In the present study, the chief objective was to examine the effectiveness and efficacy of partial replacement of cement with supplementary cementitious materials and also determine their influence on different gradations of single-size natural coarse aggregates in NFC on the strength properties, including density, compressive, split tensile, flexural strength along with abrasion resistance and permeation properties of water permeability, porosity, and water absorption. Concrete microstructure and XRD analyses were also performed in this study. Based on the laboratory test, the following main conclusions can be derived from present study:

5.1 STRENGTH PROPERTIES

5.1.1 Compressive Strength

- The optimum replacement level of FA with cement in NFC was 20%, with a 3.1% increase in compressive strength at 90-day. The maximum compressive strength achieved was 15.31 MPa at 20% replacement of FA at 365-day. It is due to the slow pozzolanic reaction of FA at early ages, but improvement in fineness and pozzolanic activity of FA contribute to an overall improvement in cement paste quality at later ages.
- Partial replacement of cement in NFC with MK results in significant improvement in its compressive strength with the maximum gain in respective strength by 46% at 20% replacement level at 90-day. The maximum compressive strength achieved was 19.79 MPa at 20% replacement of MK at 365-day. It can be attributed to the high reactivity of MK due to the presence of higher SiO_2 content.
- The optimum replacement level of SF as SCM in NFC was suggested as 10% for maximum strength enhancement, wherein a compressive strength of 15.22 MPa was achieved at 365-day.
- Using RHA as SCM in NFC for strength enhancement, an optimum replacement level of 5% is suggested where the highest compressive strength gain of 25.04% was observed at 90-day.
- The use of smaller-sized aggregates in NFC mixes provides better compressive strength than when larger-sized aggregates are used to prepare the same. The maximum percentage

increase in compressive strength was 15.18% at 365-day achieved with NFC-4.75 compared to NFC-9.5 of curing. The smaller size aggregates increase the surface area of cement matrix and packing efficiency, thus reducing voids and making NFC mixes denser.

5.1.2 Split Tensile Strength

- The optimum replacement level of FA in NFC was 20%, with a 15.79% rise in split tensile strength for 90-day testing. The maximum strength attained was 2.30 MPa at 20% replacement of FA at 365-day.
- The replacement of cement in the NFC mix by 20% of MK increased in split tensile strength at 365-day. The maximum strength obtained was 3.23 MPa at 20% replacement of MK at 365-day.
- On using SF as SCM in the NFC mix, the increase in tensile strength was 9.47% at 10% replacement of SF. The maximum tensile strength was 2.18 MPa at 10% SF at 365-day.
- The optimum replacement of RHA as SCM in the NFC mix was 5% with 1.90 MPa strength at 365-day.
- NFC mixes made with smaller size aggregates showed higher strength than achieved by using larger-sized aggregates. The maximum percentage increase in split tensile strength was 17.33% at 365-day for NFC-4.75 compared to NFC-9.5.

5.1.3 Flexural Strength

- The optimum replacement level of FA with cement in NFC was 20%, with an 11.74% increase in flexural strength at 90-day. At early ages, the strength decreased with the increasing replacement levels of FA due to the slow pozzolanic reaction of FA. But at later ages, strength increased, and maximum flexural strength was 3.89 MPa achieved.
- The replacement of cement by 20% MK increased flexural strength by 24.91% at 90-day. The maximum strength observed was 3.98 MPa at 20% replacement of MK at 365-day.
- A significant improvement in flexural strength was spotted in NFC mixes prepared with SF replacement with a maximum percentage increase of 28.11% at a 10% replacement level. The maximum flexural strength of 4.04 MPa was attained at 10% SF at 365-day.
- On replacing cement with increasing RHA, flexural strength marginally decreases.
- A similar trend was observed in flexural strength in which NFC mixes made with smaller size aggregates showed higher strength than achieved by using larger-sized aggregates.

The maximum percentage increase in flexural strength was 16.56% at 365-day for NFC-4.75 compared to NFC-9.5. The compact size of smaller aggregate resists the initial crack at the surface of the loading and improves the bond strength of NFC mixes. The flexural strength was adequate for use as pavement material and was well within the acceptable limits as per ACI guidelines.

5.1.4 Abrasion Resistance

- The abrasion resistance of NFC mix containing FA increased with increasing replacement levels. As the amount of FA replacement increased, percentage mass loss decreased. The percentage mass loss decreased from 31% to 20% at 5% to 20% replacement of FA. The optimum 20% replacement of FA was observed.
- In addition to improved compressive and flexural strength of pervious concrete with optimum 20% replacement of MK, abrasion resistance also significantly improves, pointing that they can be economically as well as effectively used in pavements for low to medium traffic applications. The percentage mass loss decreased from 31% to 20% at 5% to 20% replacement of MK.
- At optimum replacement of cement in NFC with 10% SF and 5% RHA, a significant improvement in abrasion resistance is observed along with compressive and flexural strength properties, which further justifies the use of NFC with SF and RHA as SCMs in optimum replacement levels of cement.
- The use of smaller-sized aggregates in NFC mixes improved the abrasion resistance because smaller-sized aggregates provide denser packing and a better bond with cement matrix, which is preferable for pavement concrete such as parking lots and city streets driveways etc.

5.1.5 Microstructure

- The microstructure of NFC containing FA showed the formation of a higher amount of CSH gel at later ages, as seen from SEM images.
- Microstructural SEM analysis of different NFC mixes prepared with MK shows a higher CSH gel formation concentration, leading to a dense microstructure and higher strengths.
- The microstructural SEM analysis shows a higher concentration of CSH gel formation at 10% replacement of SF.

- The SEM analysis shows the non-uniform distribution of ash decreased the degree of compaction of the mix at higher replacement levels of RHA.
- The microstructural analysis shows the denser microstructure of NFC-4.75 compared to NFC-9.5 at each curing age.

5.1.6 XRD Phase Analysis

- The XRD analysis of NFC mix with FA indicates the primary phase of silicon dioxide, calcium hydroxide, and calcium carbonate.
- The XRD spectrum shows the primary phase of silicon dioxide, calcium hydroxide, calcium carbonate, calcium silicate hydrate, and gismondine peaks.
- XRD spectrum indicates that major phases formed in NFC mix using SF and RHA remain the same. But an additional peak of C-S-H gel was noted in the NFC-SF10 mix, accompanying the quartz peak. In the case of RHA replacement, the primary phase was quartz, which does not participate in the pozzolanic activity.

5.2 PERMEATION PROPERTIES

5.2.1 Water Permeability

- Permeation properties of water permeability reduce slightly but are well within acceptable limits for NFC with increasing MK levels in NFC mixes due to the densification of a matrix. On the other hand, with an increase in FA levels in NFC mixes, water permeability was observed due to pore size refinement and the presence of continuous voids. Overall, water permeability levels of NFC mixes prepared with FA and MK replacement are suitable for drainage purposes in the road pavements with low to medium traffic and load applications.
- The permeability properties decrease marginally with increasing SF and RHA replacement at optimum levels without considerably affecting the drainage properties for use in road pavements.
- The water permeability of NFC mix prepared with 4.75 mm aggregates was 50% lower at 28-day as compared to NFC mix prepared with 9.5 mm sized aggregate. The water permeability values were well within the acceptable limits vis-à-vis drainage in pavement applications when small-sized aggregates were used and possessed adequate strength for NFC to be used for structural applications in medium traffic pavement applications.

5.2.2 Porosity

- An increase in replacement levels of FA in NFC mixes and increased porosity was observed due to pore size refinement and continuous voids.
- The porosity reduced slightly but was well within acceptable limits for NFC with increasing MK levels in NFC mixes due to the densification of a matrix.
- The porosity decreased marginally with increasing SF and RHA replacement at optimum levels. The average porosity values of different NFC mixes were in the range of 12% to 18.5%, which is within the range stated in ACI.
- The average porosity of approximately 26.5% was found for NFC prepared with a 4.75 mm aggregate size, which is acceptable as per ACI 522R guidelines and would not compromise their drainage properties in field applications.

5.2.3 Density

- The density was increased with the increasing replacement levels of FA at later ages due to improvement in pozzolanic activity and pore refinement structure. The average density was observed from 1900 kg/m^3 to 2200 kg/m^3, acceptable as per ACI 522R guidelines.
- On increasing replacement levels of MK, the density also increased. The average density was 2000 kg/m^3 to 2200 kg/m^3.
- The density of NFC mixes prepared with SF increased at 10% replacement of SF. Beyond 10% replacement, the density decreased. The average density was 2000 to 2200 kg/m^3.
- The density of NFC prepared with RHA increased at 5% replacement level at all curing ages. Beyond that percentage replacement, the density values were decreased. The average density was 2000 kg/m^3 to 2200 kg/m^3.
- The density of the NFC mixes decreased as the size of aggregates used increased. The maximum density was obtained with NFC-4.75 at all the curing ages. The average density values of different aggregate sizes lie in 1768 to 1900 kg/m^3 and within the acceptable limits of ACI 522R. It is expected that the durability and the performance of NFC mixes would significantly improve with increasing density obtained by using smaller-sized aggregates in NFC for structural applications in pavements subjected to low traffic.

5.2.4 Water Absorption

- The water absorption values decreased with the increased replacement levels of FA and

MK. The decrease in water absorption was observed at all curing ages of NFC mixes.

- The decrease in water absorption values was observed with increasing SF and RHA replacement of cement in NFC but lies well within the acceptable limits for NFC.

5.2.5 Drying Shrinkage

- The drying shrinkage of NFC mixes decreased with the increase in percentage replacement of FA. The shrinkage strains were comparable at a 5% replacement of FA with control mix.
- The decrease in drying shrinkage was observed with an increasing replacement percentage of MK. At early ages, up to 28-day, the shrinkage strains were compared with the control mix, but a noticeable difference was detected after 28-day of drying.
- With the increasing replacement of SF, the drying shrinkage was significantly decreased at all drying periods.
- The drying shrinkage of NFC mix containing RHA was decreased with the increase in percentage replacement. The shrinkage strains were comparable at later ages with the control mix.

5.3 Future Scope of Research

- The study of interfacial transition zone in NFC is very important and the changes in strength due to addition of various SCMs need to be explored in details.
- The several waste materials that cause environmental problems, such as rice stubble, bagasse ash, foundry sand, waste glass, and waste tires, can be investigated for use in NFC to prepare economical concrete mix while handling the issue of waste utilization.
- The durability properties of NFC for use in pavements with SCMs needs elaborative research concentrating on resistance to freezing and thawing, carbonation curing, resistance to sulfate attack and acid attack etc.
- Effect of clogging of NFC needs to be extensively studied and development of field test procedures is necessary for same.
- The addition of various kinds of fibers, polymers and nano-materials in NFC can be explored to enhance its strength properties.
- Flow of water in NFC being a complex phenomenon, there is a need to develop a mathematical model to study the effect of water flow property.
- The effect of various chemicals in storm water for drainage can be useful contribution.

REFERENCES

ACI Committee 522, 2010. Report on Pervious Concrete. Am. Concr. Institute, Farmingt. Hills, Mich 42.

ACI Committee 522, 2006. ACI 522R-06. Pervious concrete. Am. Concr. Institute, Farmingt. Hills, Mich.

Adil, G., Kevern, J.T., Mann, D., 2020. Influence of silica fume on mechanical and durability of pervious concrete. Constr. Build. Mater. 247, 118453. https://doi.org/10.1016/j.conbuildmat.2020.118453

Agar Ozbek, A.S., Weerheijm, J., Schlangen, E., Van Breugel, K., 2013. Dynamic behavior of porous concretes under drop weight impact testing. Cem. Concr. Compos. 39, 1–11. https://doi.org/10.1016/j.cemconcomp.2013.03.012

Akbari, H., Pomerantz, M., Taha, H., 2001. Cool surfaces and shade trees to reduce energy use and improve air quality in urban areas. Sol. energy 70, 295–310.

Anderson, I., Dewoolkar, M.M., 2015. Laboratory freezing-and-thawing durability of fly ash pervious concrete in a simulated field environment. ACI Mater. J. 112, 603–611. https://doi.org/10.14359/51687921

Araújo, R.A., De Menezes, A.L.R., Cabral, K.C., Nóbrega, A.K.C., Martinelli, A.E., Dantas, K.G.M., 2019. Evaluation of the pozzolanic activity of red ceramic waste using mechanical and physicochemical methods. Ceramica 65, 461–469. https://doi.org/10.1590/0366-69132019653752649

Asaeda, T., Ca, V.T., 2000. Characteristics of permeable pavement during hot summer weather and impact on the thermal environment. Build. Environ. 4, 363–375.

ASTM C 618, 2009. Standard Specification for Coal Fly ash and Raw or Calcined Natural Pozzolan for Use as a Mineral Admixture in Concrete. Am. Soc. Test. Mater.

ASTM C157/C157M, 1999. Standard Test Method for Length Change of Hardened Hydraulic-Cement Mortar and Concrete. Am. Soc. Test. Mater.

ASTM C1688-14a, 2014. Standard Test Method for Density and Void Content of Freshly Mixed Pervious Concrete. Am. Soc. Test. Mater.

ASTM C1747/C1747M, 2015. Standard Test Method for Determining Potential Resistance to Degradation of Pervious Concrete by Impact and Abrasion. Am. Soc. Test. Mater. https://doi.org/10.1520/C1747

ASTM C1754, 2012. Standard Test Method for Density and Void Content of Hardened Pervious Concrete. Am. Soc. Test. Mater. https://doi.org/10.1520/C1754

ASTM C642, 2013. Standard Test Method for Density, Absorption, and Voids in Hardened Concrete. Am. Soc. Test. Mater.

Barišić, I., Galić, M., Grubeša, I.N., 2017. Pervious concrete mix optimization for sustainable pavement solution, in: IOP Conference Series: Earth and Environmental Science. https://doi.org/10.1088/1755-1315/90/1/012091

Bhutta, M.A.R., Hasanah, N., Farhayu, N., Hussin, M.W., bin Md Tahir, M., Mirza, J., 2013. Properties of porous concrete from waste crushed concrete (recycled aggregate). Constr. Build. Mater. 47, 1243–1248. https://doi.org/10.1016/j.conbuildmat.2013.06.022

Bhutta, M.A.R., Tsuruta, K., Mirza, J., 2012. Evaluation of high-performance porous concrete properties. Constr. Build. Mater. 31, 67–73. https://doi.org/10.1016/j.conbuildmat.2011.12.024

BIS: 2386 (Part 3), 1963. Methods of Test for Aggregates for Concrete Specific Gravity, Density, Voids, Absorption And Bulking.

BIS: 2386 (Part 4), 1963. Methods of Test for Aggregates for Concrete Part IV Mechanical of Indian Standards Aggregates for Concrete.

BIS: 4031 (Part 11), 1988. Methods of physical tests for hydraulic cement, Part 11: Determination of density.

BIS: 4031 (Part 4), 1997. Determination of Consistency of Standard Cement Paste.

BIS: 4031 (Part 5), 1988. Determination of Initial and Final Setting Time.

BIS: 4031 (Part 6), 1988. Detremination of Compressive Strength of Hydraulic Cement other than Masonary Cement.

BIS: 516, 1959. Indian Standard Methods of Tests for Strength of Concrete. Bureau of Indian Standards, New Delhi, India. https://doi.org/10.3403/02128947

BIS: 5816, 1999. Indian Standard Splitting Tensile Strength of Concrete - Test Method. Bureau of Indian Standards, New Delhi, India.

BIS: 650, 1991. Indian Standard Sand for Testing Cement — Specification.

BIS: 8112, 2013. Indian Standard 43 Grade Ordinary Portland Cement- Specification. Bureau of Indian Standards, New Delhi, India.

BIS:12727, 1989. No-Fines Cast in Situ Cement Concrete-Code of Practice. Bur. Indian Stand. New Delhi, India.

BIS 3812, 2013. Specification for Pulverized Fuel Ash, Part-1: For Use as Pozzolana in Cement, Cement Mortar and Concrete. Bureau of Indian Standards, New Delhi, India.

Brooks, J.J., Megat Johari, M.A., 2001. Effect of metakaolin on creep and shrinkage of concrete.

Cem. Concr. Compos. 23, 495–502. https://doi.org/10.1016/S0958-9465(00)00095-0

Cackler E.T. et al., 2006. Evaluation of US and European concrete pavement noise reduction methods, National Concrete Pavement Technology Center, Concrete Pavement Surface Characteristics Project Reort, Lowa State University.

Chandrappa, Anush K., Biligiri, K.P., 2016a. Characterization of Fundamental Properties of Pervious Concrete Paving Mixtures Characterization of Fundamental Properties of Pervious Concrete Paving Mixtures.

Chandrappa, Anush K, Biligiri, K.P., 2016. Pervious concrete as a sustainable pavement material-Research findings and future prospects: A state-of-the-art review. Constr. Build. Mater. https://doi.org/10.1016/j.conbuildmat.2016.02.054

Chandrappa, Anush K., Biligiri, K.P., 2016b. Development of pavement-surface temperature predictive models: Parametric approach. J. Mater. Civ. Eng. 28. https://doi.org/10.1061/(ASCE)MT.1943-5533.0001415

Chang, J.J., Yeih, W., Chung, T.J., Huang, R., 2016. Properties of pervious concrete made with electric arc furnace slag and alkali-activated slag cement. Constr. Build. Mater. 109, 34–40. https://doi.org/10.1016/j.conbuildmat.2016.01.049

Chen, X., Wang, H., Najm, H., Venkiteela, G., Hencken, J., 2019. Evaluating engineering properties and environmental impact of pervious concrete with fly ash and slag. J. Clean. Prod. 237, 117714. https://doi.org/10.1016/j.jclepro.2019.117714

Chen, Y., Wang, K., Wang, X., Zhou, W., 2013. Strength, fracture and fatigue of pervious concrete. Constr. Build. Mater. 42, 97–104. https://doi.org/10.1016/j.conbuildmat.2013.01.006

Chindaprasirt, P., Jaturapitakkul, C., Sinsiri, T., 2005. Effect of fly ash fineness on compressive strength and pore size of blended cement paste. Cem. Concr. Compos. 27, 425–428. https://doi.org/10.1016/j.cemconcomp.2004.07.003

Chopra, D., Siddique, R., Kunal, 2015. Strength, permeability and microstructure of self-compacting concrete containing rice husk ash. Biosyst. Eng. 130, 72–80. https://doi.org/10.1016/j.biosystemseng.2014.12.005

Ćosić, K., Korat, L., Ducman, V., Netinger, I., 2015. Influence of aggregate type and size on properties of pervious concrete. Constr. Build. Mater. 78, 69–76. https://doi.org/10.1016/j.conbuildmat.2014.12.073

Deo, O., Neithalath, N., 2011. Compressive response of pervious concretes proportioned for desired porosities. Constr. Build. Mater. 25, 4181–4189. https://doi.org/10.1016/j.conbuildmat.2011.04.055

Deo, O., Neithalath, N., 2010. Compressive behavior of pervious concretes and a quantification of the influence of random pore structure features. Mater. Sci. Eng. A 528, 402–412. https://doi.org/10.1016/j.msea.2010.09.024

Dinakar, P., Sahoo, P.K., Sriram, G., 2013. Effect of Metakaolin Content on the Properties of High Strength Concrete. Int. J. Concr. Struct. Mater. 7, 215–223. https://doi.org/10.1007/s40069-013-0045-0

Dong, Q., Wu, H., Huang, B., Shu, X., Wang, K., 2013. Investigation into Laboratory Abrasion Test Methods for Pervious Concrete. J. Mater. Civ. Eng. 25, 886–892. https://doi.org/10.1061/(asce)mt.1943-5533.0000683

Elango, K.S., Revathi, V., 2017. Fal-G Binder Pervious Concrete. Constr. Build. Mater. 140, 91–99. https://doi.org/10.1016/j.conbuildmat.2017.02.086

Ferguson, B.K., 2005. Porous pavements. Boca Raton, Florida: CRC Press.

Fu, T.C., Yeih, W., Chang, J.J., Huang, R., 2014. The Influence of Aggregate Size and Binder Material on the Properties of Pervious Concrete. Adv. Mater. Sci. Eng. 2014, 963971. https://doi.org/10.1155/2014/963971

Ganesan, K., Rajagopal, K., Thangavel, K., 2008. Rice husk ash blended cement: Assessment of optimal level of replacement for strength and permeability properties of concrete. Constr. Build. Mater. 22, 1675–1683. https://doi.org/10.1016/j.conbuildmat.2007.06.011

Gao, R.D., Xu, Q.F., Li, X.M., Du, M.S., 2014. Experimental Research on Pervious Concrete Mixed with Polypropylene Split Fiber(PPSF). Adv. Mater. Res. 1065–1069, 1894–1898. https://doi.org/10.4028/www.scientific.net/amr.1065-1069.1894

Gesoğlu, M., Güneyisi, E., Khoshnaw, G., Ipek, S., 2014. Investigating properties of pervious concretes containing waste tire rubbers. Constr. Build. Mater. 63, 206–213. https://doi.org/10.1016/j.conbuildmat.2014.04.046

Ghafoori, N., Dutta, S., 1995. Laboratory investigation of compacted no-fines concrete for paving materials. J. Mater. Civ. Eng. 7, 183–191.

Gill, A.S., Siddique, R., 2017. Strength and micro-structural properties of self-compacting concrete containing metakaolin and rice husk ash. Constr. Build. Mater. 157, 51–64. https://doi.org/10.1016/j.conbuildmat.2017.09.088

Golden, J.S., 2004. The built environment induced urban heat island effect in rapidly urbanizing arid regions–a sustainable urban engineering complexity. Environ. Sci. 1, 321–349.

Grubeša, I.N., Barišić, I., Ducman, V., Korat, L., 2018. Draining capability of single-sized pervious concrete. Constr. Build. Mater. 169, 252–260. https://doi.org/10.1016/j.conbuildmat.2018.03.037

Güneyisi, E., Gesoğlu, M., Karaoğlu, S., Mermerdaş, K., 2012. Strength, permeability and shrinkage cracking of silica fume and metakaolin concretes. Constr. Build. Mater. 34, 120–130. https://doi.org/10.1016/j.conbuildmat.2012.02.017

Güneyisi, E., Gesoğlu, M., Mermerdaş, K., 2008. Improving strength, drying shrinkage, and pore structure of concrete using metakaolin. Mater. Struct. Constr. 41, 937–949. https://doi.org/10.1617/s11527-007-9296-z

Hadi, M.N.S., Al-Azzawi, M., Yu, T., 2018. Effects of fly ash characteristics and alkaline activator components on compressive strength of fly ash-based geopolymer mortar. Constr. Build. Mater. 175, 41–54. https://doi.org/10.1016/j.conbuildmat.2018.04.092

Hassan, A.A.A., Lachemi, M., Hossain, K.M.A., 2012. Effect of metakaolin and silica fume on the durability of self-consolidating concrete. Cem. Concr. Compos. 34, 801–807. https://doi.org/10.1016/j.cemconcomp.2012.02.013

Hesami, S., Ahmadi, S., Nematzadeh, M., 2014. Effects of rice husk ash and fiber on mechanical properties of pervious concrete pavement. Constr. Build. Mater. 53, 680–691. https://doi.org/10.1016/j.conbuildmat.2013.11.070

Huang, B., Wu, H., Shu, X., Burdette, E.G., 2010. Laboratory evaluation of permeability and strength of polymer-modified pervious concrete. Constr. Build. Mater. 24, 818–823. https://doi.org/10.1016/j.conbuildmat.2009.10.025

Ibrahim, A., Mahmoud, E., Yamin, M., Patibandla, V.C., 2014. Experimental study on Portland cement pervious concrete mechanical and hydrological properties. Constr. Build. Mater. 50, 524–529. https://doi.org/10.1016/j.conbuildmat.2013.09.022

Ibrahim, H.A., Abdul Razak, H., 2016. Effect of palm oil clinker incorporation on properties of pervious concrete. Constr. Build. Mater. 115, 70–77. https://doi.org/10.1016/j.conbuildmat.2016.03.181

IRC 44, 2017. Guidelines for Cement Concrete Mix Design for Pavements. Indian Roads Congr.

Jain, A.K., Chouhan, J.S., Goliya, S.S., 2011. Effect of Shape and Size of Aggregate on Permeability of Pervious Concrete. J. Eng. Res. Stud. 2, 48–51.

JIS A 5371, 2016. Precast unreinforced concrete products, Japanese Standards 690 Association. JIS.

Karthikeyan, B., Dhinakaran, G., 2018. Influence of ultrafine TiO2 and silica fume on performance of unreinforced and fiber reinforced concrete. Constr. Build. Mater. 161, 570–576. https://doi.org/10.1016/j.conbuildmat.2017.11.133

Kevern, J., Wang, K., Suleiman, M.T., Schaefer, V.R., 2005. Mix design development for pervious concrete in cold weather climates, in: Proceedings of the 2005 Mid-Continent Transportation Research Symposium.

Kevern, J.T., Biddle, D., Cao, Q., 2015. Effects of Macrosynthetic Fibers on Pervious Concrete Properties. J. Mater. Civ. Eng. 27, 06014031. https://doi.org/10.1061/(asce)mt.1943-5533.0001213

Kevern, J.T., Wang, K., Schaefer, V.R., 2010. Effect of coarse aggregate on the freeze-thaw durability of pervious concrete. J. Mater. Civ. Eng. 22, 469–475. https://doi.org/10.1061/(ASCE)MT.1943-5533.0000049

Khankhaje, E., Salim, M.R., Mirza, J., Hussin, M.W., Rafieizonooz, M., 2016. Properties of sustainable lightweight pervious concrete containing oil palm kernel shell as coarse aggregate. Constr. Build. Mater. 126, 1054–1065. https://doi.org/10.1016/j.conbuildmat.2016.09.010

Khassaf, S.I., Jasim, A.T., Mahdi, F.K., 2014. Investigation The Properties Of Concrete Containing Rice Husk Ash To Reduction The Seepage In Canals. Int. J. Sci. Technol. Res. 3, 348–354.

Khatib, J.M., Clay, R.M., 2004. Absorption characteristics of metakaolin concrete. Cem. Concr. Res. 34, 19–29. https://doi.org/10.1016/S0008-8846(03)00188-1

Khatib, J.M., Hibbert, J.J., 2005. Selected engineering properties of concrete incorporating slag and metakaolin. Constr. Build. Mater. 19, 460–472. https://doi.org/https://doi.org/10.1016/j.conbuildmat.2004.07.017

Kothari, A., 2017. Effects of Fly Ash on the properties of Alkali Activated Slag Concrete. Degree Proj.

Kou, S.C., Poon, C.S., 2013. Long-term mechanical and durability properties of recycled aggregate concrete prepared with the incorporation of fly ash. Cem. Concr. Compos. 37, 12–19. https://doi.org/10.1016/j.cemconcomp.2012.12.011

Kuang, X., Sansalone, J., Ying, G., Ranieri, V., 2011. Pore-structure models of hydraulic conductivity for permeable pavement. J. Hydrol. 399, 148–157. https://doi.org/10.1016/j.jhydrol.2010.11.024

Lang, L., Duan, H., Chen, B., 2019. Properties of pervious concrete made from steel slag and magnesium phosphate cement. Constr. Build. Mater. 209, 95–104. https://doi.org/10.1016/j.conbuildmat.2019.03.123

Le, H.T., Nguyen, S.T., Ludwig, H.M., 2014. A Study on High Performance Fine-Grained Concrete Containing Rice Husk Ash. Int. J. Concr. Struct. Mater. 8, 301–307. https://doi.org/10.1007/s40069-014-0078-z

Li, H., Harvey, J., Ge, Z., 2014. Experimental investigation on evaporation rate for enhancing evaporative cooling effect of permeable pavement materials. Constr. Build. Mater. 65, 367–375. https://doi.org/10.1016/j.conbuildmat.2014.05.004

Li, H., Zhang, M. hua, Ou, J. ping, 2006. Abrasion resistance of concrete containing nano-particles for pavement. Wear 260, 1262–1266. https://doi.org/10.1016/j.wear.2005.08.006

Lian, C., Zhuge, Y., 2010. Optimum mix design of enhanced permeable concrete - An experimental investigation. Constr. Build. Mater. 24, 2664–2671. https://doi.org/10.1016/j.conbuildmat.2010.04.057

Lian, C., Zhuge, Y., Beecham, S., 2011. The relationship between porosity and strength for porous concrete. Constr. Build. Mater. 25, 4294–4298. https://doi.org/10.1016/j.conbuildmat.2011.05.005

Limbachiya, M., Meddah, M.S., Ouchagour, Y., 2012. Use of recycled concrete aggregate in fly-ash concrete. Constr. Build. Mater. 27, 439–449. https://doi.org/10.1016/j.conbuildmat.2011.07.023

Luck, J.D., Workman, S.R., Coyne, M.S., Higgins, S.F., 2008. Solid material retention and nutrient reduction properties of pervious concrete mixtures. Biosyst. Eng. 100, 401–408.

Macedo, A.R.S., Silva, A.S., Da Luz, D.S., Ferreira, R.L.S., Lourenço, C.S., Gomes, U.U., 2020. Study of the effect of diatomite on physico-mechanical properties of concrete. Ceramica 66, 50–55. https://doi.org/10.1590/0366-69132020663772561

Maguesvari, M.U., Narasimha, V.L., 2013. Studies on Characterization of Pervious Concrete for Pavement Applications. Procedia - Soc. Behav. Sci. 104, 198–207. https://doi.org/10.1016/j.sbspro.2013.11.112

Maria, F. Di, Mersky, R.L., Daskal, S., Ayalon, O., Ghosh, S.K., 2020. Sustainable Waste Management: Policies and Case Studies, Sustainable Waste Management: Policies and Case Studies. Springer Singapore, Singapore. https://doi.org/10.1007/978-981-13-7071-7

Mehta, A., Ashish, D.K., 2019. Silica fume and waste glass in cement concrete production: A review. J. Build. Eng. 100888. https://doi.org/10.1016/j.jobe.2019.100888

Mehta, P.K., 2004. High-performance, high-volume fly ash concrete for sustainable development. Int. Work. Sustain. Dev. Concr. Technol. 3–14.

Miller, J.D., Kim, H., Kjeldsen, T.R., Packman, J., Grebby, S., Dearden, R., 2014. Assessing the impact of urbanization on storm runoff in a peri-urban catchment using historical change in impervious cover. J. Hydrol. 515, 59–70. https://doi.org/10.1016/j.jhydrol.2014.04.011

Mineral Commodity Summaries (USGS), 2020. . U.S Dep. Inter. U.S Geol. Surv. 1–39.

Mineral Commodity Summaries (USGS), 2011. . U.S Dep. Inter. U.S Geol. Surv. 1–295. https://doi.org/10.3133/mineral2011

Mohseni, E., Khotbehsara, M.M., Naseri, F., Monazami, M., Sarker, P., 2016. Polypropylene fiber reinforced cement mortars containing rice husk ash and nano-alumina. Constr. Build. Mater. 111, 429–439. https://doi.org/10.1016/j.conbuildmat.2016.02.124

Monteiro, P.J.M., Miller, S.A., Horvath, A., 2017. Towards sustainable concrete. Nat. Mater. 16, 698–699. https://doi.org/10.1038/nmat4930

Montes, F., 2006. Pervious concrete: characterization of fundamental properties and simulation of microstructure.

Mrakovčić, S., Čeh, N., Jugovac, V., 2014. Effect of aggregate grading on pervious concrete properties. Gradjevinar 66, 107–113. https://doi.org/10.14256/JCE.977.2013

National Ready Mixed Concrete Association, 2004. Freeze Thaw Resistance of Pervious Concrete.

Nguyen, D.H., Boutouil, M., Sebaibi, N., Baraud, F., Leleyter, L., 2017. Durability of pervious concrete using crushed seashells. Constr. Build. Mater. 135, 137–150. https://doi.org/10.1016/j.conbuildmat.2016.12.219

Nguyen, D.H., Boutouil, M., Sebaibi, N., Leleyter, L., Baraud, F., 2013. Valorization of seashell by-products in pervious concrete pavers. Constr. Build. Mater. 49, 151–160. https://doi.org/10.1016/j.conbuildmat.2013.08.017

Olutoge, F.A., Adesina, P.A., 2019. Effects of rice husk ash prepared from charcoal-powered incinerator on the strength and durability properties of concrete. Constr. Build. Mater. 196, 386–394. https://doi.org/10.1016/j.conbuildmat.2018.11.138

Padhi, R.S., Patra, R.K., Mukharjee, B.B., Dey, T., 2018. Influence of incorporation of rice husk ash and coarse recycled concrete aggregates on properties of concrete. Constr. Build. Mater. 173, 289–297. https://doi.org/10.1016/j.conbuildmat.2018.03.270

Parasivamurthy, P., Jawali, V., Kirankumar, B. V, Patil, M.B., 2010. Improving ground water recharge using pervious cement concrete made of aggregates recycled from crushed concrete wastes, in: World Environmental and Water Resources Congress 2010: Challenges of Change - Proceedings of the World Environmental and Water Resources Congress 2010. pp. 2917–2926. https://doi.org/10.1061/41114(371)301

Park, S.B., Jang, Y. Il, Lee, J., Lee, B.J., 2009. An experimental study on the hazard assessment and mechanical properties of porous concrete utilizing coal bottom ash coarse aggregate in Korea. J. Hazard. Mater. 166, 348–355. https://doi.org/10.1016/j.jhazmat.2008.11.054

Patel, V.N., Modhera, C.D., Chavda, M.M., Panseriya, M.M., 2018. Effect of metakaolin on mechanical properties of different grades concretes inclusion of recycled aggregates from C & D waste and ceramic waste. Int. J. Eng. Technol. 7, 138–142. https://doi.org/10.14419/ijet.v7i3.29.18543

Qin, Y., Hiller, J.E., 2014. Understanding pavement-surface energy balance and its implications on cool pavement development. Energy Build. 85, 389–399.

https://doi.org/10.1016/j.enbuild.2014.09.076

Qing-Xin, Z., Wei, S., Chang-wen, M., 2009. Effect and mechanism of interaction between fly ash proportion and water-binder ratio on the creep characteristics of high performance concrete. China Civ. Eng. J. 42, 76–82.

Rashad, A.M., 2013. A preliminary study on the effect of fine aggregate replacement with metakaolin on strength and abrasion resistance of concrete. Constr. Build. Mater. 44, 487–495. https://doi.org/10.1016/j.conbuildmat.2013.03.038

Rawat, V., Kumar, R., Sachan, A.K., Tripathi, D., 2021. Effect of Steel Fibre on Mechanical Properties of Metakaolin-Mixed Concrete. Lect. Notes Civ. Eng. 135 LNCE, 101–110. https://doi.org/10.1007/978-981-33-6389-2_11

Saboo, N., Shivhare, S., Kori, K.K., Chandrappa, A.K., 2019. Effect of fly ash and metakaolin on pervious concrete properties. Constr. Build. Mater. 223, 322–328. https://doi.org/10.1016/j.conbuildmat.2019.06.185

Sanusi, G., Dauda, D., Khalil, I.., 2014. An Assessment of the Durability Properties of Binary Concrete 6, 22–30.

Sata, V., Ngohpok, C., Chindaprasirt, P., 2016. Properties of pervious concrete containing high-calcium fly ash. Comput. Concr. 17, 337–351. https://doi.org/10.12989/cac.2016.17.3.337

Shannag, M.J., 2000. High strength concrete containing natural pozzolan and silica fume. Cem. Concr. Compos. 22, 399–406. https://doi.org/10.1016/S0958-9465(00)00037-8

Shen, W., Shan, L., Zhang, T., Ma, H., Cai, Z., Shi, H., 2013. Investigation on polymer-rubber aggregate modified porous concrete. Constr. Build. Mater. 38, 667–674. https://doi.org/10.1016/j.conbuildmat.2012.09.006

Siddique, R., 2007. Waste Materials and By-Products in Concrete, Springer Science & Business Media. Springer Science & Business Media.

Siddique, R., 2004. Performance characteristics of high-volume Class F fly ash concrete. Cem. Concr. Res. 34, 487–493. https://doi.org/10.1016/j.cemconres.2003.09.002

Siddique, R., Aggarwal, P., Aggarwal, Y., 2012. Mechanical and durability properties of self-compacting concrete containing fly ash and bottom ash. J. Sustain. Cem. Mater. 1, 67–82. https://doi.org/10.1080/21650373.2012.726820

Siddique, R., Jameel, A., Singh, M., Barnat-Hunek, D., Kunal, Aït-Mokhtar, A., Belarbi, R., Rajor, A., 2017. Effect of bacteria on strength, permeation characteristics and micro-structure of silica fume concrete. Constr. Build. Mater. 142, 92–100. https://doi.org/10.1016/j.conbuildmat.2017.03.057

Siddique, R., Kadri, E.H., 2011. Effect of metakaolin and foundry sand on the near surface characteristics of concrete. Constr. Build. Mater. 25, 3257–3266. https://doi.org/10.1016/j.conbuildmat.2011.03.012

Siddique, R., Khan, M.I., 2011. Supplementary Cementing Materials, Engineering Materials. Springer Berlin Heidelberg, Berlin, Heidelberg. https://doi.org/10.1007/978-3-642-17866-5

Siddique, R., Khatib, J.M., 2010. Abrasion resistance and mechanical properties of high-volume fly ash concrete. Mater. Struct. Constr. 43, 709–718. https://doi.org/10.1617/s11527-009-9523-x

Siddique, R., Singh, K., Kunal, P., Singh, M., Corinaldesi, V., Rajor, A., 2016. Properties of bacterial rice husk ash concrete. Constr. Build. Mater. 121, 112–119. https://doi.org/10.1016/j.conbuildmat.2016.05.146

Singh, D., Singh, S.P., 2020. Influence of recycled concrete aggregates and blended cements on the mechanical properties of pervious concrete. Innov. Infrastruct. Solut. 5, 66. https://doi.org/10.1007/s41062-020-00314-x

Sreedhar, S., Biligiri, K.P., 2016. Comprehensive laboratory evaluation of thermophysical properties of pavement materials: Effects on urban heat island. J. Mater. Civ. Eng. 28, 1–12. https://doi.org/10.1061/(ASCE)MT.1943-5533.0001531

Sun, Z., Lin, X., Vollpracht, A., 2018. Pervious concrete made of alkali activated slag and geopolymers. Constr. Build. Mater. 189, 797–803. https://doi.org/10.1016/j.conbuildmat.2018.09.067

Sustainable Development, 1987. United Nations Conference on Environment and Development (UNCED), Earth Summit [WWW Document]. URL https://en.wikisource.org/wiki/Page:Brundtland_Report.djvu/25

Talsania, S., Pitroda, J., Vyas, C.M., 2015. Effect of rice husk ash on properties of pervious concrete. Int. J. Adv. Eng. Res. Stud. 296, 299.

Tang, W.C., Lo, T.Y., 2009. Mechanical and fracture properties of normal-and high-strength concretes with fly ash after exposure to high temperatures. Mag. Concr. Res. 61, 323–330. https://doi.org/10.1680/macr.2008.00084

Tangpagasit, J., Cheerarot, R., Jaturapitakkul, C., Kiattikomol, K., 2005. Packing effect and pozzolanic reaction of fly ash in mortar. Cem. Concr. Res. 35, 1145–1151. https://doi.org/10.1016/j.cemconres.2004.09.030

Tennis, P.D., Leming, M.L., Akers, D.J., 2004. Pervious concrete pavements. Portland Cement Association Skokie, IL.

Tho-In, T., Sata, V., Chindaprasirt, P., Jaturapitakkul, C., 2012. Pervious high-calcium fly ash geopolymer concrete. Constr. Build. Mater. 30, 366–371. https://doi.org/10.1016/j.conbuildmat.2011.12.028

Uma Maguesvari, M., Sundararajan, T., 2017. Influence of fly ash and fine aggregates on the characteristics of pervious concrete. Int. J. Appl. Eng. Res. 12, 1598–1609.

United Nations, 2014. World Urbanization Prospects: The 2014 Revision, Highlights (ST/ESA/SER.A/352), New York, United. https://doi.org/10.4054/DemRes.2005.12.9

Van Tuan, N., Ye, G., Van Breugel, K., Fraaij, A.L.A., Bui, D.D., 2011. The study of using rice husk ash to produce ultra high performance concrete. Constr. Build. Mater. 25, 2030–2035. https://doi.org/10.1016/j.conbuildmat.2010.11.046

Wang, K., Schaefer, V.R., Kevern, J.T., Suleiman, M.T., 2006. Development of mix proportion for functional and durable pervious concrete, in: NRMCA Concrete Technology Forum: Focus on Pervious Concrete. pp. 1–12.

Wild, S., Khatib, J.M., Jones, A., 1996. Relative strength, pozzolanic activity and cement hydration in superplasticised metakaolin concrete. Cem. Concr. Res. 26, 1537–1544. https://doi.org/10.1016/0008-8846(96)00148-2

Woo, S.K., Song, Y.C., Won, J.P., 2011. Enhanced durability performance of face slab concrete in Concrete-Faced Rock-filled Dam using fly ash and PVA fibre. KSCE J. Civ. Eng. 15, 875–882. https://doi.org/10.1007/s12205-011-1231-8

Wu, H., Huang, B., Shu, X., Dong, Q., 2011. Laboratory Evaluation of Abrasion Resistance of Portland Cement Pervious Concrete. J. Mater. Civ. Eng. 23, 697–702. https://doi.org/10.1061/(asce)mt.1943-5533.0000210

Wu, H., Liu, Z., Sun, B., 2016. Freeze-Thaw Resistance of Field and Laboratory Produced Portland Cement Pervious Concrete, in: Geotechnical Special Publication. pp. 26–33. https://doi.org/10.1061/9780784480090.004

Wu, W., Wang, R., Zhu, C., Meng, Q., 2018. The effect of fly ash and silica fume on mechanical properties and durability of coral aggregate concrete. Constr. Build. Mater. 185, 69–78. https://doi.org/https://doi.org/10.1016/j.conbuildmat.2018.06.097

Yahia, A., Kabagire, K.D., 2014. New approach to proportion pervious concrete. Constr. Build. Mater. https://doi.org/10.1016/j.conbuildmat.2014.03.025

Yang, J., Jiang, G., 2003. Experimental study on properties of pervious concrete pavement materials. Cem. Concr. Res. 33, 381–386. https://doi.org/10.1016/S0008-8846(02)00966-3

Yang, T., Zhu, H., Zhang, Z., 2017. Influence of fly ash on the pore structure and shrinkage characteristics of metakaolin-based geopolymer pastes and mortars. Constr. Build. Mater. 153, 284–293. https://doi.org/10.1016/j.conbuildmat.2017.05.067

Yen, T., Hsu, T.H., Liu, Y.W., Chen, S.H., 2007. Influence of class F fly ash on the abrasion-erosion resistance of high-strength concrete. Constr. Build. Mater. 21, 458–463.

https://doi.org/10.1016/j.conbuildmat.2005.06.051

Yue, Y., Wang, J.J., Bai, Y., 2018. Tracing the status of silica fume in cementitious materials with Raman microscope. Constr. Build. Mater. 159, 610–616. https://doi.org/10.1016/j.conbuildmat.2017.11.015

Zaetang, Y., Wongsa, A., Sata, V., Chindaprasirt, P., 2017. Influence of mineral additives on the properties of pervious concrete. Indian J. Eng. Mater. Sci. 24, 507–515.

Zaetang, Y., Wongsa, A., Sata, V., Chindaprasirt, P., 2013. Use of lightweight aggregates in pervious concrete. Constr. Build. Mater. 48, 585–591. https://doi.org/10.1016/j.conbuildmat.2013.07.077

Zhang, D., Han, P., Yang, Q., Mao, M., 2020. Shrinkage Effects of Using Fly Ash instead of Fine Aggregate in Concrete Mixtures. Adv. Mater. Sci. Eng. 2020. https://doi.org/10.1155/2020/2109093

Zhang, D., Mao, M., Zhang, S., Yang, Q., 2019. Influence of stress damage and high temperature on the freeze–thaw resistance of concrete with fly ash as fine aggregate. Constr. Build. Mater. 229, 116845. https://doi.org/10.1016/j.conbuildmat.2019.116845

Zhong, R., Leng, Z., Poon, C. sun, 2018. Research and application of pervious concrete as a sustainable pavement material: A state-of-the-art and state-of-the-practice review. Constr. Build. Mater. 183, 544–553. https://doi.org/10.1016/j.conbuildmat.2018.06.131

Zhou, J., Zheng, M., Wang, Q., Yang, J., Lin, T., 2016. Flexural fatigue behavior of polymer-modified pervious concrete with single sized aggregates. Constr. Build. Mater. 124, 897–905. https://doi.org/10.1016/j.conbuildmat.2016.07.136